Analysis of Ionospheric Data Sets to Identify Periodic Signatures Matching Atmospheric Planetary Waves

Andrew D. Norton

Thesis submitted to the Faculty of the
Virginia Polytechnic Institute and State University
in partial fulfillment of the requirements for the degree of

Master of Science
in
Aerospace Engineering

Scott L. England, Chair
Mayuresh J. Patil
Colin S. Adams

December 14, 2020
Blacksburg, Virginia

Keywords: Atmosphere-Ionosphere Coupling, Planetary Wave, Equatorial Ionosphere, Ionospheric Dynamo, Rossby-Gravity Wave

Analysis of Ionospheric Data Sets to Identify Periodic Signatures Matching Atmospheric Planetary Waves

Andrew D. Norton

(ABSTRACT)

Atmospheric planetary waves play a role in introducing variability to the low-latitude ionosphere. To better understand this coupling, this study investigates times when oscillations seen in both atmospheric planetary waves and ionospheric data-sets have similar periodicity. The planetary wave data-set used are temperature observations made by Sounding of the Atmosphere using Broadband Emission Radiometry (SABER). These highlight periods during which 2-Day westward propagating wave-number 3 waves are evident in the mesosphere and lower thermosphere. The ionospheric data-set is Total Electron Content (TEC), which is used to identify periods during which the ionosphere appears to respond to the planetary waves. Data from KP and F10.7 indices are used to determine events that may be of external origin. A 17-year time-span from 2002 to 2018 is used for this analysis so that both times of solar minimum and maximum can be studied. To extract the periods of this collection of data a Morlet Wavelet analysis is used, along with thresholding to indicate events when similar periods are seen in each data-set. Trends are then determined, which can lead to verification of previous assumptions and new discoveries.

Analysis of Ionospheric Data Sets to Identify Periodic Signatures Matching Atmospheric Planetary Waves

Andrew D. Norton

(GENERAL AUDIENCE ABSTRACT)

The thermosphere and ionosphere are impacted by many sources. The sun and the magnetosphere externally impact this system. Planetary waves, which originate in the lower atmosphere, internally impact this system. This interaction leads to periodic signatures in the ionosphere that reflect periodic signatures seen in the lower atmosphere, the sun and the magnetosphere. This study identifies these times of similar oscillations in the neutral atmosphere, the ionosphere, and the sun, in order to characterize these interactions. Events are cataloged through wavelet analysis and thresholding techniques. Using a time-span of 17 years, trends are identified using histograms and percentages. From these trends, the characteristics of this coupling can be concluded. This study is meant to confirm the theory and provide new insights that will hopefully lead to further investigation through modeling. The goal of this study is to gain a better understanding of the role that planetary waves have on the interaction of the atmosphere and the ionosphere.

Dedication

I dedicate this thesis to my friends and family. I want to especially thank my parents for their constant encouragement and belief.

Acknowledgments

I would first like to thank my advisor Dr. Scott L. England for his guidance and advice in this research process. I would also like to thank Dr. Mayuresh J. Patil and Dr. Colin S. Adams for serving on my Advisory Committee. Lastly, I would like to thank Dr. Guiping Lui providing additional guidance and generating the SABER data used for this study.

Contents

List of Figures ix

List of Tables xiii

1 Introduction 1

1.1 Earth's Upper Atmosphere 1

1.1.1 Ionosphere 4

1.2 Neutral Atmosphere and Ionosphere Coupling 6

1.2.1 Atmospheric Waves 7

1.2.2 Ionospheric Dynamo 9

1.2.3 Signatures of Planetary Waves in the Ionosphere 9

1.3 Statistical Studies 11

2 Data 12

2.1 SABER 13

2.2 Ground-based TEC 14

2.3 Solar Data 16

3 Methods **18**

3.1 TEC Data Selection 19

3.2 Wavelet Analysis & Threshold Techniques 26

3.2.1 Wavelet Analysis 26

3.2.2 Threshold Techniques 28

3.3 Comparison Techniques 32

3.3.1 Timeline Table Method 34

3.3.2 Histograms Method 37

3.3.3 Percentages Method 39

3.4 Wavelength Analysis 41

4 Results & Discussion **43**

4.1 Duration 44

4.2 Planetary Wave Amplitude 46

4.3 Location 48

4.4 Solar Activity 52

5 Conclusions **54**

Bibliography **58**

Appendices **63**

Appendix A Timelines **64**

A.1 Japan 64

A.2 Central America/Caribbean 69

A.3 South America 74

Appendix B Histograms **79**

B.1 Duration 79

B.2 Planetary Wave Amplitude 89

B.2.1 Upper Latitude Band 89

B.2.2 Middle Latitude Band 99

B.2.3 Lower Latitude Band 109

B.3 Number of Latitude Bands 119

B.4 Specific Latitude Band 129

B.5 Solar Level 139

List of Figures

1.1 Temperature profile of the upper atmosphere [14]. 3

1.2 Density profiles of the neutral atmosphere [14]. 4

1.3 Electron density profile of the ionosphere [4]. 6

1.4 Depiction of a Rossby wave. 8

1.5 Diagram of the E-region Dynamo showing how the build up of charges can create an electrostatic field that leads to plasma motion at higher altitudes in the ionosphere [7]. 10

2.1 Example of a SABER Amplitude plot of a 2-Day westward propagating wave-number 3 wave. 15

2.2 Example of a TEC map on May 12, 2017 at 2:00 UTC. 16

2.3 F10.7 data from 2002 to 2018. 17

3.1 Total Availability of the Ground-Based Total Electron Content data. The contour plot strength is the total number of data points at each location over the 17 years. The magnetic equator is also shown. Black outline has a contour value of 75% of the maximum value. 20

3.2 The three major TEC regions of interest. The left shows the overall Japan region, the middle shows two areas in the South American region, and the left shows the Central America/Caribbean region. Black outline has a contour value of 75% of the maximum value. . . . 21

3.3 The yearly availability of the TEC data for the South American region from 2007 to 2018. The magnetic equator is also shown in each of the plots. Black outline has a contour value of 75% of the maximum value. 23

3.4 An availability of plot of TEC for the Japan region showing the first method for dividing the major TEC regions. Any point inside red lines is considered part of the region. 24

3.5 A map showing each TEC region of interest. Each region is defined by a selection of points and each different color signifies a different region. The magnetic equator is the magenta colored line. 25

3.6 The left plot shows each latitude and longitude point included in the lower Japan region. The right plot is a contour plot of the magnetic latitude. 25

3.7 Example of a Morlet Wavelet. 27

3.8 The top plot is the summed TEC in the lower Japan region over the 17-year span. The bottom plot is power spectrum generated from the wavelet analysis over the 17-year span. 29

3.9 The SABER Amplitude plot of the 2-Day westward propagating wave-number 3 wave from 2002 to 2018. The dotted lines show how the latitude bands were defined. 30

3.10 The top plot shows the half-year threshold method. The bottom plot is the top latitude band of the SABER amplitude band. 31

3.11 Each plot is the maximum SABER amplitude at each time-step for each latitude band. Each plot shows the rolling threshold value by the black solid line. 33

3.12 Examples of Planetary Wave, Solar and Ambiguous Forcing using timeline plots 35

3.13 Histograms of the Saber Duration Distribution and Saber Mean Amplitude Distribution for the top latitude band. 38

3.14 The left plot is an example histogram of the number of SABER latitude bands a TEC region's events show up in. The right plot is an example histogram of which of the SABER latitude bands the TEC region's events show up in. The left region is for the first Japan region and the right is for the third South American Region 39

3.15 Example of a Solar Level Histogram for the Japan region. 40

3.16 Plots used to calculate wavelength. The plots include an amplitude plot and phase plot dependent on altitude and latitude. The third plot is the plots dependent on altitude with a best-fit line. 42

4.1 The distribution in duration of the SABER events using a threshold value of 1.2 standard deviations. 45

4.2 The distribution in duration of the TEC events in one of the Central American/Caribbean regions using a threshold value of 1.4 standard deviations. 45

4.3 The distribution in the Mean Amplitude of the SABER events using a threshold value of 1.2 standard deviations. 49

4.4 A histogram showing a concurrence in the peak latitude band and the TEC region position. This is a histogram for one of the Central America/Caribbean regions using a threshold value of 1.5 standard deviations. 51

List of Tables

4.1 Duration percentage table. The second column is the number of TEC concurrent with SABER events, the third is the percentage out of the total, the fourth is the number of just SABER occurrences and the fifth is the efficiency percentage. 47

4.2 Duration percentage table. The second column is the number of TEC concurrent with SABER events, the third is the percentage out of the total, the fourth is the number of just SABER occurrences and the fifth is the efficiency percentage. 50

4.3 A table of concurrence percentages. 51

4.4 Duration percentage table. The second column is the number of TEC concurrent with SABER events, the third is the percentage out of the total, the fourth is the number of just SABER occurrences and the fifth is the efficiency percentage. 53

Chapter 1

Introduction

The vertical coupling seen between the atmosphere and the ionosphere is believed to be heavily influenced by atmospheric planetary waves. The goal of this study is to gain a better understanding of this vertical coupling. This is done by first reviewing what is already known about the impact that these planetary-scale waves have on the ionosphere. This chapter will start by defining both the neutral upper atmosphere and the ionosphere. Then, sources and attributes of atmospheric waves will be discussed along with how they affect the ionosphere. This will include an explanation of the ionospheric dynamo and describe how planetary wave signatures can reach higher altitudes. Finally, a previous statistical study focused on this interaction will be discussed.

1.1 Earth's Upper Atmosphere

The upper atmosphere of Earth is a very complex region. It is important to understand the physics of this region because it is where many spacecraft operate. Some of the impacts that this region has on spacecraft includes, radio propagation inter-

ference, increased satellite drag, satellite erosion, and much more. In order to better predict the impact that space weather has on spacecraft one must have a good understanding of the many complex interactions that exist in this region. This section will describe both of the two main components of the upper atmosphere, neutral and charged.

Earth's upper atmosphere is unlike the atmosphere we commonly think of. There are many complexities in the temperature profile of the upper atmosphere. The regions of the neutral atmosphere can be defined by a temperature profile shown in Figure 1.1. Starting from the surface of the Earth the temperature decreases due to radiative cooling [14]. This region extends to 10 km and is called the Troposphere. The tropopause is where the temperature reaches a local minimum. A temperature increase is seen as the altitude increases, which is due to UV radiation at wavelengths above 242 nm. This region, the stratosphere, reaches a maximum altitude of 50 km, with the local maximum being called the stratopause. The temperature begins to decrease once more to the absolute minimum temperature in the upper atmosphere, 160 K. This region is called the mesosphere. The decrease in temperature is once again a result of radiative cooling but is specifically due to the trace gas, carbon dioxide [14]. Above the mesopause, the absolute minimum, the temperature begins to rapidly increase. This region of rapid heating is called the thermosphere. Once again, the rise in temperature is a result of solar radiation heating the atmosphere, but the rate of increase is attributed to the absence of effective heat loss processes at this altitude [14]. The thermopause is at the top of the thermosphere and has an altitude of around 600 km. The temperature reaches a limiting value of 1000K at

around 200 km. A depiction of the neutral density profile in the upper atmosphere is shown in Figure 1.2. As one can see the total density decreases exponentially with altitude as does most of the neutral particles. Atomic oxygen decreases at a much smaller rate to a production increase due to radiative recombination. This low-density region is characterized by a rising temperature profile and a change in composition with altitude.

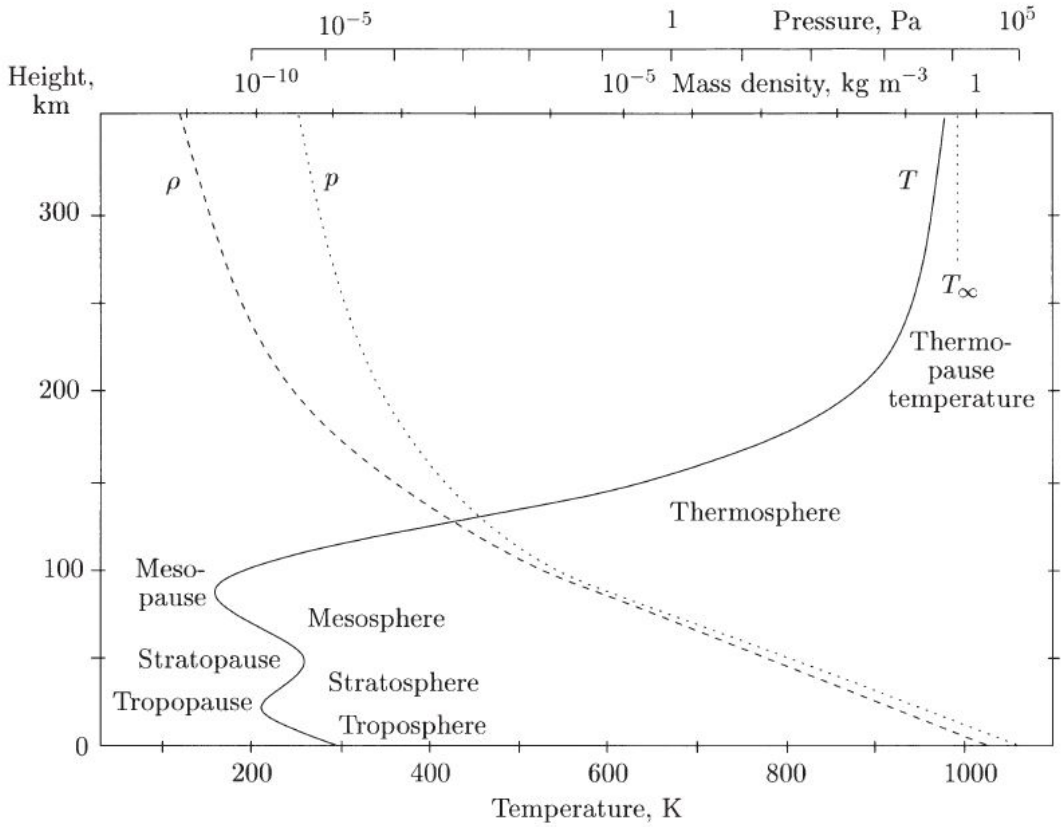

Figure 1.1: Temperature profile of the upper atmosphere [14].

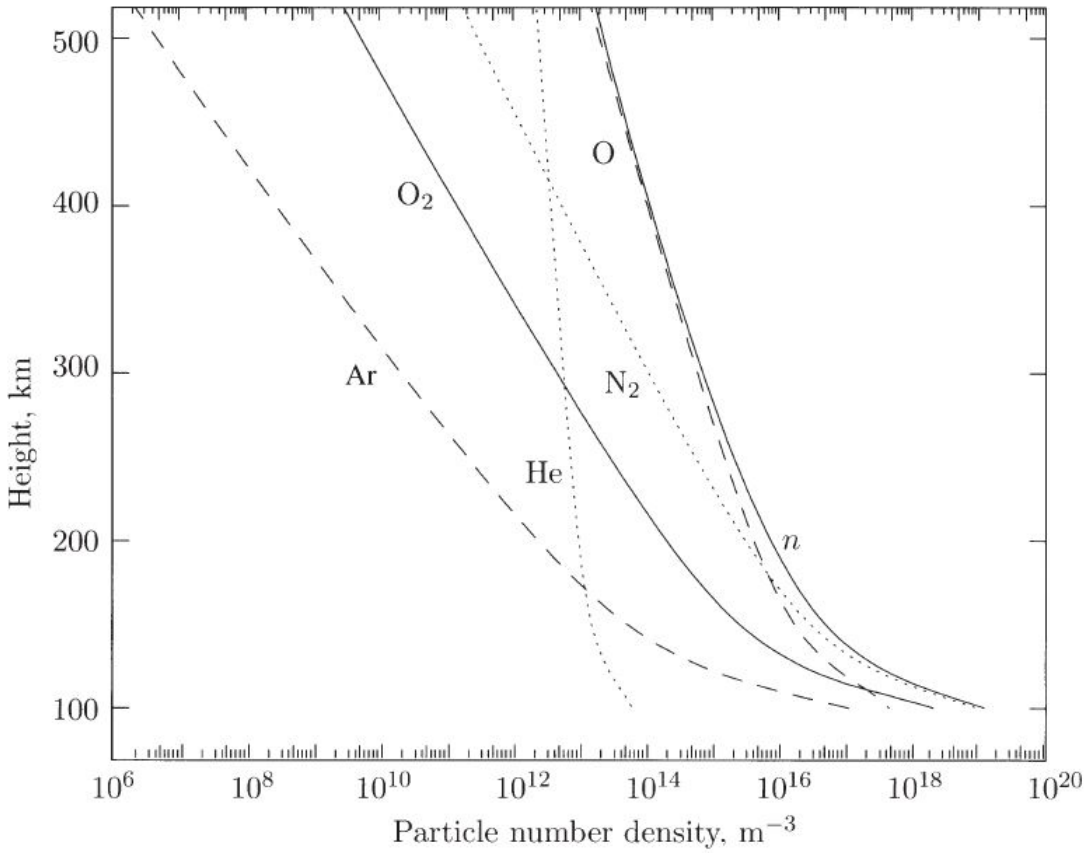

Figure 1.2: Density profiles of the neutral atmosphere [14].

1.1.1 Ionosphere

The ionosphere is the ionized component of the upper atmosphere. This charged region has an altitude range from about 50 km to 1000 km, which contains all of the thermosphere and some of the mesosphere and the exosphere. The ionosphere can be divided into three regions, D, E, and F. Each of these regions have different compositions. The D region is composed of $H_3O^+.(H_2O)_n$ and NO_3^- and has an altitude range of 50 km to 90 km [14]. The E region is composed of O_2^+ and NO^+ ions and

has an altitude range of 90 km to 170 km [14]. The F region is primarily composed of O^+ and has an altitude range of 170 km to 1000 km [14]. The primary source of production for these ions is the photoionization of neutral gases. An example of this photoionization is shown by the following equation.

$$X + photon(\lambda \leq 100nm) \longrightarrow X^+ + e$$

Where X is a neutral atom or molecule. The photon must have a high enough energy to ionize the neutral gas, which corresponds to having a wavelength lower than about 100 nm. Each of these three regions are produced by different types of solar radiation. The E and F regions are a result of both X-ray and Extreme Ultraviolet (EUV) radiation [14]. The D region is also attributed to X-ray radiation but is also a result of Lyman α radiation [14]. A physical representation of each of these regions can be easily seen in the electron density profile, which is shown in Figure 1.3. Both of the peaks for the E and F regions can be easily seen during both the day and the night. The D region peak can barely be seen during the day and is non-existent during the night. The E region of the ionosphere is important because this is where it is believed coupling between the atmosphere and the ionosphere exists. The F-region is important because it dominates electron density, which is the ionospheric metric that will be analyzed for this study.

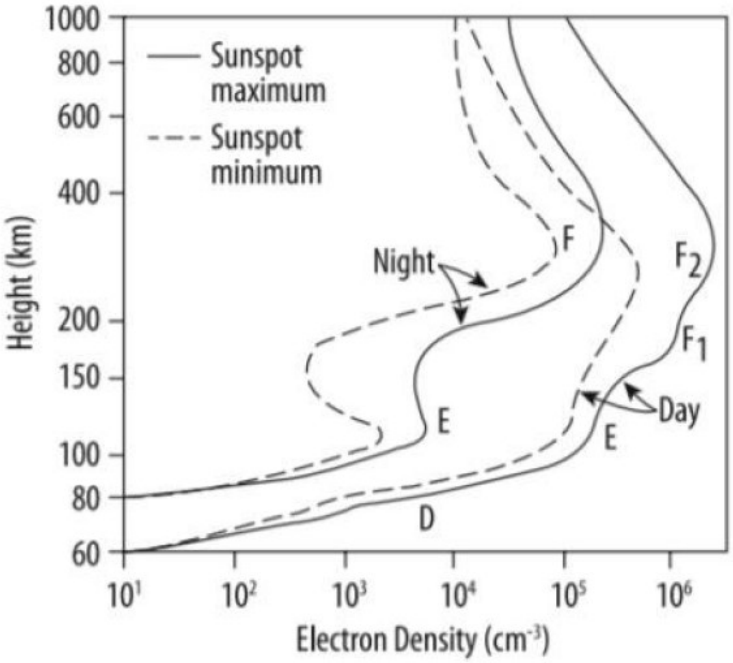

Figure 1.3: Electron density profile of the ionosphere [4].

1.2 Neutral Atmosphere and Ionosphere Coupling

The atmosphere-ionosphere system starts in the lower atmosphere and extends to the upper layers of the ionosphere. Since this system contains both a partially charged region, the ionosphere, and the hottest neutral atmosphere region, the thermosphere, there are many complexities in the dynamics. This region of the atmosphere is affected by both external and internal processes. Above the upper atmosphere, magnetospheric, solar, and geomagnetic processes influence the atmosphere-ionosphere system [24]. Below this region, planetary waves internally influence perturbations in the upper atmosphere [24]. In this section, atmospheric waves and the ionospheric dynamo will be explained. In addition, their role in the atmosphere-ionosphere sys-

tem will be discussed.

1.2.1 Atmospheric Waves

There are many waves seen internal to Earth's atmosphere. Some are small-scale waves, like gravity waves, that only have a scale of about 10-100 km [18]. Some are larger-scale waves like tides and planetary-scale waves. This study focuses on planetary waves, which are defined as large scale perturbations of pressure, temperature, winds, and composition seen in the Earth's atmosphere [18]. These waves originate in the lower atmosphere and have the capability to modulate atmospheric tides, which will be discussed in further detail shortly. There are several types of large-scale waves, for example, Kelvin waves, Rossby waves, and the mixed Rossby-gravity waves. The location source of these waves varies, as Rossby waves originate in mid-latitude regions while Kelvin and Rossby-gravity waves are equatorial [18]. This study is focused on equatorial waves since they are seen to have the most impact on the ionosphere.

Kelvin waves and Rossby-gravity waves are examples of waves that are trapped in the equatorial region of the Earth's atmosphere. The Kelvin waves tend to have a period range from 2.5 to 5 days. The focus of this study, the Rossby-gravity wave, can be attributed to the quasi-2-day wave [22]. This wave is a waywardly propagating wave that is most commonly observed in the stratosphere. It has characteristics of both Rossby and gravity waves. The generation and evolution of Rossby waves are highly dependent upon vorticity relationships in the atmosphere.

The source of Rossby waves is westerlies, eastward wind, that are compressed due to the earth's terrain and tropopause, which leads to a horizontal expansion [5]. This expansion leads to decreased vorticity which, transports air in the northern hemisphere towards lower latitudes. The restoring force for Rossby waves is the Coriolis force. A Rossby wave is depicted in Figure 1.4. Gravity waves are formed by air being vertically displaced. The buoyancy force tries to restore equilibrium, which produces the wave. These waves have a much smaller scale than Rossby waves.

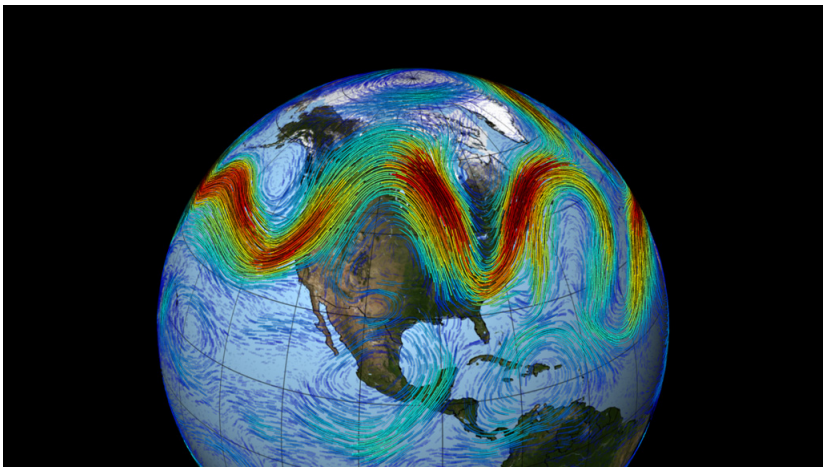

Figure 1.4: Depiction of a Rossby wave.

Tides are another atmospheric wave. These are defined as global scale oscillations that are dependent on solar and lunar forcing. The tides created by the moon are generated by lunar gravitation. Solar tides are caused by solar radiation and large-scale latent heat release [11]. There are two main periods for tides, diurnal and semi-diurnal. The solar diurnal and semi-diurnal tides have periods of 24 and 12 hours, respectively. The lunar diurnal and semi-diurnal tides have periods of 24.8 and 12.4 hours, respectively. These waves can also be migrating or non-migrating.

Like other atmospheric waves explained in this section, tides cause perturbations in the pressure, temperature, winds, and composition of the Earth's atmosphere. Tides are important to this study because of their interaction with planetary waves.

1.2.2 Ionospheric Dynamo

The ionospheric dynamo is what links the atmosphere to the ionosphere [16]. In the lower portion of the ionosphere there is a dynamo region where collisions with neutrals are still prominent. The E-region dynamo is dependent upon atmospheric winds and Earth's magnetic field. The ionospheric dynamo is created by atmospheric winds moving plasma in a direction that is non-parallel to geomagnetic field lines. The different ion and electron motion caused by atmospheric winds results in a current. Gradients created in the conductivity and winds in this region creates charge build-ups, which imposes an electrostatic field. When this field is mapped to higher altitudes in the F-region, plasma motion is created by $E \times B$ drift. This plasma motion causes variations in the F-region electron density. Figure 1.5 is a diagram of the E-region dynamo. This interaction between neutrals and charged plasma is why planetary waves have the capability to impact the variability in the ionosphere.

1.2.3 Signatures of Planetary Waves in the Ionosphere

The previous section explained the connection that the atmosphere has with the ionosphere in the ionospheric dynamo. It still has not been explained how these lower

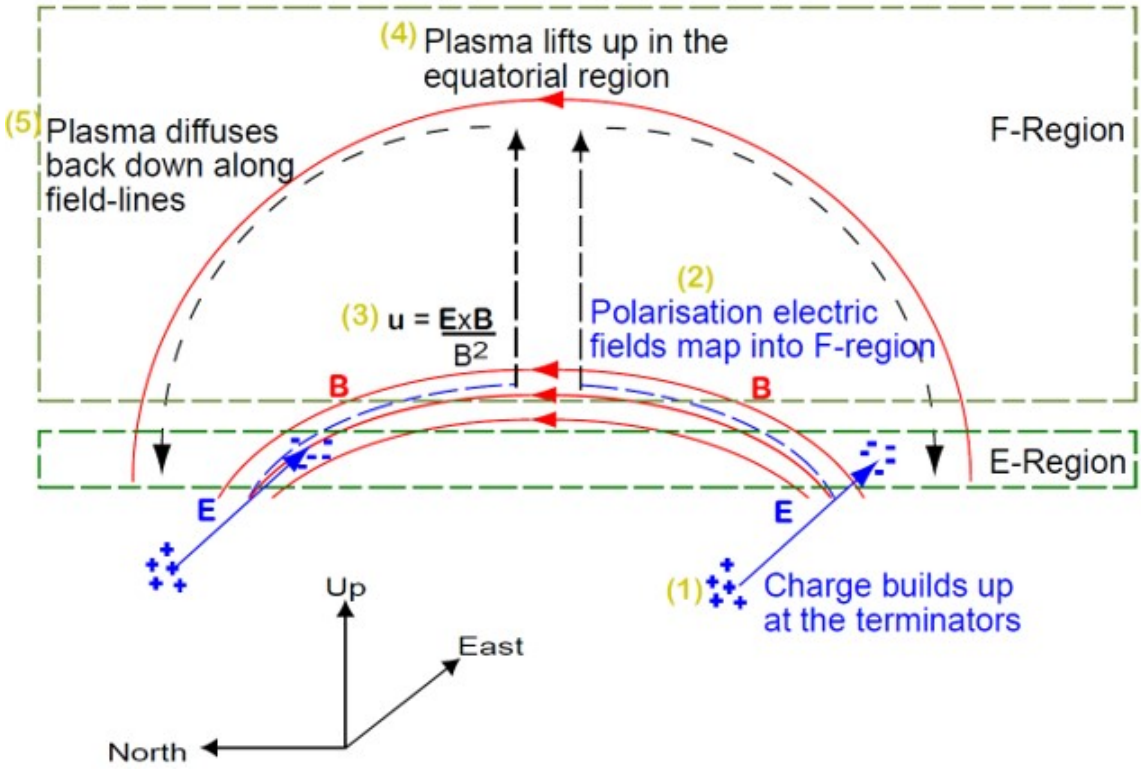

Figure 1.5: Diagram of the E-region Dynamo showing how the build up of charges can create an electrostatic field that leads to plasma motion at higher altitudes in the ionosphere [7].

atmospheric planetary waves reach E-region altitudes. It is most commonly believed that this is accomplished through tidal modulation. This is when planetary waves can impose their signatures on tides through modifying tidal amplitudes. When there are two waves that are propagating coincidentally, there are linear and non-linear interactions. Through numerical studies it has been seen that these non-linear interactions can lead to very large tidal amplitudes with planetary wave signatures [19]. This process of non-linear advection occurs when the waves reach sufficient (non-linear) amplitudes. Observations suggest this occurs in the 90-100 km region,

and thus atmospheric data from this altitude range will be used as a measure of the periodic signatures in the atmosphere during this study. As these waves reach the E-region they cause variations in the dynamo region which modifies the F-region of the ionosphere. Ion density and Total Electron Content (TEC) perturbations are heavily dependent on variations in the F-region. This is how similar signatures are seen between low atmosphere planetary waves and the electron density of the ionosphere.

1.3 Statistical Studies

There have been other statistical studies analyzing atmospheric and ionospheric coupling, one of which focuses on the quasi-3-day wave [8]. This study uses SABER temperature data to determine when there is a planetary wave present in the lower atmosphere. TEC is used for analyzing variations in the ionosphere. Both of these data-sets are used in the present study and will be further explained in the following chapter. The quasi-3-day wave can be attributed to "Ultrafast" Kelvin waves (UFWS) which have a period range of 2.5 to 5 days. This study analyzed 3 eastward propagating 3-day waves (E1-E3). From 2002 to 2012, a total of 300 waves were identified. 66% of these waves could be linked to 3-day signatures existing in the ionosphere. The waves that correspond to ionospheric signatures all had longer vertical wavelengths and larger amplitudes, which matches theory. This study was very influential for the present study as it is the baseline for the overall approach, although the detailed data-sets and methodology are different.

Chapter 2

Data

In order to perform an analysis of the ionospheric and atmospheric coupling, the correct data needs to be selected. This chapter will discuss the selection process for each type of data-set. The three types include ionospheric, planetary wave, and solar. SABER temperature data is used for planetary waves; Ground-based TEC is used for the ionosphere, and F10.7 and KP are used for solar activity. Each section in this chapter will discuss how these data-sets are generated. There are multiple constraints considered in this selection process. The most important of these is the duration. The collection of data-sets is limited to ones that have a 17-year time span from January of 2002 to December of 2018. This is because there is usually 1-2 good periods with strong 2-day waves per year, so to study anything in a statistical sense, at least 15 years are required to have a sample size of at least 30. Another constraint for the ionospheric and atmospheric data is geographic location. This study is primarily interested in the low-latitude coupling, so the data needs to have a range of at least -45 to 45 degrees in latitude. Another need in this selection process is the data collection rate. In other words, the time-steps in the data must be reasonably short, due to the fact that 2-day oscillations are of interest. Needing a 17-year time span and small time-steps leads to large data-sets.

2.1 SABER

Temperature data from SABER (Sounding of the Atmosphere using Broadband Emission Radiometry) is used as the planetary wave data in this study. This is a limb-scanning infrared instrument that scans the horizon in 10 broadband channels that range from 1.27 to 17 μm [6]. SABER is on board the TIMED (Thermosphere, Ionosphere, Mesosphere, Energetics, and Dynamic) spacecraft, which launched in December of 2000. SABER started taking measurements in January of 2002, which is the beginning of the selected 17-year span. Kinetic temperature is calculated using CO_2 emissions, where SABER uses radiance measurements from two CO_2 15 μm channels, one narrow and one wide bandpass channels. These channels can estimate the pressure with altitude, which can be used to calculate the kinetic temperature using local-thermodynamic-equilibrium (LTE) conditions. One can not always assume LTE conditions in the Mesosphere and Lower Thermosphere (MLT) so the kinetic temperature is inferred using radiance measurements in the narrow CO_2 channel [10]. This allows a temperature profile to be generated from 10 km to 130 km in altitude. Every 60 days the TIMED spacecraft performs a yaw flip and allows for northward and southward facing phases, which have a latitude range of -52 to 83 degrees and -83 to 52 degrees, respectively [6]. Due to the TIMED orbit and the SABER remote sensing geometry, these measurements have a continuous latitude range from -50 degrees to 50 degrees.

Now that temperature data fits the conditions required for this study, 2-day wave signatures need to be identified. This is accomplished using a 2-D least

squares fitting, which is detailed in [23]. This is a proven method for planetary wave signatures as it has been successfully used in the following studies: [1], [2], [3], [8], [9], [12], [13], [17], [21]. It is important to note that this study did not perform this 2-D least square fittings, it is simply being described. The temperature is grouped in 10 degree latitude bands from -50 to 50 degrees and temperature values are fit to sinusoidal functions with a period range from 1.5 to 2.5 days [9]. An example of the SABER data is shown in Figure 2.1.

2.2 Ground-based TEC

The ionospheric data-set of choice is Total Electron Content. TEC is defined as the total number of electrons along a path from a satellite transmitter to a ground-based receiver. This metric is very important in GPS theory and design. The TEC data used for this study was developed using the MAPGPS software package, which produces TEC maps processed from GPS data. It is important to note that this study did not process the GPS signals into TEC, it is simply being described. The goal of this software is to produce reliable data using all available GPS receivers, not just ones like the IGS or CORS networks [15]. The maps created by this software display TEC values different from the original definition given. This study is more interested in zenith TEC values, which are defined by a path that is perpendicular to the ground and ends at a certain ”pierce height”. Zenith TEC is not measurable but is estimated using a collection of TEC values from different GPS receivers over a 24-hour period. As one can expect, the location of these zenith TEC values must be in close proximity

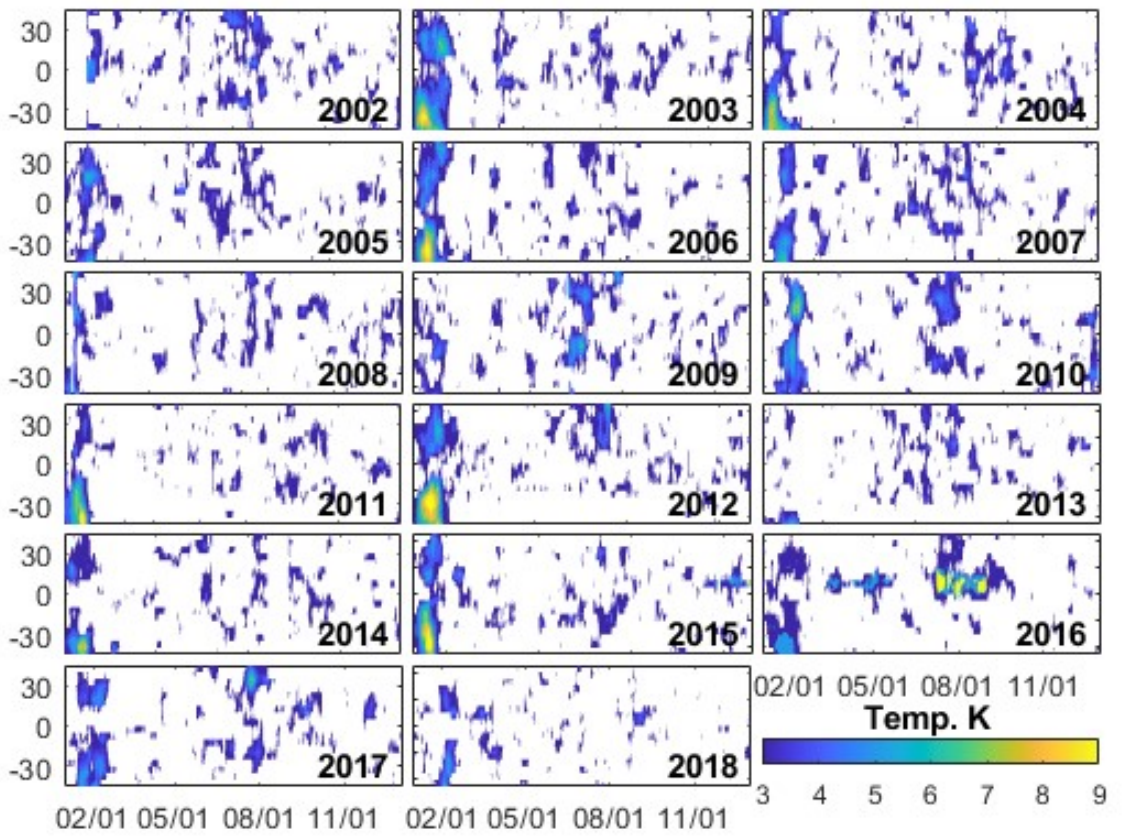

Figure 2.1: Example of a SABER Amplitude plot of a 2-Day westward propagating wave-number 3 wave.

to the ground station. In order to produce reliable data, this MAPGPS software is data-driven, so there are no smoothing or modeling techniques used to estimate TEC values in locations with no ground-stations [15]. A plot showing this restriction is Figure 2.2. The TEC data is given in TECU which is equivalent to 10^{16} electrons/m^2. The process of selecting the usable data for this analysis is described in Chapter 3. The TEC data used for this study is from Madrigal, which is a web-based database

that includes the data produced by this MAPGPS software. The span of the available data dates back to 2000 and is updated regularly. The TEC maps have a resolution of 1 degree by 1 degree and are given in 5-minute intervals.

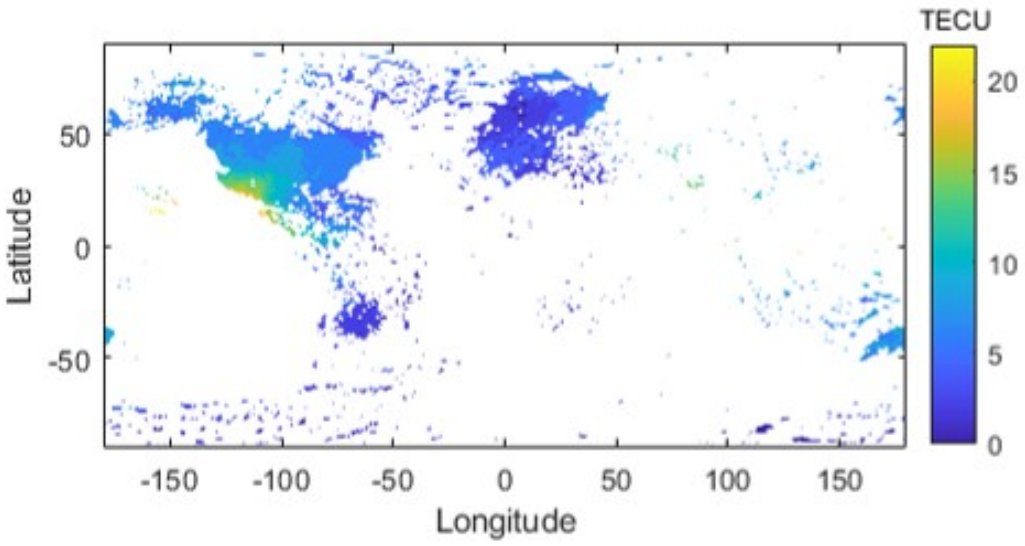

Figure 2.2: Example of a TEC map on May 12, 2017 at 2:00 UTC.

2.3 Solar Data

Two metrics are used for analyzing solar activity, F10.7 and KP. F10.7 is the solar radio flux measured at 10.7 cm and is a reliable data-set for measuring the activity of the Sun. It also has been recorded for many years dating back to 1947, which is obviously in the time-range of this study. This is a good estimate of the solar activity because this type of emission is produced high in the chromosphere and low in the corona of the solar atmosphere. This data-set is also recorded in solar flux units

(sfu). For this study, F10.7 data is retrieved from NASA's OMNIWeb database. A plot of F10.7 is shown in Figure 2.3, which clearly shows times of solar minimum and maximum. The other metric used to detect 2-day oscillations in solar activity is KP. Planetary K-Index (KP) is a good representation of the severity of Earth's geomagnetic storms. KP effectively measures the disturbances in the horizontal component of Earth's magnetic. This is an index so there are no units associated with this measurement. It is given as an integer from 0-9, where the higher the number the more severe the geomagnetic storm. This is a good estimate of solar activity because disturbances in the magnetic field are highly impacted by the solar wind. This data-set also fits the timeline of this study, as it was first recorded in 1938.

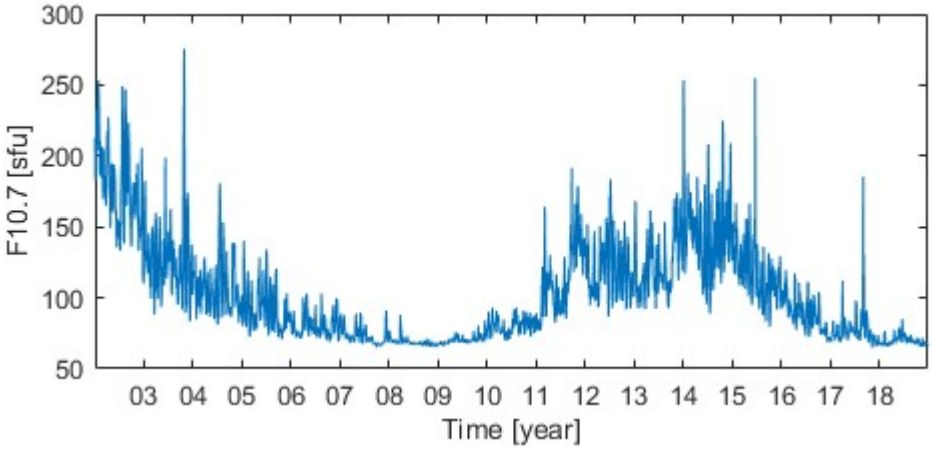

Figure 2.3: F10.7 data from 2002 to 2018.

Chapter 3

Methods

This chapter will detail the methods used to determine times of similar periodicity in the ionosphere and atmosphere. The data selection process for Ground-Based Madrigal Total Electron Content will also be discussed. Due to the inconsistent time availability of the TEC data, there are only a select few regions that are usable for this study. Also, other constraints such as magnetic latitude limit the regions that can be deemed useful. This chapter will also discuss the wavelet analysis used on these refined data sets, along with the thresholding methods used to determine when these periodicities are the most prevalent. Once the strongest 2-day oscillations are extracted from the Atmospheric, Ionospheric, and Solar data, comparison techniques are used to characterize the interactions of interest. These techniques include creating timelines to visualize the coupling, developing histograms to identify trends, and calculating percentages to back up the trends with numbers.

3.1 TEC Data Selection

There are both theoretical and practical reasons for why Total Electron Content is chosen to be the best metric for characterizing the ionosphere. The theoretical reasons are explained in Chapter 1. This section details practically why TEC is the ionospheric metric for this analysis. First, it is very important that the ionospheric data is low in geographic and magnetic latitudes. Second, there must be consistent data throughout the 2002 to 2018 time-span for which this study is focused on. Both of these constraints lead to the decision to select Ground-Based Madrigal TEC data as the ionospheric metric. The specifics of this data-set are explained in the previous chapter; this chapter is mostly concerned with spatial and temporal availability.

The ground-based TEC has drops in coverage in both location and time. The drops in location coverage are because the data is being measured by ground stations therefore, the availability is constrained to the locations of these ground stations. To choose which regions would be best, an availability plot is created. This is shown in Figure 3.1.

Specifically, it is a contour plot displaying the total number of data points at each latitude and longitude over the 17-year span. As one can see, the best regions for coverage are the United States, Europe, Japan, and New Zealand regions. The United States and Europe are not at low enough geographic and magnetic latitudes and the span of their geographic longitude is too large. The New Zealand region also would not be considered low-latitude. This leads to looking at areas with not the best coverage but suitable coverage. The two regions chosen, along with the

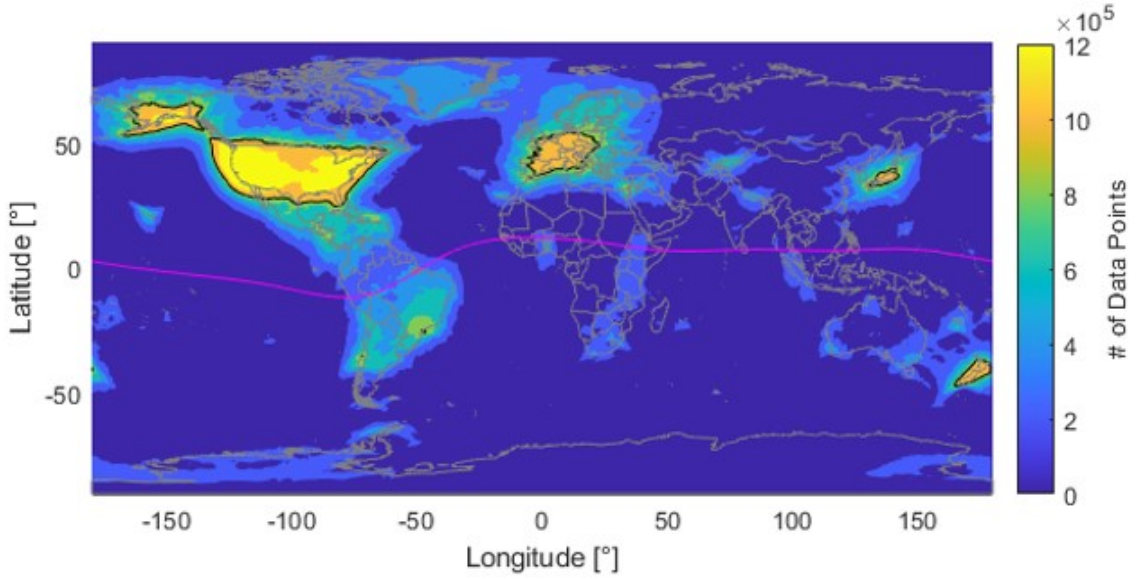

Figure 3.1: Total Availability of the Ground-Based Total Electron Content data. The contour plot strength is the total number of data points at each location over the 17 years. The magnetic equator is also shown. Black outline has a contour value of 75% of the maximum value.

Japan region, are the South American Region, and the Central American/Caribbean region. The South American Region is very interesting for this analysis because of its low magnetic latitude. The Central American/Caribbean region is of interest due to its low geographic latitude and relatively low magnetic latitude. Due to these constraints, the areas best suited for this study are narrowed down to these three areas, Japan, South America, and Central America/Caribbean. These three regions are shown in Figure 3.2 and each geographic point considered is contained within the black outlines.

The total availability is not the only parameter used to define the regions of interest. It is also important to consider how consistent the ground station coverage

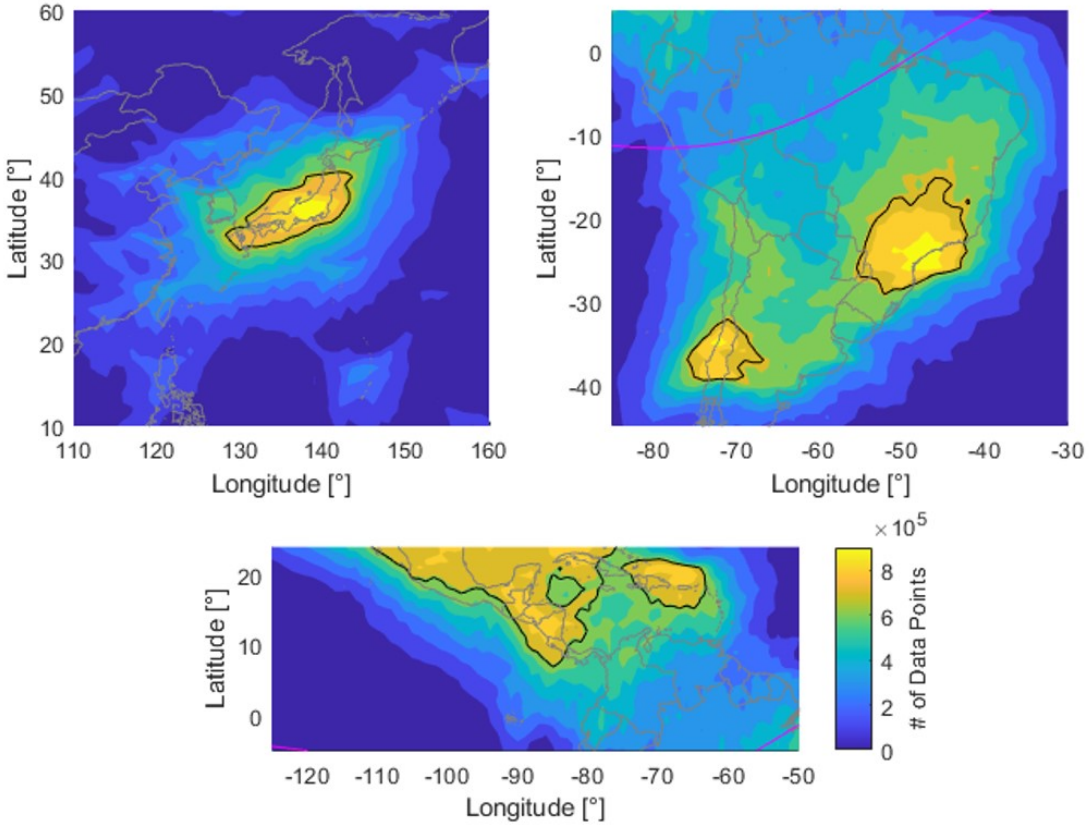

Figure 3.2: The three major TEC regions of interest. The left shows the overall Japan region, the middle shows two areas in the South American region, and the left shows the Central America/Caribbean region. Black outline has a contour value of 75% of the maximum value.

is. Figure 3.3 shows the method used to determine consistency. A contour plot is generated for each year, 2002 to 2018, with an overall scale so that each year can be easily compared. By far the most consistent region anywhere on Earth is Japan. The ground coverage was just as strong as it was in 2002 as it was in 2018. There were only two years that were inconsistent; 2014 had an excess number of data points recorded and 2016 had a lack of data points recorded. The Japan region is

deemed usable because of its great coverage even in the early years of the time-span. The South American and Central American/Caribbean regions both have similar consistency plots. The South American plot is shown in Figure 3.3. For both of these areas, there is a lack of coverage at the beginning of the time-span of interest, which is about 2002 to 2007. In 2008 the coverage begins to increase and both of the regions become completely covered. Although there is a lack of coverage in the early years of the time-span, it is deemed acceptable for this study. For each of the three regions, it is determined that the total 17-year availability plot should be used to explicitly define the boundaries of each region because it is the best representation of the overall time-span.

The regions of interest are still not defined well enough. Each major area, Japan, South America, and Central American/Caribbean needs to be divided into smaller sub-regions. The goal in defining each sub-region is to have a geographic and magnetic latitude range no more than about 10 degrees and a geographic longitude range no more than about 10 degrees as well. There were two methods considered to achieve this. The first is to define each region by a rectangle, which can be interpreted as defining a range of geographic latitudes and longitudes. This method is displayed in Figure 3.4. The advantage of this method is code efficiency. Although this method would save on time, the boundaries are subjective, and it has the possibility of including regions with low coverage.

The preferred method, which is shown in Figure 3.5, defines the regions by a collection of points rather than a range of points. This method lowers the possibility of including areas with a lack of coverage but requires more computational effort.

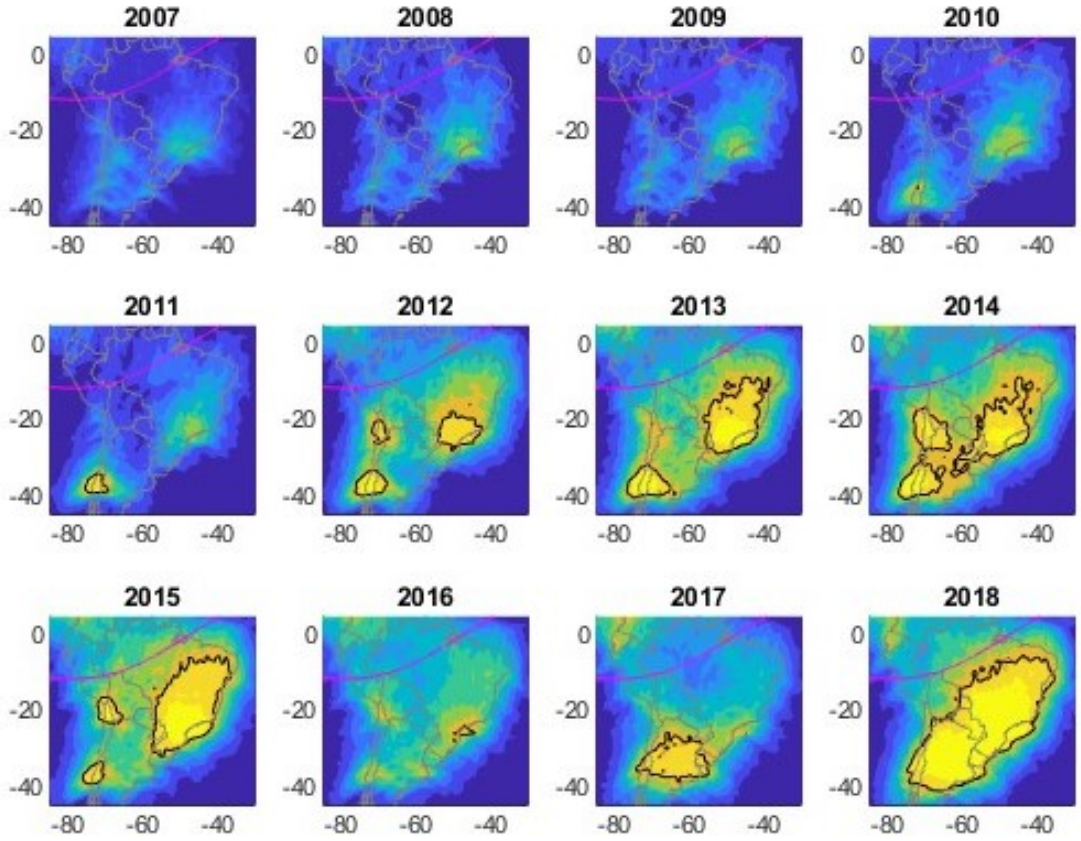

Figure 3.3: The yearly availability of the TEC data for the South American region from 2007 to 2018. The magnetic equator is also shown in each of the plots. Black outline has a contour value of 75% of the maximum value.

This method is preferred because increased coverage and reliability of the data is worth the extra computational time. When defining the regions with this method, some user input and slight tweaking is required to minimize the latitudinal and longitudinal ranges. Finally, there are nine regions defined; two in the Japan region, four in the South American region, and three in the Central American/Caribbean region, all of which are clearly displayed in Figure 3.5. It is important to note that not every sub-region within the major region is connected. This is important

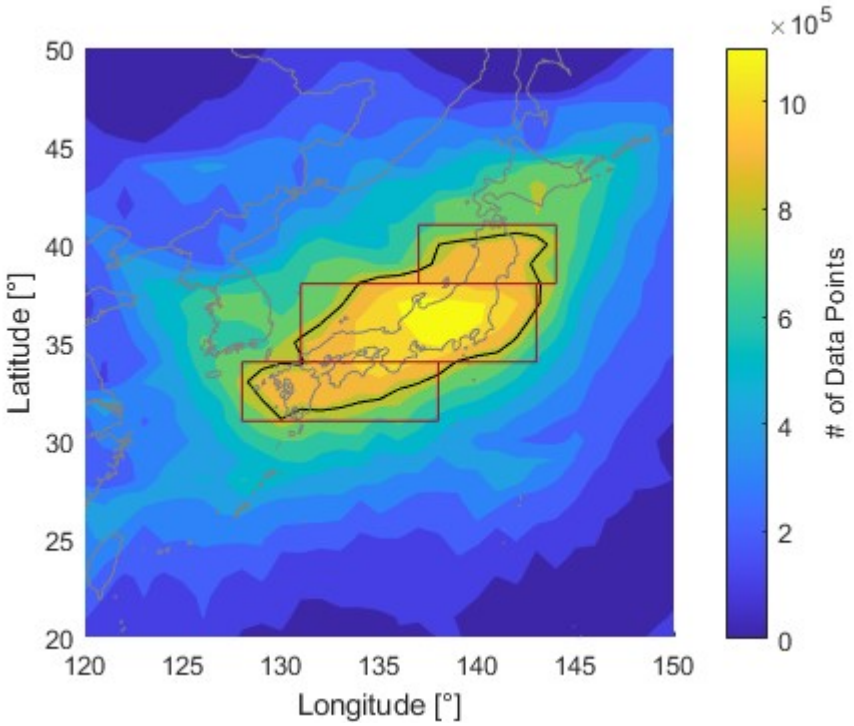

Figure 3.4: An availability of plot of TEC for the Japan region showing the first method for dividing the major TEC regions. Any point inside red lines is considered part of the region.

when analyzing the results as regions that are connected within the major region are expected to produce similar results, while regions that are not connected within the major region could have slightly differing results. Figure 3.6 shows why this second method is preferred. It helps maximize the reliability of the ionospheric data that is being interpreted. The two sources of unreliability in the TEC data are lack of coverage and high magnetic latitude. This method maximizes reliability by being heavily constrained by coverage and low latitudes.

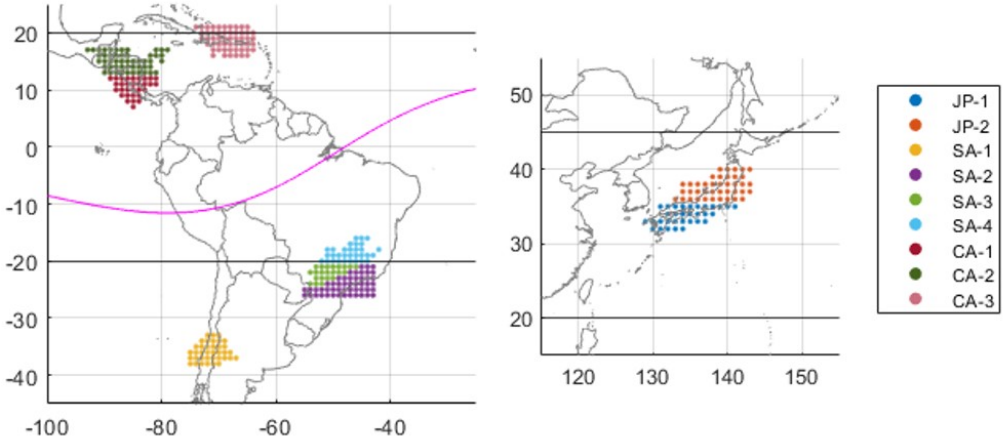

Figure 3.5: A map showing each TEC region of interest. Each region is defined by a selection of points and each different color signifies a different region. The magnetic equator is the magenta colored line.

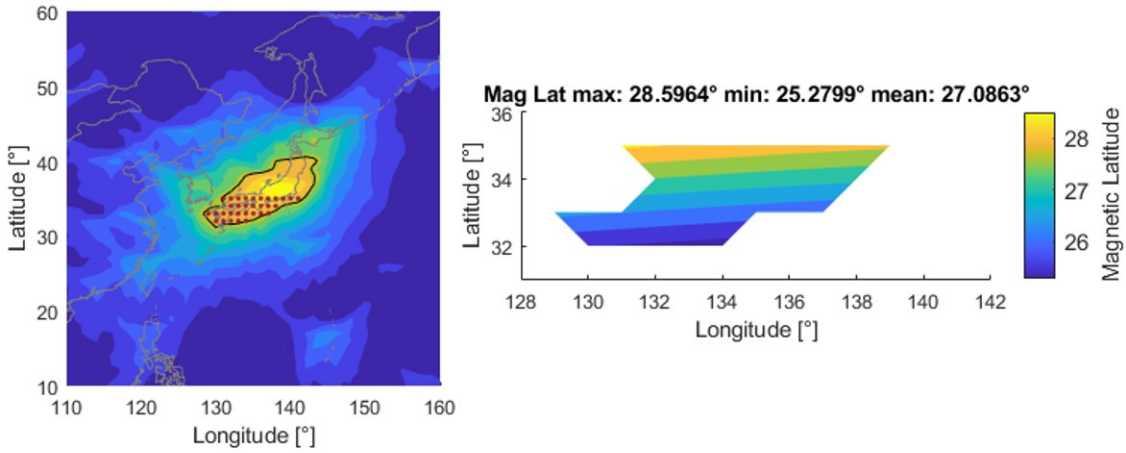

Figure 3.6: The left plot shows each latitude and longitude point included in the lower Japan region. The right plot is a contour plot of the magnetic latitude.

3.2 Wavelet Analysis & Threshold Techniques

This section will detail the methods used to determine occurrences of strong 2 day oscillations in each of the three major data sets, atmospheric, ionospheric, and solar. Once every data-set is modified to only have one dependent variable, time, wavelet analysis is performed. For this study, a Morlet Wavelet transform is used to determine times where a 2-day periodicity is most prevalent. To extract these occurrences multiple methods of thresholding are used. This is the most subjective part of this analysis because of the impact that thresholding can have on the results. This will be discussed in further detail in Chapter 4.

3.2.1 Wavelet Analysis

In order to perform a wavelet analysis on a data-set, it must be one dimensional, only dependent in time. This happens to already be the case with the solar data, F10.7 and KP. This is not the case for the Ground-Based TEC data, which has temporal and spatial dependence. For the case of ionospheric data, the total electron content is summed across each of the 9 regions. This means that regions with larger areas will have larger values for TEC, but this is not an issue because this analysis is only concerned with relative oscillations in the data. This will create nine separate time-series for TEC which now can be analyzed further.

Now that the data of interest is converted from multidimensional to one dimensional, a wavelet analysis can be run. This wavelet analysis is run on the TEC,

F10.7, and KP time-series. The steps of Wavelet analysis will not be described in detail, but how and why this analysis is used will be explained. A wavelet transform is chosen for this study since the waves of interest are propagating waves. In most practices, a Windowed Fourier transform is used, but this only works well with stationary waves. The most common wavelet is chosen for this study, a Morlet Wavelet. This wavelet is a plane wave modulated by a Gaussian [20]. A Morlet wavelet is defined by the equation below and an example can be seen in Figure 3.7.

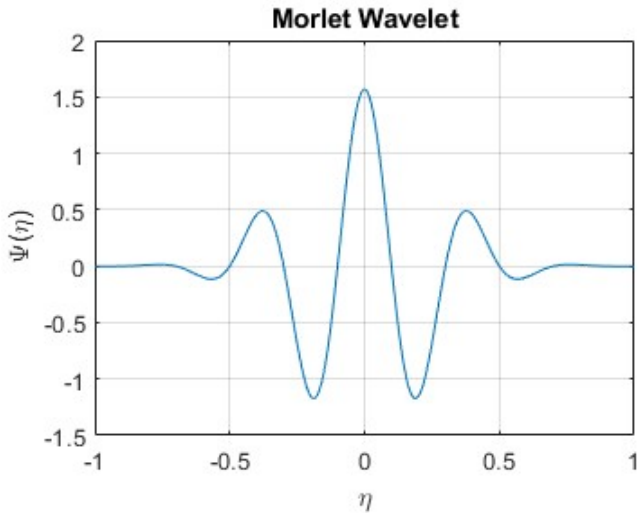

Figure 3.7: Example of a Morlet Wavelet.

$$\Psi_0(\eta) = \pi^{-1/4} e^{i\omega_0 \eta} e^{-\eta^2/2}$$

Where $Psi_0(\eta)$ is the wavelet function, η is a non dimensional time parameter and ω_0 is the non dimensional frequency. Using this wavelet a power spectrum can be generated from a time-series. An example of a power spectrum generated from a time-series is shown as a contour plot in Figure 3.8. The power spectrum

displays, at each time-step, which oscillations are the most prevalent. In Figure 3.8 one can see large signatures in the 20-30 day range from 2002 to 2006 and 2011 to 2017. There is also a secondary signature picked up at around the 2-day period, which is what this study is focused on. It is important to note that if this analysis was investigating larger periods around a year-long there would be parts of the contour plot that would unreliable. This is called the cone of influence, where the range of acceptable data decreases from the start and beginning the larger the period of interest is. For example, if one is looking for a 2-year oscillation in this data set, the first and last several years would have to be excluded. This is not an issue for this analysis because it is only interested in 2-day periods in a 17-year span.

3.2.2 Threshold Techniques

TEC varies with latitude and longitude while SABER only varies with latitude, which makes the conversion to one dimension somewhat simpler. The SABER data is also split up into separate regions, -45 to -20 degrees, -20 to 20 degrees, and 20 to 45 degrees in latitude. This breakdown is shown by the 17-year SABER Amplitude Plot in Figure 3.9. At each time-step, the maximum amplitude in each latitude band is recorded, which creates three separate time-series. Wavelet analysis is not required for SABER since it has already been constrained to the 2-Day westward propagating wave-number 3 wave. The SABER time-series is shown in Figure 3.10, where the bottom plot is the SABER Amplitude plot, and the upper plot shows the time-series with one of the thresholding techniques. All of these time-series are used

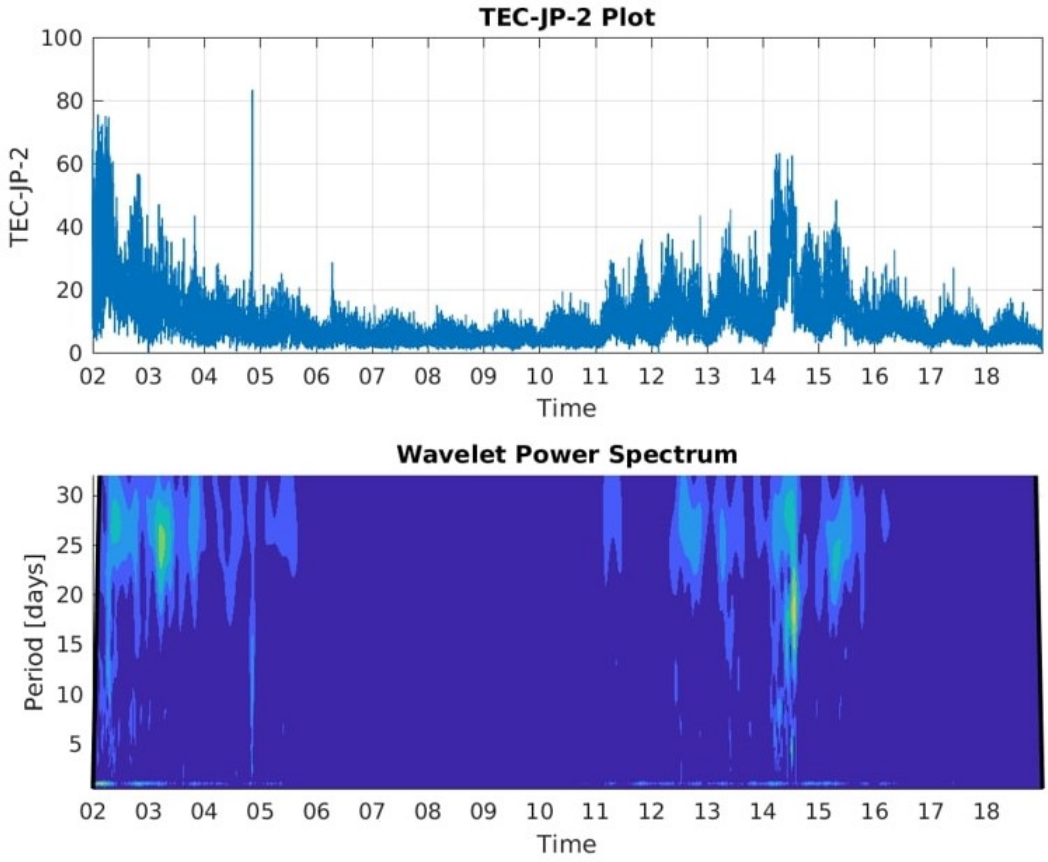

Figure 3.8: The top plot is the summed TEC in the lower Japan region over the 17-year span. The bottom plot is power spectrum generated from the wavelet analysis over the 17-year span.

to determine the occurrences of strong 2-day oscillations, which is accomplished with several threshold techniques.

The first technique used is to determine one threshold over the entire 17-year span. The threshold value is determined using a certain number of standard deviations above the median of the data. The issue with this method is seen best in the Solar data, specifically the F10.7 data. As an artifact of wavelet analysis, in times

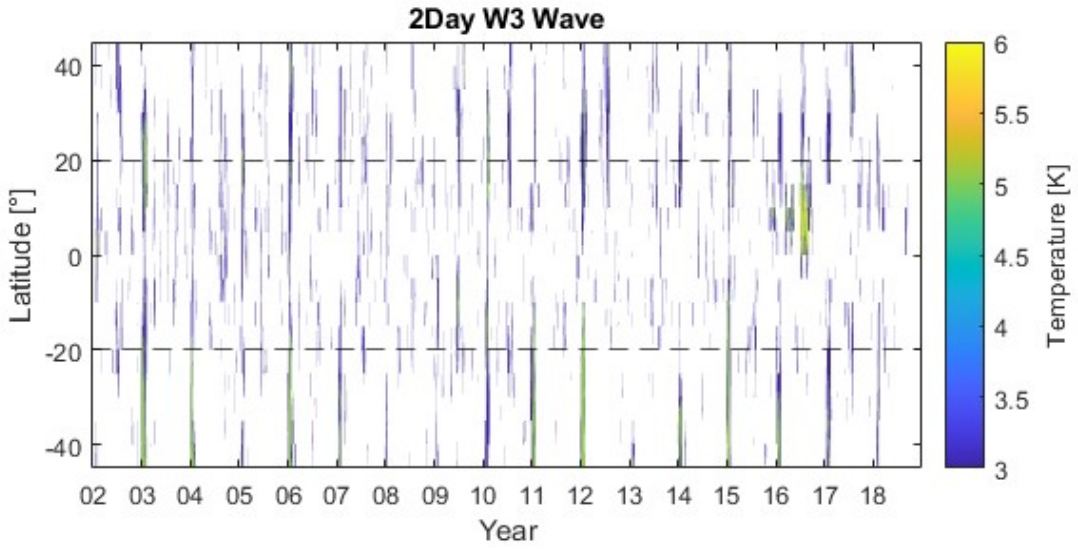

Figure 3.9: The SABER Amplitude plot of the 2-Day westward propagating wave-number 3 wave from 2002 to 2018. The dotted lines show how the latitude bands were defined.

of solar minimum, the wavelet analysis identifies a weaker strength than in times of solar maximum. This leads to no oscillations registering in the solar minimum. The next technique used threshold values for smaller time-spans, which include a year time-span, a half-year time-span, and a modified half-year time-span. The half-year works better, especially for the SABER data which in most years has a peak in the first half of the year and another peak in the second half of the year. The modified half-year thresholding uses the second threshold value in the year for the first half. This is shown in Figure 3.10.

Although this half-year technique works well with SABER and the other data-sets during certain half-year time-spans it does not work for all of them, which is also shown in Figure 3.10. If there is an abnormally large peak during a half-year

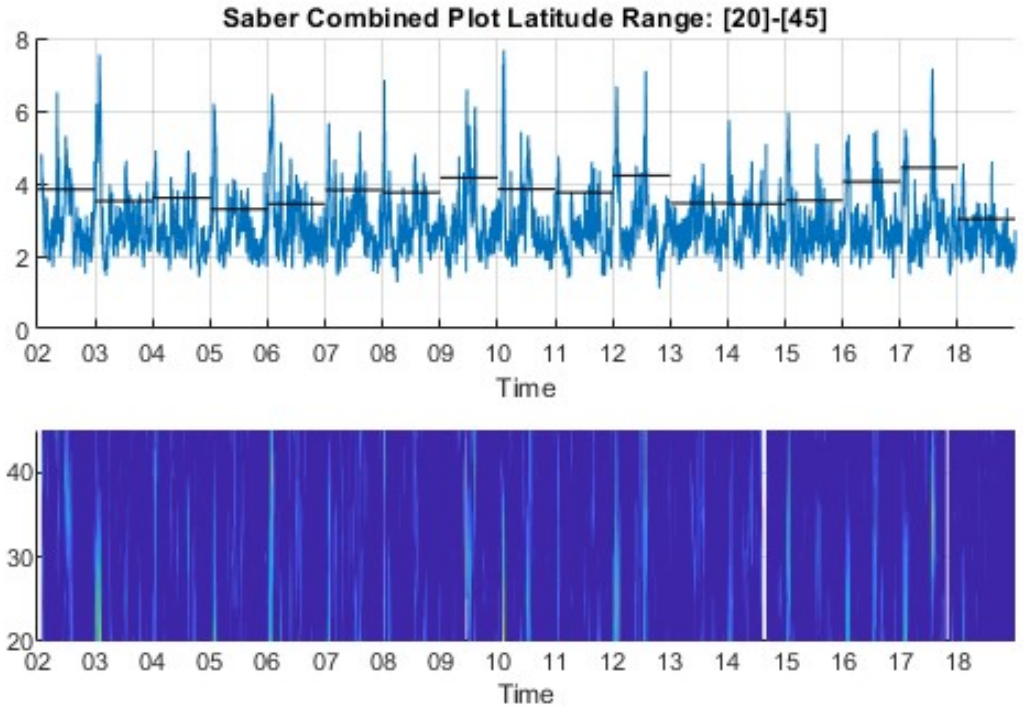

Figure 3.10: The top plot shows the half-year threshold method. The bottom plot is the top latitude band of the SABER amplitude band.

time-span the thresholding method will not record other peaks that would normally be considered notable. This leads to the preferred method of using a rolling threshold value. For every time-step, the median and standard deviation are determined over ninety days with the time-step situated in the middle of this span. This is the best method for determining occurrences that have large peaks relative to the entire data-set and peaks that are large only compared to the data points in closer proximity. This rolling thresholding technique is shown in Figure 3.11. Using this technique, a collection of ranges where there is a strong 2-day oscillation is determined. For each of these ranges the start and stop times are recorded where durations can be

calculated. Other than surpassing the threshold value, these events have several other constraints. First of all, the events must have a duration of at least 8 days. This is a reasonable value since each occurrence will exhibit at least 4 periods and should eliminate false signatures. In addition, if ranges are within 4 days of one another they are considered to be the same occurrence. This means the start time will be the beginning of the first occurrence and the end time will be the end of the second occurrence, but the duration calculation will not include the 4 days in between.

3.3 Comparison Techniques

Now that events have been cataloged, the last step is comparison. This study uses multiple techniques to characterize the similarities between each data-set. The first technique is meant to be a visualizer for the data-sets. A large amount of timelines are created to display the possible types of coupling that could exist. The second comparison technique is generating a large amount of histograms. These histograms include SABER distributions, TEC and SABER concurrence distributions, and the same TEC and SABER distributions with ambiguous events eliminated, this will be explained in further detail later in this section. The final comparison technique used in this study is to calculate a few percentages that best characterize the ionospheric and atmospheric coupling seen in this 17-year span.

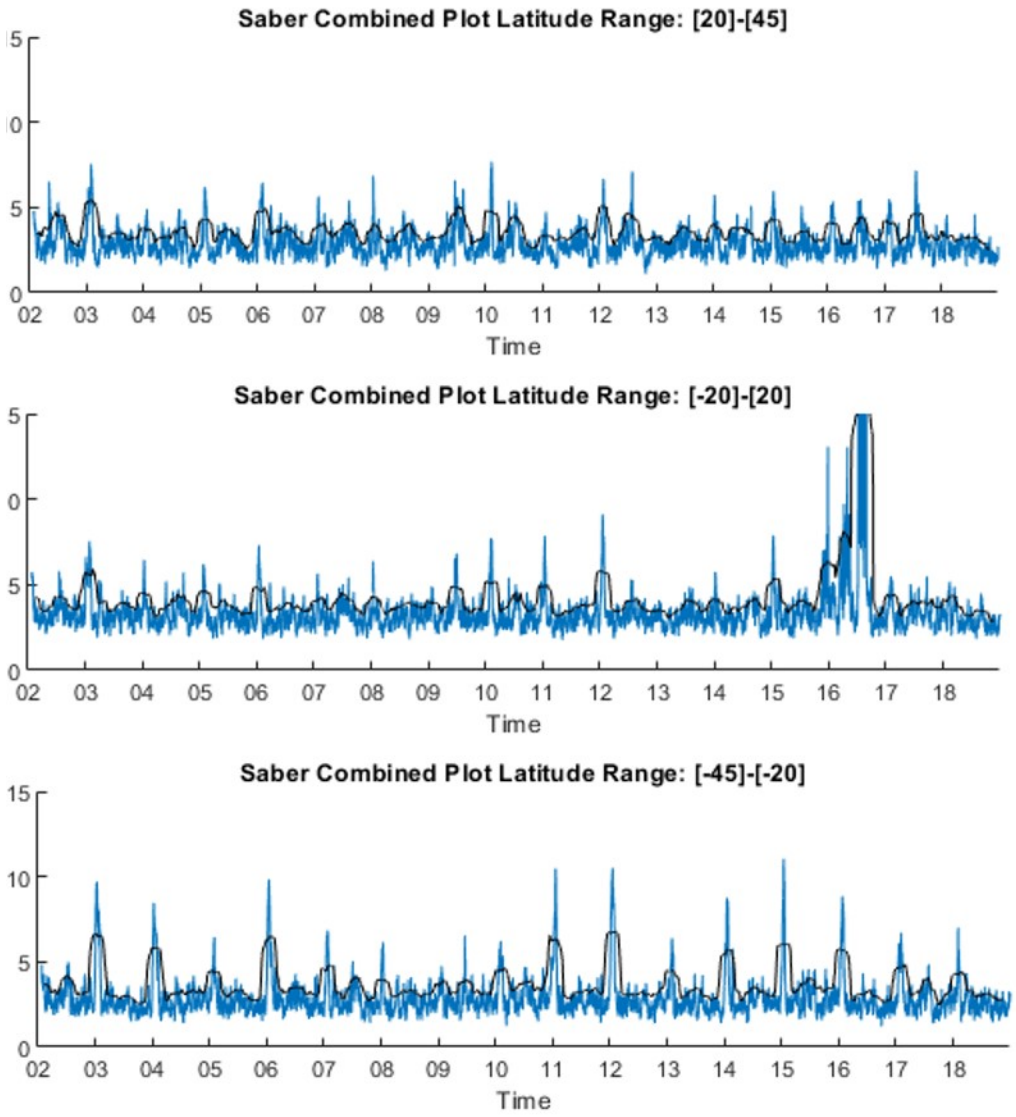

Figure 3.11: Each plot is the maximum SABER amplitude at each time-step for each latitude band. Each plot shows the rolling threshold value by the black solid line.

3.3.1 Timeline Table Method

The first step in the comparison process is to visualize each of the occurrences. This helps with validating both the wavelet analysis and threshold techniques. A timeline is set up for the entire 2002-2018 span and it compares the SABER data-set, both of the Solar data-sets, and one of the Major TEC data-sets, Japan, South America, or Central America/Caribbean. Timelines can be found in the Appendix. This allows for a visual check on the previously described methods. It can easily be seen if one of the occurrences saturates the timeline or if there is an absence of occurrences. This technique also makes it easy to check some yearly trends. For example, the timelines confirms the fact there should be a longer SABER oscillation at the beginning of the year with a shorter one later in the year. The timelines also visualize the geographical variance for the Major TEC regions. It can easily be seen that, most of the time, when an oscillation is seen in TEC it is seen throughout the entire region, but here are times when this is not the case.

This technique is a confirmation that there are events that occur due to different types of forcing. There are three types of events, where events are described as concurrent signatures seen in two or more data-set groups. The first is planetary wave forcing where the response in the ionospheric data, TEC, is clearly due to activity seen in the planetary wave data, SABER. An example of this type of event is shown in the top plot in Figure 3.12. This event clearly shows up in all regions of both the SABER and TEC data-sets and does not register in either of the Solar data-sets. The second classification for events is solar forcing, which can be seen

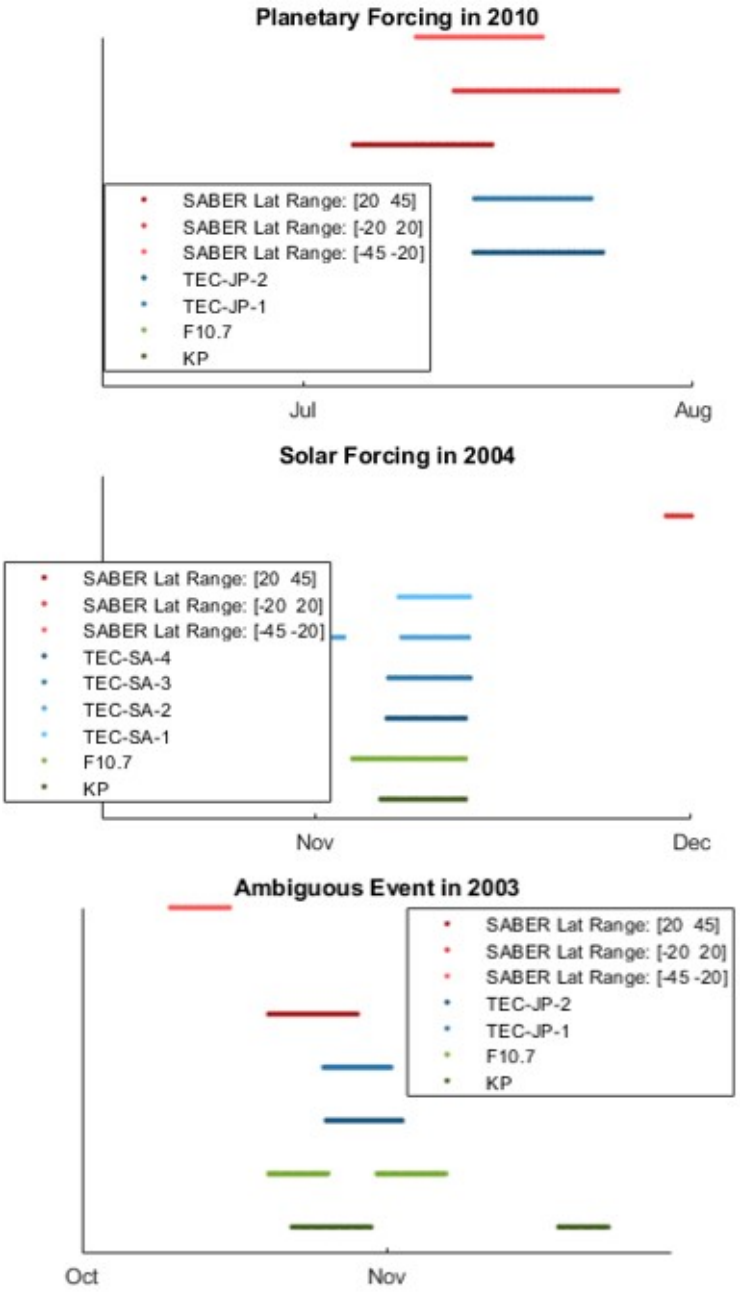

Figure 3.12: Examples of Planetary Wave, Solar and Ambiguous Forcing using timeline plots

in the middle plot in Figure 3.12. As one would suspect for this type of event, the signature picked up across all TEC regions for South America is concurrent with both the F10.7 and KP data-sets, with no signature in the SABER data. The final classification is an ambiguous event. This is where a 2-day oscillation is clearly identified in the ionospheric data but it is concurrent with both planetary wave and solar data events. This classification is shown in the bottom plot in Figure 3.12. The reason why this type of event must be recorded is because there is a clear event in the TEC data but it can not be determined what type of forcing caused it.

The timeline method is useful for visualizing the events of significance but does not make it easy to determine trends in the data. If the time-span was shorter it would be easy to identify these events by eye but due to the 17-year span, it is much more time-efficient to use computational methods to characterize the events. The significance of the threshold value is also being analyzed so having a variable threshold would greatly increase the number of timelines generated. Due to a large number of events, it was determined the most effective method would be to compare these occurrences computationally. Two functions were created to identify times of concurrence between each of the occurrences. To be clearer, occurrences are just when a 2-day oscillation is identified in any of the data-sets. For each data-set, catalogs are created for each occurrence, where the start time, end time, and duration are recorded. The first function used to compare these occurrence catalogs simply identifies times of concurrence. Concurrence is defined as any overlap between the occurrences or if the occurrences are within 4 days of one another. The second function is much like the first except it eliminates concurrent occurrences. The

importance of this function will be detailed later in this section. Using a combination of these two functions, a series of data-sets can be created to help quantify the impact that planetary wave forcing and solar forcing have on the ionosphere.

3.3.2 Histograms Method

The goal of this study is to investigate the relationship that planetary waves have with the ionosphere. This is why the most important comparison to analyze is the 2-day oscillation periods for TEC that are concurrent with occurrences in the 2-day SABER data. The previous section describes how every one of these occurrences is cataloged and now it is time to analyze them. There are two methods used to analyze these occurrences; the first is to use histograms and the second is to calculate useful percentages. The goal of the histograms is to identify trends in the events to either prove what is already known by theory or make discoveries. Percentages are used in conjunction with the histograms to put numbers behind the trends seen. This subsection will detail the types of histograms and percentages generated.

There are several metrics to take into consideration. The first one investigated was the duration of these TEC/SABER occurrences. To have a basis to compare to, the SABER duration distribution was also generated. An example of this histogram is shown in Figure 3.13. The next metric is the mean amplitude in Kelvin that is seen in SABER during the duration of these occurrences. Once again, these histograms are compared to the mean amplitude distribution seen in just the SABER occurrences, which is shown in Figure 3.13. The next two histograms fo-

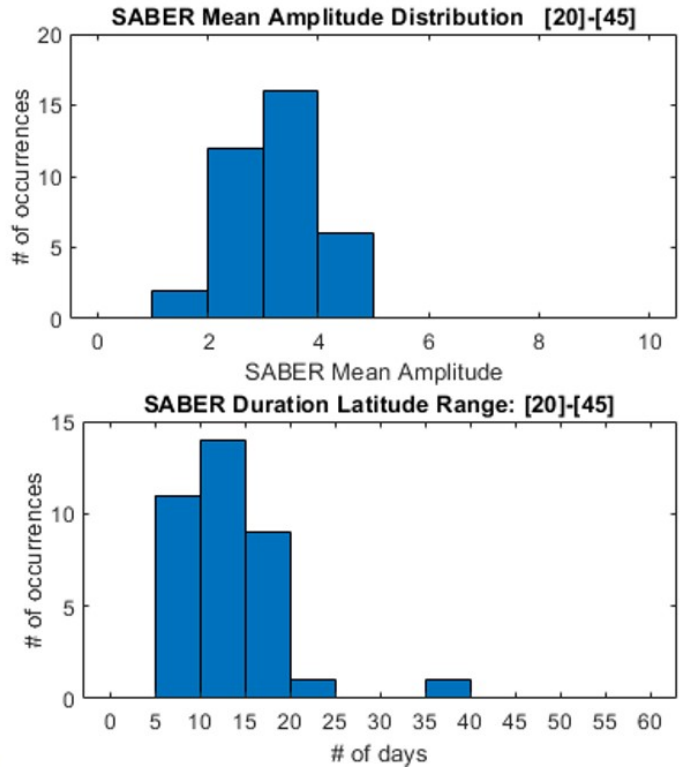

Figure 3.13: Histograms of the Saber Duration Distribution and Saber Mean Amplitude Distribution for the top latitude band.

cus on the SABER latitude bands. The first portrays the number of bands a TEC event shows up in. The other is focused on which latitude bands the TEC event registers in SABER. These two histograms will give a picture of how the latitudinal position affects the atmospheric and ionospheric coupling. Examples of both of these histograms are shown in Figure 3.14. The second histogram needs to be weighted because of the variation of total SABER occurrences in each SABER latitude band. The weighted number of occurrences is calculated by dividing the number of TEC events by the number of SABER events. The last histogram investigates how the solar level affects this coupling by displaying the number of occurrences that are

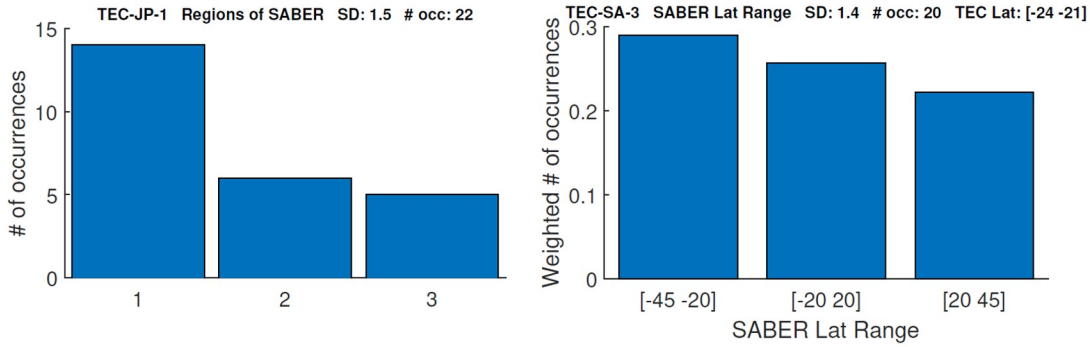

Figure 3.14: The left plot is an example histogram of the number of SABER latitude bands a TEC region's events show up in. The right plot is an example histogram of which of the SABER latitude bands the TEC region's events show up in. The left region is for the first Japan region and the right is for the third South American Region

during times of solar maximum, minimum, or mean. Once again, an example of this plot is shown in Figure 3.15. As one can see these numbers need to be weighted due to the fact that this timeline does not have equal times of solar maximum, minimum, and mean. To be specific, this 17-year span is 57.75% solar minimum, 31.95% solar mean, and 10.30% solar maximum. The number of occurrences is weighted simply by dividing by the fraction of time there is solar minimum, maximum, or mean.

3.3.3 Percentages Method

To more easily identify trends seen in the histograms and provide numbers to back up these trends, percentages for each major result category are calculated. For the duration metric, the percentage of short, medium, and long occurrences are calculated. For SABER Mean Amplitude, the percentage of higher and lower strength waves is

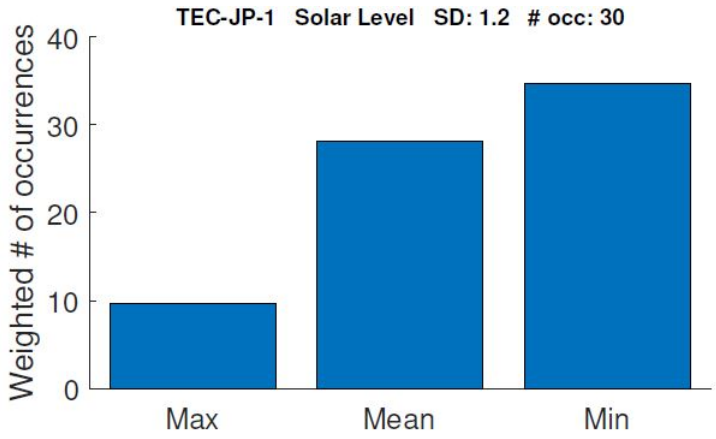

Figure 3.15: Example of a Solar Level Histogram for the Japan region.

calculated. Much like the histograms these percentages need to be split up into the SABER latitude bands. The percentage of occurrences that show up in one, two, or three SABER latitude bands are calculated. In addition, the percentage of times that a signature is picked up in the same SABER latitude band as the TEC region of interest is calculated. For example, the number of times one of the Japan regions has a signature show up in the upper SABER latitude band. The final percentage calculated is solar level percentages. To determine the effect that the Sun has on this coupling, the same histograms and percentages are created but occurrences that were also concurrent with solar events are eliminated. In other words, the results were recalculated with the ambiguous events removed.

3.4 Wavelength Analysis

Another metric that needs to be investigated is the wavelength of the planetary waves. It is important to be able to determine the wavelengths that produce coupling in the atmosphere and ionosphere. This would also be able to prove the theory stated in Chapter 1. As described in Chapter 2, the SABER data has phase values that depend on latitude, altitude, and time. Since there is no efficient way of computationally determining the wavelength of these events, this process is done semi-manually. The SABER events have already been determined computationally, but the accompanying phase plots vary greatly in usefulness. There are only 7 cases that had phase plots that could be used. An example of one of these is shown in Figure 3.16. On the left side of the Amplitude plot, there is a consistently strong response across all altitudes, which is needed to calculate the phase. On the phase plot, there is a clear variation in the phase, which decreases with altitude within the latitude band determined by the phase plot. The wavelength plot is generated by plotting the averaged phase over the appropriate latitude over each altitude, which is only 5 altitudes. The wavelength of this wave is determined by calculating the slope of the best fit line. There are only 7 cases out of 31 that had good R^2 values that are close to 1. In addition, values of wavelength vary from 25 km to 60 km. It was decided that no conclusions could be made from this analysis because of the number of acceptable values and the lack of range in altitude. It is difficult to determine wavelengths greater than the 20 km range that was available.

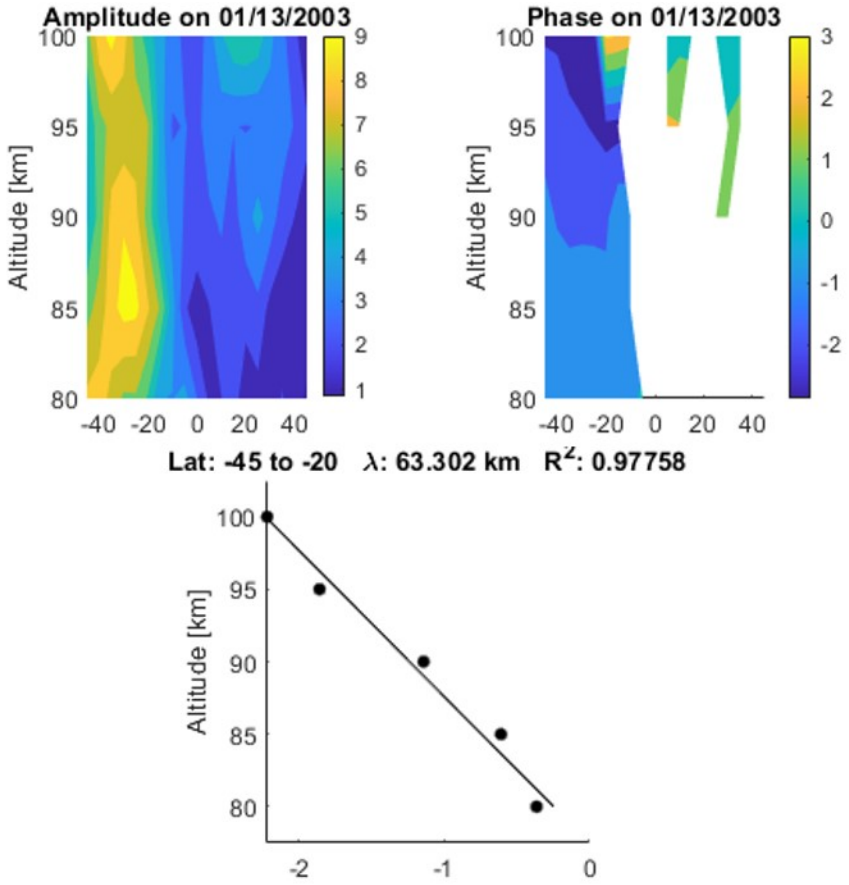

Figure 3.16: Plots used to calculate wavelength. The plots include an amplitude plot and phase plot dependent on altitude and latitude. The third plot is the plots dependent on altitude with a best-fit line.

Chapter 4

Results & Discussion

This chapter will discuss the results found by using the techniques described in the previous chapter. The full collection of timelines are in the Appendix A. This comparison technique verifies that there is clear and obvious coupling and that there will be sensible results gathered from both the histograms and the percentages. This chapter will discuss the results of both the histograms and the percentages and is divided into the 4 main metrics that were analyzed, duration, SABER amplitude, location, and solar level. For the histograms there are 9 TEC regions, 4 threshold values, 3 SABER latitude bands, and 5 types of histograms; this leads to a large number of histograms generated, so this section will only be showing a few histograms. The full collection of histograms is in Appendix B. Before the results are explained the thresholding needs to be discussed. Since threshold values have a large impact on trends and percentages, there has to be an analysis of the threshold values along with the four other metrics. Since both the histograms and the percentages are using the portion of TEC that is concurrent with SABER, it is best to vary the threshold value for TEC and hold the threshold values for SABER, F10.7, and KP constant. The range of threshold values used for TEC is 1.2 to 1.5 standard deviations above the rolling median value. The other threshold values were determined by analyzing

the threshold plots, Figure 3.11, to make sure all the significant events were recorded. The SABER threshold value used in this analysis is 1.2 standard deviations, and for both F10.7 and KP, 1.5 standard deviations.

4.1 Duration

Duration is an important metric when analyzing the characteristics of this coupling. Both the SABER event distributions and the TEC concurrent with SABER distributions are generated. Conclusions for the TEC/SABER data can be surmised but this is irrelevant when it is not compared exclusively to the SABER distribution. Figure 4.1 shows the duration distribution for each SABER latitude band. Most of the events for SABER fall between 5 days and 30 days. It is important to note that this lower limit is somewhat misleading; in the previous chapter, the minimum value is set at 8 days. The longest event is recorded in the upper latitude band and has a duration of 35-40 days. The most important takeaway from these distributions is that the majority of SABER events last from 8-15 days, which is relatively small compared to the full range of duration. The histograms for the TEC events tend to show a different distribution in duration. A majority of the TEC events have a duration that exceeds 15 days, with a peak in either the 15-20- or 20-25-day range. The TEC events also have a broader range of duration as the range extends to 50 days. The TEC events exhibit more of a Gaussian distribution with minimums on both sides of the maximum. A good example of this is shown in Figure 4.2.

The TEC events concurrent with SABER events are now divided up into

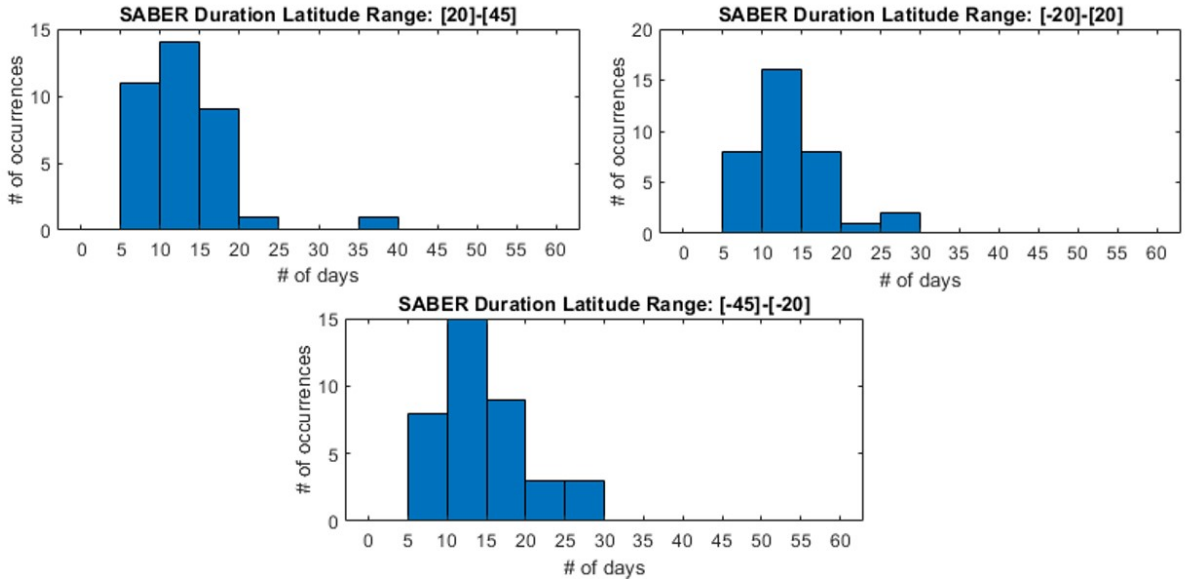

Figure 4.1: The distribution in duration of the SABER events using a threshold value of 1.2 standard deviations.

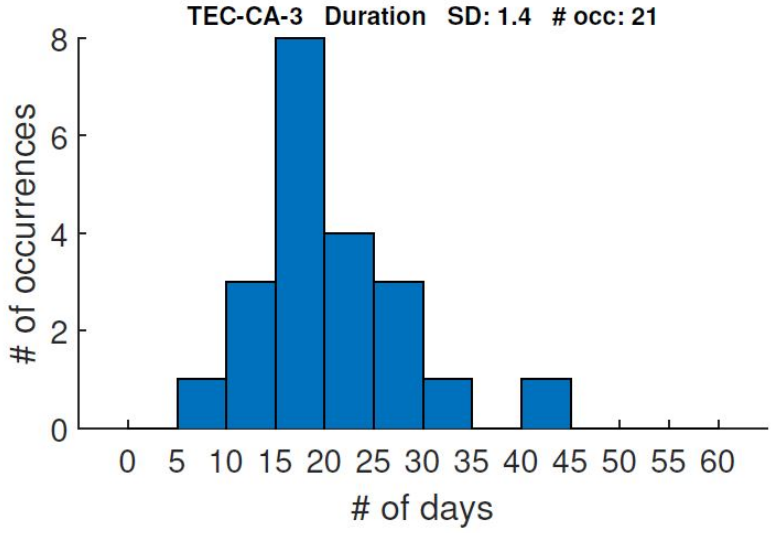

Figure 4.2: The distribution in duration of the TEC events in one of the Central American/Caribbean regions using a threshold value of 1.4 standard deviations.

three categories, short, medium, and long. A short duration event is described as an event that lasts less than 15 days. A long duration is any event that lasts more than 25 days. Finally, a medium duration event is any event that falls between 15 to 25 days. This categorization helps to easily determine the type of TEC event. It is important to note that in this chapter when I refer to TEC events I am really referring to TEC events concurrent with SABER. The first percentage seen in Table 4.1 is just the number of TEC events with a certain duration length over the total number of TEC events. The second percentage is the efficiency percentage. This is needed because the first percentage alone does not tell you how the SABER data is impacting the TEC data. To determine the efficiency of the planetary waves for each duration length, the number of TEC events is divided by the number of SABER events. This is why in some of the cases the percentages exceed 100%. As one can see the majority of the TEC durations are of medium length, where the majority of SABER event durations are of small length. This result would suggest that the ionosphere rattles longer than the atmosphere as a result of this coupling. This result could also be caused by the thresholding techniques, although the different TEC threshold values produce the same result.

4.2 Planetary Wave Amplitude

The next metric to help understand atmospheric and ionospheric coupling is planetary wave amplitude. As described in Chapter 2, the 2-day SABER data used in this study is the wave's amplitude, which is actually just the temperature in Kelvin. The

Table 4.1: Duration percentage table. The second column is the number of TEC concurrent with SABER events, the third is the percentage out of the total, the fourth is the number of just SABER occurrences and the fifth is the efficiency percentage.

SD:1.2				
Category	# of TEC	Percent	# of SABER	Efficiency Percent
Short Duration	70	25.27%	648	10.80%
Medium Duration	142	51.26%	279	50.90%
Long Duration	65	23.47%	54	120.37%
SD:1.3				
Short Duration	66	25.88%	648	10.19%
Medium Duration	128	50.20%	279	45.88%
Long Duration	61	23.92%	54	112.96%
SD:1.4				
Short Duration	65	28.14%	648	10.03%
Medium Duration	114	49.35%	279	40.86%
Long Duration	52	22.51%	54	96.30%
SD:1.5				
Short Duration	60	30.93%	648	9.26%
Medium Duration	96	49.48%	279	34.41%
Long Duration	38	19.59%	54	70.37%

larger the amplitude the stronger the planetary wave. From the SABER amplitude plots described in Chapter 3, it can be determined that there is definitely a variation in wave strength between the three latitude bands. Just like with duration, the Amplitude distribution of the SABER events needs to be examined. This is shown in Figure 4.3. To calculate this mean amplitude, first, the maximum amplitude is recorded for each time step in each latitude band. Then the mean is calculated over the duration of each event. The peak for the -45 to -20 degree and -20 to 20 degree latitude bands is in the 2-3 K range. The peak for the 20 to 45 degree latitude band

is in the 3-4 K range. The lower latitude band has a much larger range than the other bands, while the upper band has the most Gaussian-like distribution. These histograms are recreated for the 9 TEC regions for each of the SABER Latitude band. Due to the number of histograms, the percentages are better at describing the impact that wave amplitude has on this coupling. The percentages can be seen in Table 4.2. Much like with duration, the wave amplitude is put into categories, small and large amplitudes. Any amplitude under 3 K is considered small, and any amplitude over 3 K is considered large. As one can see, in both the lower and middle latitude bands, there is a higher percentage of TEC events with a small amplitude. In the upper latitude band, there are more events with a large amplitude. With just this information one would conclude that TEC responds better to weaker waves in the lower and middle latitude bands, and stronger waves in the upper latitude band. This result is most likely due to the fact that the upper latitude band tends to have stronger waves than the other two bands, which is seen in the SABER Mean Amplitude distributions. It is important to note that there is an abnormally large amplitude in the SABER in the middle latitude band of 2016, which can be seen in Figure 2.1. This calculation is most likely erroneous and is ignored for these results.

4.3 Location

The reason for dividing up both the TEC and SABER data into smaller geographic regions is to understand how location affects this coupling. The first aspect to investigate is how large of a geographic impact the planetary waves have on the

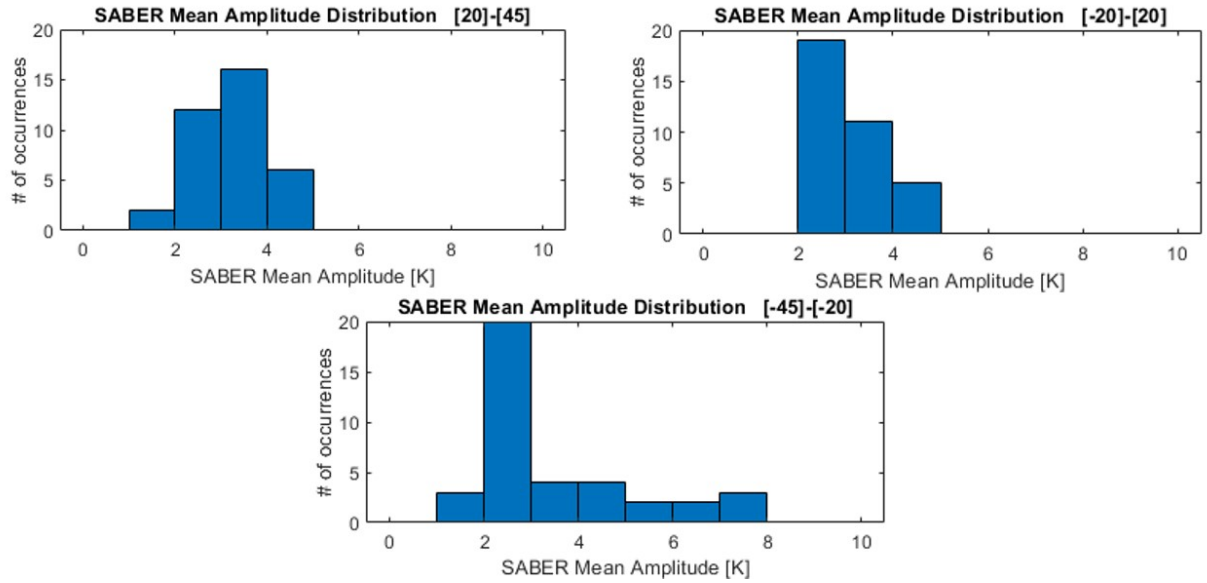

Figure 4.3: The distribution in the Mean Amplitude of the SABER events using a threshold value of 1.2 standard deviations.

ionosphere. This is accomplished by determining how many latitude bands each TEC event shows up in. The overwhelming result is that most of the TEC events are attributed to a SABER event spanning only one latitude band. This was followed by events that span 2 latitude bands and then 3 latitude bands. Although this is the result it can not be surmised that single latitude band events have a greater impact on the ionosphere. This trend is most likely due to the fact that there are simply more events that only span one latitude band. The other set of histograms used to determine the impact of location is the ones that investigate *which* latitude bands have the most impact. For each of the nine regions, it is determined if the peak number of occurrences is in the same latitude band that the region of interest is positioned in. An example of this is shown in Figure 4.4. The region of interest is the first Central America/Caribbean region which has a latitude range of 7 to

Table 4.2: Duration percentage table. The second column is the number of TEC concurrent with SABER events, the third is the percentage out of the total, the fourth is the number of just SABER occurrences and the fifth is the efficiency percentage.

Category	# of TEC	Percent
SD:1.2		
Small Amp. 20 to 45	60	45.45%
Large Amp. 20 to 45	72	54.55%
Small Amp. -20 to 20	88	63.77%
Large Amp. -20 to 20	50	36.23%
Small Amp. -45 to -20	93	62.84%
Large Amp. -45 to -20	55	37.16%
SD:1.3		
Small Amp. 20 to 45	54	46.55%
Large Amp. 20 to 45	62	53.45%
Small Amp. -20 to 20	75	63.56%
Large Amp. -20 to 20	43	36.44%
Small Amp. -45 to -20	86	62.77%
Large Amp. -45 to -20	51	37.23%
SD:1.4		
Small Amp. 20 to 45	51	48.57%
Large Amp. 20 to 45	54	51.43%
Small Amp. -20 to 20	68	65.38%
Large Amp. -20 to 20	36	34.62%
Small Amp. -45 to -20	78	62.90%
Large Amp. -45 to -20	46	37.10%
SD:1.5		
Small Amp. 20 to 45	40	47.62%
Large Amp. 20 to 45	44	52.38%
Small Amp. -20 to 20	58	65.91%
Large Amp. -20 to 20	30	34.09%
Small Amp. -45 to -20	64	62.75%
Large Amp. -45 to -20	38	37.25%

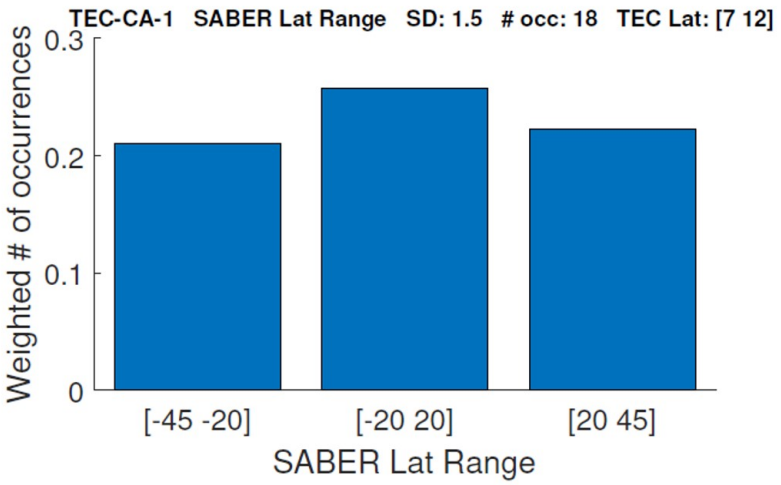

Figure 4.4: A histogram showing a concurrence in the peak latitude band and the TEC region position. This is a histogram for one of the Central America/Caribbean regions using a threshold value of 1.5 standard deviations.

12 degrees. There is a peak seen in the -20 to 20 degrees latitude band, which is where this region is positioned. This instance would be described as a concurrence. A check for concurrence is done on each of the nine regions at each threshold value. The results are shown in Table 4.3. The TEC threshold has a noticeable impact on the results of this analysis. As the threshold value increases the percentage of histograms that have a concurrent peak increase. The raised threshold is most likely eliminating weaker events, which means that if there is a strong 2-day oscillation in the ionosphere is more likely due to a planetary wave event in close proximity.

Table 4.3: A table of concurrence percentages.

Category	Percentage			
	SD:1.2	SD:1.3	SD:1.4	SD:1.5
Concurrence	11.11%	22.22%	55.56%	66.67%

4.4 Solar Activity

The final metric is solar activity. The solar level can be put into three categories, minimum, maximum, and mean. F10.7 was used to determine the times of these solar levels, as the event's solar level was determined by the mean of the F10.7 value over the duration. Below 100 sfu is considered solar minimum, above 150 sfu is considered solar maximum, and in between is considered solar mean. Due to the fact that there is a disproportional amount of time spent in each solar level, the occurrences needed to be weighted, which was described in Chapter 3. The histograms show a peak in mean solar level. This is not the expected result, but it is mostly due to the fact that these results are only weighted based on time and not the SABER events. The percentages will look into the results weighted based on SABER events, which are shown in Table 4.4. These percentages are efficiency percentages, as they are calculated as the number of TEC events divided by the number of SABER events. The slightly largest percentage of events occur in solar minimum, which is the expected result. The smallest percentage of events occur in solar maximum. This means that planetary waves are more efficient at impacting the ionosphere during times of solar minimum. Removing the ambiguous events from this data-set also had a large impact on the results. The trend is the same but the separation in the percentages is much more significant. The percentage of events in the solar maximum category have decreased significantly relative to the other events. This means that a majority of the events at times of solar maximum are actually ambiguous events.

Table 4.4: Duration percentage table. The second column is the number of TEC concurrent with SABER events, the third is the percentage out of the total, the fourth is the number of just SABER occurrences and the fifth is the efficiency percentage.

	All Occ.		Eliminated Ambig.	
		SD:1.2		
Category	# of TEC	Percent	# of TEC	Percent
Solar Max.	16	25.40%	9	4.31%
Solar Mean	105	28.46%	82	39.23%
Solar Min.	156	28.42%	118	56.46%
		SD:1.3		
Solar Max.	13	20.63%	8	4.47%
Solar Mean	96	26.02%	64	35.75%
Solar Min.	146	26.59%	107	59.78%
		SD:1.4		
Solar Max.	12	19.05%	6	3.77%
Solar Mean	86	23.31%	59	37.11%
Solar Min.	133	24.23%	94	59.12%
		SD:1.5		
Solar Max.	9	14.29%	3	2.29%
Solar Mean	71	19.24%	50	38.17%
Solar Min.	114	20.77%	78	59.54%

Chapter 5

Conclusions

It is known that there is a vertical coupling between the neutral lower atmosphere and the ionosphere. Planetary waves with periods in the range of 2-30 days have a significant contribution to this ionospheric variability. This atmospheric impact on the ionosphere is most prominent in low-latitude regions, which is thought to be a result of the E-region dynamo. It is thought that some planetary wave signatures can reach the E-region of the ionosphere, where they can perturb the E-region dynamo directly, but that much of the coupling occurs through planetary wave modulation of the amplitude of atmospheric tides. These tides are able to propagate upwards more easily and thus impact the E-region dynamo. Further, any tides that can reach F-region altitudes can also directly modify the main ionospheric layer directly. In this study, we seek to understand any trends in the planetary wave coupling to the ionosphere, such that we can elucidate the nature of this coupling and provide such detailed constraints to models and other studies that are able to either observe the tides at high altitude or simulate this coupling.

Due to the multitude of different planetary waves that are seen in the atmosphere, only one type of wave is investigated in this study. This wave happens to be

the westward propagating quasi-2-day wave, which is formally called Rossby-gravity waves. This wave is chosen because it is thought to have one of the largest amplitudes of all the planetary waves in the lower atmosphere. There have been many studies that confirm this coupling by identifying similar oscillations in atmospheric and ionospheric data-sets. In previous studies, only a few events were identified at a time. The goal of this study is to use a large time-span, 17 years, to determine a large number of events that exhibit signs of coupling. With this large collection of concurrences, trends can be analyzed, and the characteristics of this coupling can be speculated.

Due to the 2-day wave being the interest of this study, this type of oscillation needs to be extracted from the available data. The method used to determine times of similar periodicity is wavelet analysis with thresholding techniques. Three types of data were analyzed in this study, planetary wave, ionospheric, and solar. SABER temperature data provides information of when the 2-day wave is present in the atmosphere at altitudes just below the E-region dynamo. Total Electron Content is used for the ionospheric activity. F10.7 solar flux and the KP index are used for solar activity. Comparing the atmospheric and ionospheric data, a collection of concurrent events is generated. Both solar activity and atmospheric waves have an impact on the ionosphere. To isolate the atmospheric and ionospheric coupling, the solar data needs to be analyzed. Ambiguous forcing events are eliminated from the comparison catalog to remove any solar bias. To characterize this coupling seen with 2-day atmospheric waves, histograms and percentages are generated. The metrics considered in this analysis are duration, wave amplitude, location, and solar level.

The following is a list of conclusions gathered from the results of this study.

- The majority of SABER events that have a 2-day oscillation, last anywhere from 8 to 15 days. The majority of 2-day TEC events that were concurrent with 2-day SABER events have a longer duration, lasting from 15 to 25 days. This finding could lead one to believe that the ionosphere rattles longer than the atmosphere as a result of this coupling. This result could also be an artifact of the thresholding techniques used.

- The majority of TEC events that were concurrent with SABER events happened to be long-duration planetary wave events lasting at least 15-days. This means that atmospheric waves that last over 15-days are more efficient in causing variability in the ionosphere.

- There were more ionospheric events that correlated to weaker atmospheric waves in both the lower and middle latitude bands. The opposite was found in the upper latitude band, where more events were correlating with stronger planetary waves. This was not expected, as one would think that larger strength waves would lead to more efficient coupling, no matter which latitude band. This led to the conclusion that the results of this analysis were just an artifact of the different strengths of waves seen in each latitude band.

- TEC events that corresponded to SABER events in the same latitude band tended to occur more frequently when the threshold value was increased. Increasing the threshold value eliminates some of the noise in the data-set and

only includes events with very strong 2-day oscillations. These results lead to the conclusion that the ionosphere is more heavily impacted by the planetary waves in close geographic proximity.

- TEC events that were concurrent with SABER events were more likely to occur at times of solar minimum than at times of solar maximum. In addition, when ambiguous events were eliminated from the data-set, the number of events during solar maximum decreased drastically. Both of these results lead one to conclude that the atmosphere has more impact on the ionosphere during times of solar minimum. This is due to the fact that solar impact on the ionosphere is low during these times.

This study is primarily interested in narrowing down the possibilities of how planetary wave oscillations cause perturbations in the ionosphere, which provides a solid target for the modeling studies. During this analysis, it was determined that the methods used had many variables that can skew results. The thresholding value was one variable that had a large influence on the trends seen. This study was meant to provide validity to previous assumptions and make discoveries about atmospheric and ionospheric coupling. It is important to note that the conflicting results are not to disprove previous assumptions but to encourage more analysis of the complexities of this coupling. This study was able to use a longer time-span to identify times of coupling between the atmosphere and ionosphere and start to determine the properties of this interaction.

Bibliography

[1] R. N. Davis, Y.-W. Chen, S. Miyahara, and N. J. Mitchell. The climatology, propagation and excitation of ultra-fast kelvin waves as observed by meteor radar, aura mls, trmm and in the kyushu-gcm. *Atmospheric Chemistry and Physics*, 12(4):1865–1879, 2012. doi: 10.5194/acp-12-1865-2012.

[2] Scott L. England, Guiping Liu, Qihou Zhou, Thomas J. Immel, Karanam K. Kumar, and Geetha Ramkumar. On the signature of the quasi-3-day wave in the thermosphere during the january 2010 ursi world day campaign. *Journal of Geophysical Research: Space Physics*, 117(A6), 2012. doi: 10.1029/2012ja017558.

[3] Jeffrey M. Forbes, Xiaoli Zhang, Scott E. Palo, James Russell, Christopher J. Mertens, and Martin Mlynczak. Kelvin waves in stratosphere, mesosphere and lower thermosphere temperatures as observed by timed/saber during 2002–2006. *Earth, Planets and Space*, 61(4):447–453, 2009. doi: 10.1186/bf03353161.

[4] John Keith Hargreaves. *Contents*. Cambridge Atmospheric and Space Science Series. Cambridge University Press, 1992.

[5] Jay R. Harman. *Rossby wave*, pages 724–727. Springer US, Boston, MA, 1987. ISBN 978-0-387-30749-7. doi: 10.1007/0-387-30749-4_151.

[6] James M. Russell III, Martin G. Mlynczak, Larry L. Gordley, Jr. Joseph J. Tansock, and Roy W. Esplin. Overview of the saber experiment and preliminary

calibration results. *Optical Spectroscopic Techniques and Instrumentation for Atmospheric and Space Research III*, 1999. doi: 10.1117/12.366382.

[7] T. J. Immel, E. Sagawa, S. L. England, S. B. Henderson, M. E. Hagan, S. B. Mende, H. U. Frey, C. M. Swenson, and L. J. Paxton. Control of equatorial ionospheric morphology by atmospheric tides. *Geophysical Research Letters*, 33 (15), 2006. doi: https://doi.org/10.1029/2006GL026161.

[8] Guiping Liu, Scott L. England, Thomas J. Immel, Harald U. Frey, Anthony J. Mannucci, and Nicholas J. Mitchell. A comprehensive survey of atmospheric quasi 3 day planetary-scale waves and their impacts on the day-to-day variations of the equatorial ionosphere. *Journal of Geophysical Research: Space Physics*, 120(4):2979–2992, 2015. doi: 10.1002/2014JA020805.

[9] Guiping Liu, Scott L. England, and Diego Janches. Quasi two-, three-, and six-day planetary-scale wave oscillations in the upper atmosphere observed by timed/saber over 17 years during 2002–2018. *Journal of Geophysical Research: Space Physics*, 124(11):9462–9474, 2019. doi: 10.1029/2019JA026918.

[10] Christopher J. Mertens, Martin G. Mlynczak, Manuel López-Puertas, Peter P. Wintersteiner, R. H. Picard, Jeremy R. Winick, Larry L. Gordley, and James M. Russell. Retrieval of mesospheric and lower thermospheric kinetic temperature from measurements of co215 μm earth limb emission under non-lte conditions. *Geophysical Research Letters*, 28(7):1391–1394, 2001. doi: 10.1029/2000gl012189.

[11] J. Oberheide, M.E. Hagan, A.D. Richmond, and J.M. Forbes. Dynamical meteorology | atmospheric tides. In Gerald R. North, John Pyle, and Fuqing Zhang, editors, *Encyclopedia of Atmospheric Sciences (Second Edition)*, pages 287 – 297. Academic Press, Oxford, second edition edition, 2015. ISBN 978-0-12-382225-3. doi: https://doi.org/10.1016/B978-0-12-382225-3.00409-6.

[12] D. Offermann, P. Hoffmann, P. Knieling, R. Koppmann, J. Oberheide, D. M. Riggin, V. M. Tunbridge, and W. Steinbrecht. Quasi 2 day waves in the summer mesosphere: Triple structure of amplitudes and long-term development. *Journal of Geophysical Research*, 116, 2011. doi: 10.1029/2010jd015051.

[13] D. Pancheva, P. Mukhtarov, B. Andonov, and J.m. Forbes. Global distribution and climatological features of the 5–6-day planetary waves seen in the saber/-timed temperatures (2002–2007). *Journal of Atmospheric and Solar-Terrestrial Physics*, 72(1):26–37, 2010. doi: 10.1016/j.jastp.2009.10.005.

[14] Gerd W. Prolss. *Physics of the Earth's Space Environment: An Introduction.* Springer, 2004.

[15] William Rideout and Anthea Coster. Automated gps processing for global total electron content data. *GPS Solutions*, 10(3):219–228, 2006. doi: 10.1007/s10291-006-0029-5.

[16] H. Rishbeth. The ionospheric e-layer and f-layer dynamos — a tutorial review. *Journal of Atmospheric and Solar-Terrestrial Physics*, 59(15):1873 – 1880, 1997. ISSN 1364-6826. doi: https://doi.org/10.1016/S1364-6826(97)00005-9.

[17] D. J. Sandford, M. J. Schwartz, and N. J. Mitchell. The wintertime two-day wave in the polar stratosphere, mesosphere and lower thermosphere. *Atmospheric Chemistry and Physics*, 8(3):749–755, 2008. doi: 10.5194/acp-8-749-2008.

[18] A.K. Smith and J. Perlwitz. Middle atmosphere | planetary waves. In Gerald R. North, John Pyle, and Fuqing Zhang, editors, *Encyclopedia of Atmospheric Sciences (Second Edition)*, pages 1 – 11. Academic Press, Oxford, second edition edition, 2015. ISBN 978-0-12-382225-3. doi: https://doi.org/10.1016/B978-0-12-382225-3.00229-2.

[19] Hector Teitelbaum and François Vial. On tidal variability induced by nonlinear interaction with planetary waves. *Journal of Geophysical Research: Space Physics*, 96(A8):14169–14178, 1991. doi: https://doi.org/10.1029/91JA01019.

[20] Christopher Torrence and Gilbert P. Compo. A practical guide to wavelet analysis. *Bulletin of the American Meteorological Society*, 79(1):61–78, 1998. doi: 10.1175/1520-0477(1998)079<0061:apgtwa>2.0.co;2.

[21] V. M. Tunbridge, D. J. Sandford, and N. J. Mitchell. Zonal wave numbers of the summertime 2 day planetary wave observed in the mesosphere by eos aura microwave limb sounder. *Journal of Geophysical Research*, 116(D11), 2011. doi: 10.1029/2010jd014567.

[22] Jack C. Wang, Loren C. Chang, Jia Yue, Wenbin Wang, and D. E. Siskind. The quasi 2 day wave response in time-gcm nudged with nogaps-alpha. *Journal of Geophysical Research: Space Physics*, 122(5):5709–5732, 2017. doi: https://doi.org/10.1002/2016JA023745.

[23] Dong L. Wu, Paul B. Hays, and Wilbert R. Skinner. A Least Squares Method for Spectral Analysis of Space-Time Series. *Journal of the Atmospheric Sciences*, 52(20):3501–3511, 10 1995. ISSN 0022-4928. doi: 10.1175/1520-0469.

[24] Erdal Yiğit, Petra Koucká Knížová, Katya Georgieva, and William Ward. A review of vertical coupling in the atmosphere–ionosphere system: Effects of waves, sudden stratospheric warmings, space weather, and of solar activity. *Journal of Atmospheric and Solar-Terrestrial Physics*, 141:1 – 12, 2016. ISSN 1364-6826. doi: https://doi.org/10.1016/j.jastp.2016.02.011. SI:Vertical Coupling.

Appendices

Appendix A

Timelines

This section contains the timelines described in Section 3.3.1.

A.1 Japan

These timelines use the TEC data for the 2 Japan sub regions. Each timeline plot shows a different standard deviation from 1.2 to 1.5 in increments of 0.1.

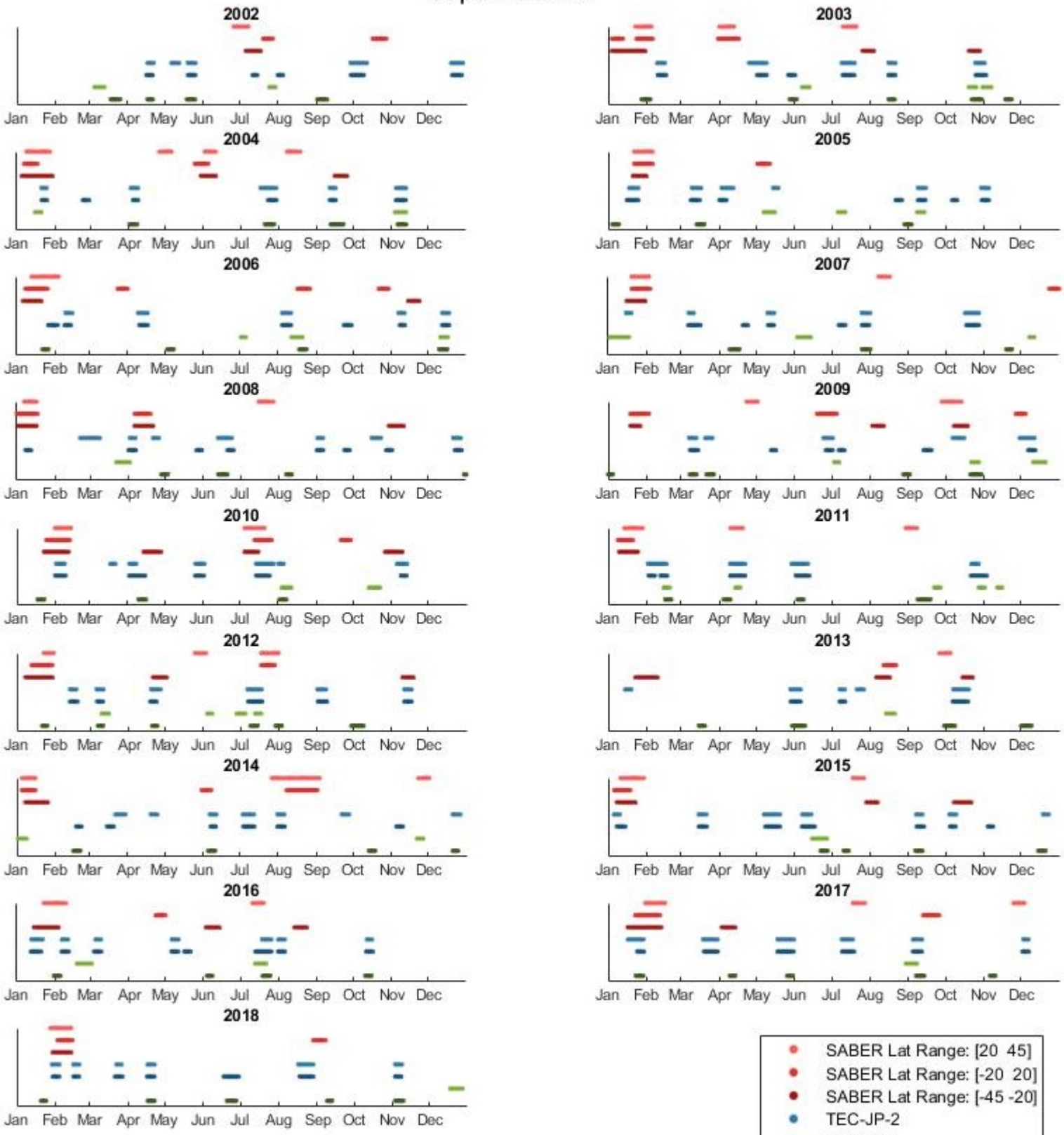
Japan SD:1.2
2002
2003
2004
2005
2006
2007
2008
2009
2010
2011
2012
2013
2014
2015
2016
2017
2018
Jan Feb Mar Apr May Jun Jul Aug Sep Oct Nov Dec
SABER Lat Range: [20 45]
SABER Lat Range: [-20 20]
SABER Lat Range: [-45 -20]
TEC-JP-2
TEC-JP-1
F10.7
KP

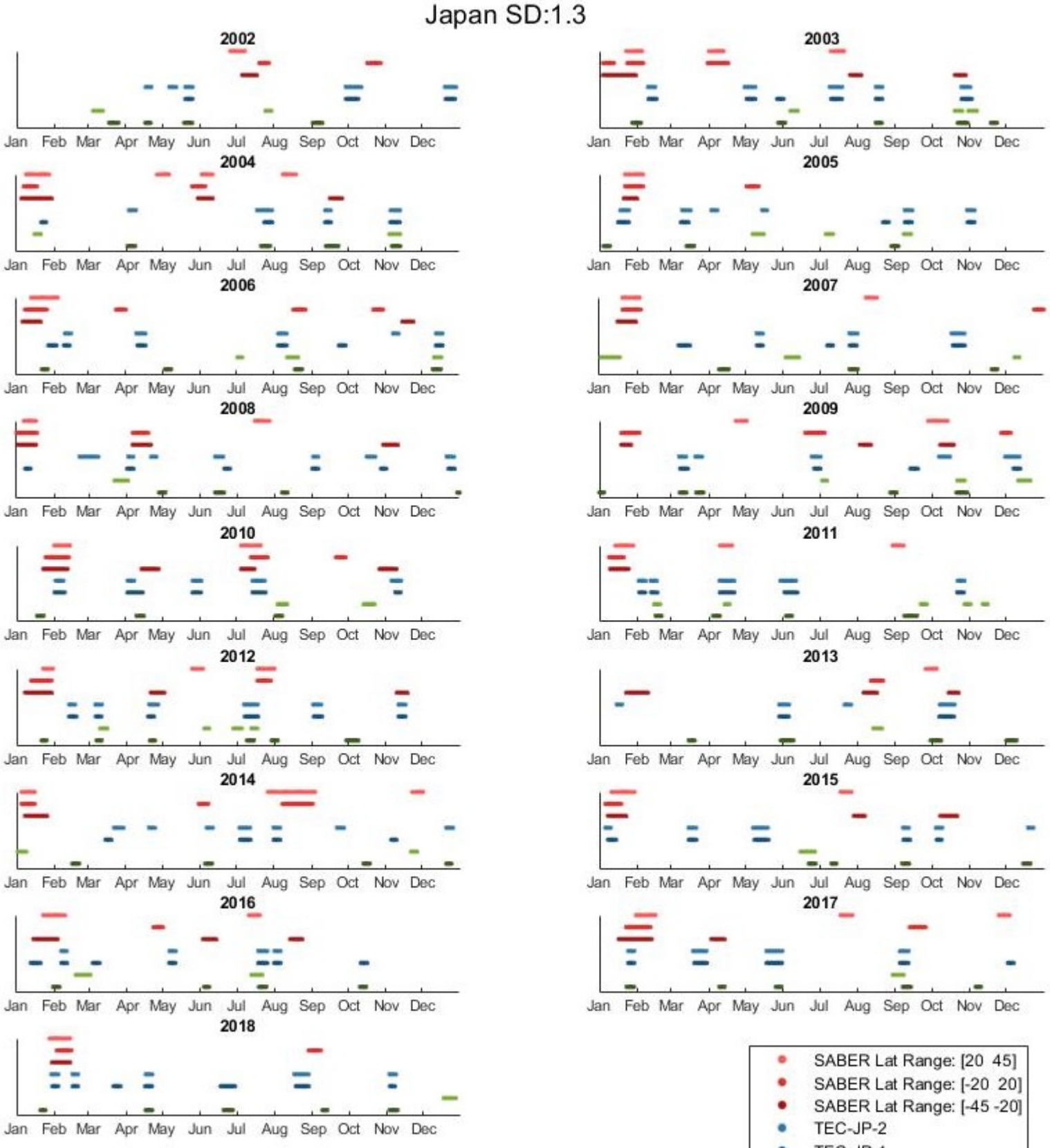
Japan SD:1.3
2002
2003
2004
2005
2006
2007
2008
2009
2010
2011
2012
2013
2014
2015
2016
2017
2018
Jan Feb Mar Apr May Jun Jul Aug Sep Oct Nov Dec
SABER Lat Range: [20 45]
SABER Lat Range: [-20 20]
SABER Lat Range: [-45 -20]
TEC-JP-2
TEC-JP-1
F10.7
KP

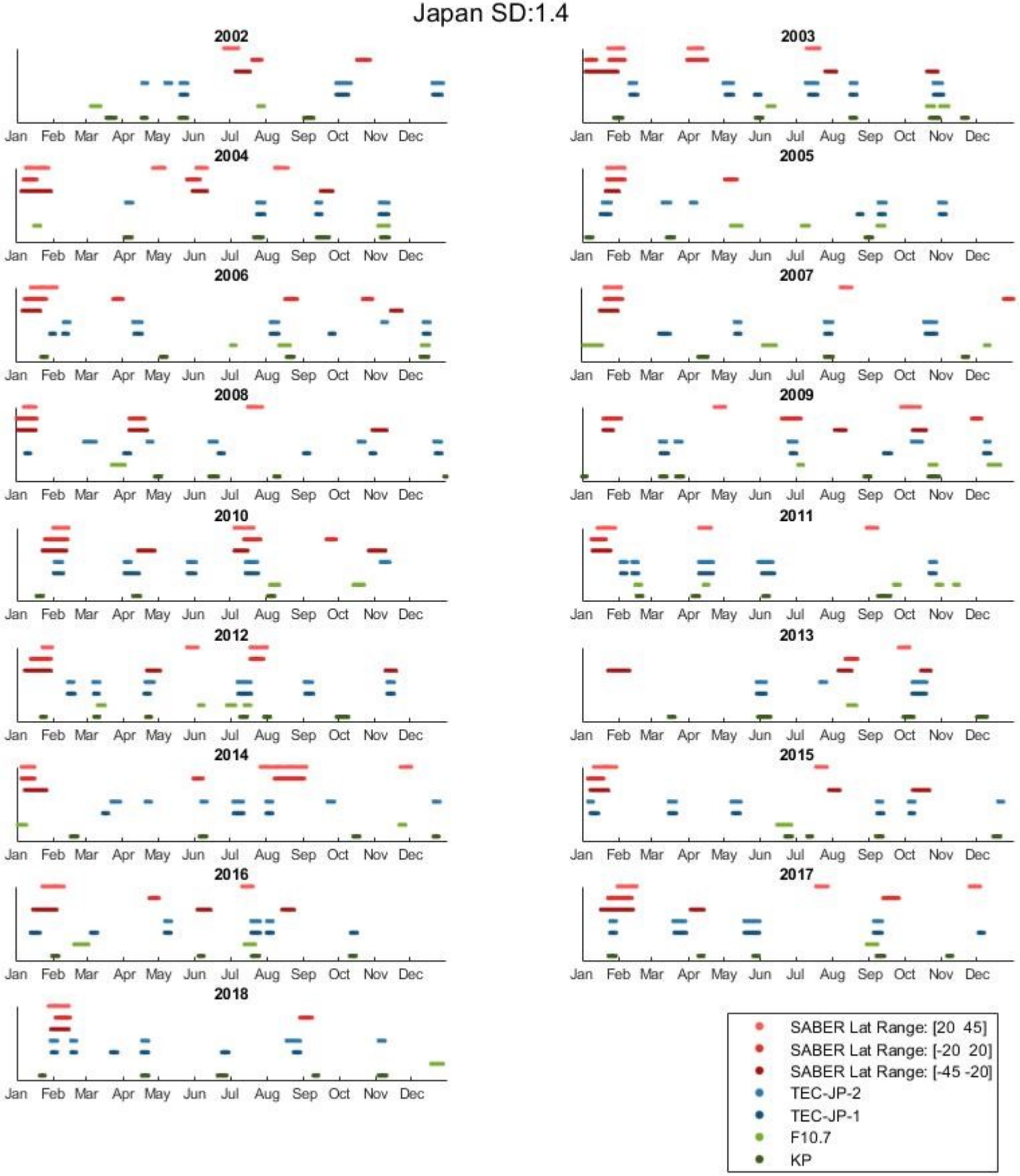
Japan SD:1.4
2002
2003
2004
2005
2006
2007
2008
2009
2010
2011
2012
2013
2014
2015
2016
2017
2018
Jan Feb Mar Apr May Jun Jul Aug Sep Oct Nov Dec
SABER Lat Range: [20 45]
SABER Lat Range: [-20 20]
SABER Lat Range: [-45 -20]
TEC-JP-2
TEC-JP-1
F10.7
KP

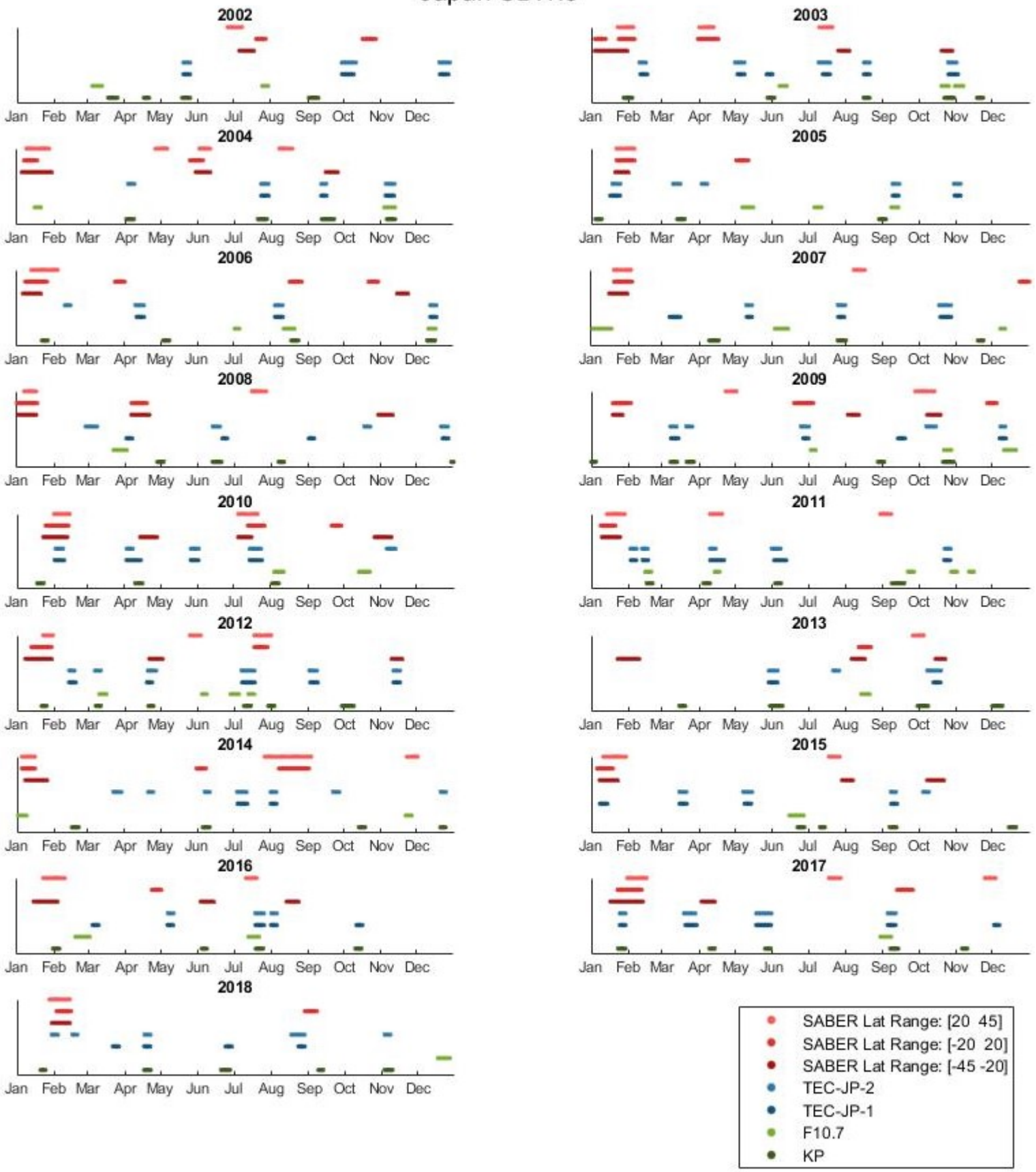
Japan SD:1.5
2002
2003
2004
2005
2006
2007
2008
2009
2010
2011
2012
2013
2014
2015
2016
2017
2018
Jan Feb Mar Apr May Jun Jul Aug Sep Oct Nov Dec
SABER Lat Range: [20 45]
SABER Lat Range: [-20 20]
SABER Lat Range: [-45 -20]
TEC-JP-2
TEC-JP-1
F10.7
KP

A.2 Central America/Caribbean

These timelines use the TEC data for the 3 Central American/Caribbean sub regions. Each timeline plot shows a different standard deviation from 1.2 to 1.5 in increments of 0.1.

Central America/Caribbean SD:1.2

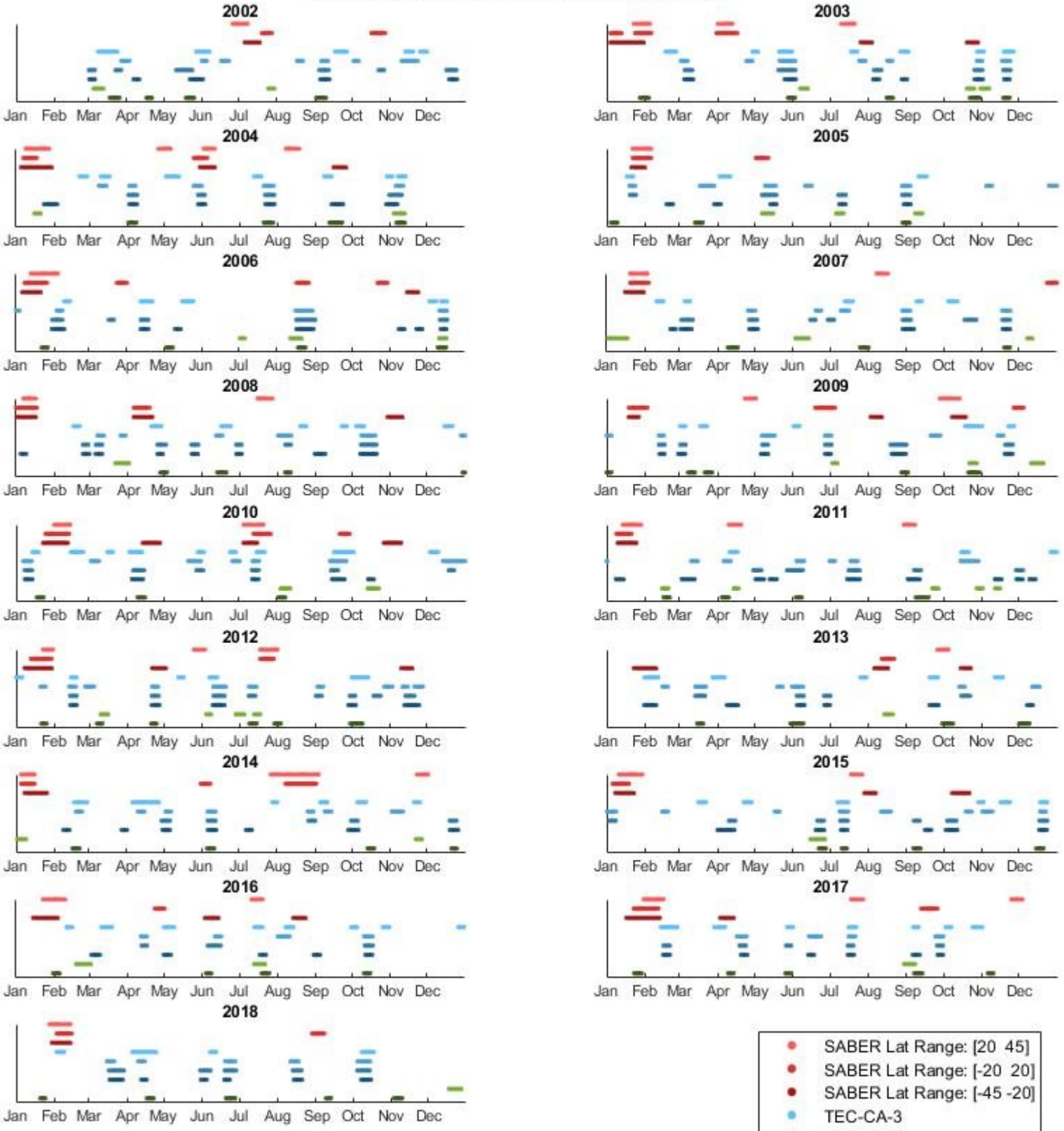

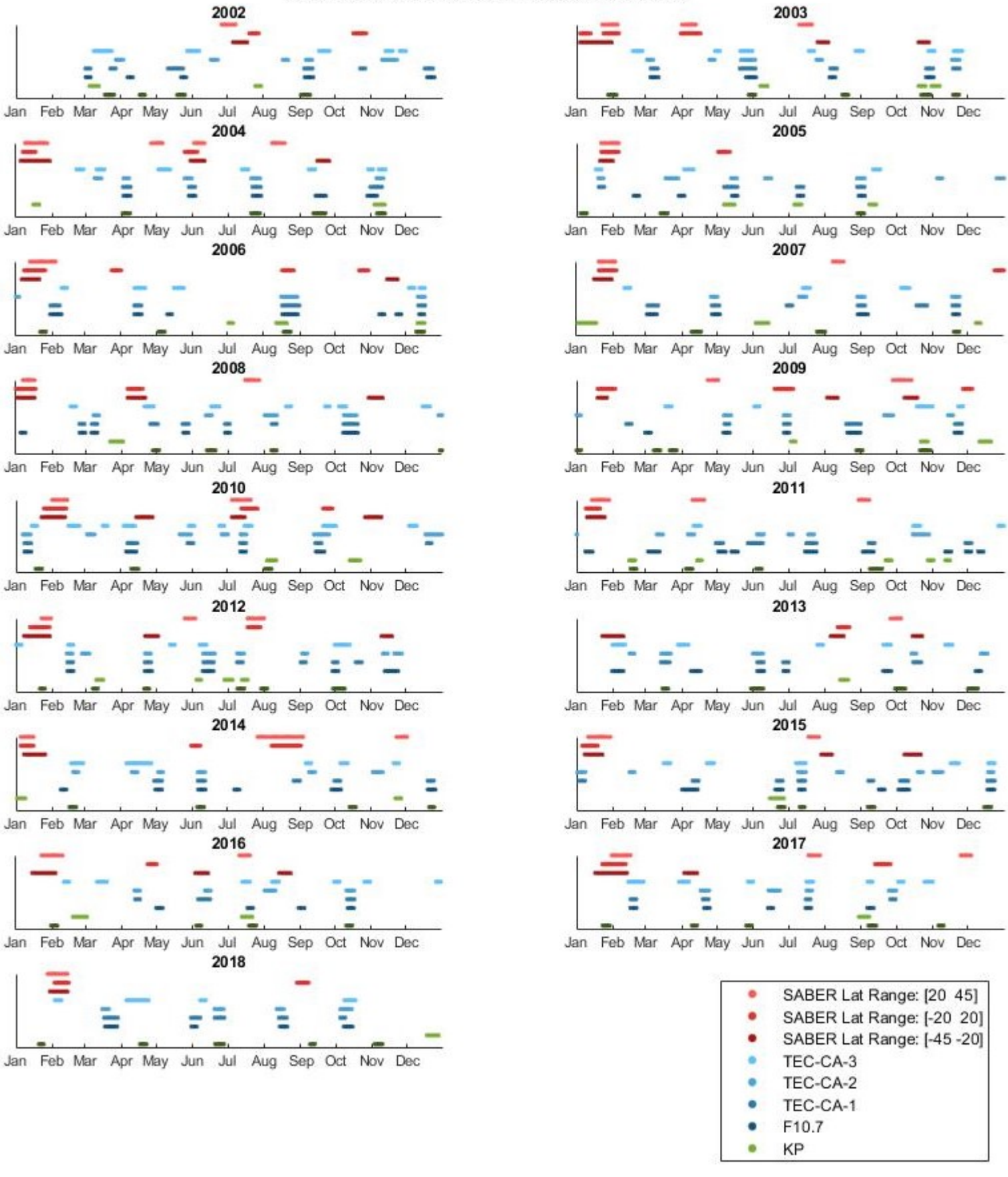
Central America/Caribbean SD:1.3
2002
2003
2004
2005
2006
2007
2008
2009
2010
2011
2012
2013
2014
2015
2016
2017
2018
Jan Feb Mar Apr May Jun Jul Aug Sep Oct Nov Dec
SABER Lat Range: [20 45]
SABER Lat Range: [-20 20]
SABER Lat Range: [-45 -20]
TEC-CA-3
TEC-CA-2
TEC-CA-1
F10.7
KP

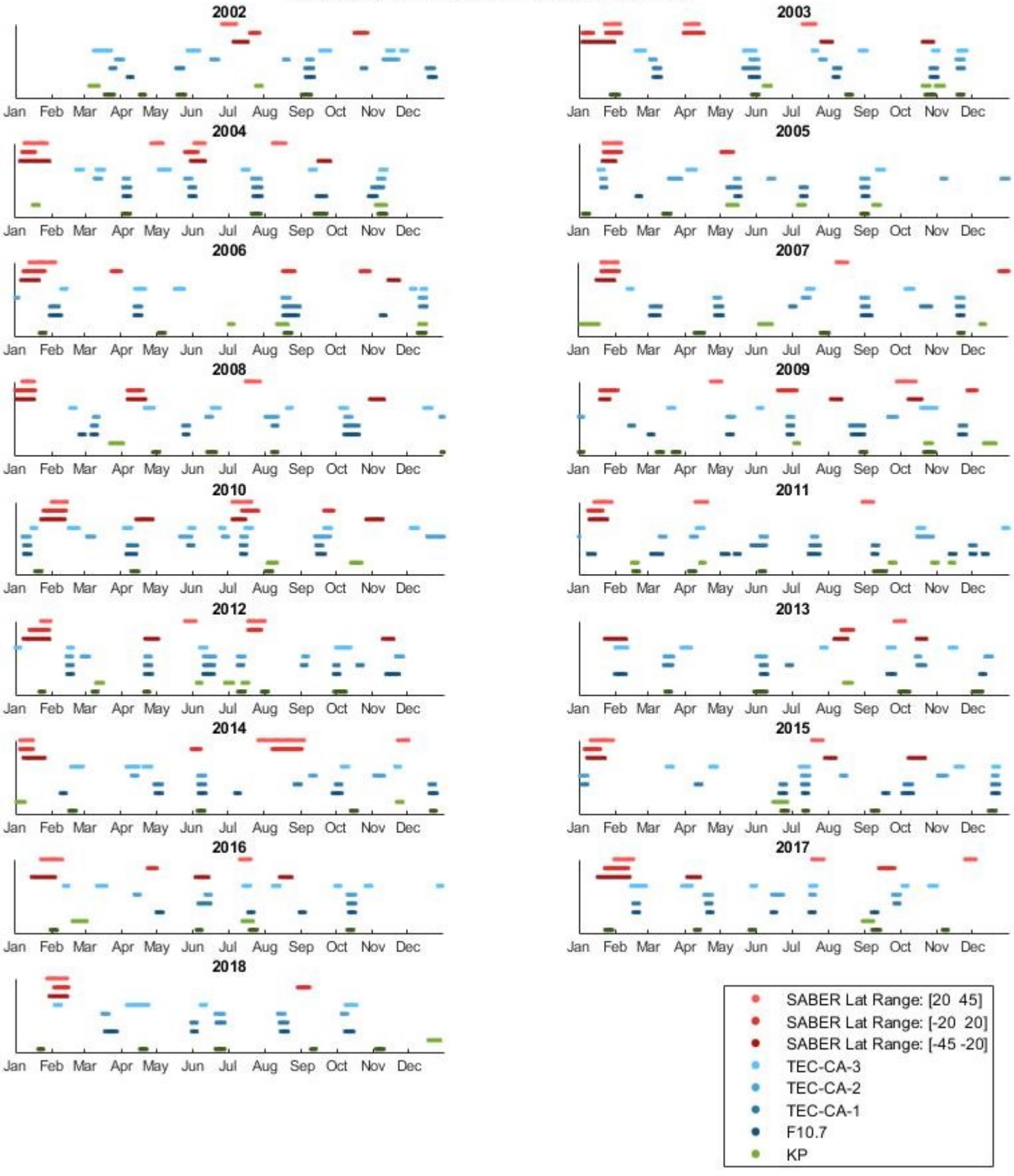
Central America/Caribbean SD:1.4
2002
2003
2004
2005
2006
2007
2008
2009
2010
2011
2012
2013
2014
2015
2016
2017
2018
Jan Feb Mar Apr May Jun Jul Aug Sep Oct Nov Dec
SABER Lat Range: [20 45]
SABER Lat Range: [-20 20]
SABER Lat Range: [-45 -20]
TEC-CA-3
TEC-CA-2
TEC-CA-1
F10.7
KP

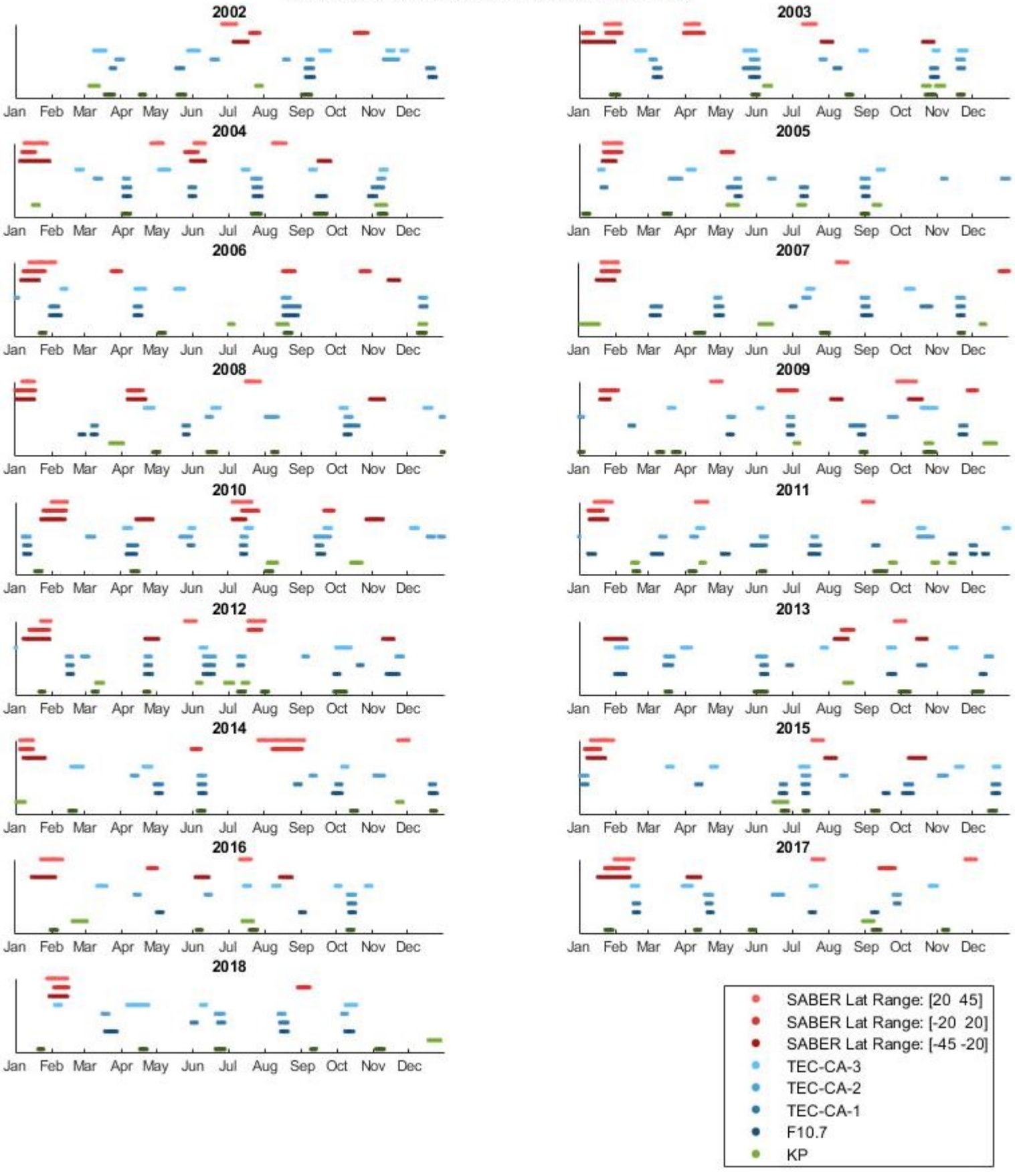
Central America/Caribbean SD:1.5
2002
2003
2004
2005
2006
2007
2008
2009
2010
2011
2012
2013
2014
2015
2016
2017
2018
Jan Feb Mar Apr May Jun Jul Aug Sep Oct Nov Dec
SABER Lat Range: [20 45]
SABER Lat Range: [-20 20]
SABER Lat Range: [-45 -20]
TEC-CA-3
TEC-CA-2
TEC-CA-1
F10.7
KP

A.3 South America

These timelines use the TEC data for the 4 South American sub regions. Each timeline plot shows a different threshold value in standard deviations from 1.2 to 1.5 in increments of 0.1.

South America SD:1.2

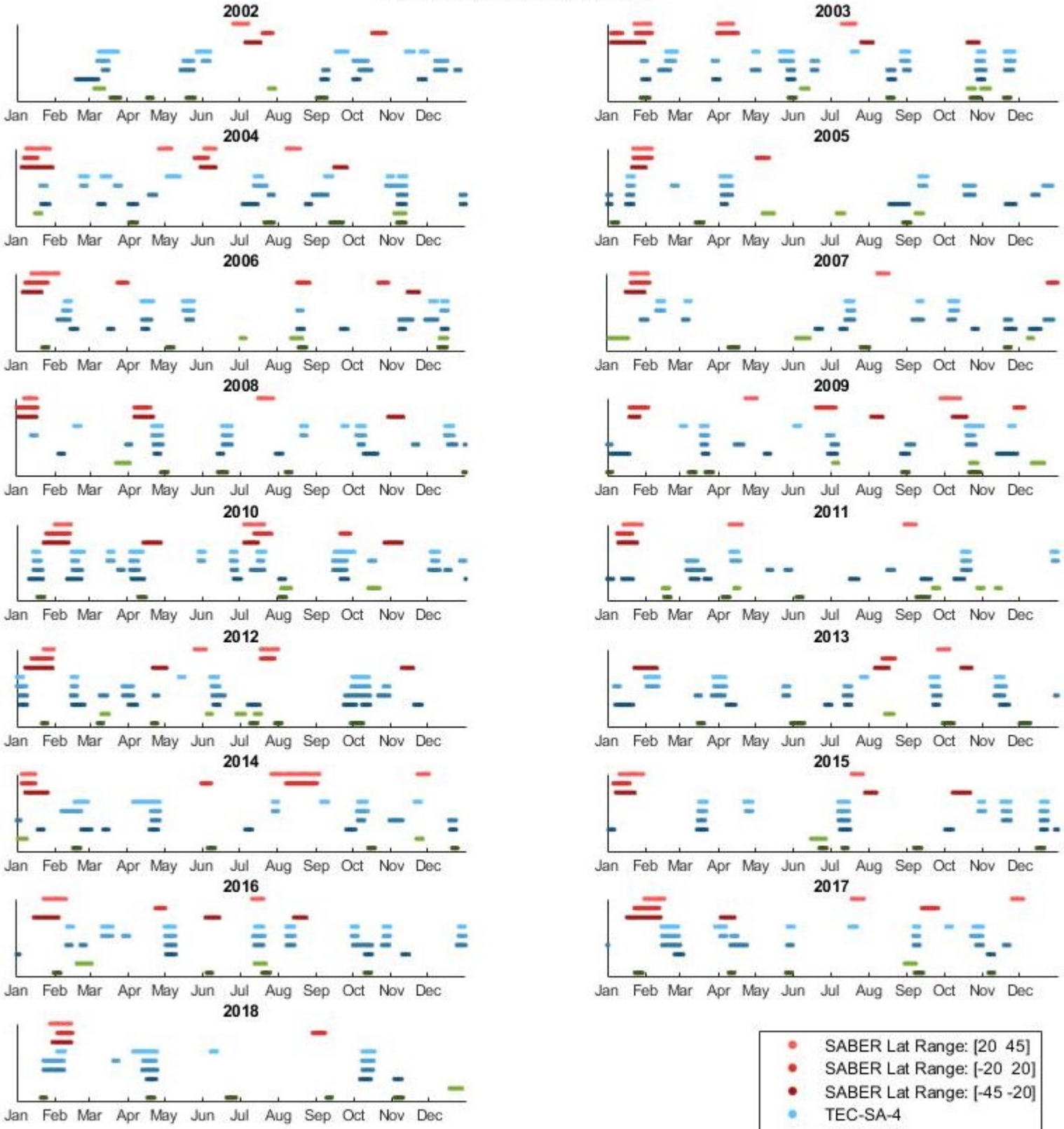

South America SD:1.3

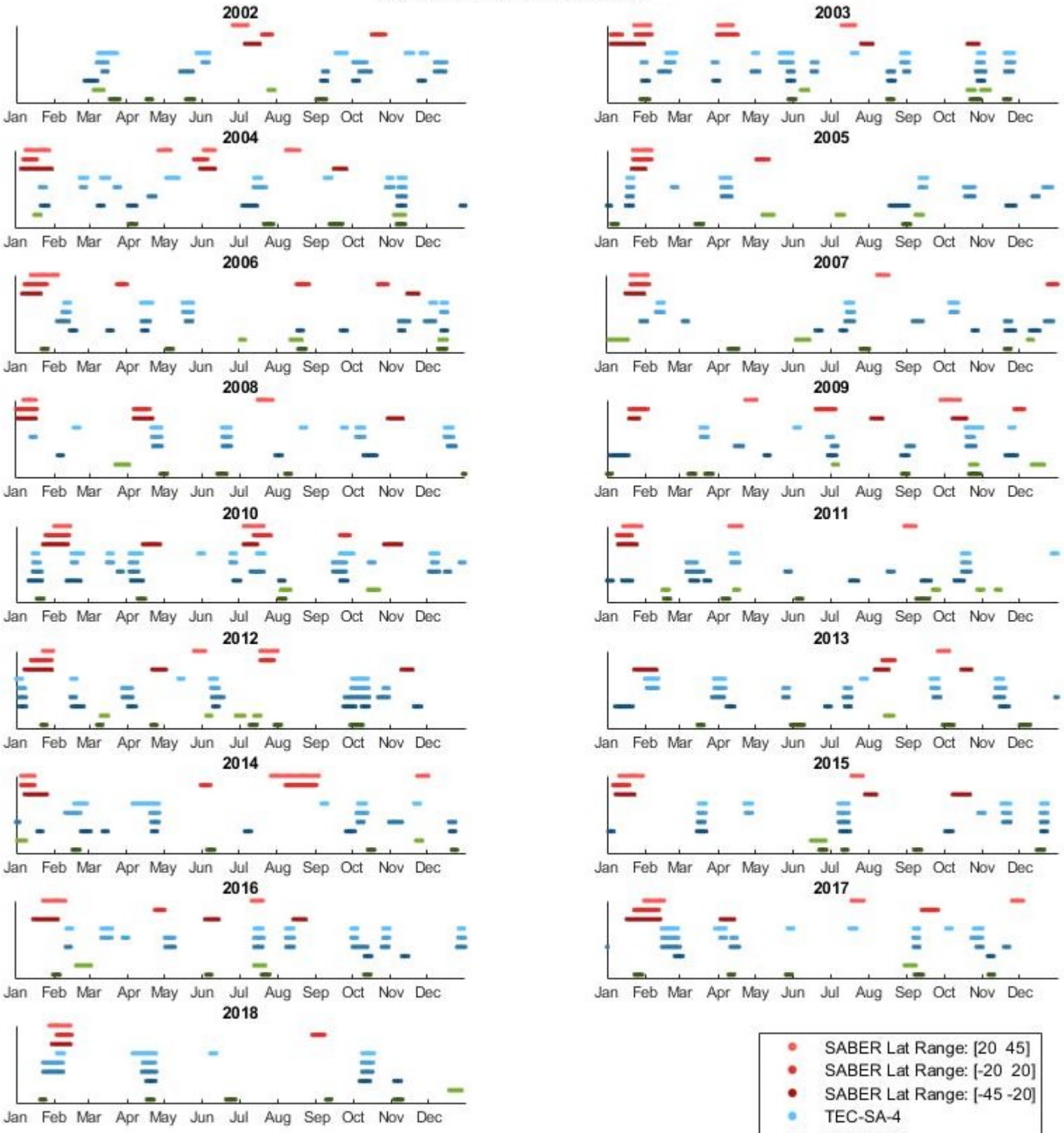

South America SD:1.4

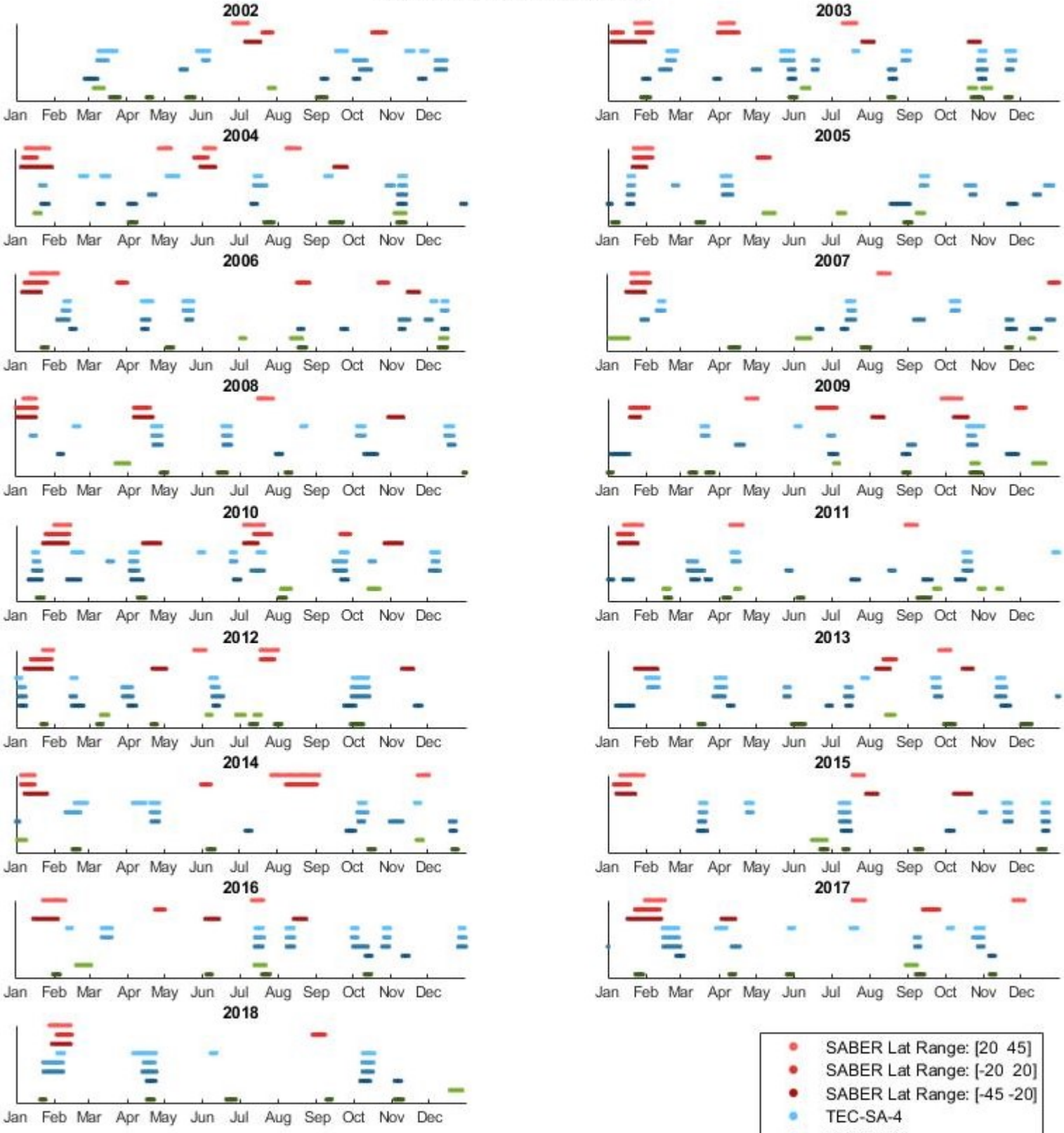

South America SD:1.5

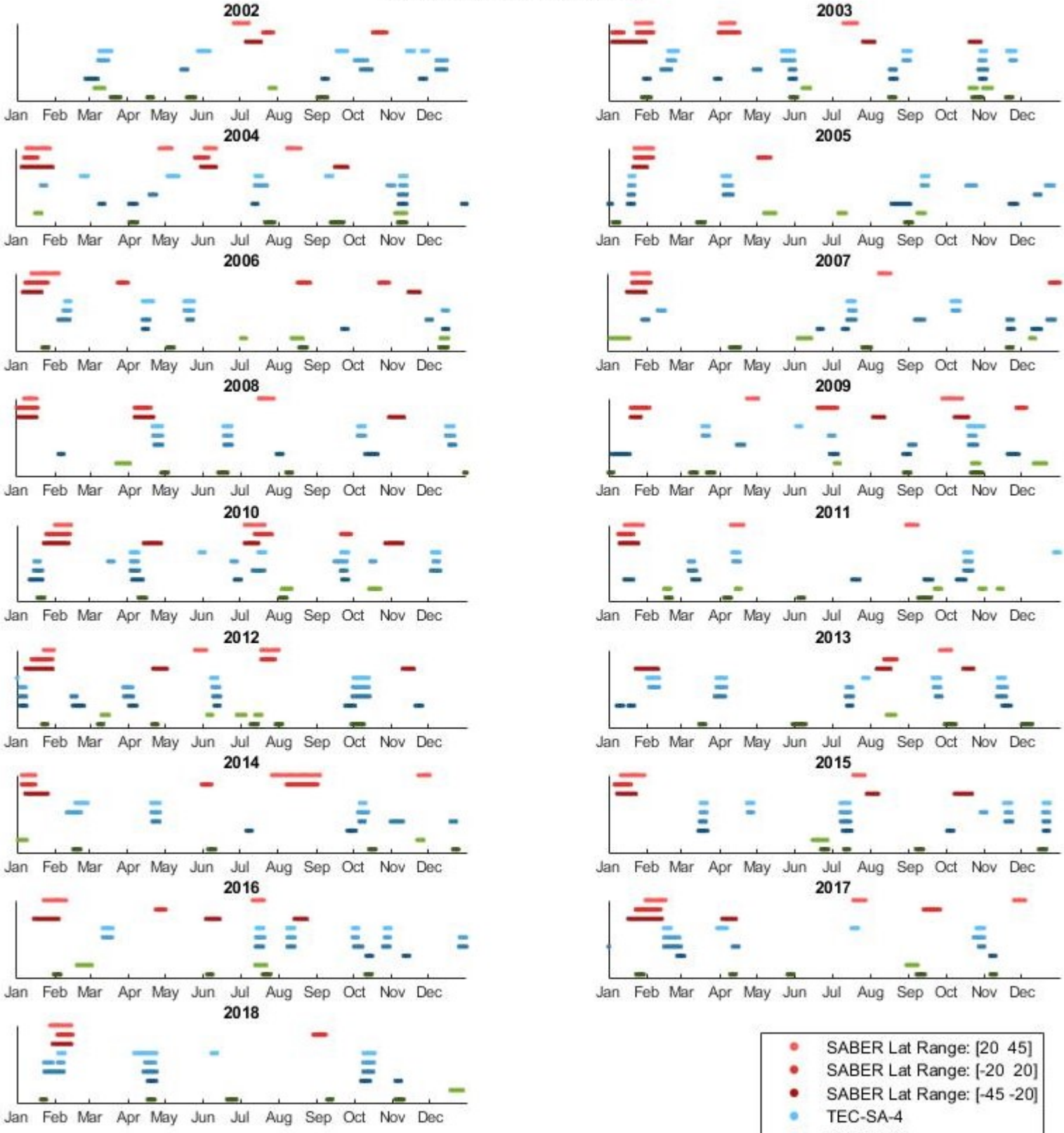

Appendix B

Histograms

These histograms are for all of the 9 TEC sub-regions and vary the threshold value from 1.2 to 1.5 standard deviations in increments of 0.1. In addition, these histograms show the TEC events concurrent with SABER on the left and the same events with the ambiguous events eliminated on the right.

B.1 Duration

This section contains the duration histograms described in Sections 3.3.2 and 4.1. These figures are similar to 4.2.

With Solar

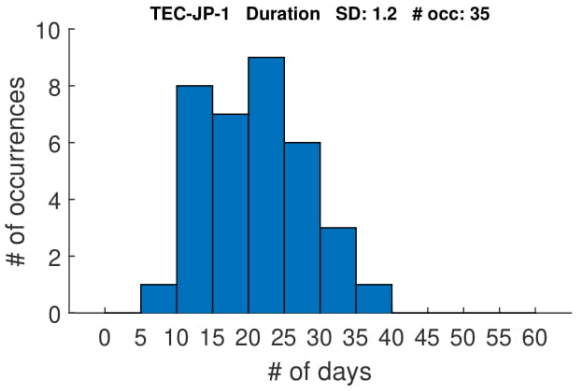

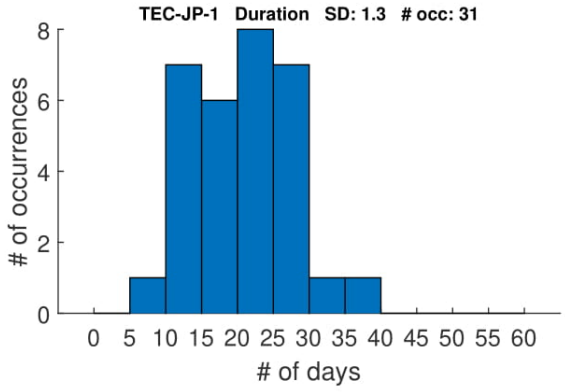

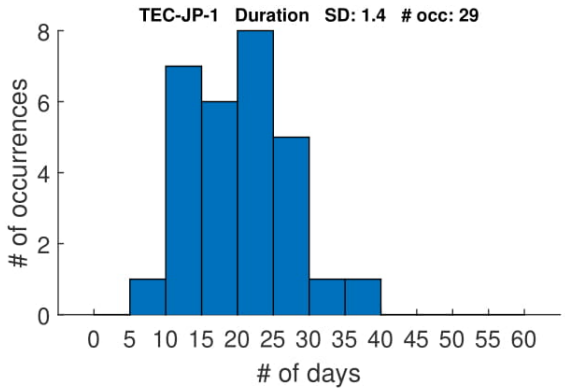

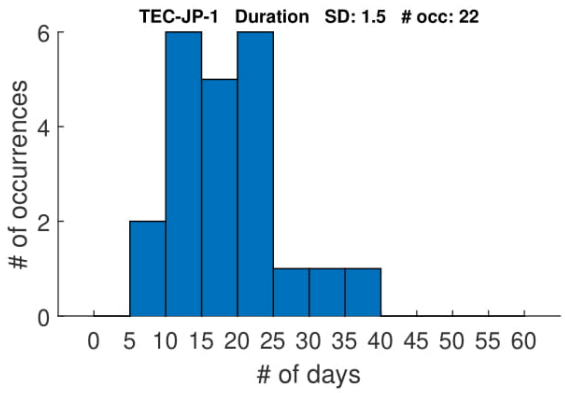

Eliminating Solar

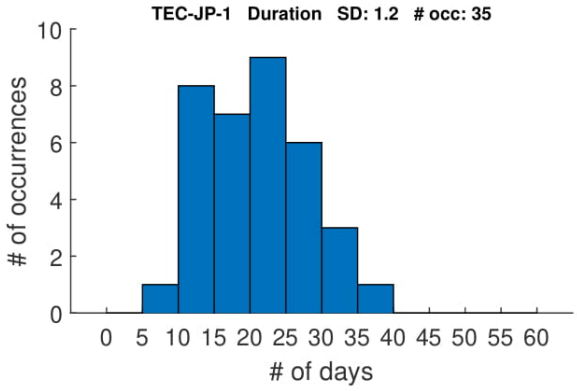

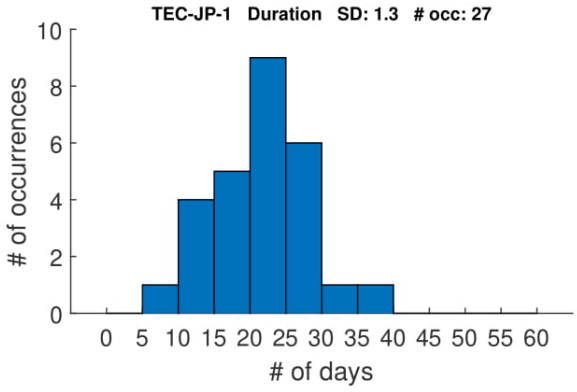

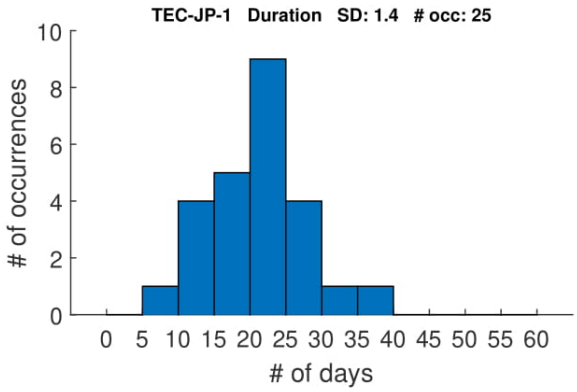

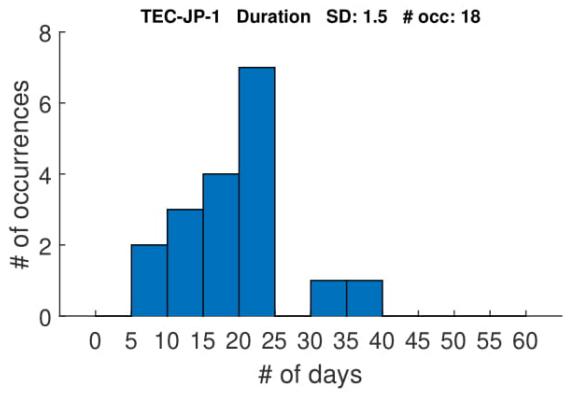

With Solar

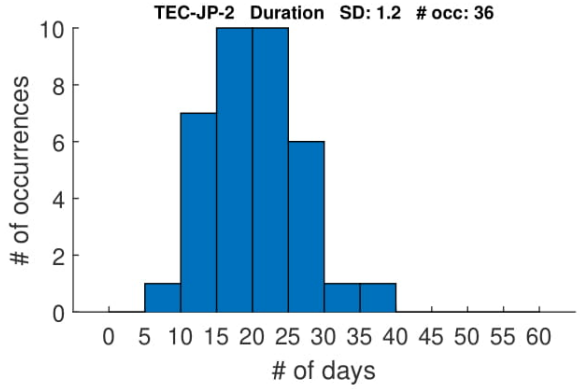

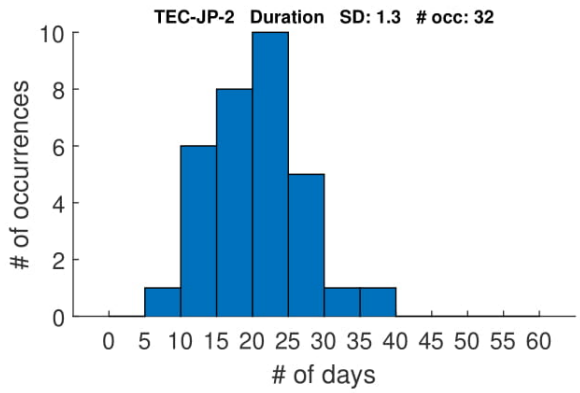

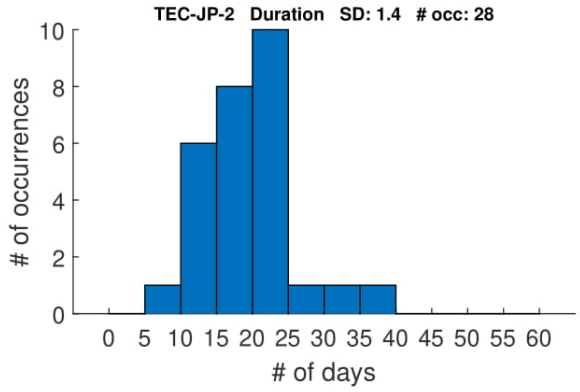

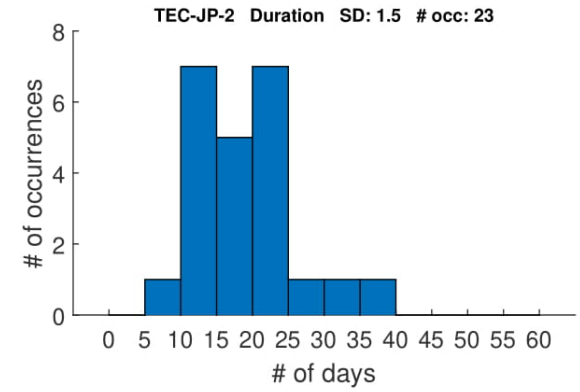

Eliminating Solar

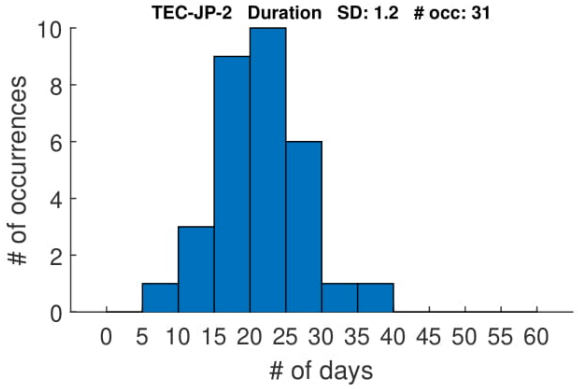

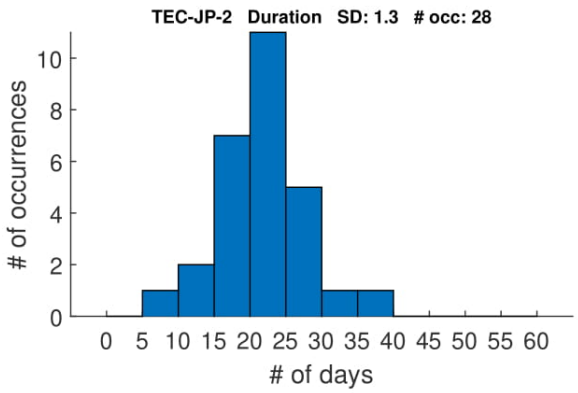

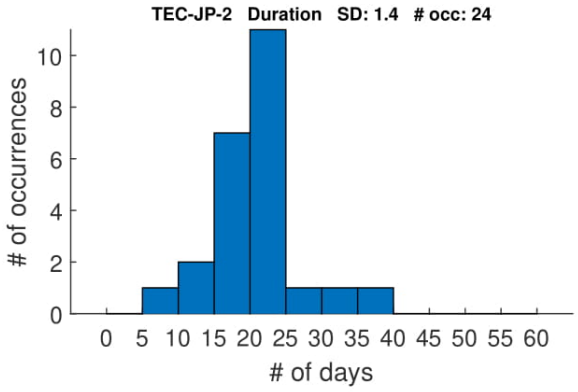

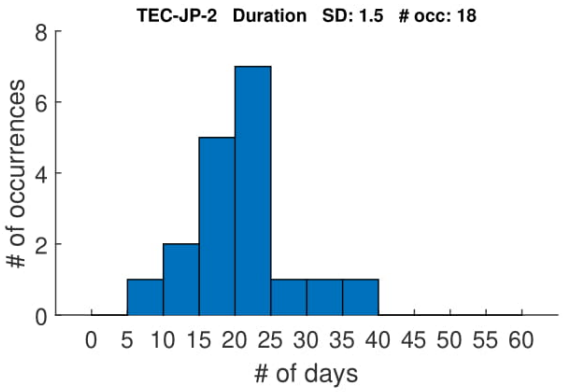

With Solar

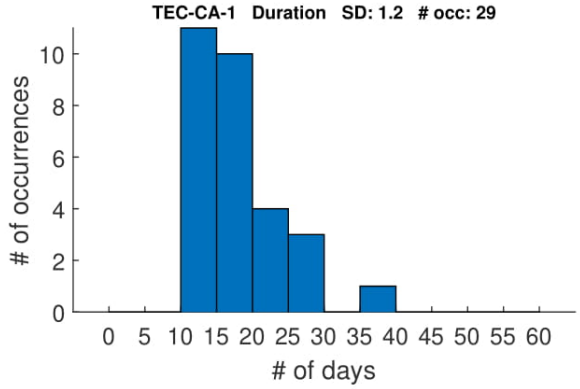

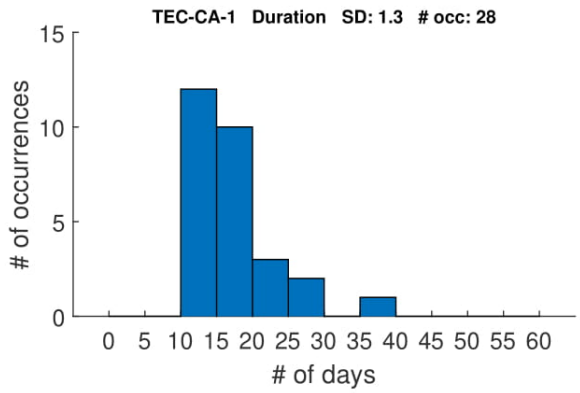

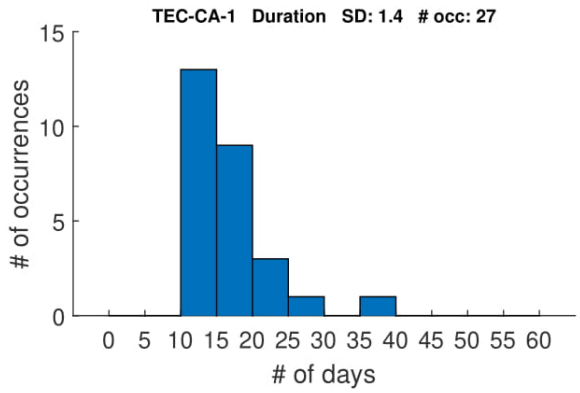

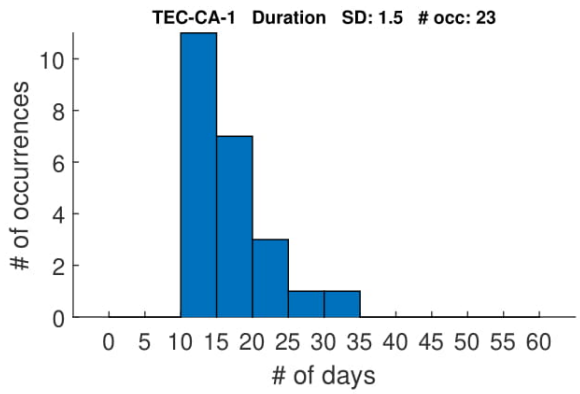

Eliminating Solar

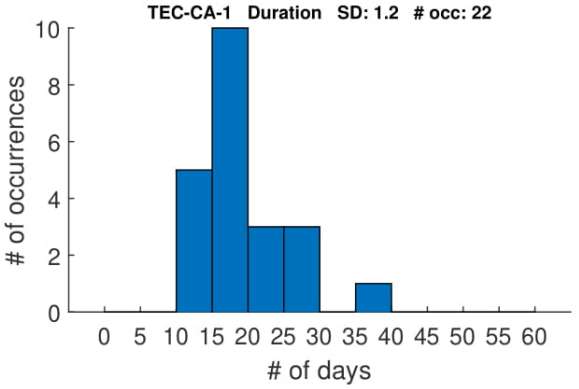

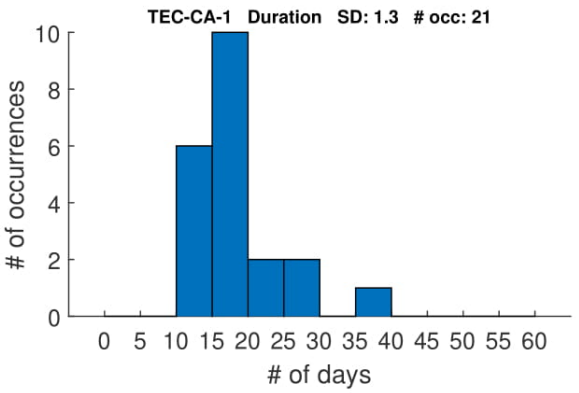

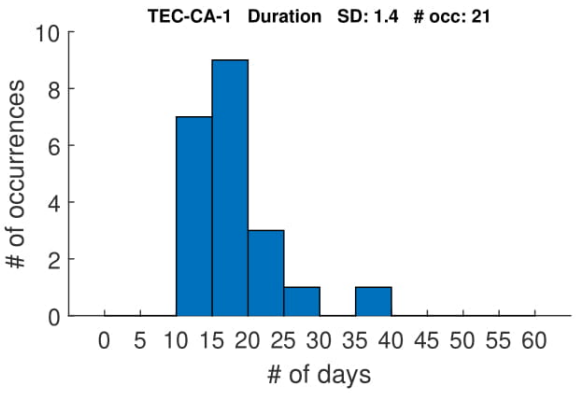

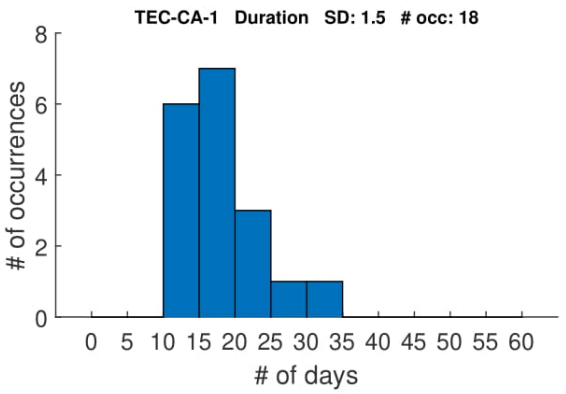

With Solar

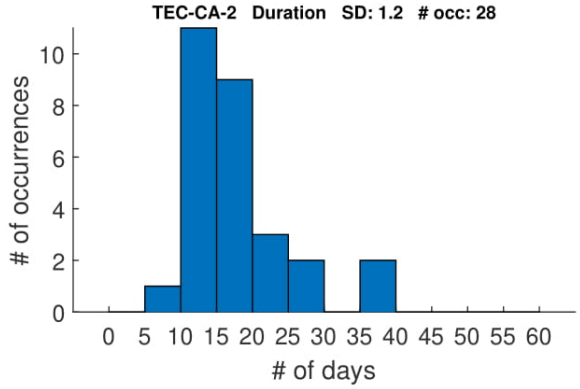

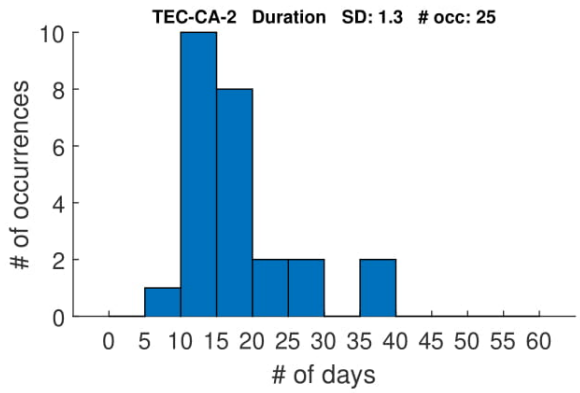

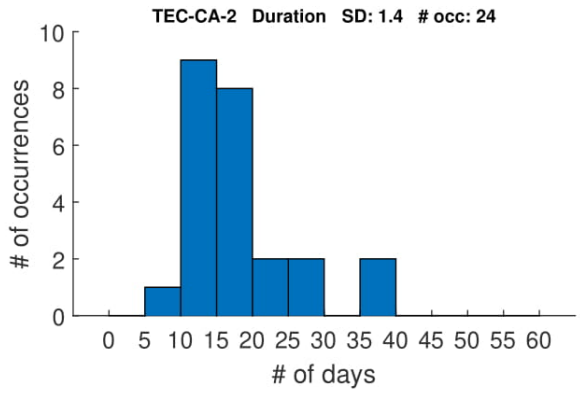

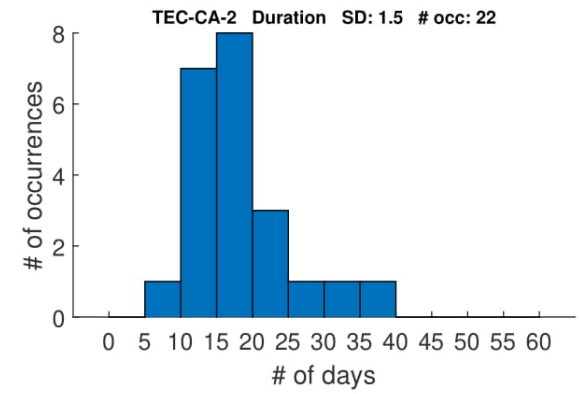

Eliminating Solar

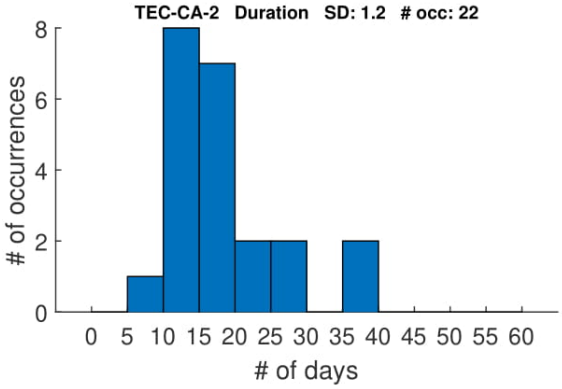

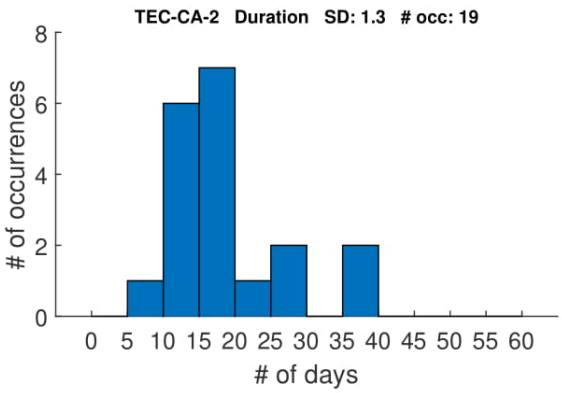

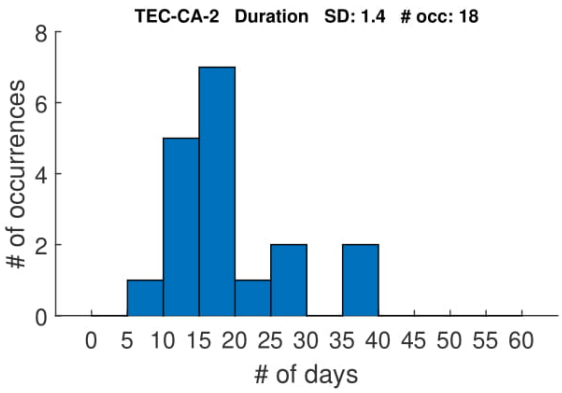

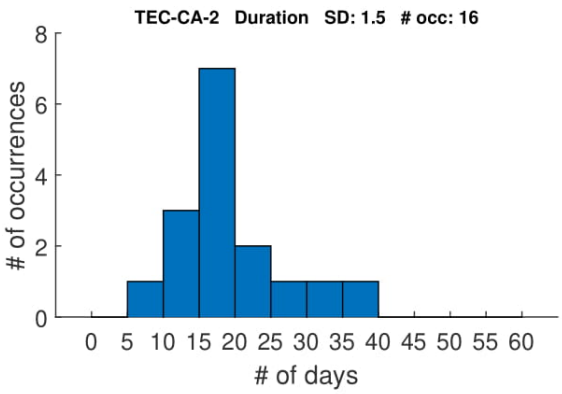

With Solar

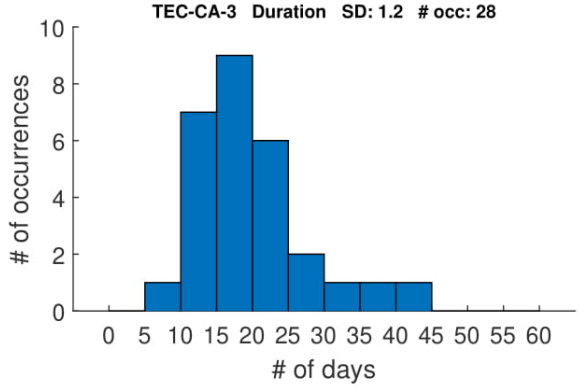

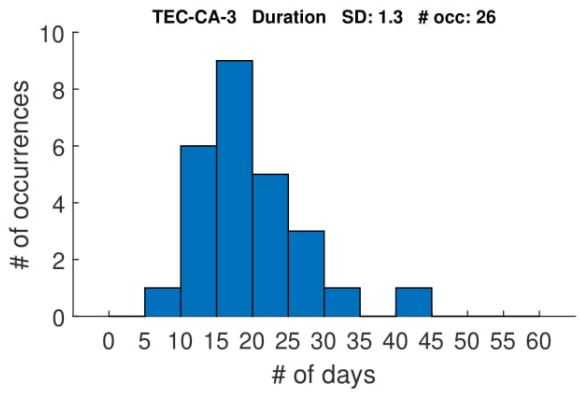

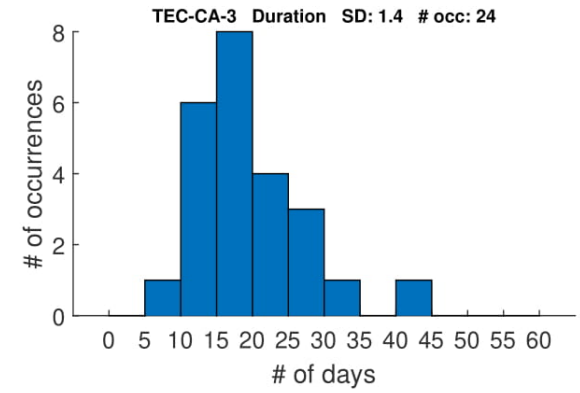

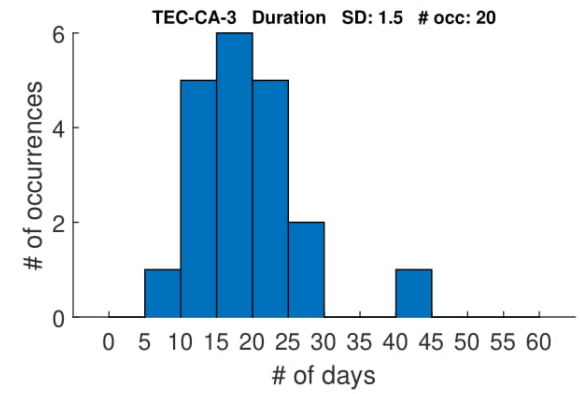

Eliminating Solar

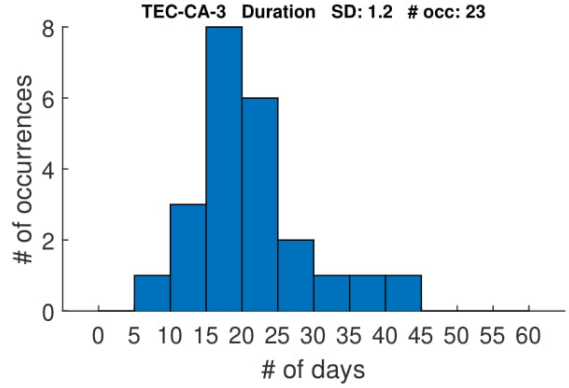

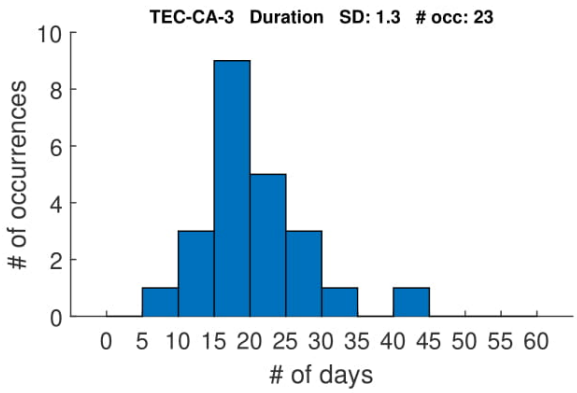

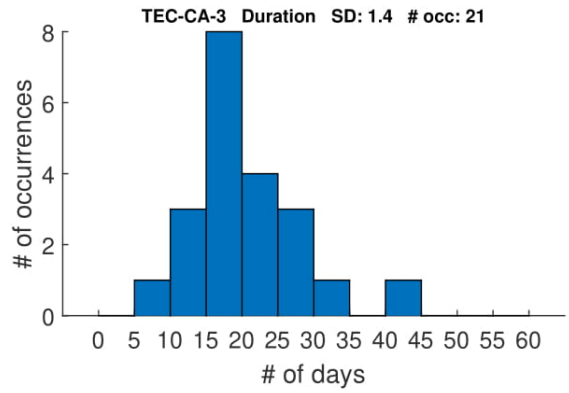

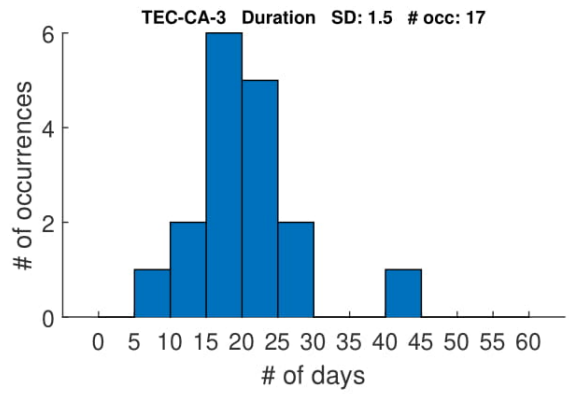

With Solar

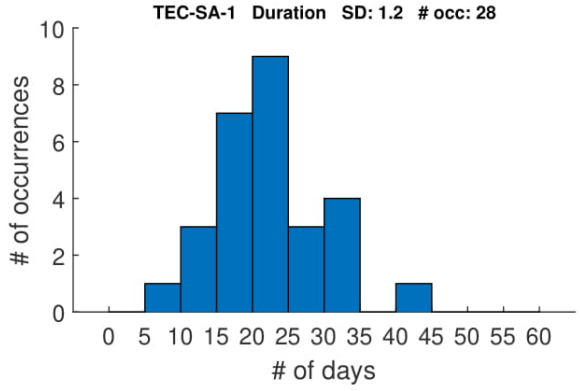

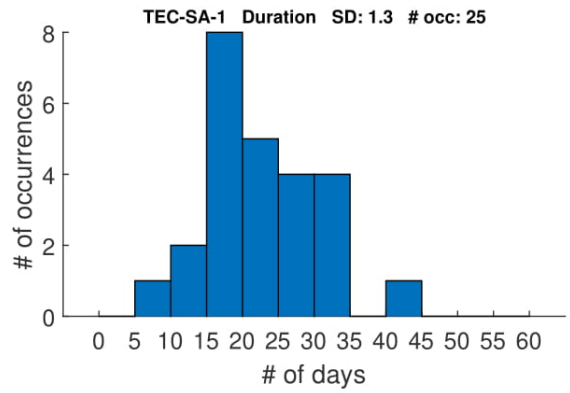

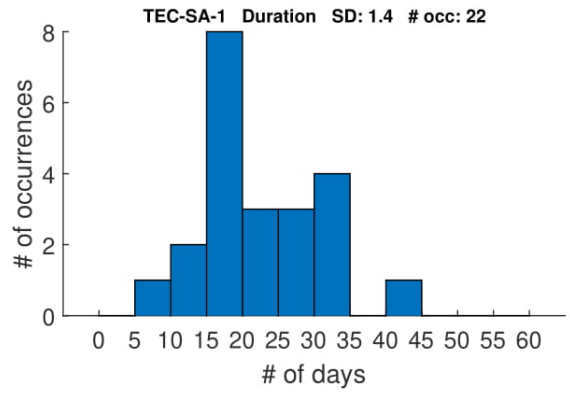

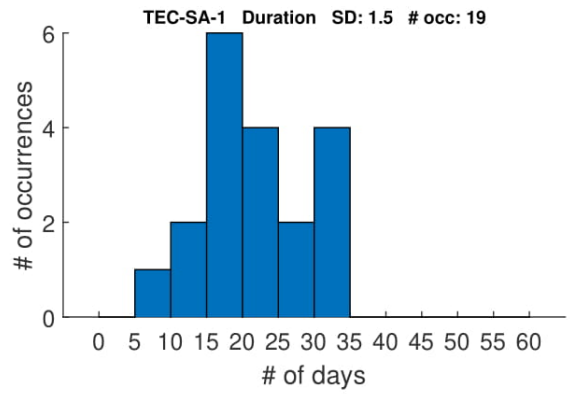

Eliminating Solar

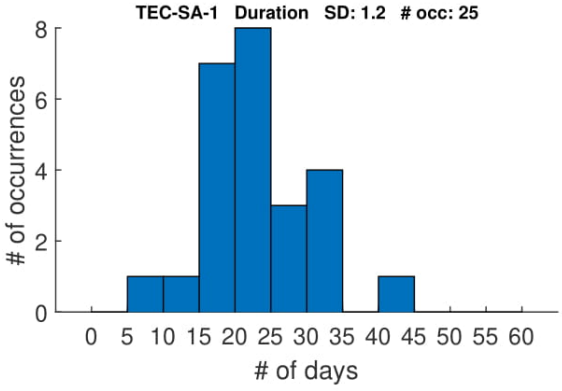

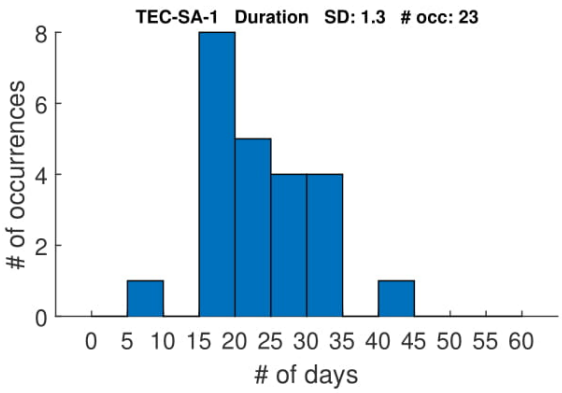

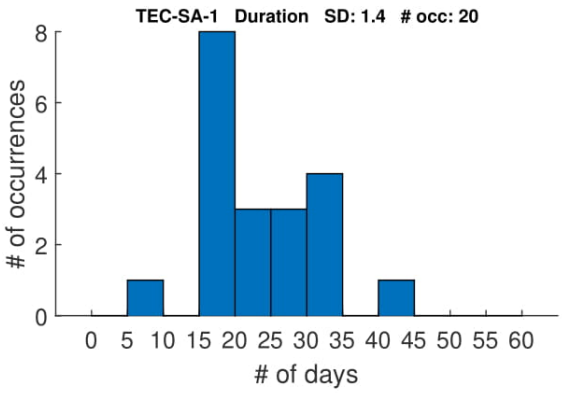

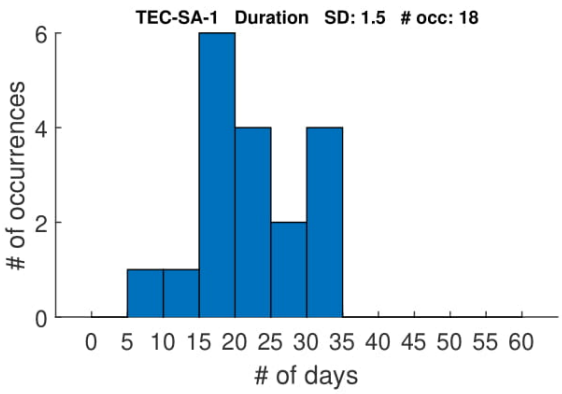

With Solar

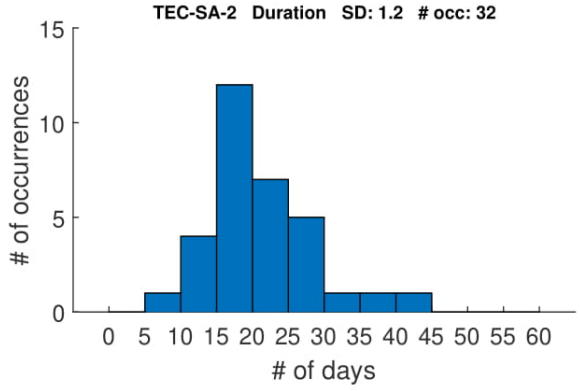

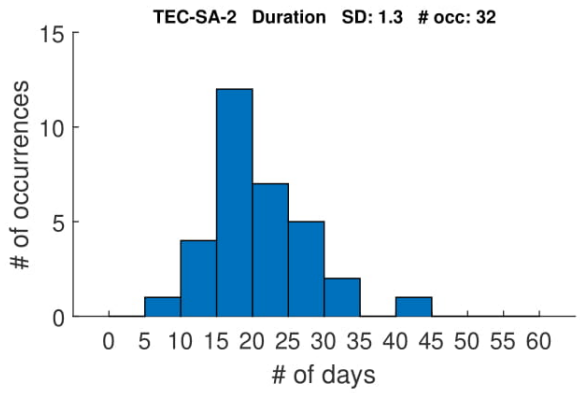

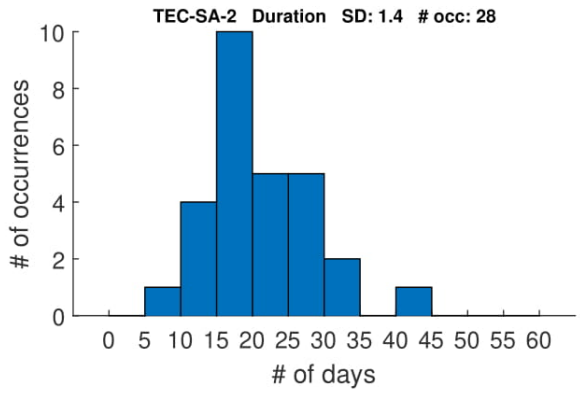

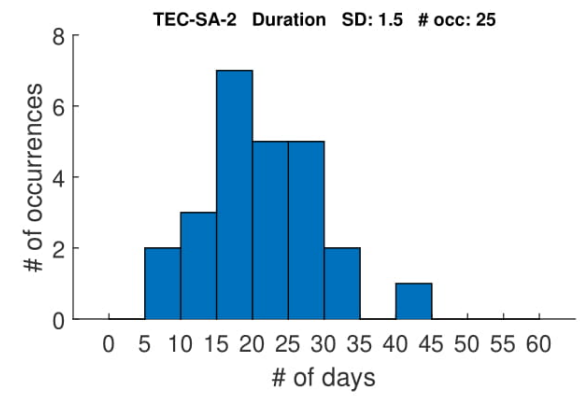

Eliminating Solar

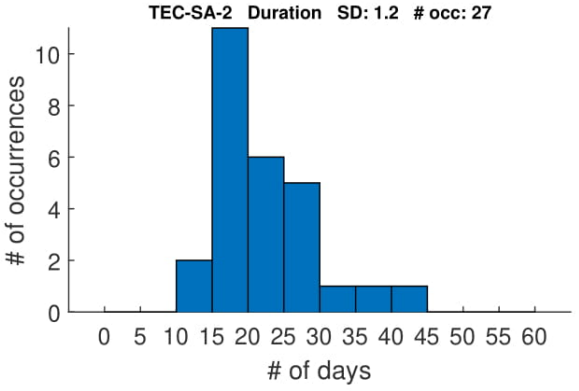

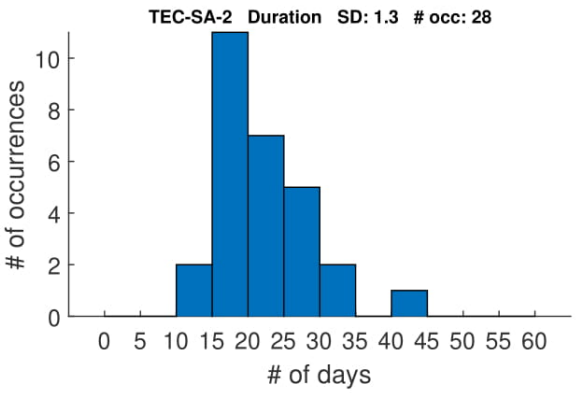

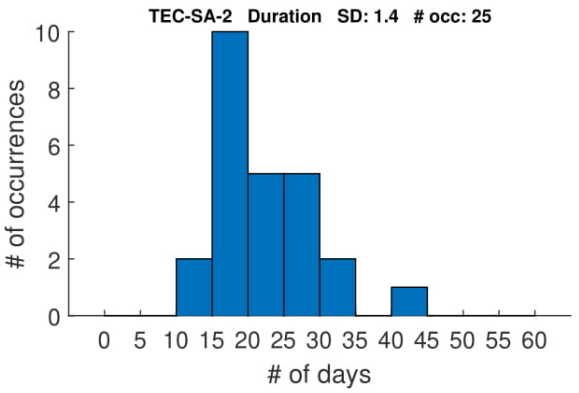

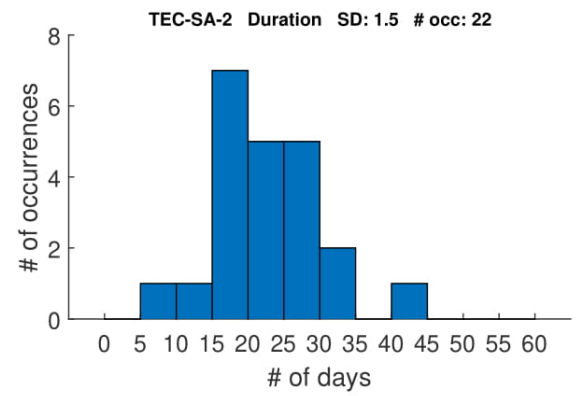

With Solar

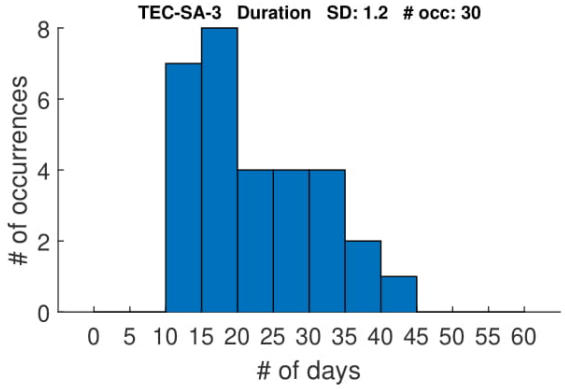

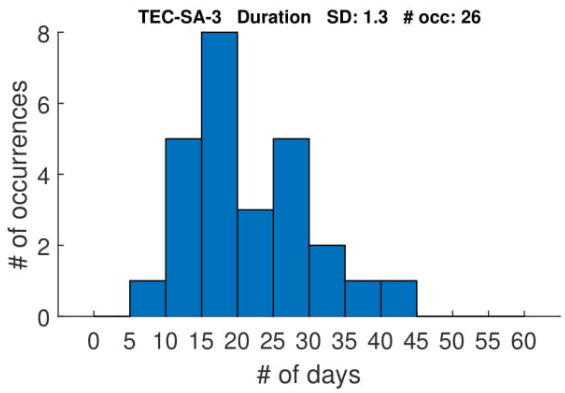

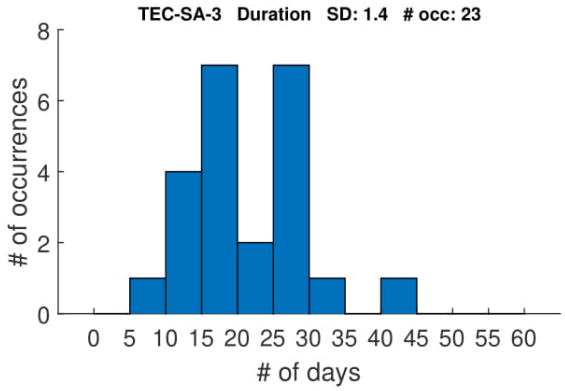

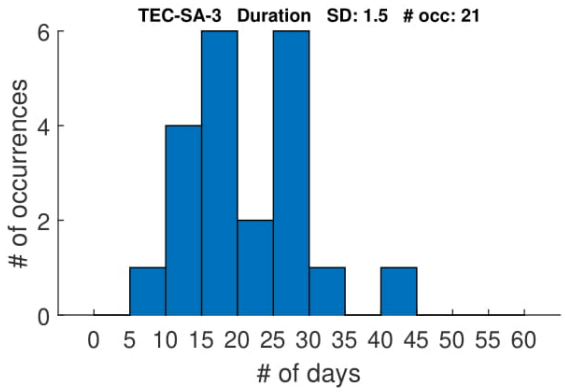

Eliminating Solar

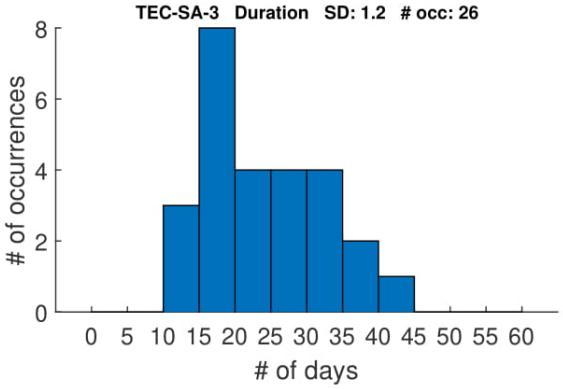

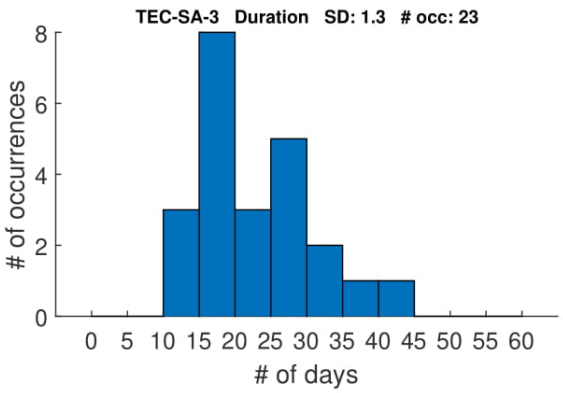

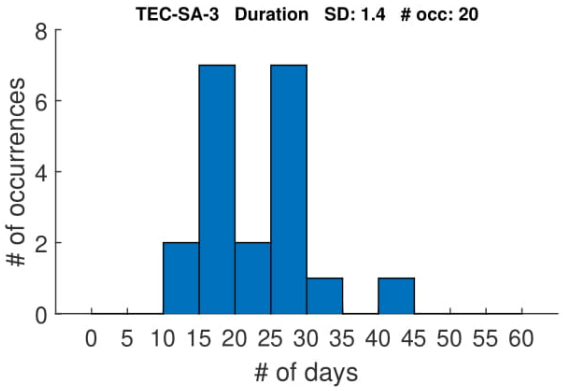

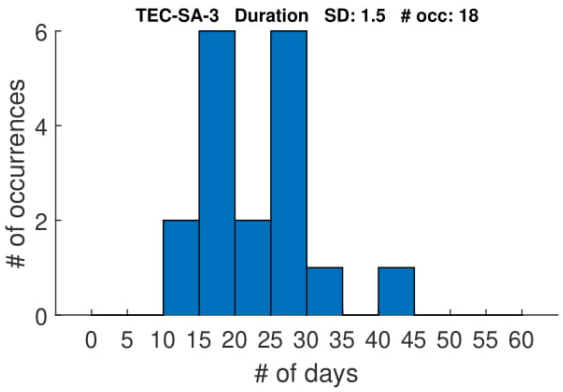

With Solar

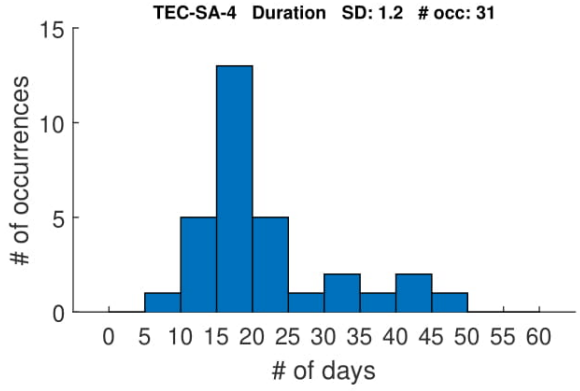

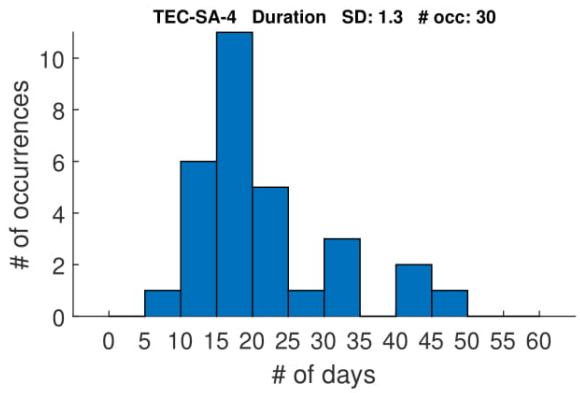

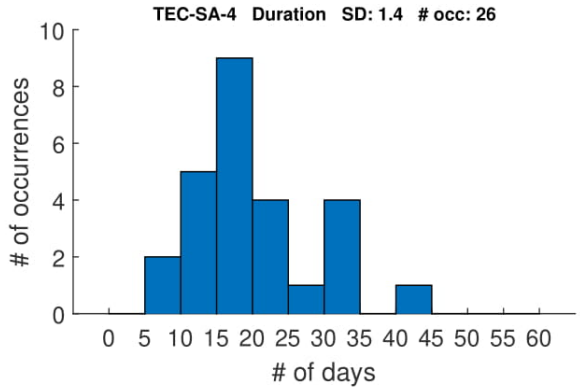

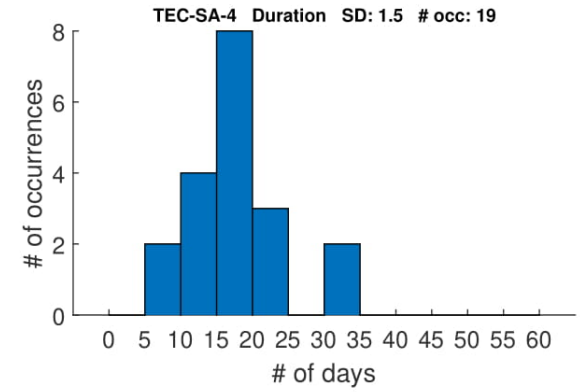

Eliminating Solar

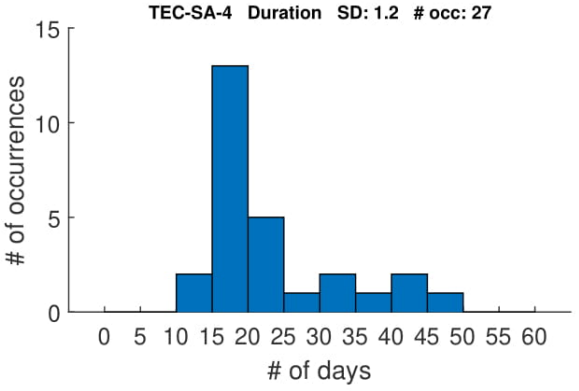

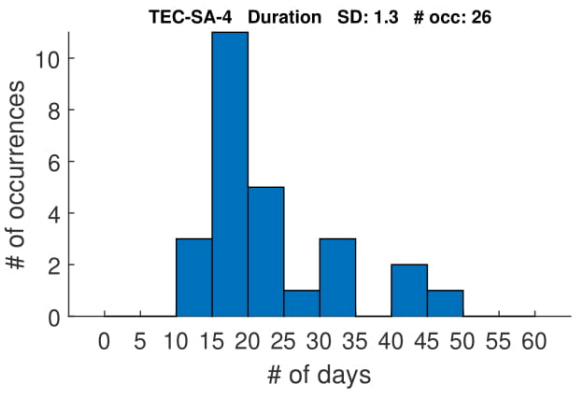

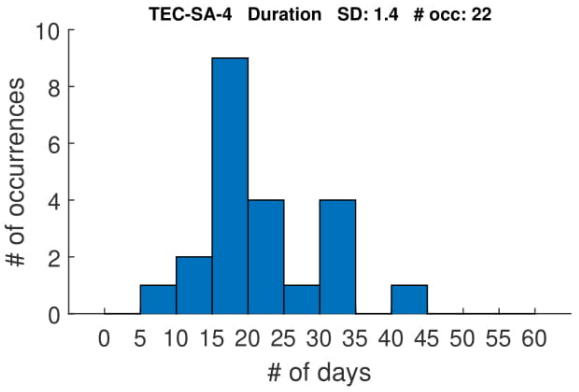

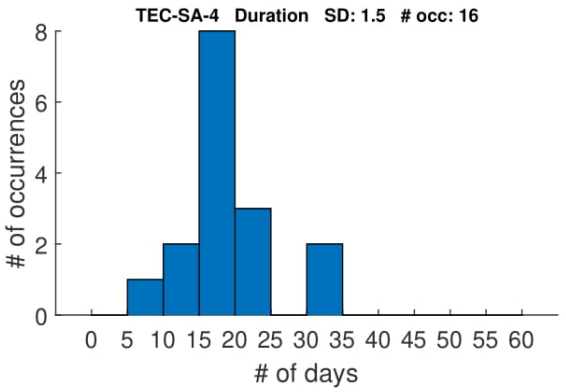

B.2 Planetary Wave Amplitude

This section contains the planetary wave amplitude histograms described in Sections 3.3.2 and 4.2.

B.2.1 Upper Latitude Band

These histograms only use the SABER events in the Upper latitude band, 20 to 45 degrees.

With Solar

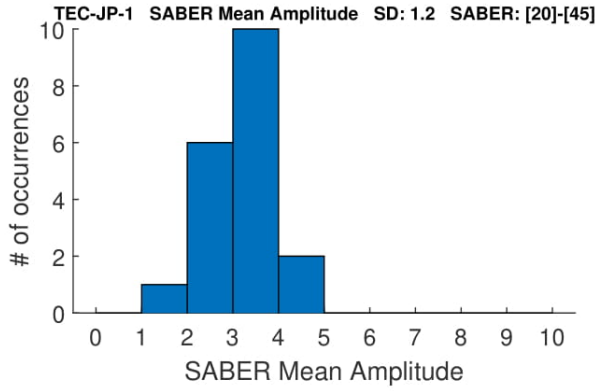

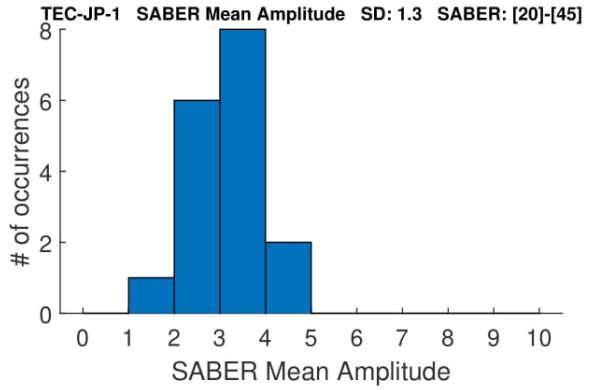

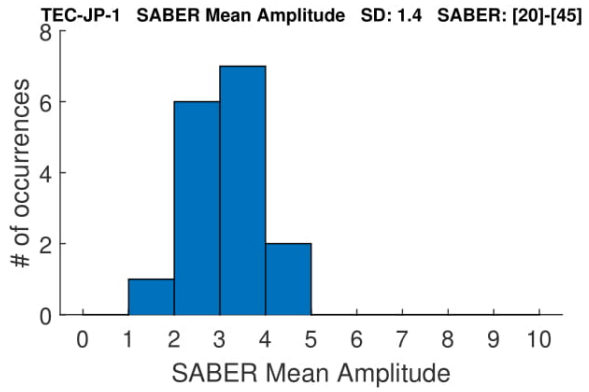

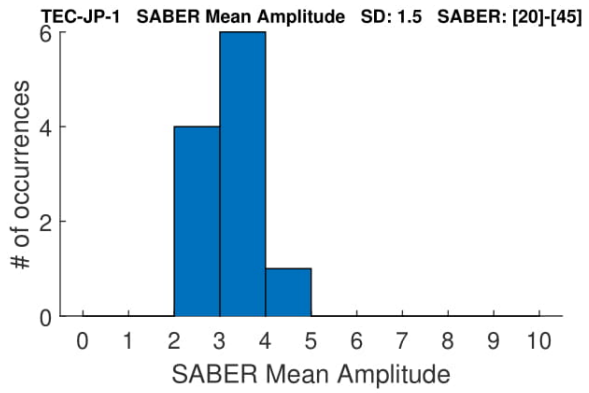

Eliminating Solar

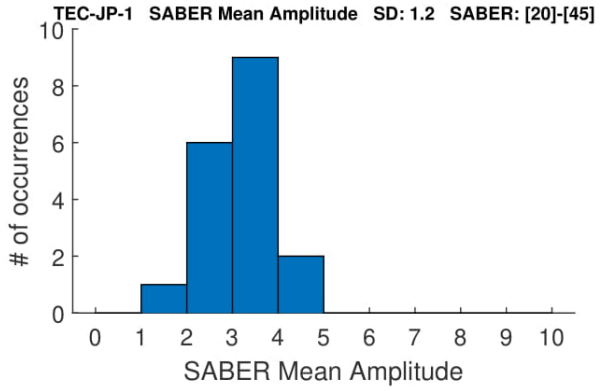

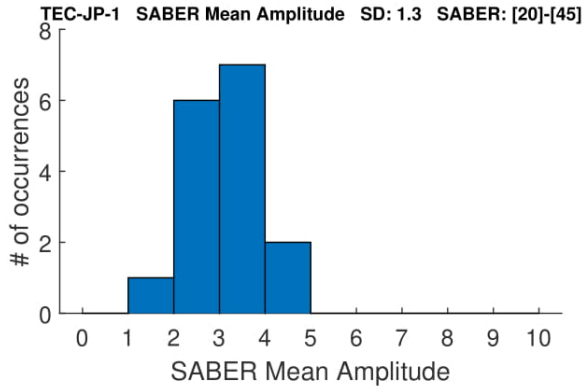

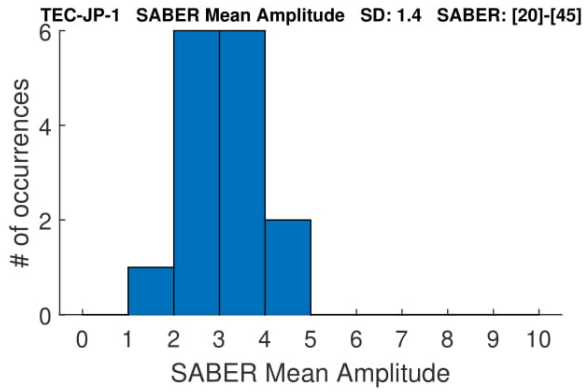

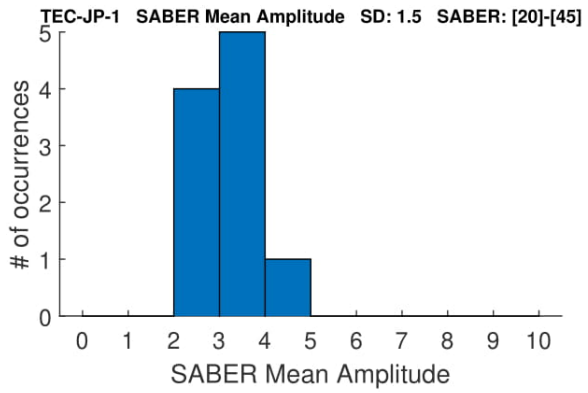

With Solar

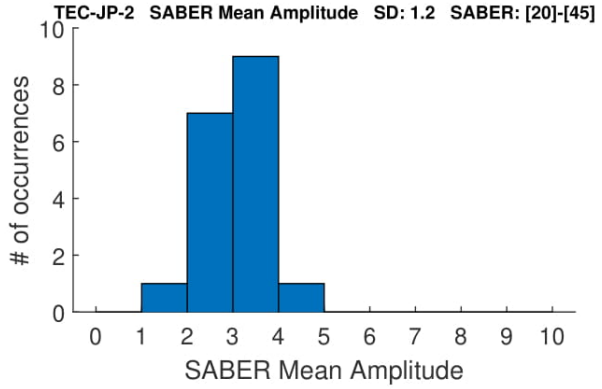

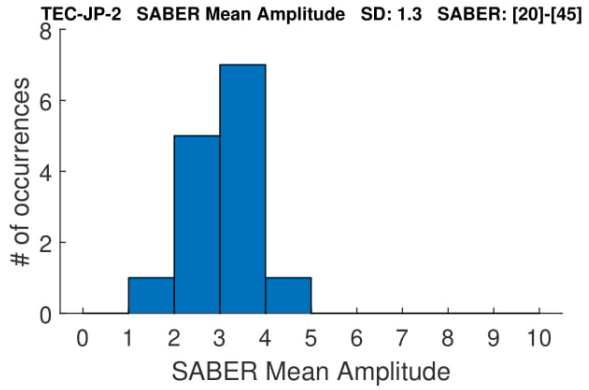

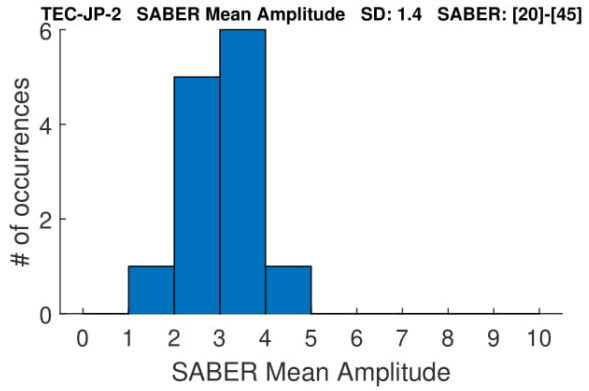

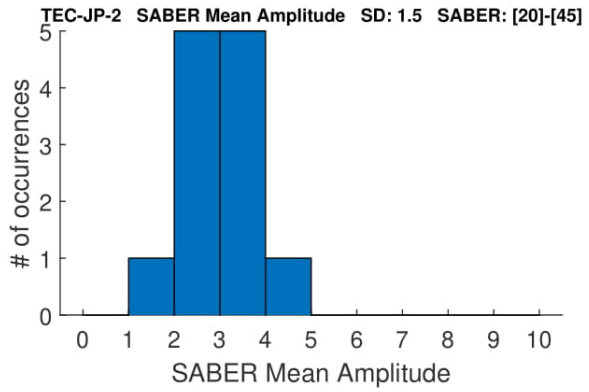

Eliminating Solar

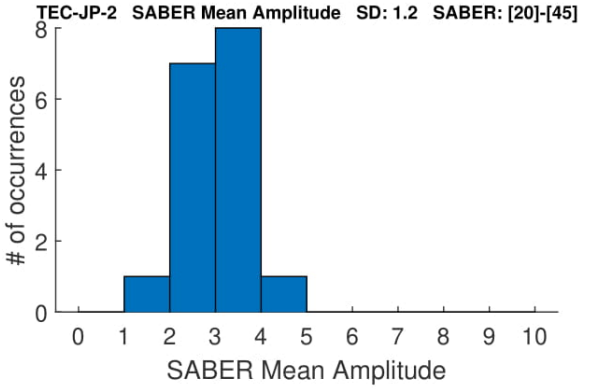

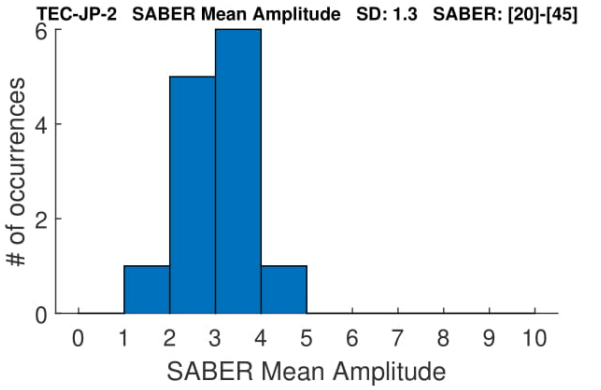

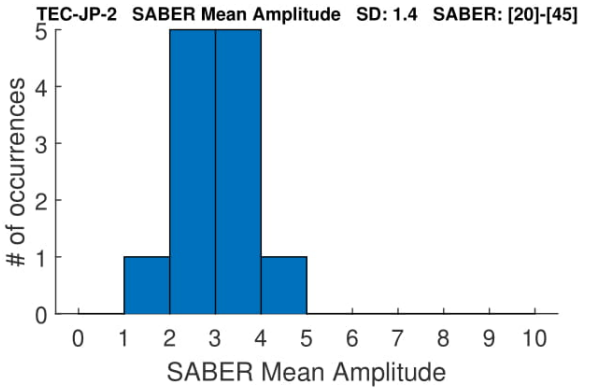

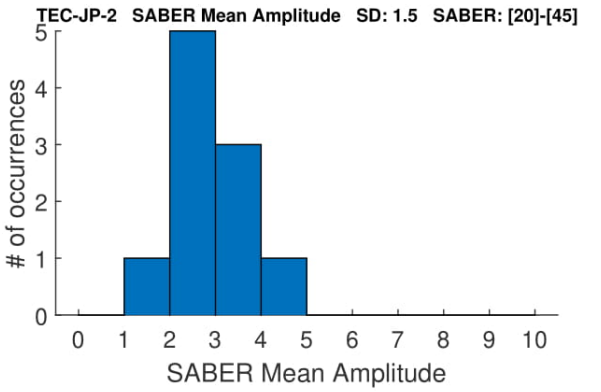

With Solar

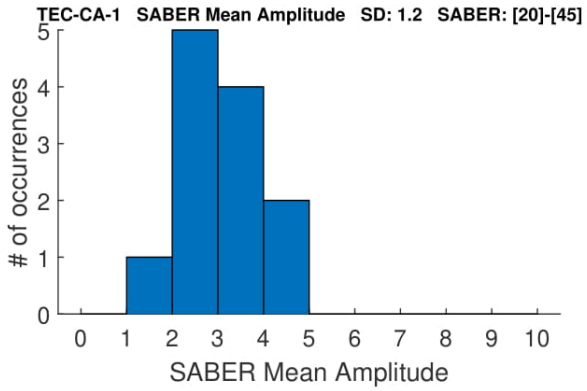

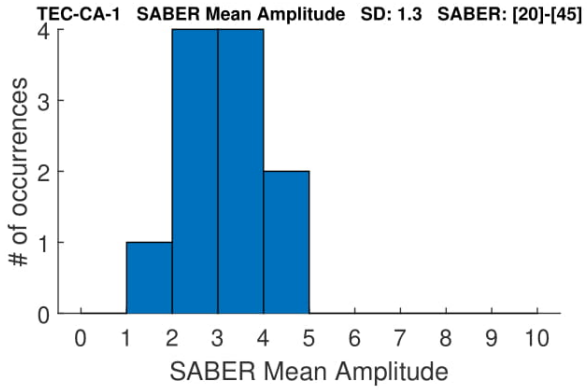

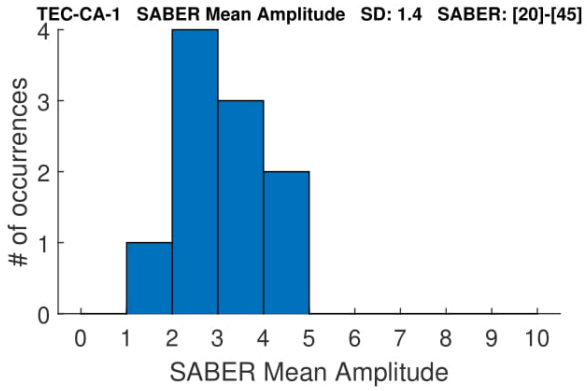

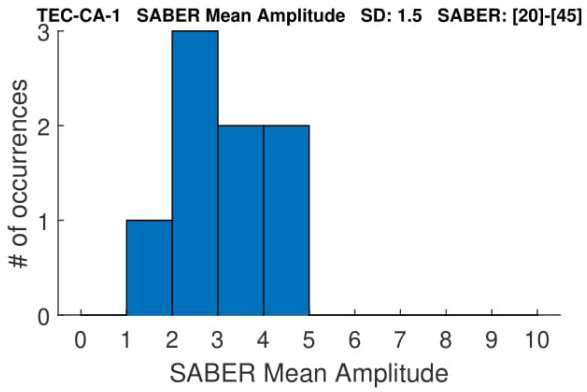

Eliminating Solar

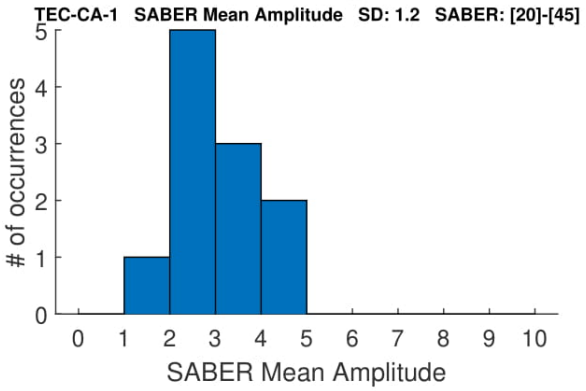

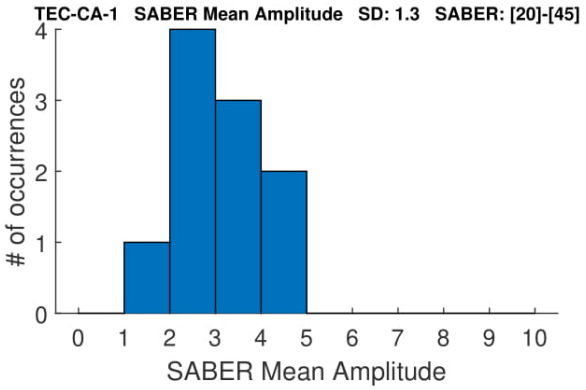

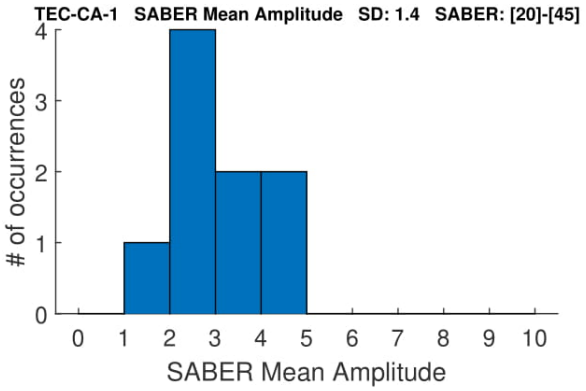

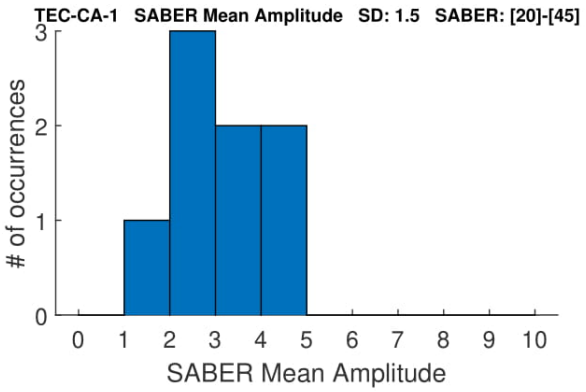

With Solar

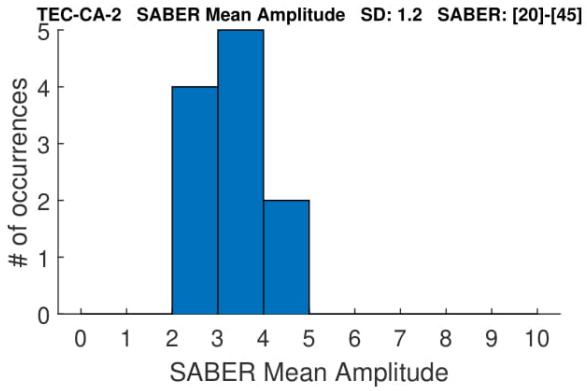

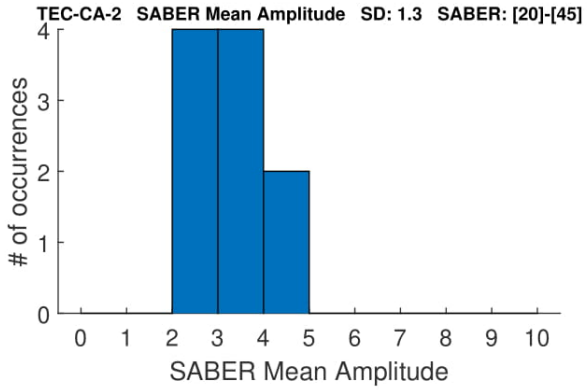

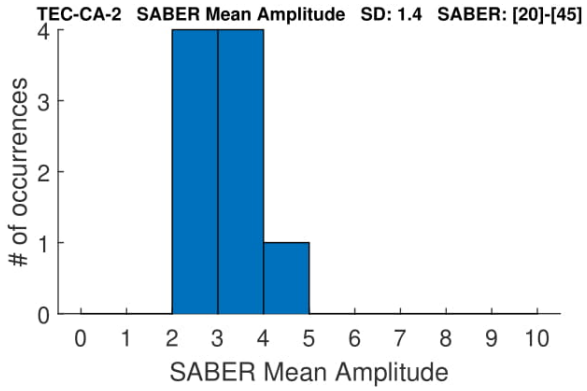

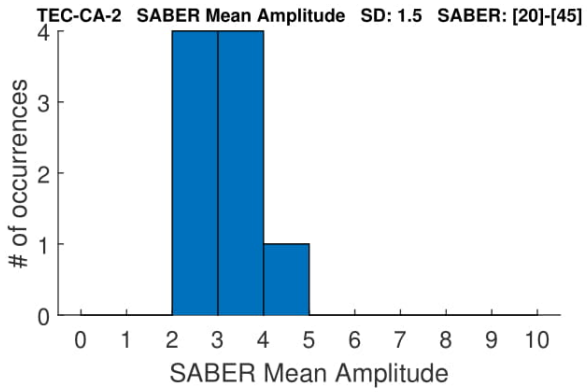

Eliminating Solar

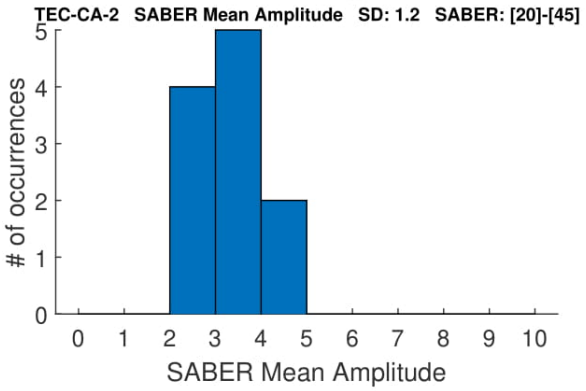

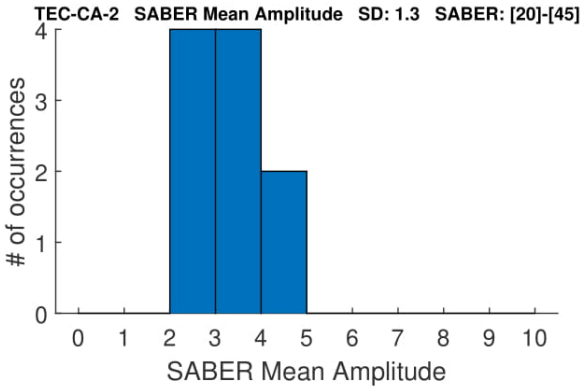

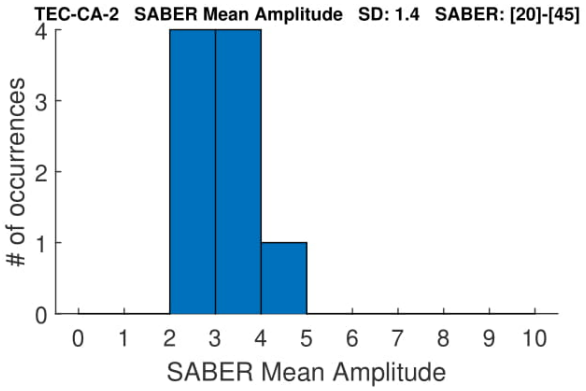

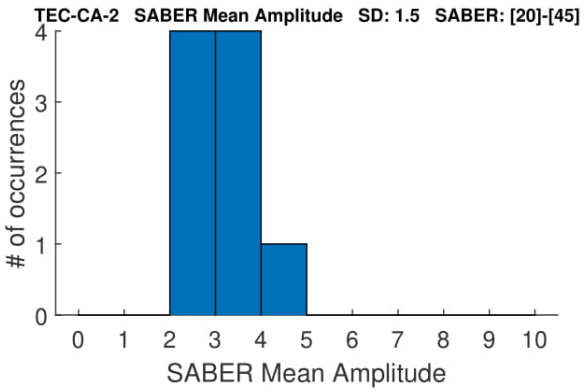

With Solar

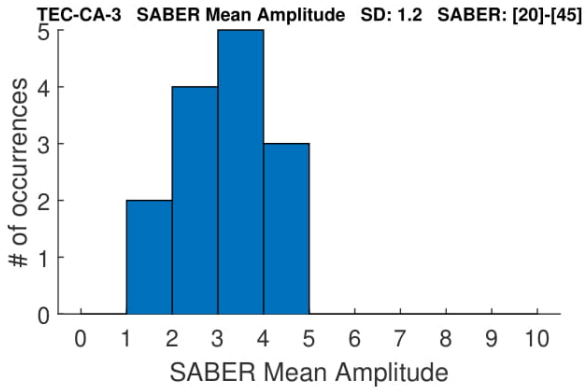

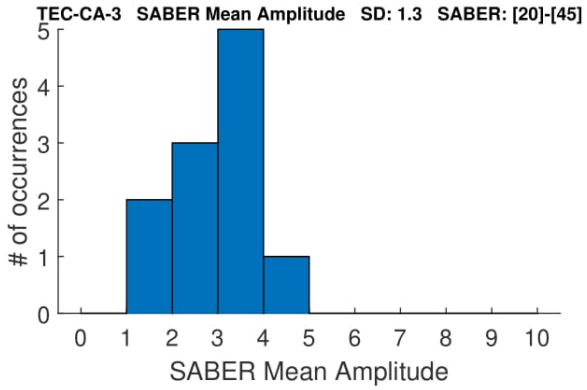

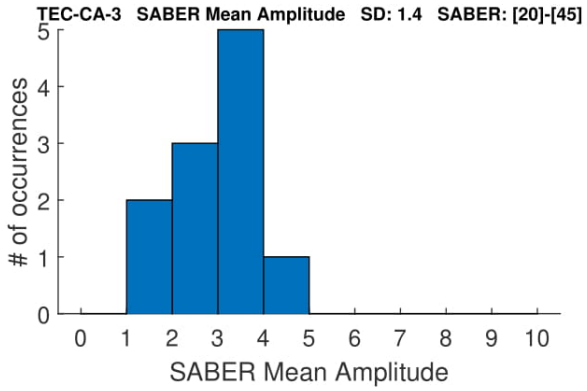

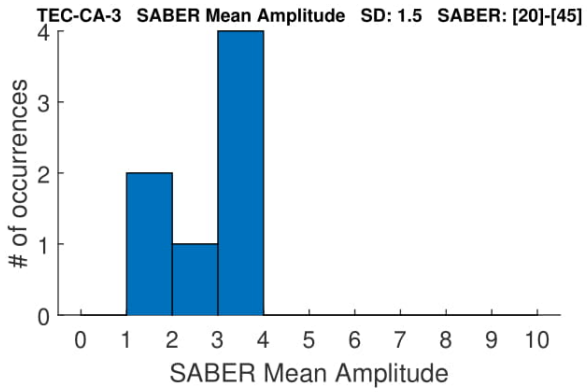

Eliminating Solar

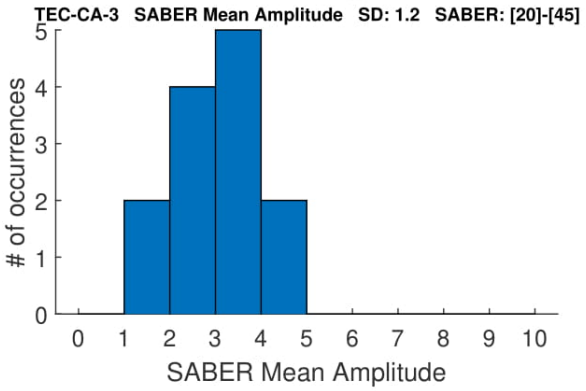

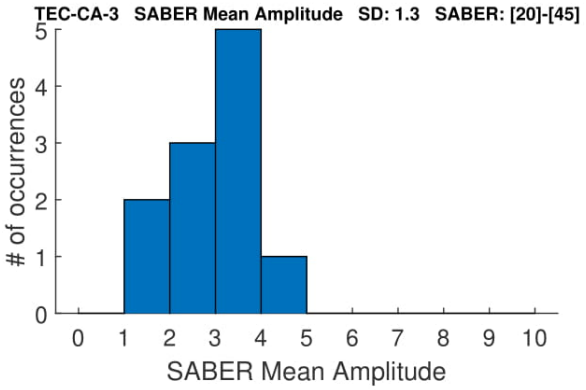

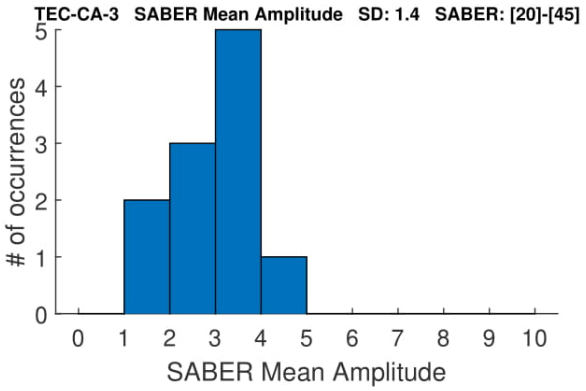

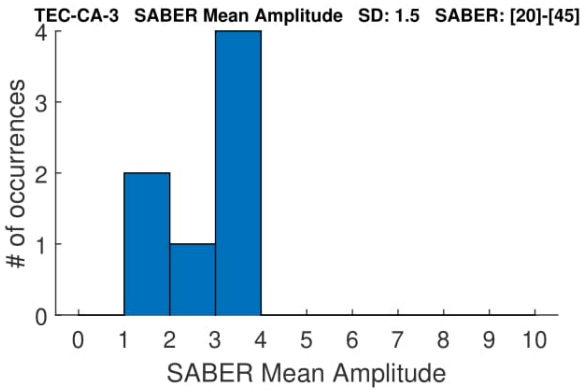

With Solar

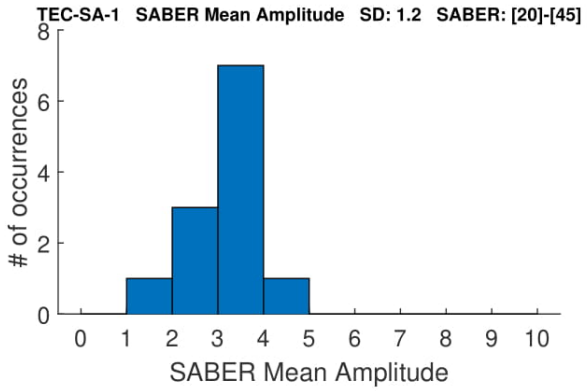

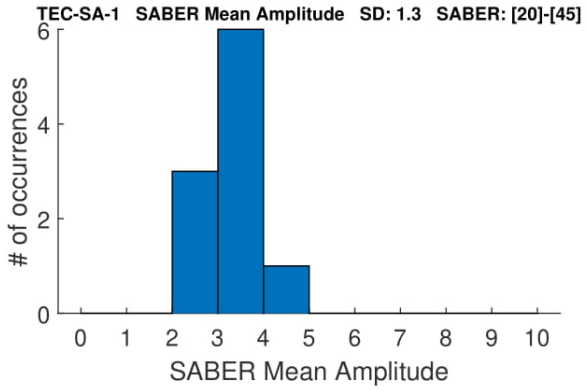

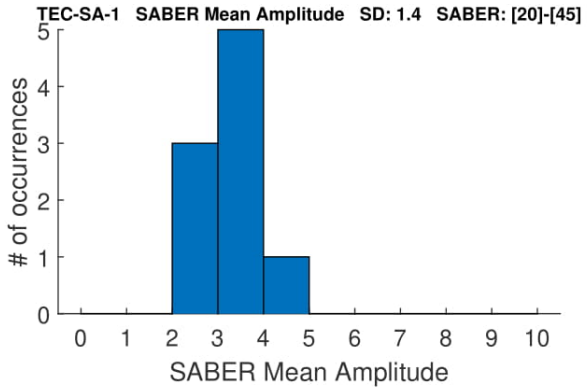

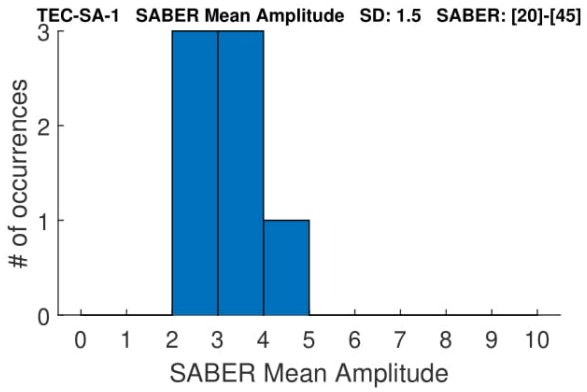

Eliminating Solar

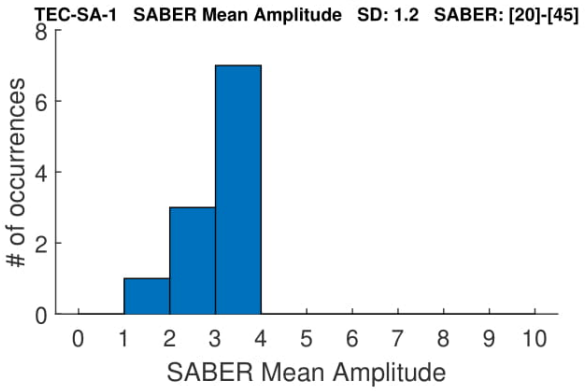

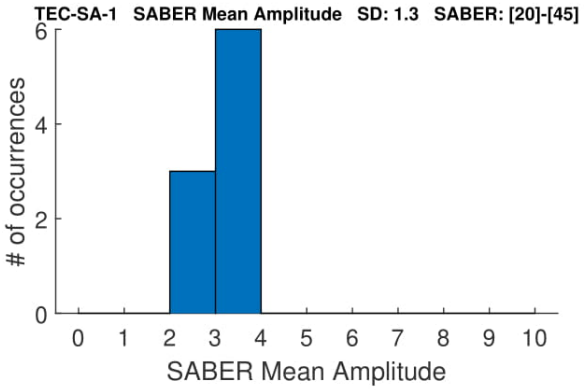

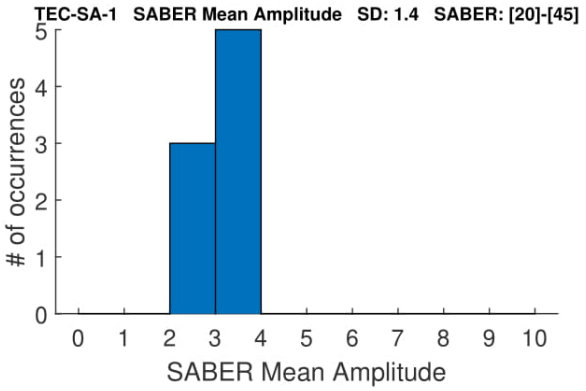

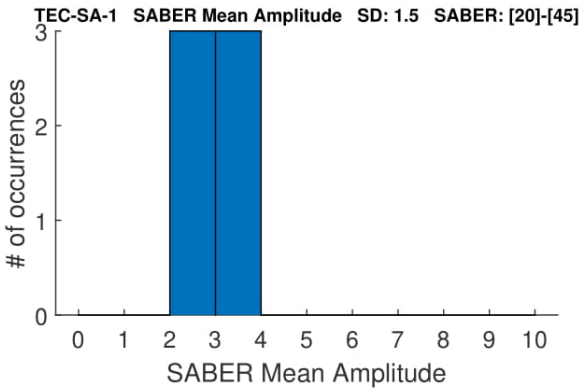

With Solar

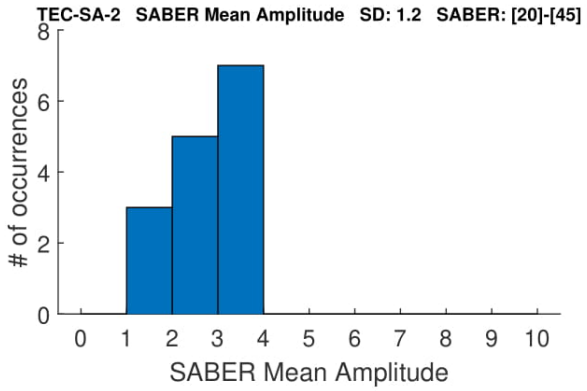

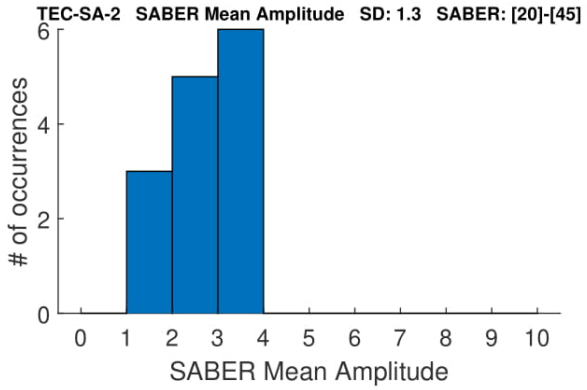

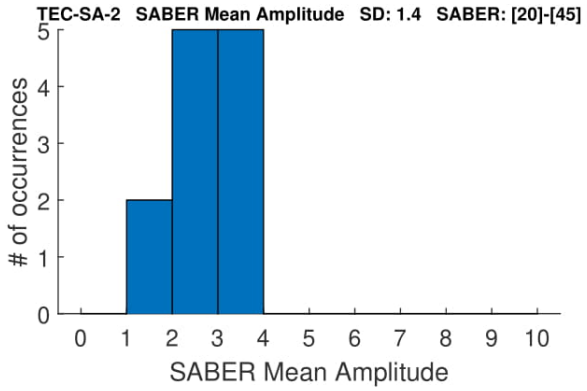

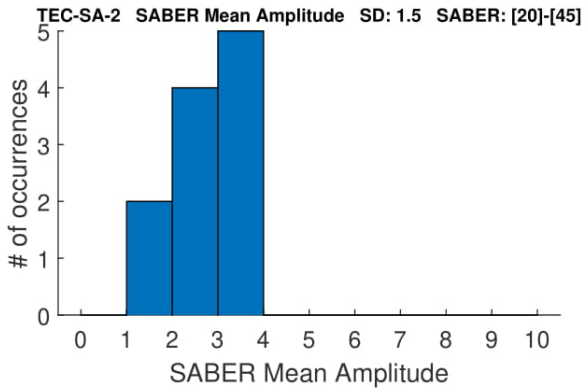

Eliminating Solar

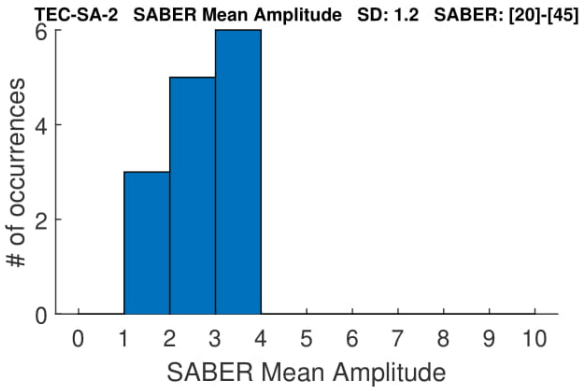

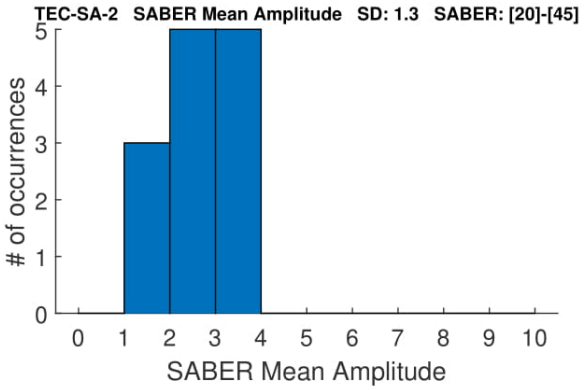

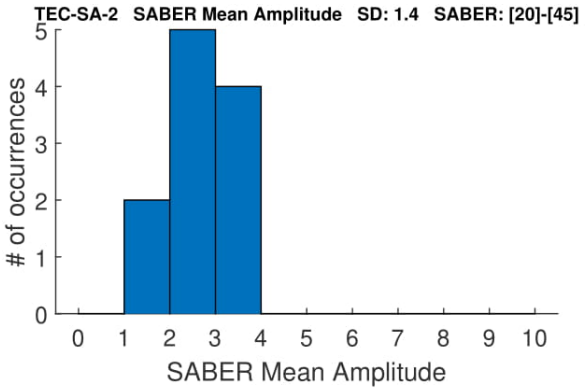

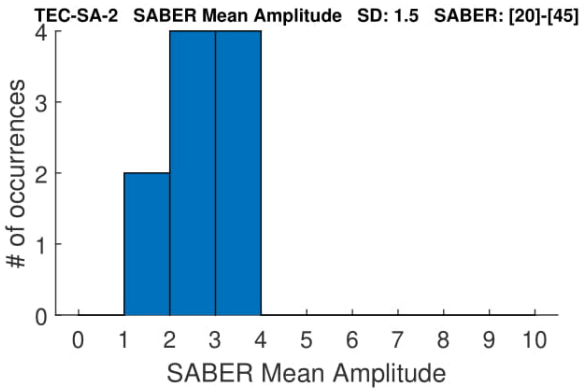

With Solar

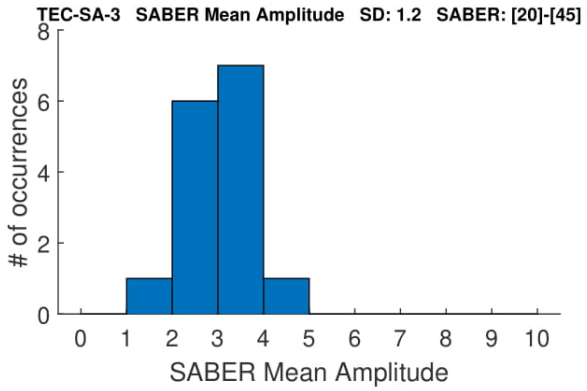

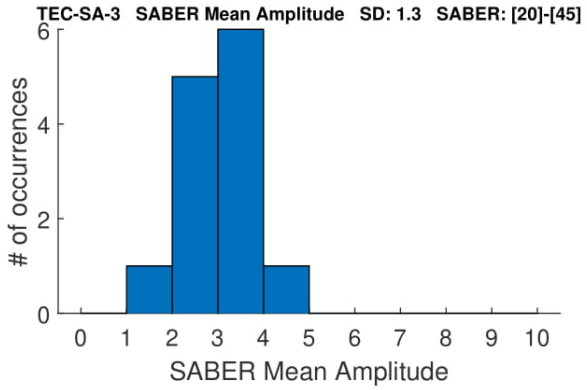

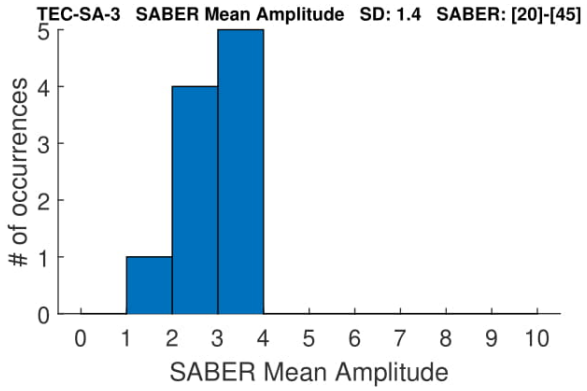

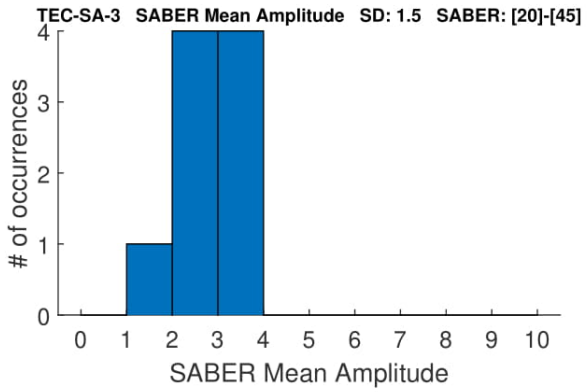

Eliminating Solar

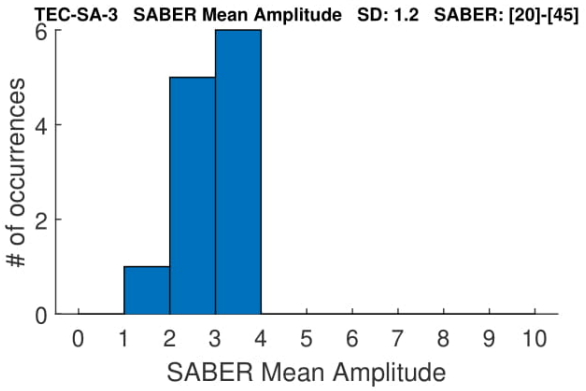

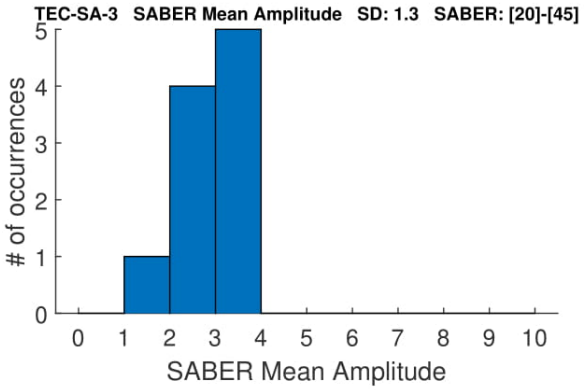

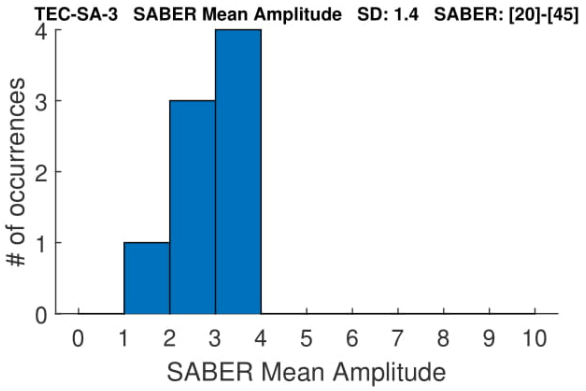

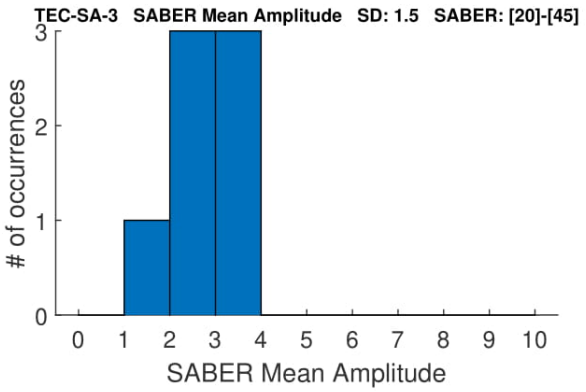

With Solar

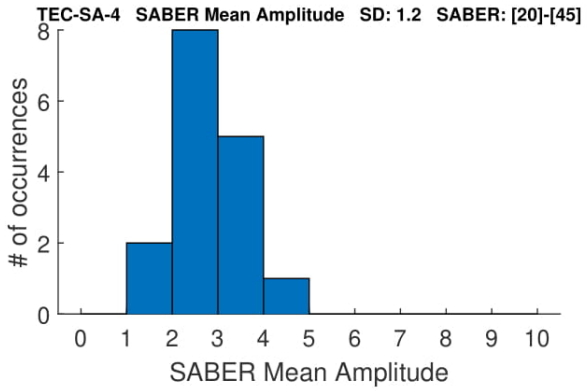

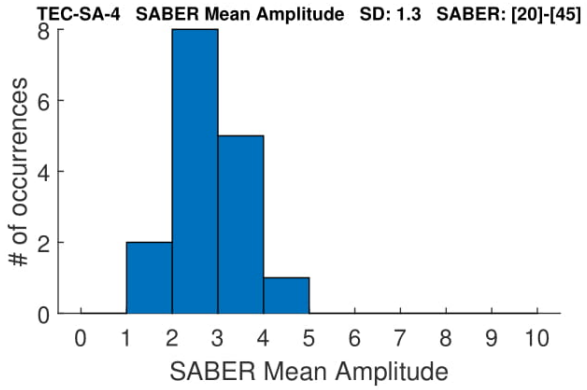

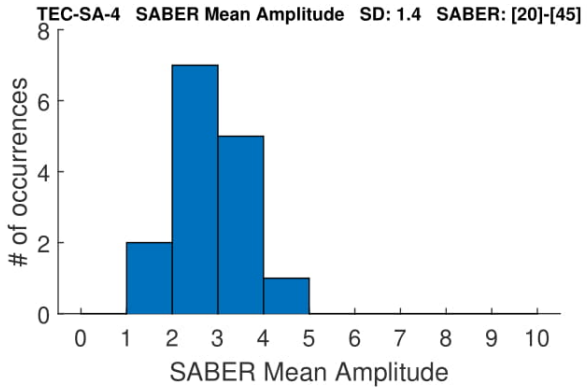

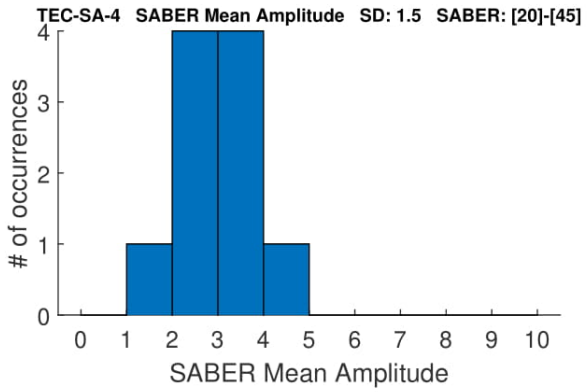

Eliminating Solar

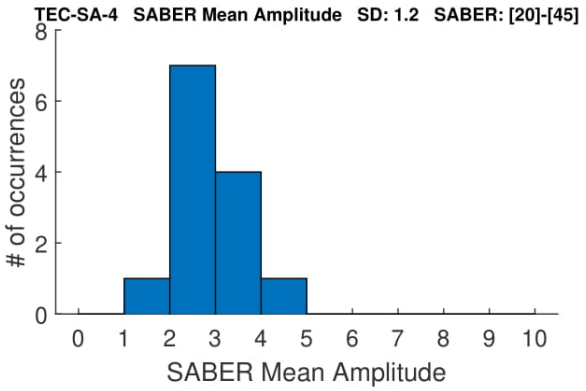

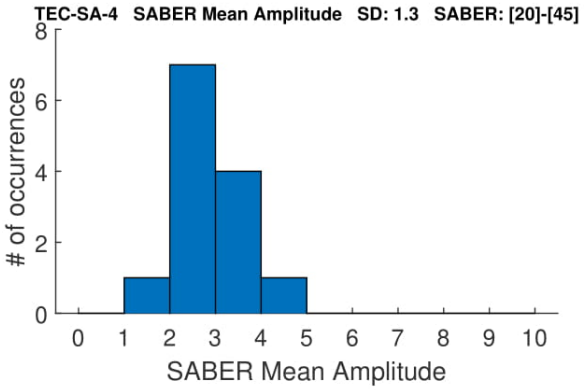

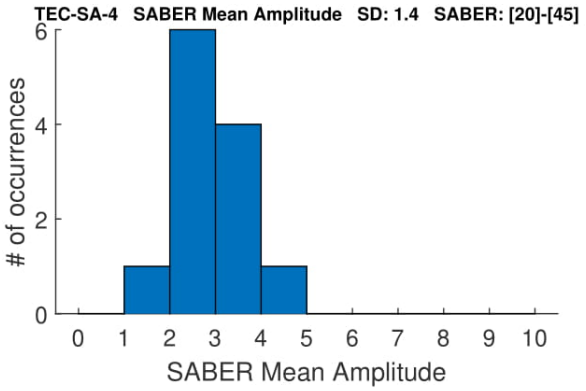

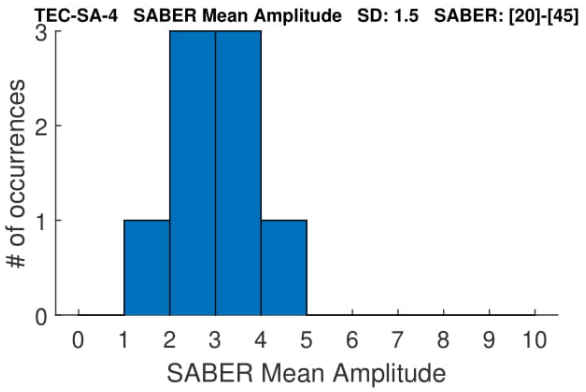

B.2.2 Middle Latitude Band

These histograms only use the SABER events in the Middle latitude band, -20 to 20 degrees.

With Solar

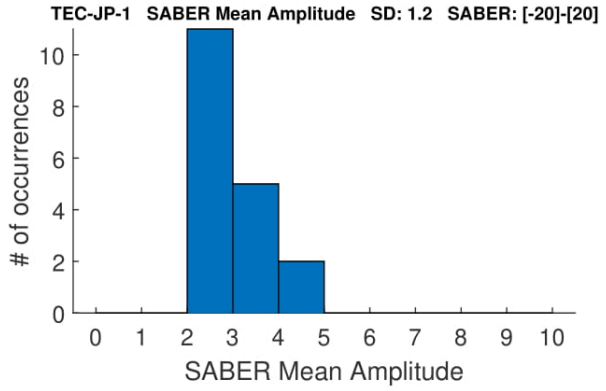

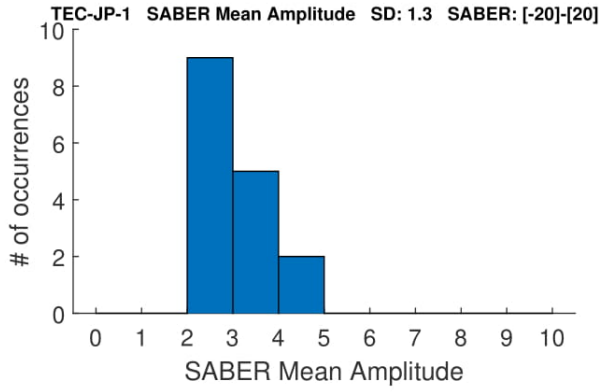

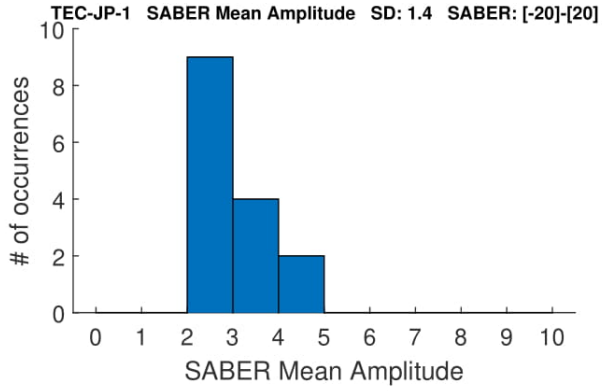

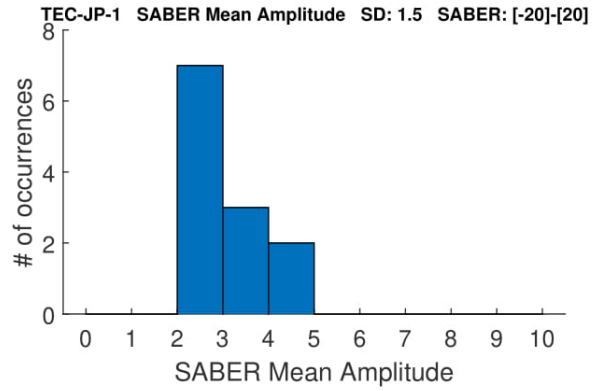

Eliminating Solar

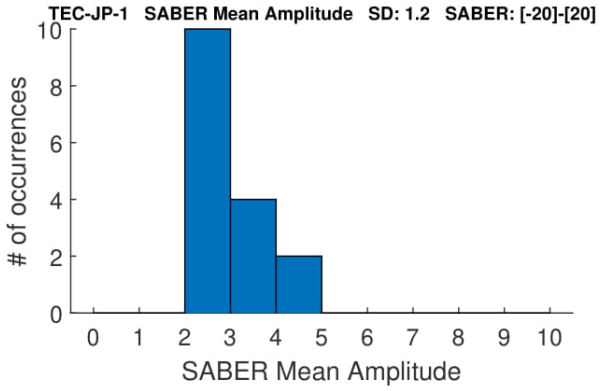

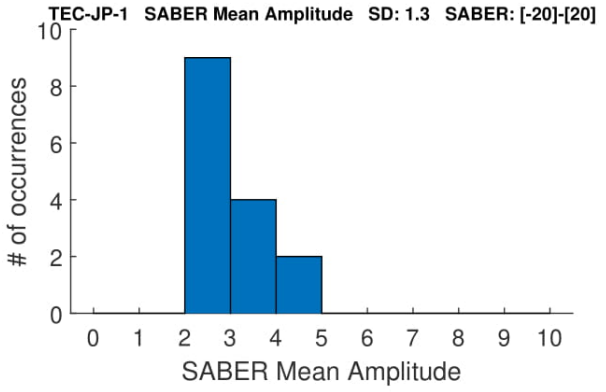

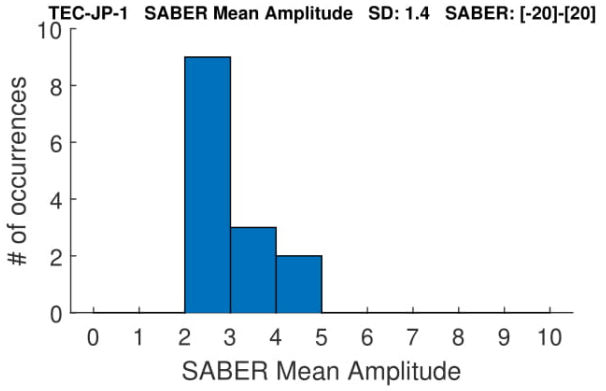

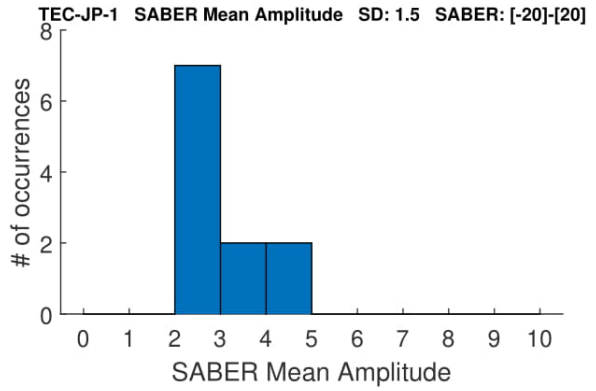

With Solar

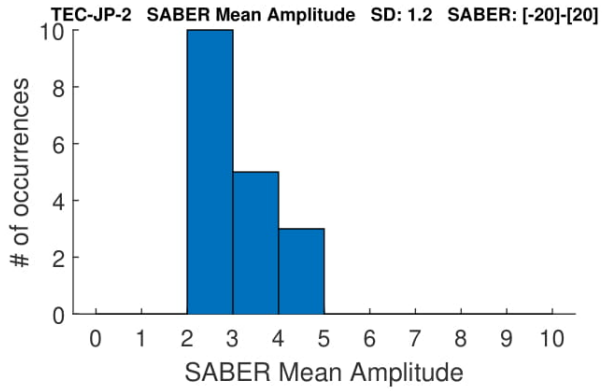

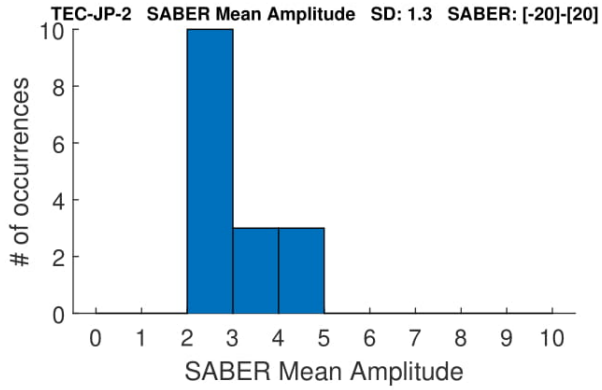

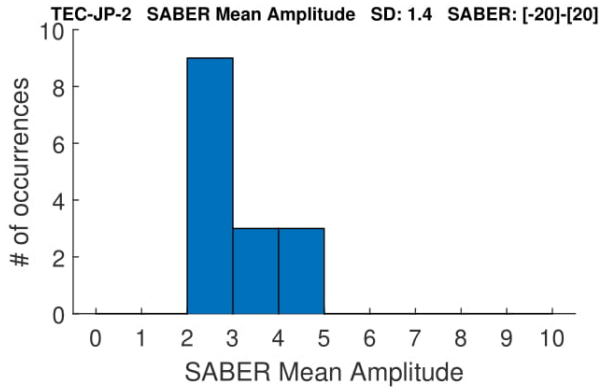

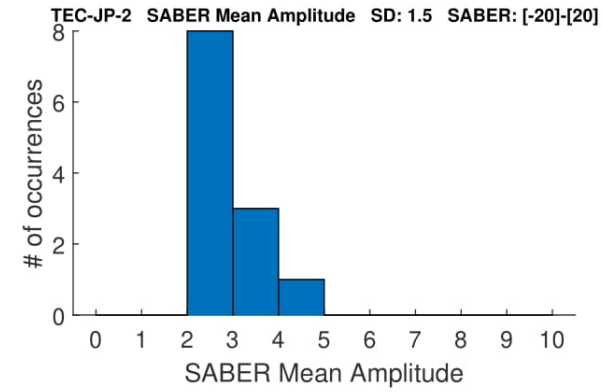

Eliminating Solar

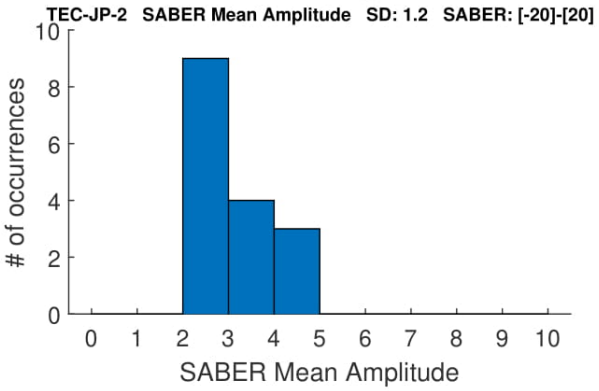

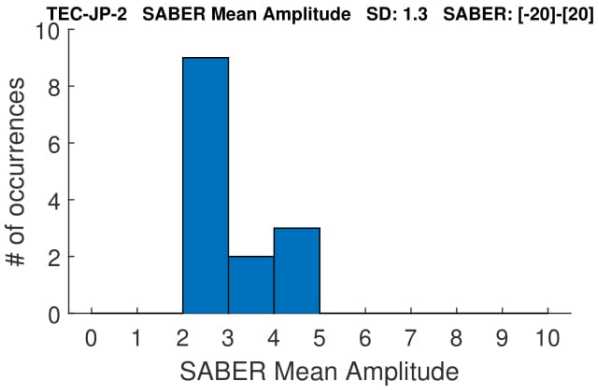

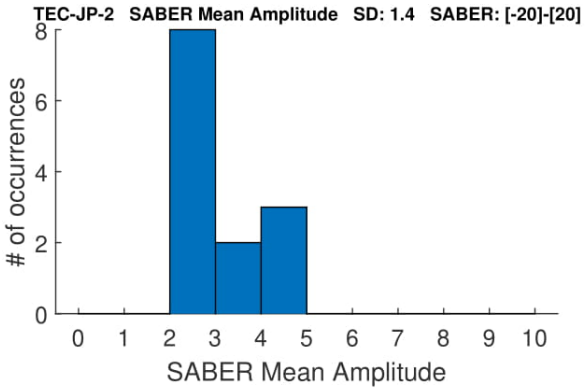

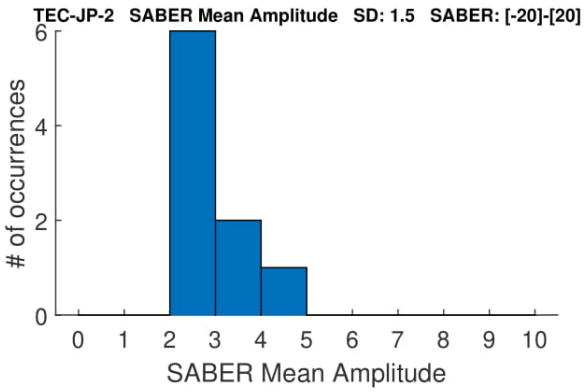

With Solar

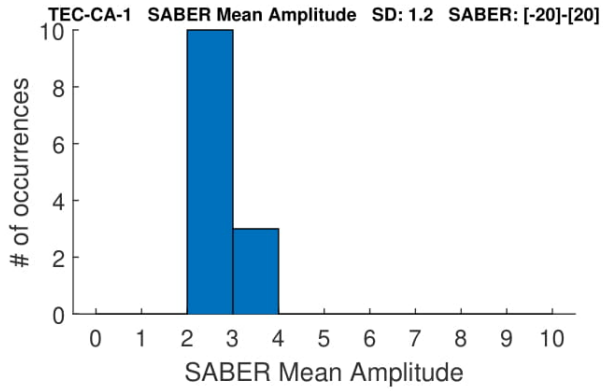

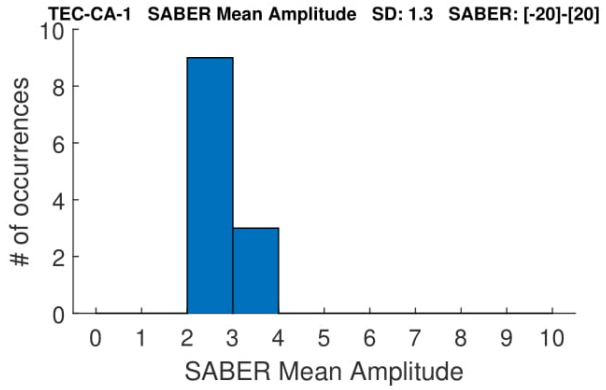

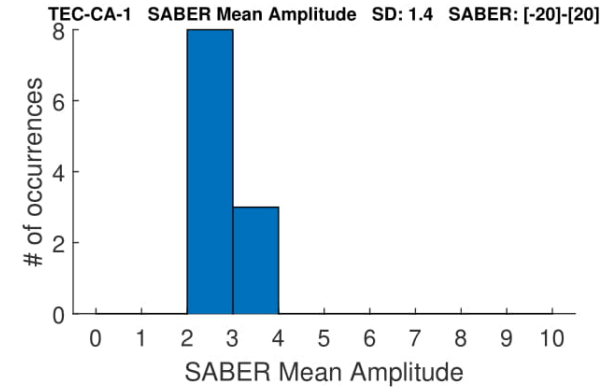

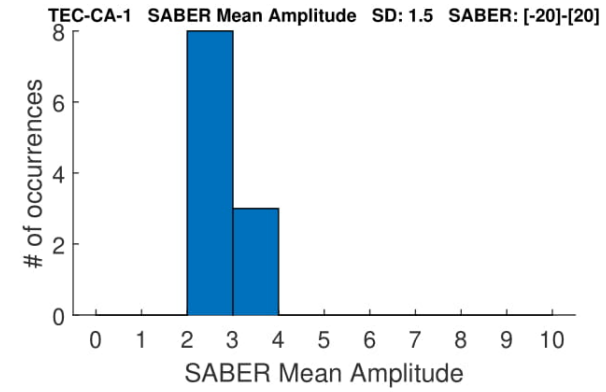

Eliminating Solar

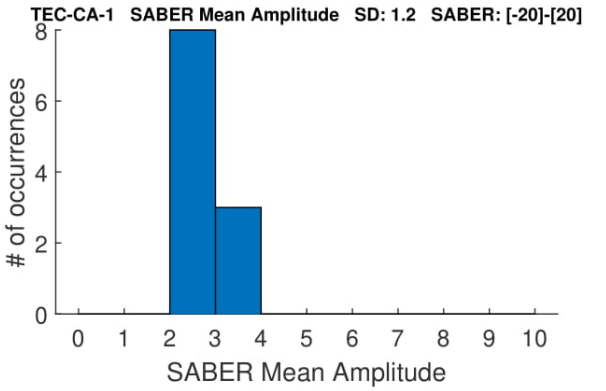

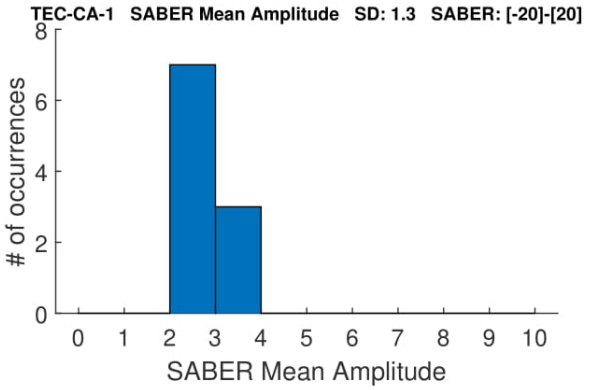

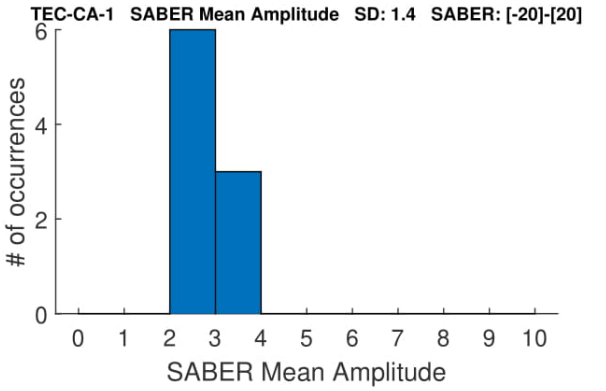

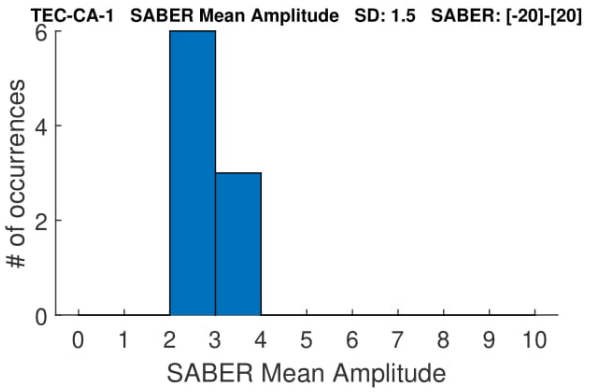

With Solar

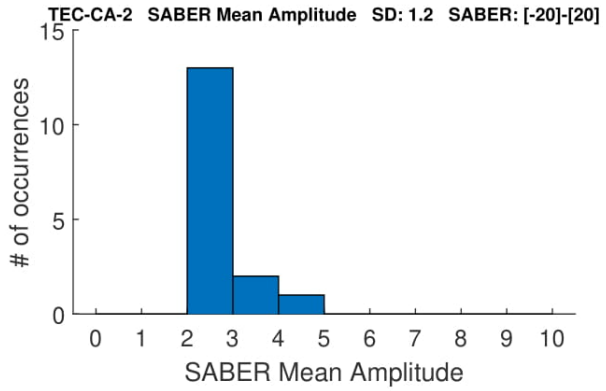

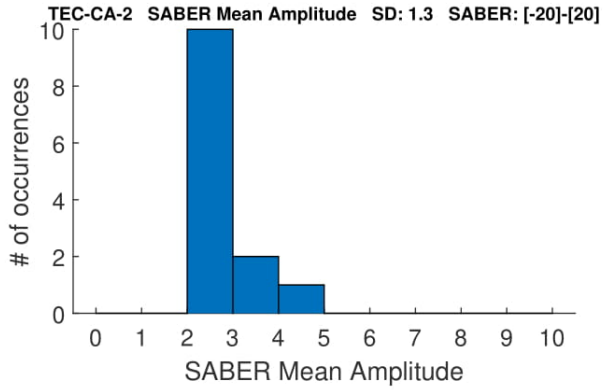

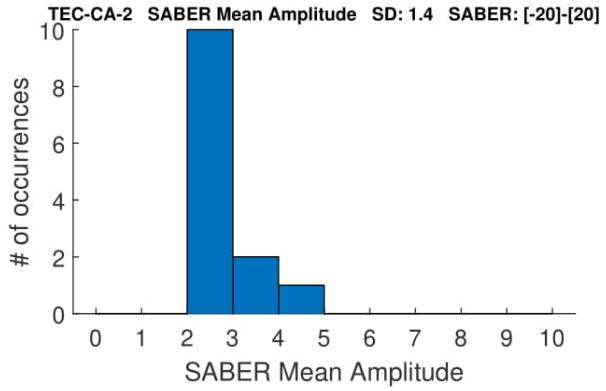

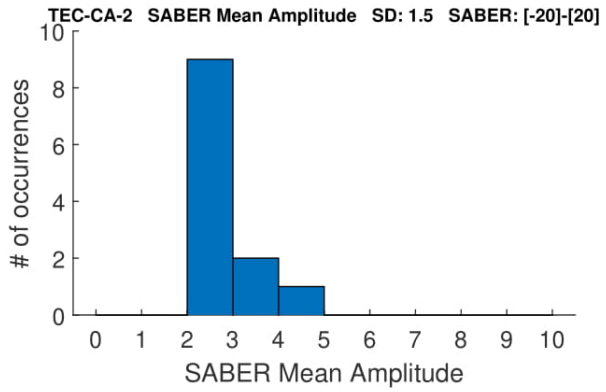

Eliminating Solar

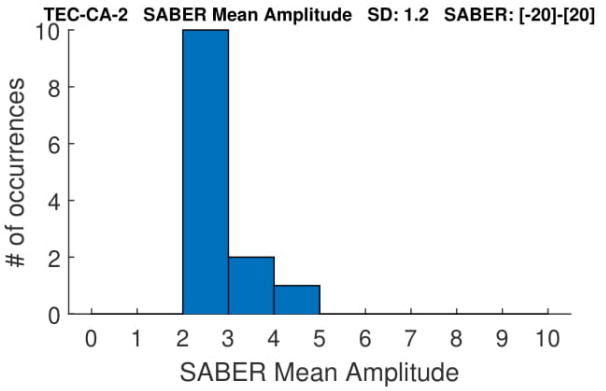

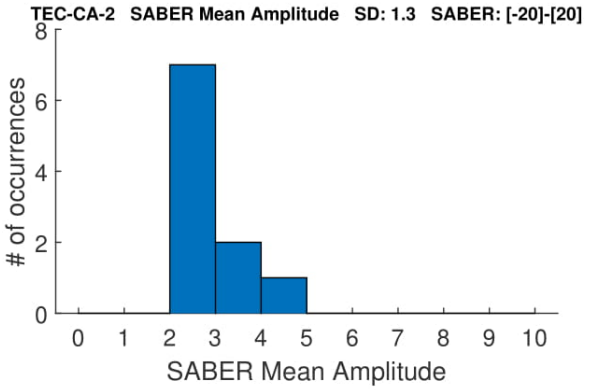

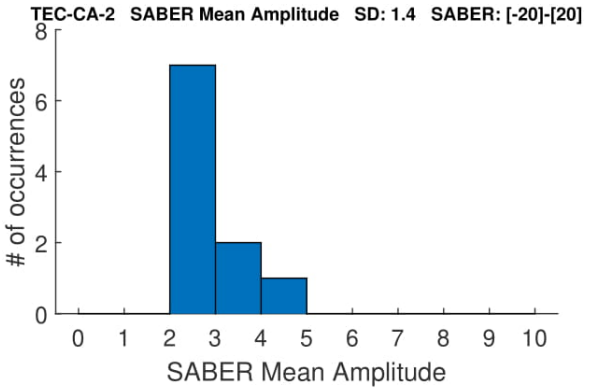

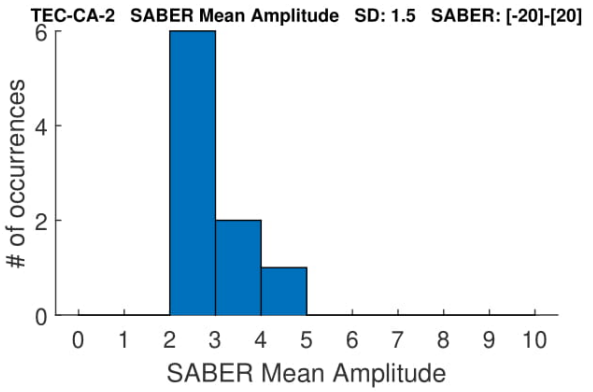

With Solar

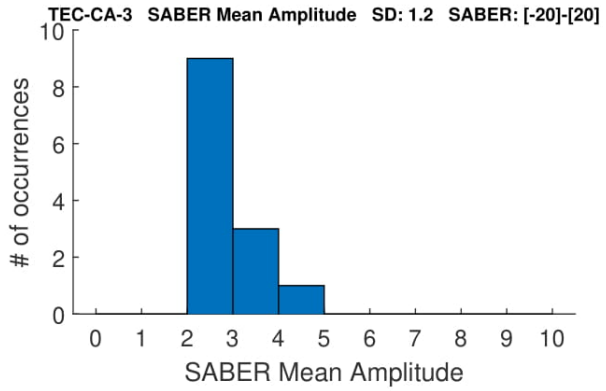

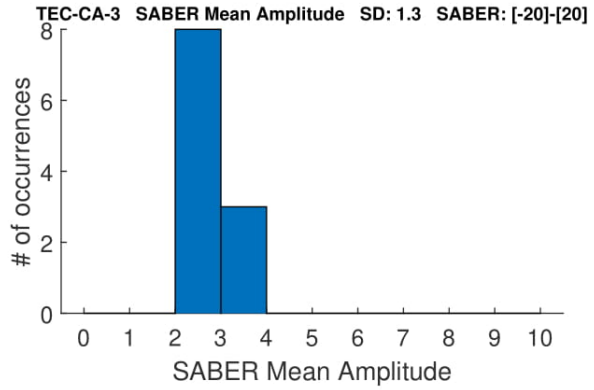

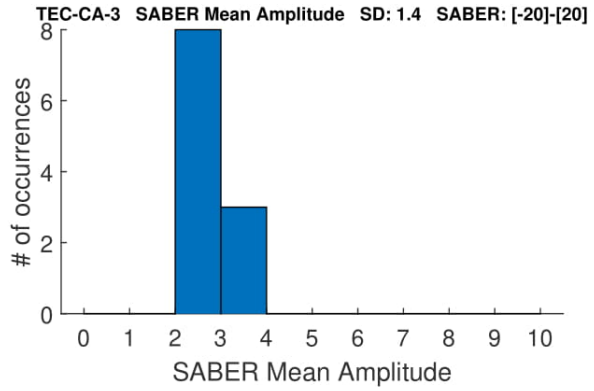

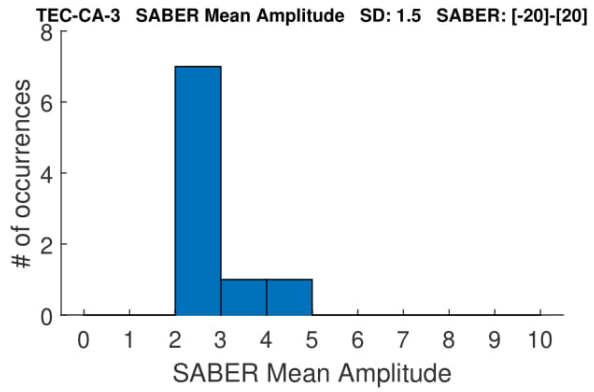

Eliminating Solar

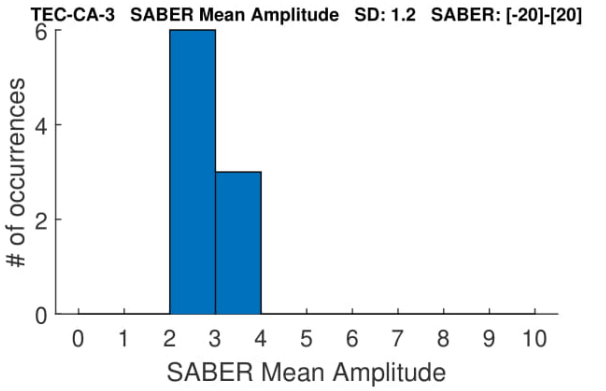

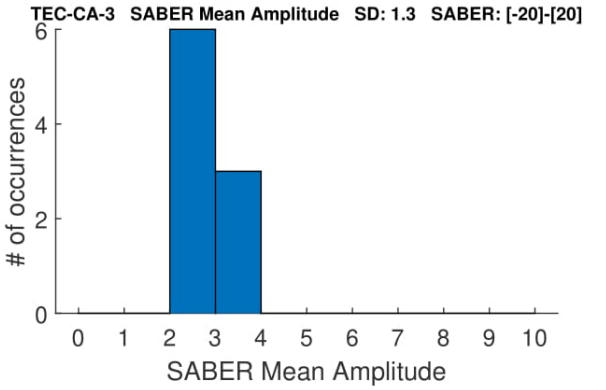

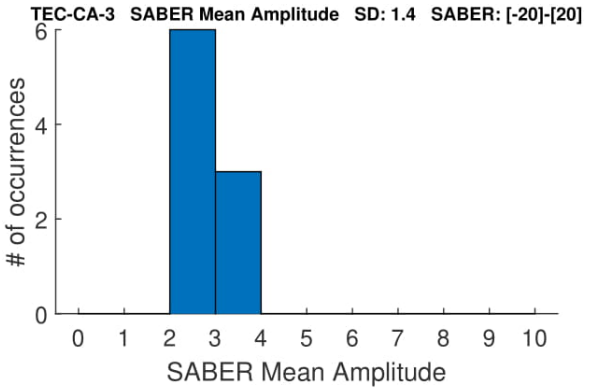

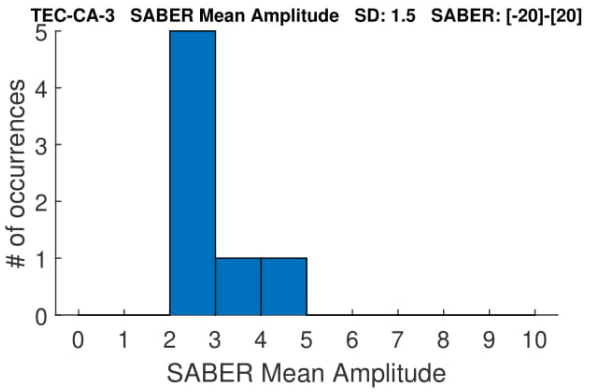

With Solar

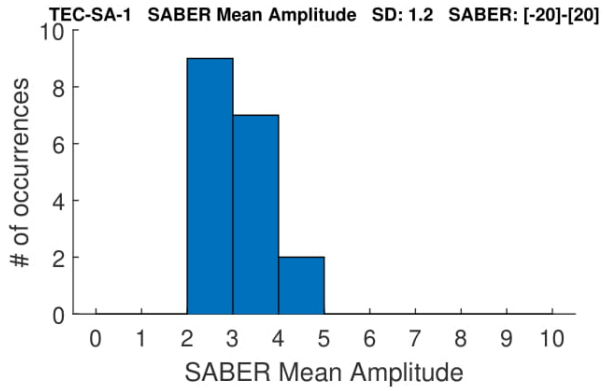

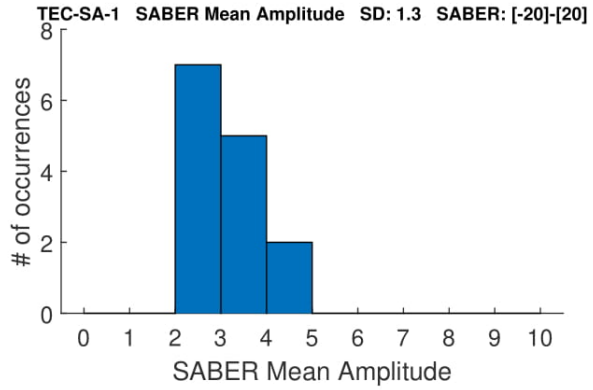

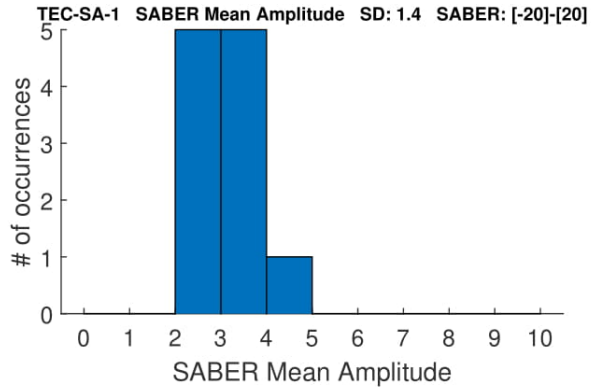

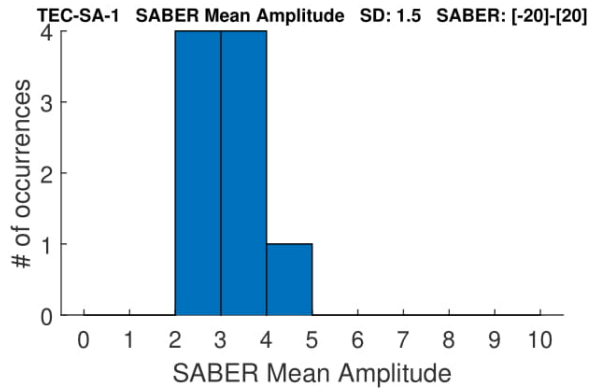

Eliminating Solar

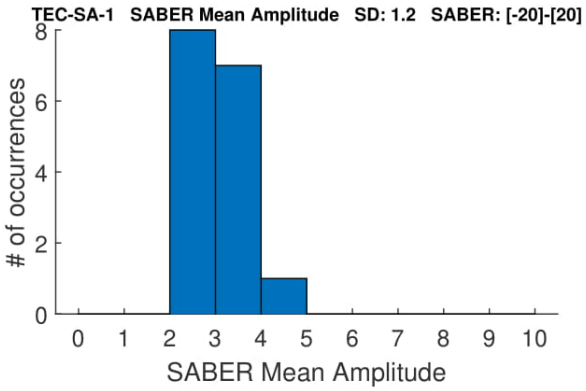

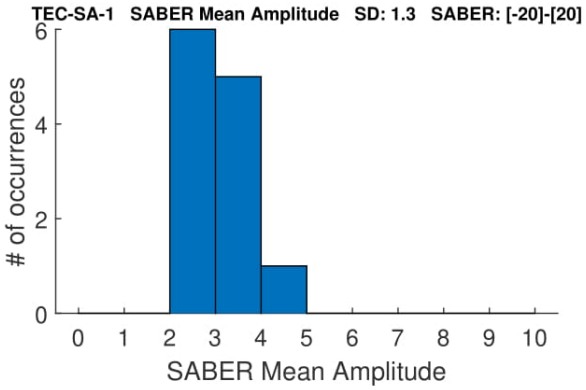

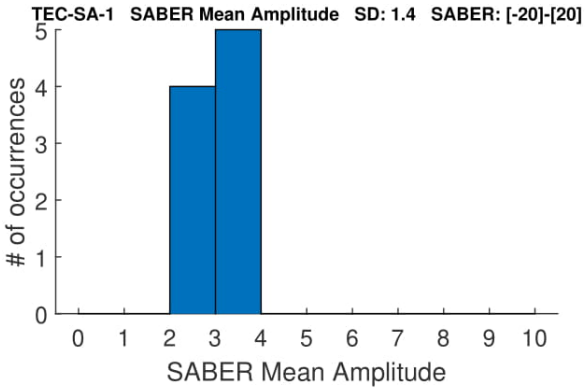

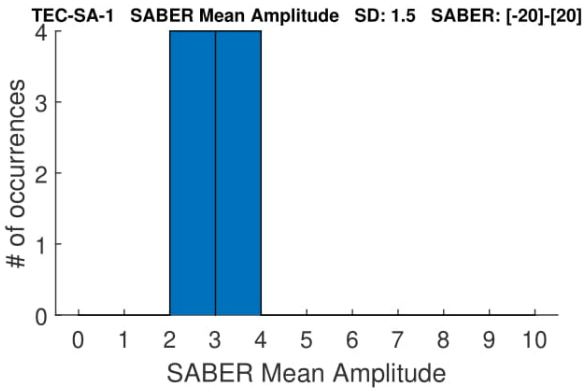

With Solar

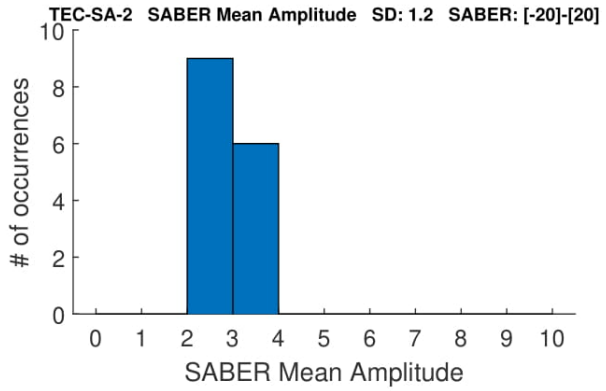

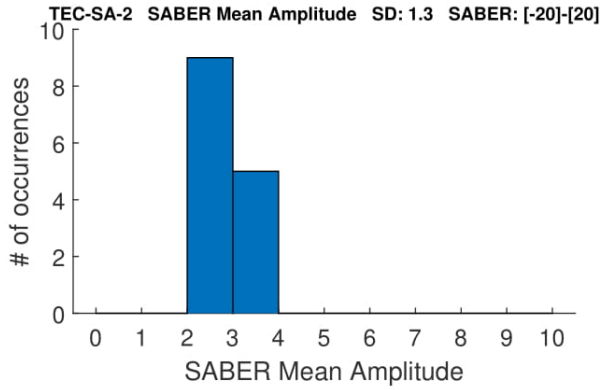

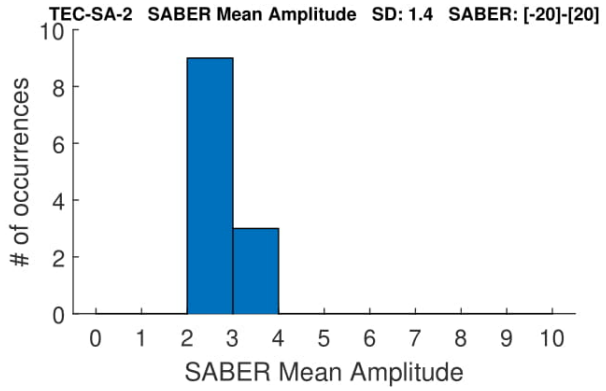

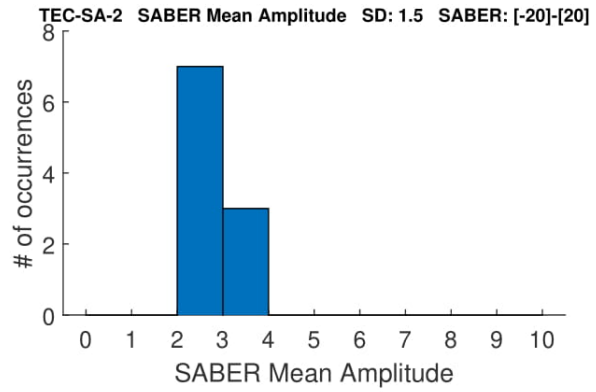

Eliminating Solar

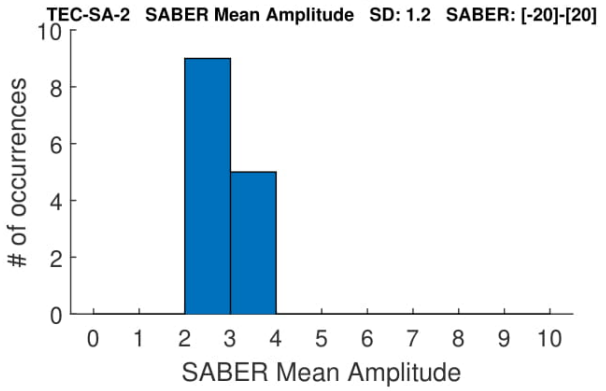

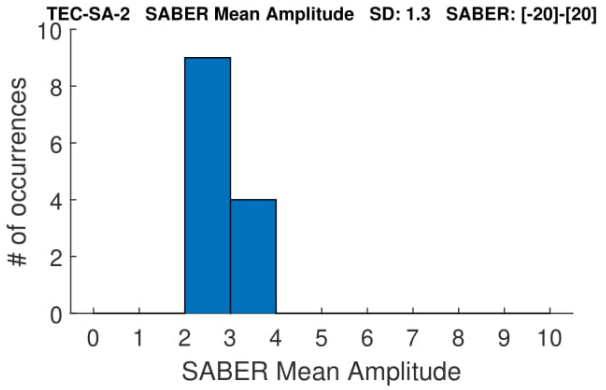

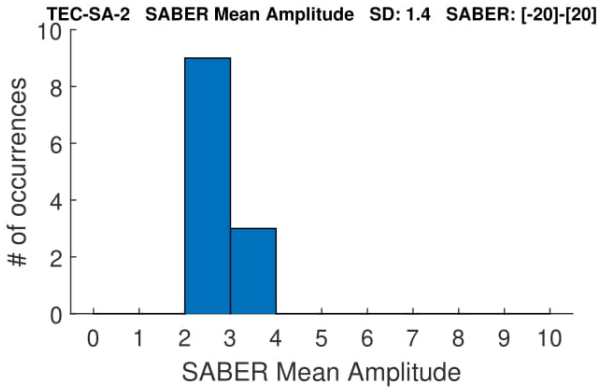

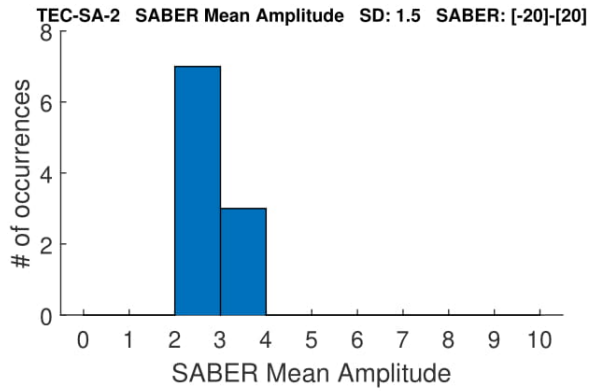

With Solar

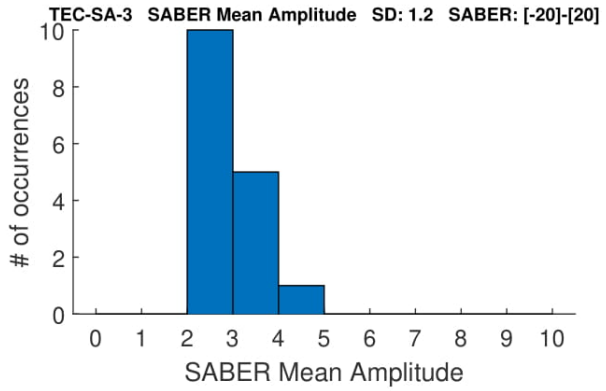

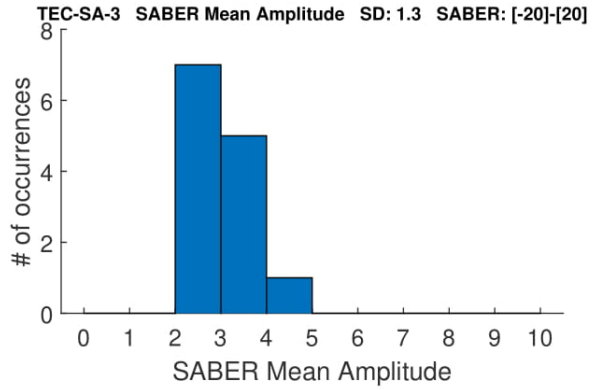

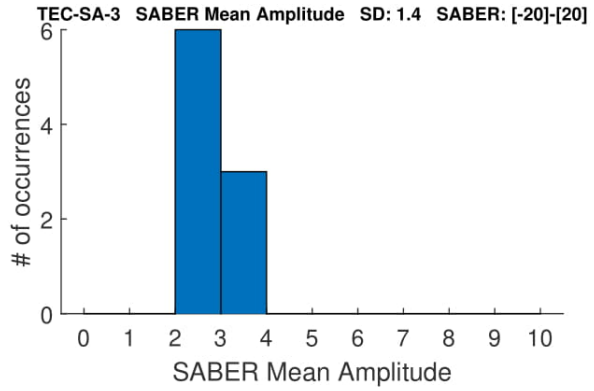

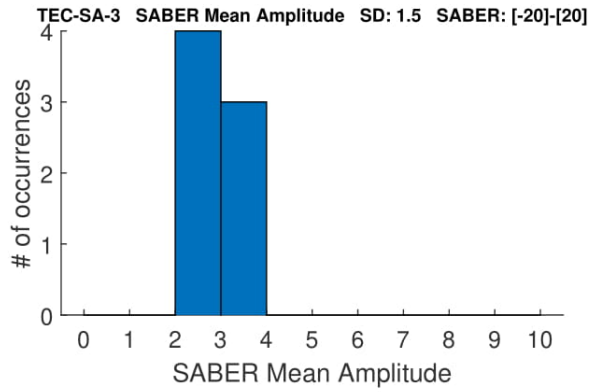

Eliminating Solar

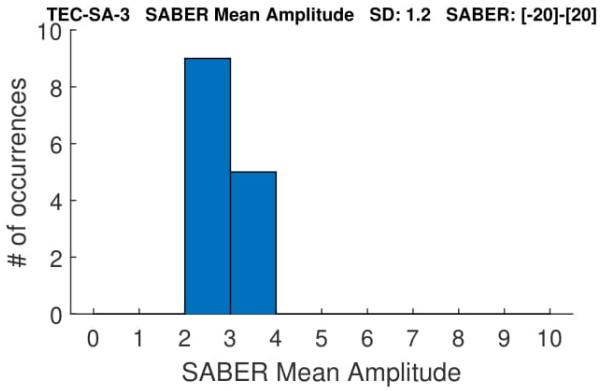

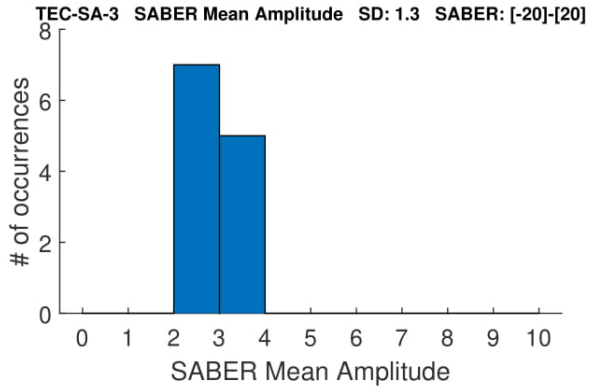

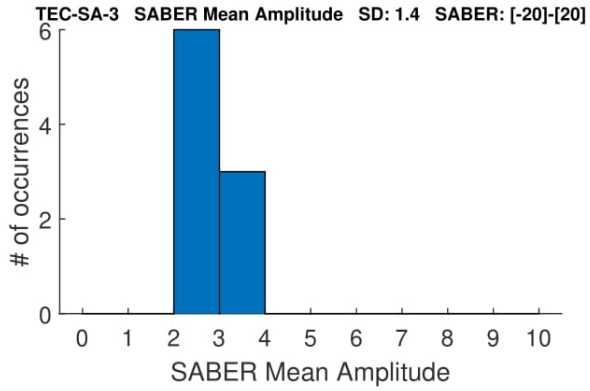

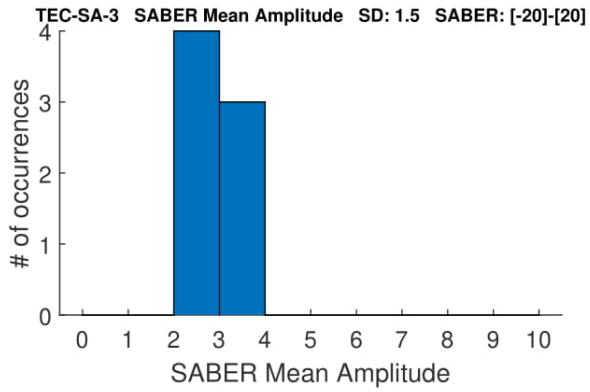

With Solar

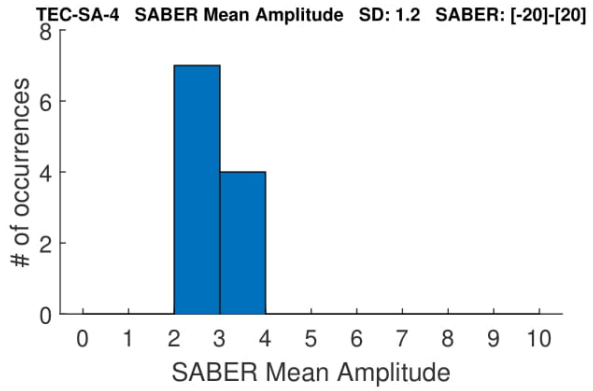

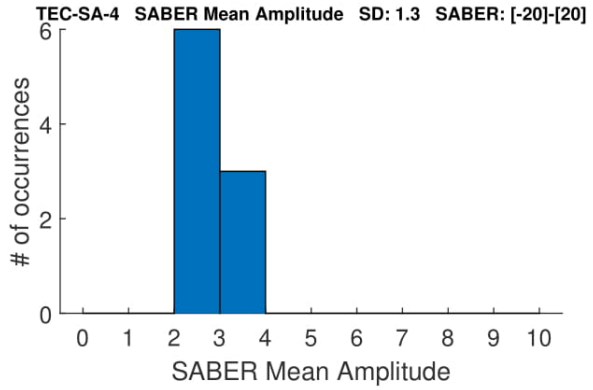

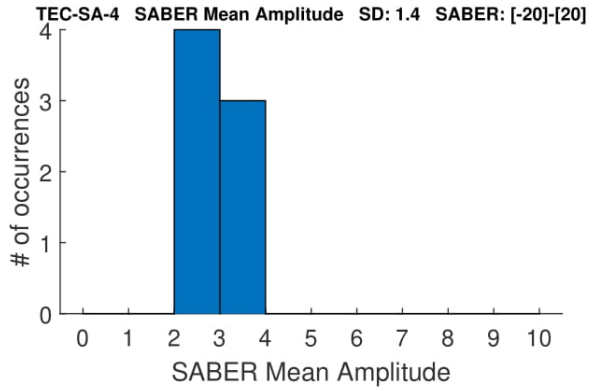

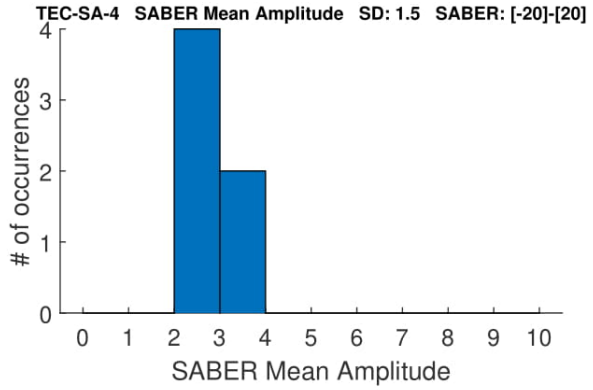

Eliminating Solar

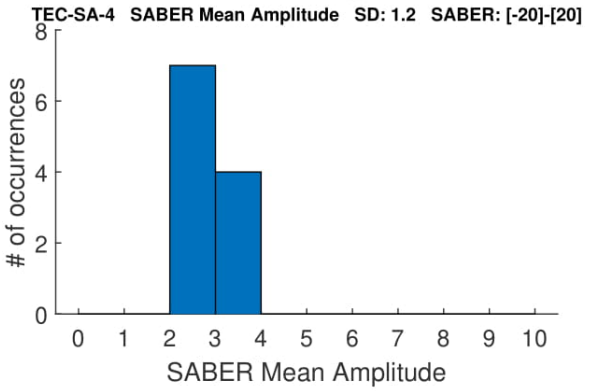

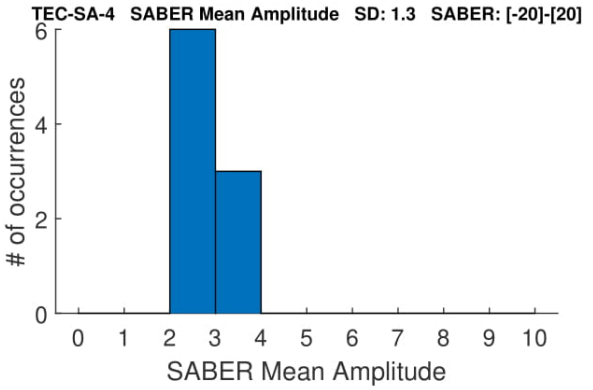

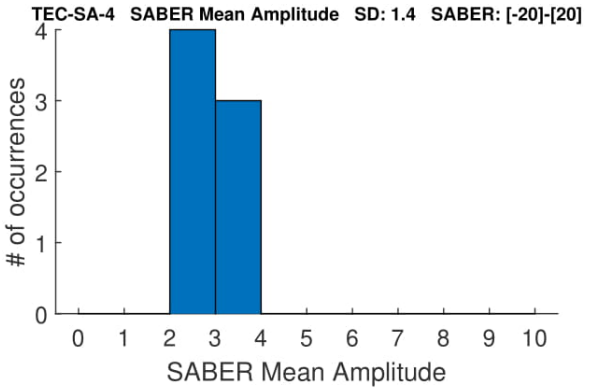

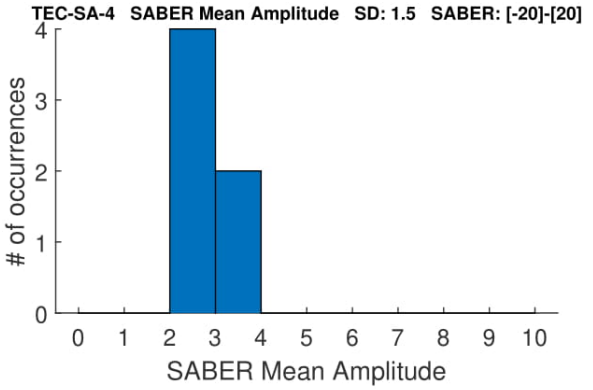

B.2.3 Lower Latitude Band

These histograms only use the SABER events in the Middle latitude band, -45 to -20 degrees.

With Solar

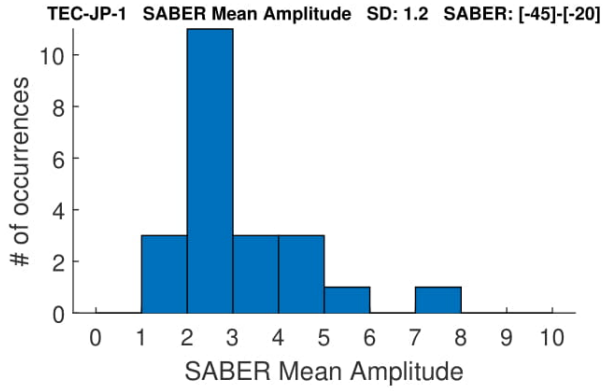

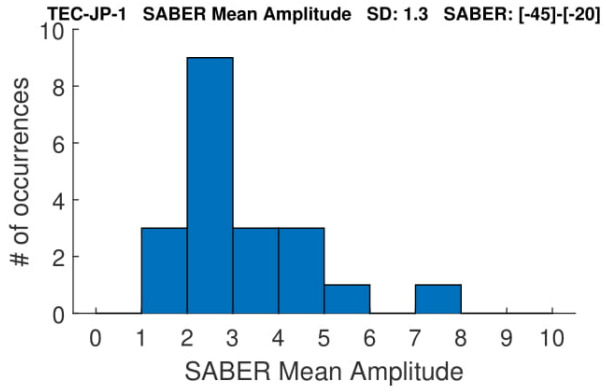

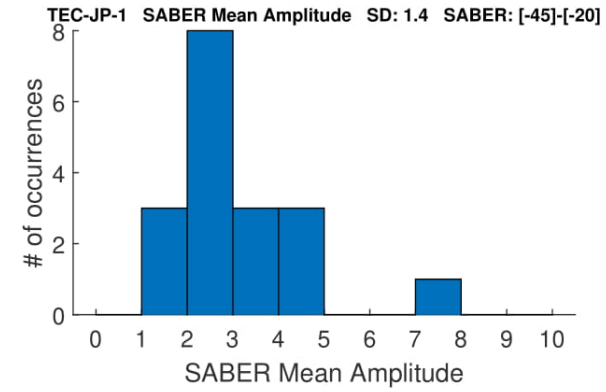

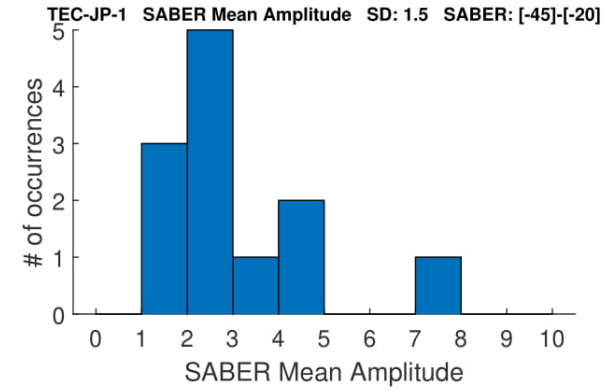

Eliminating Solar

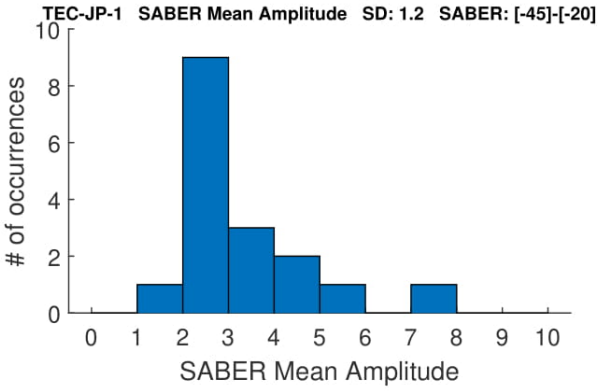

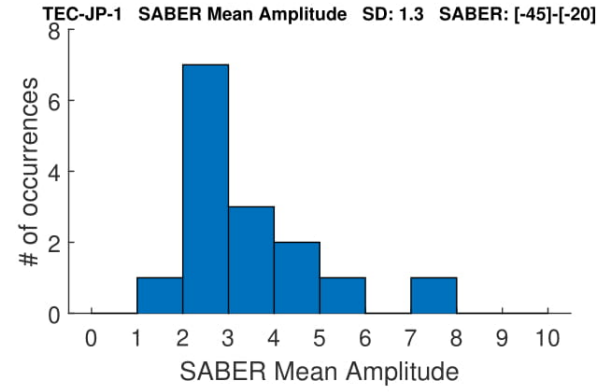

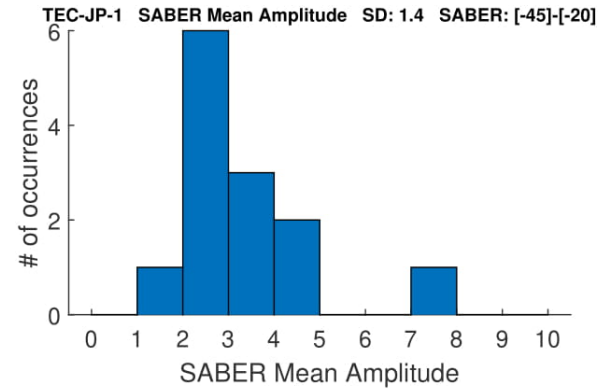

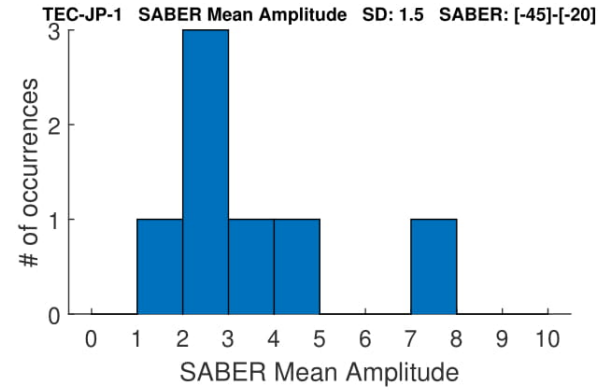

With Solar

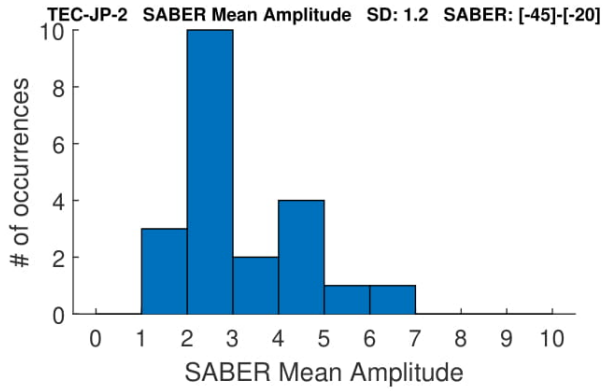

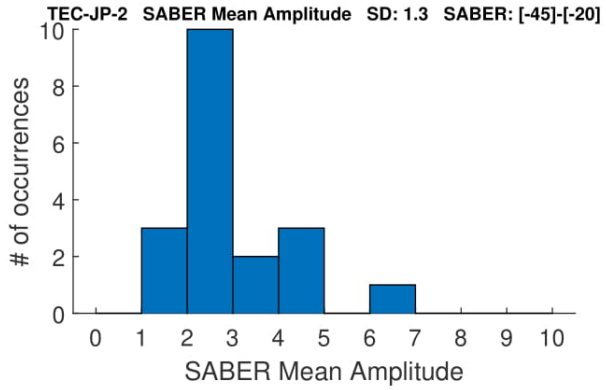

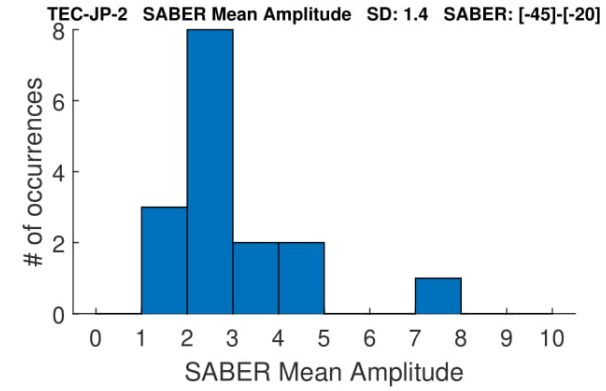

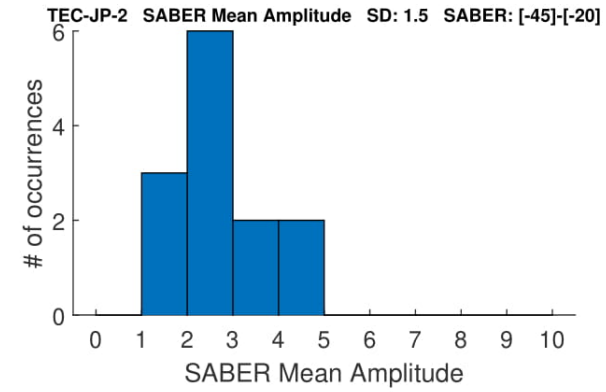

Eliminating Solar

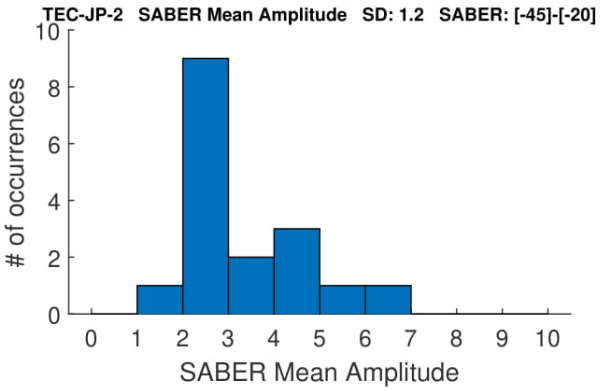

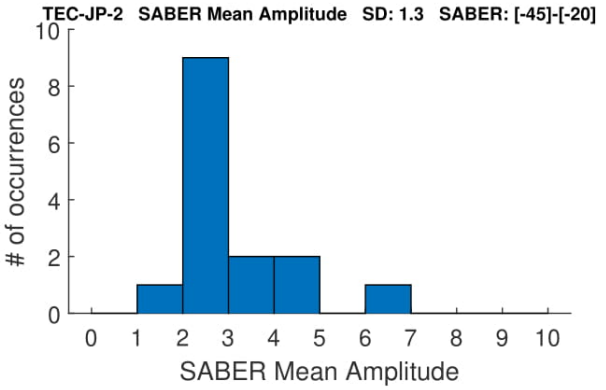

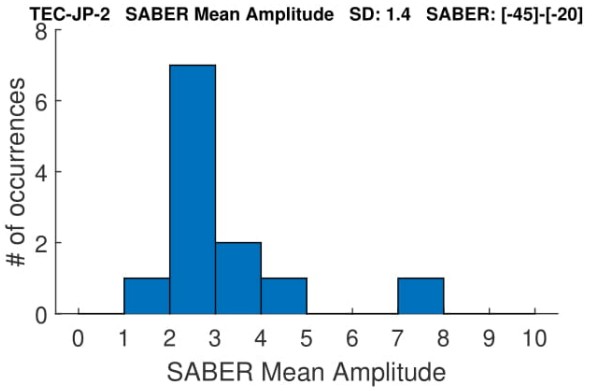

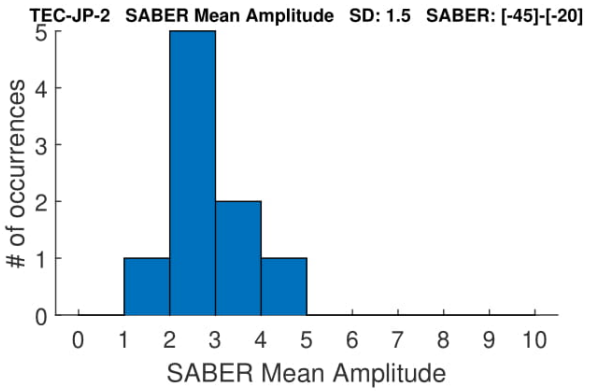

With Solar

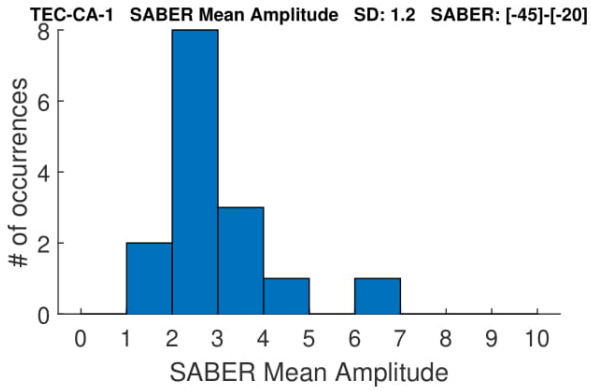

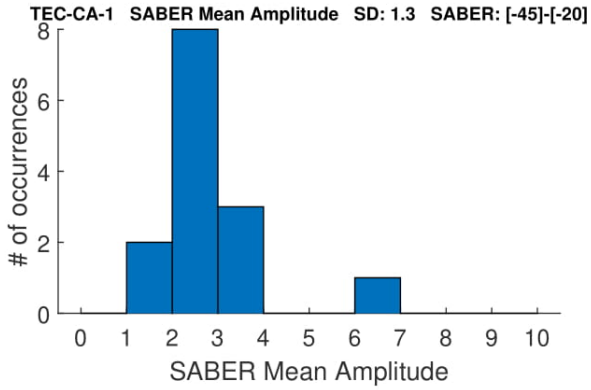

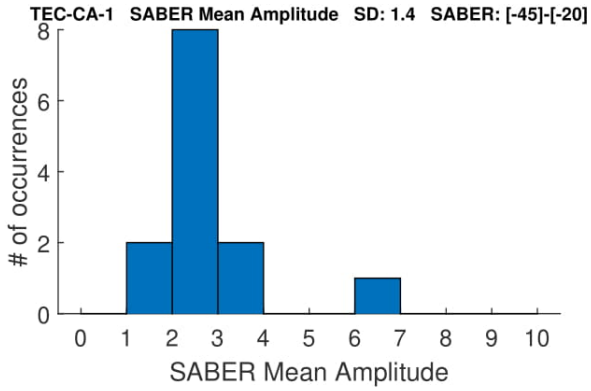

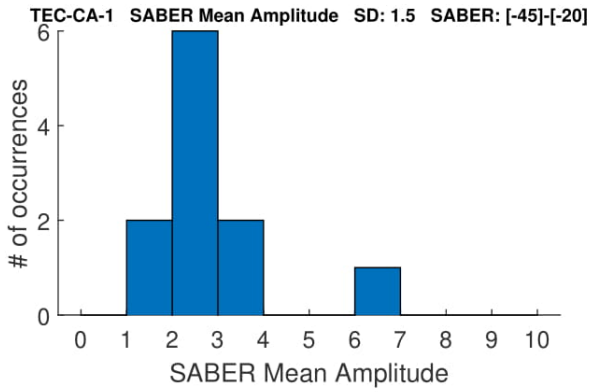

Eliminating Solar

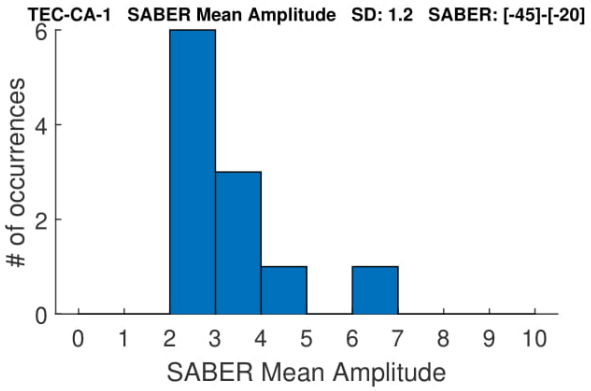

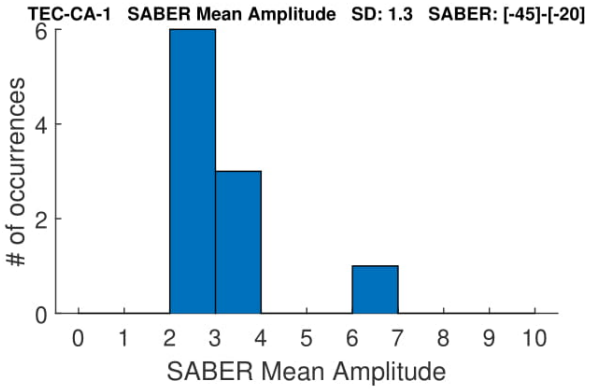

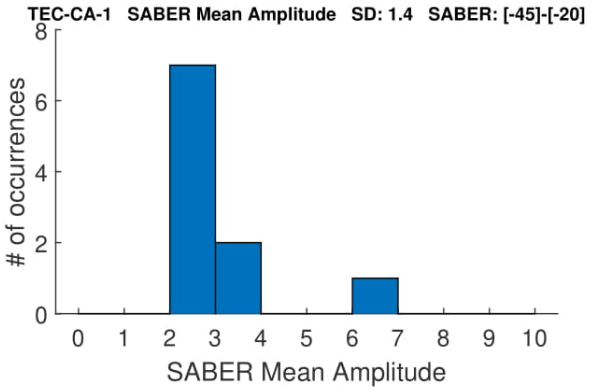

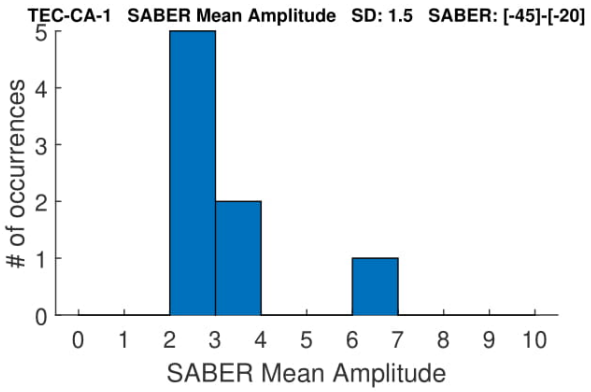

With Solar

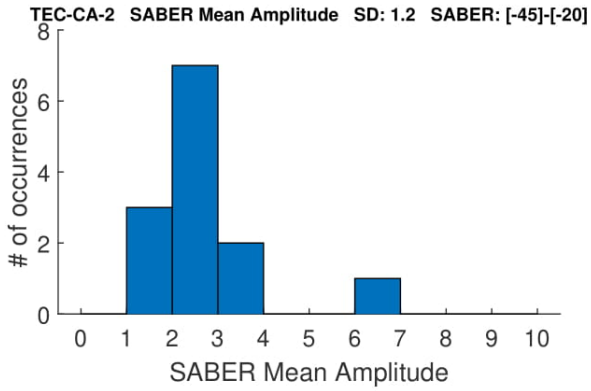

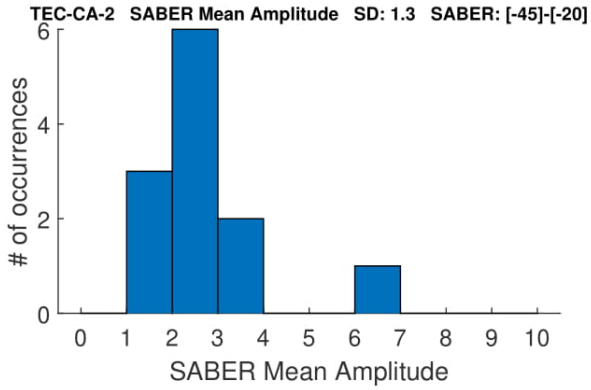

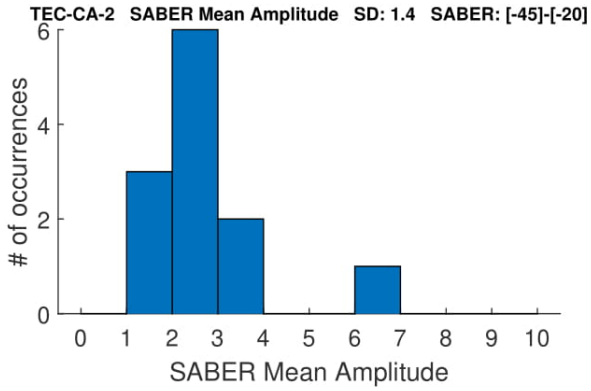

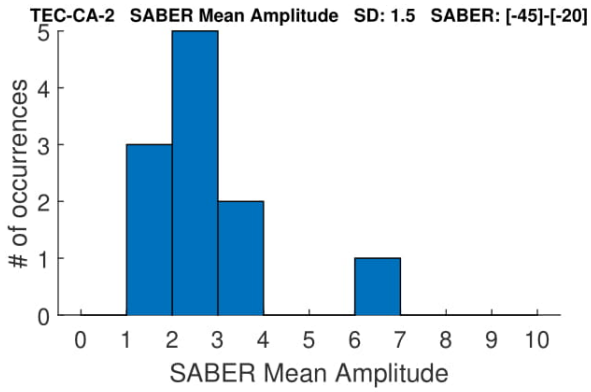

Eliminating Solar

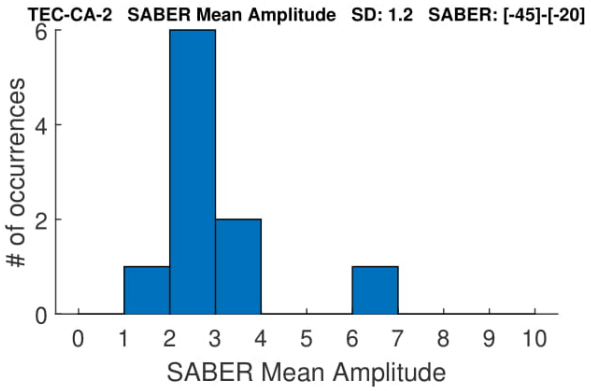

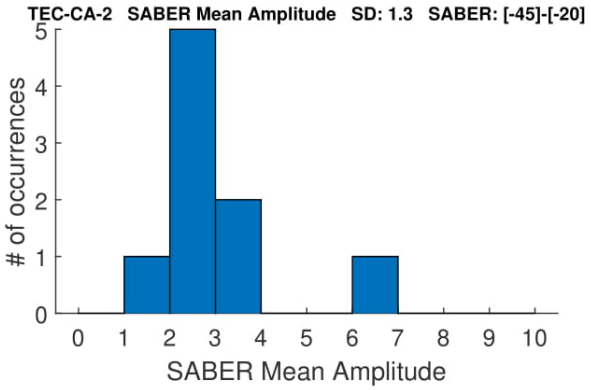

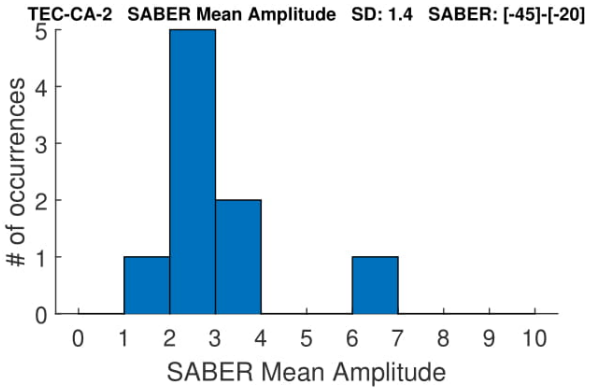

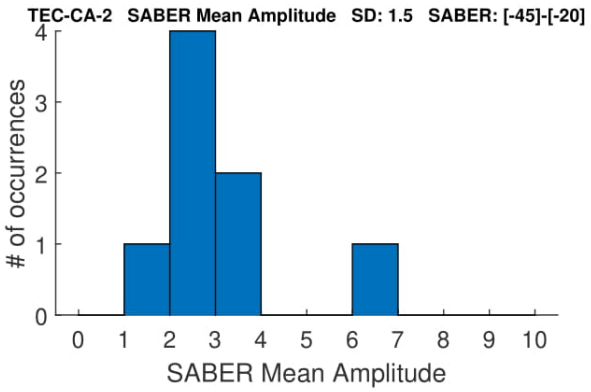

With Solar

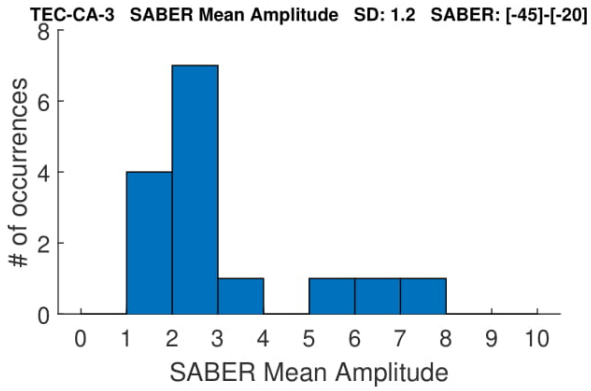

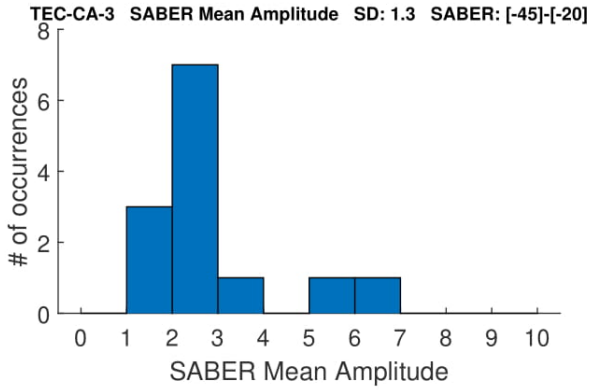

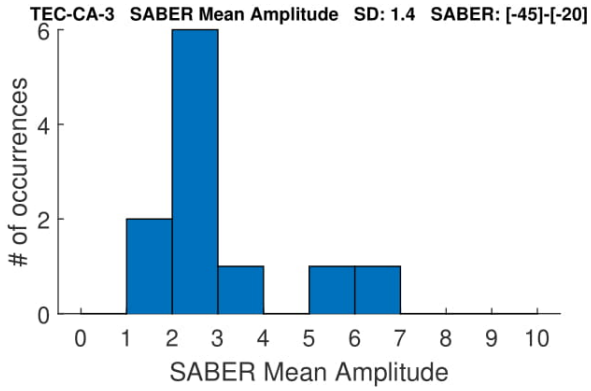

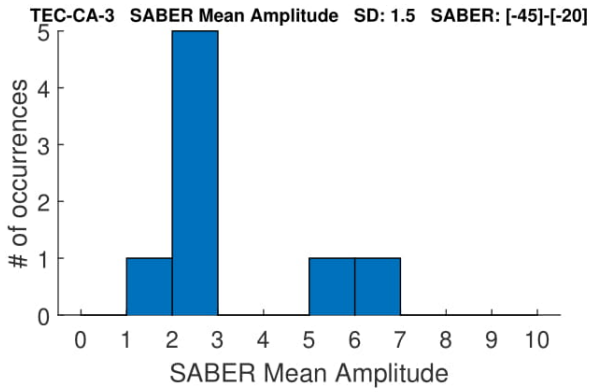

Eliminating Solar

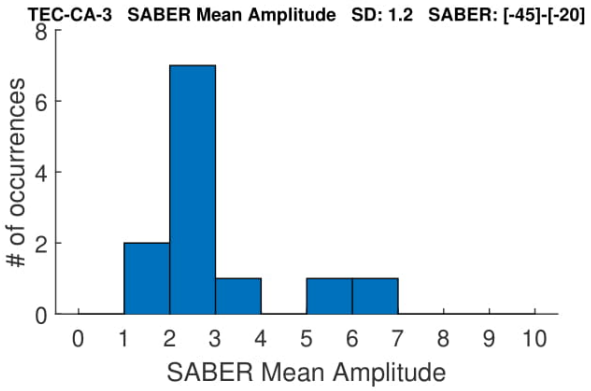

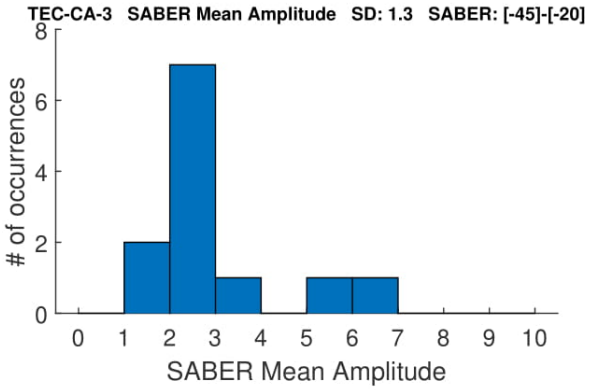

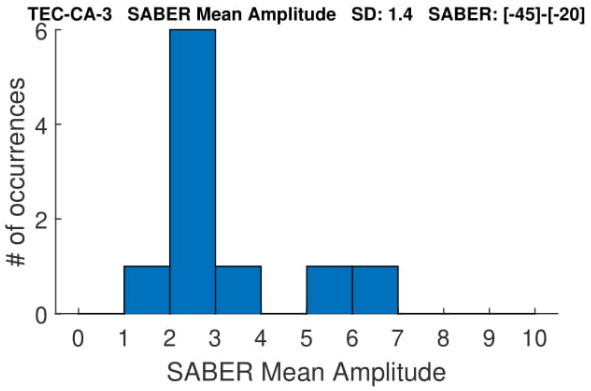

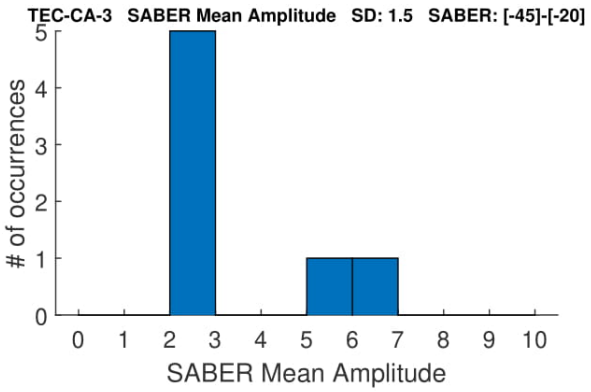

With Solar

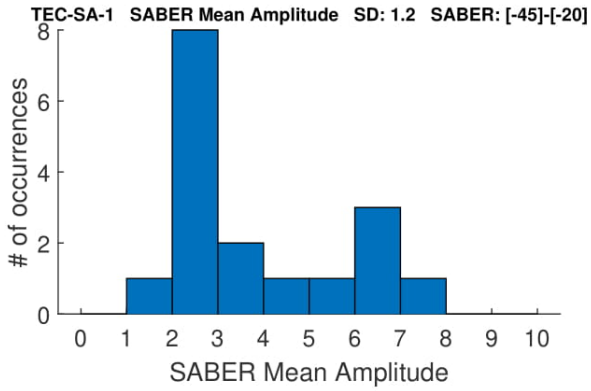

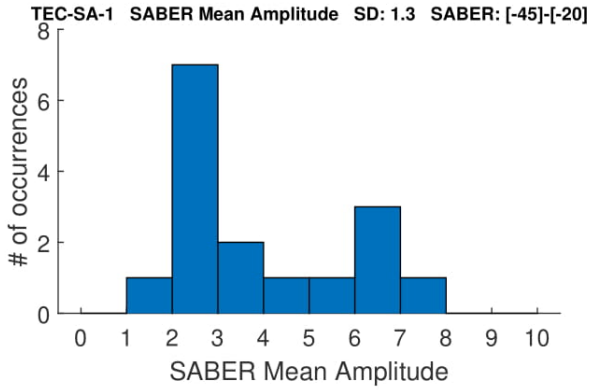

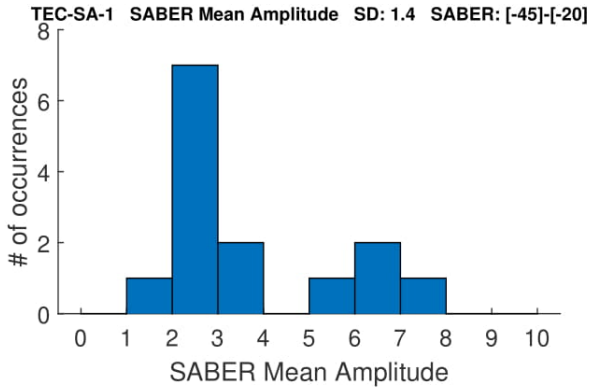

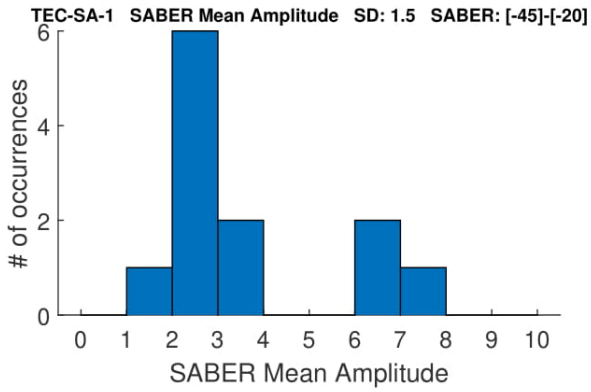

Eliminating Solar

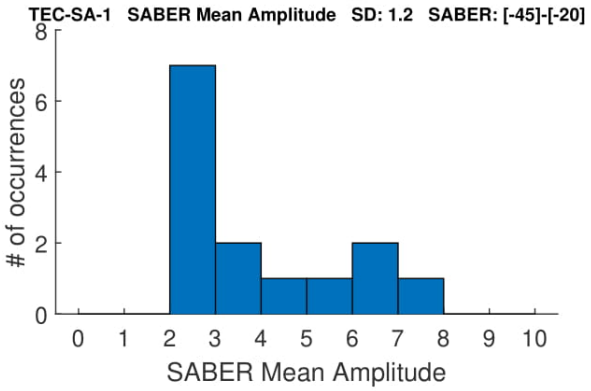

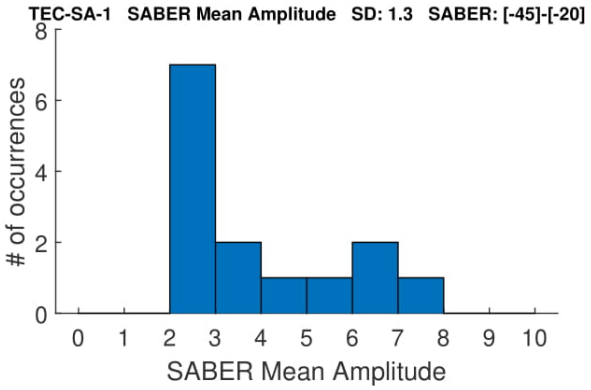

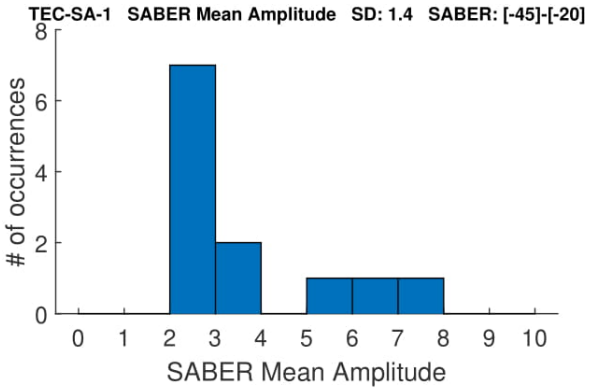

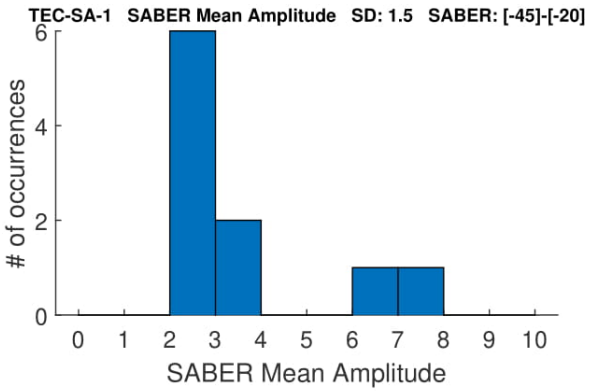

With Solar

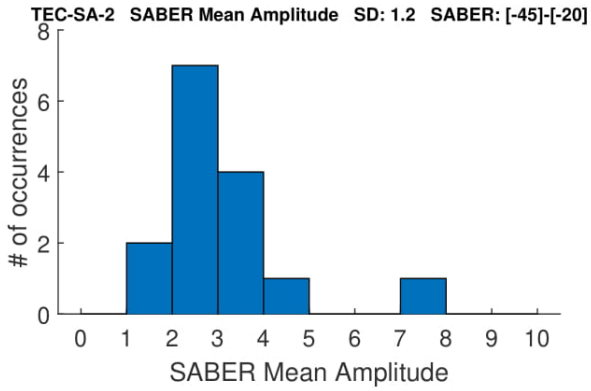

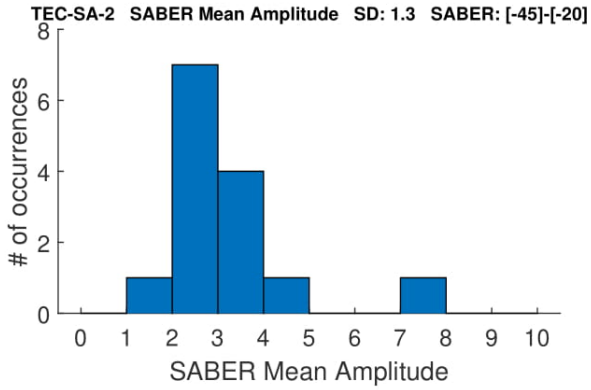

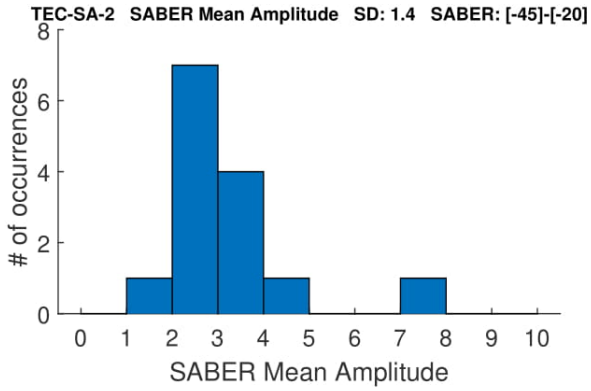

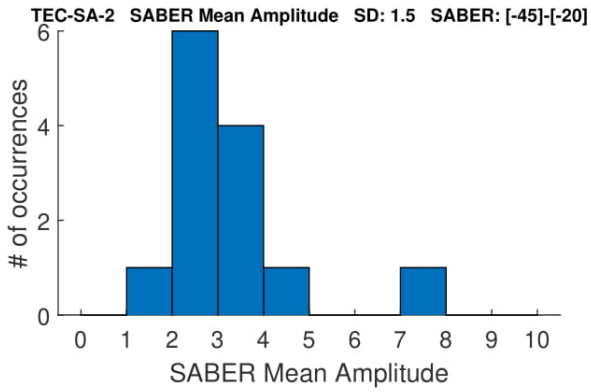

Eliminating Solar

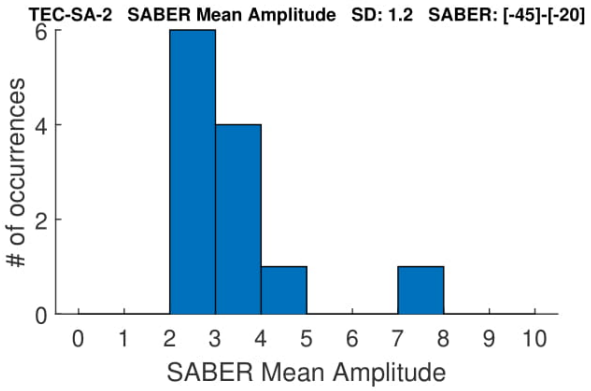

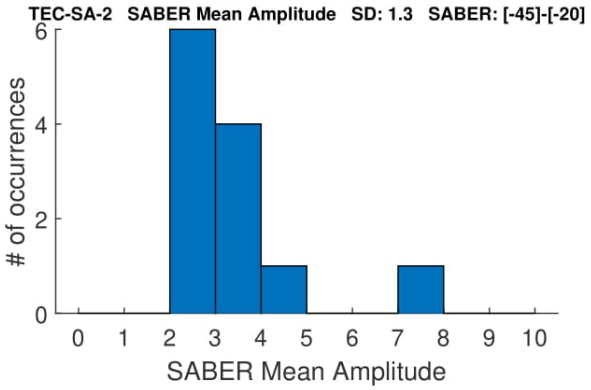

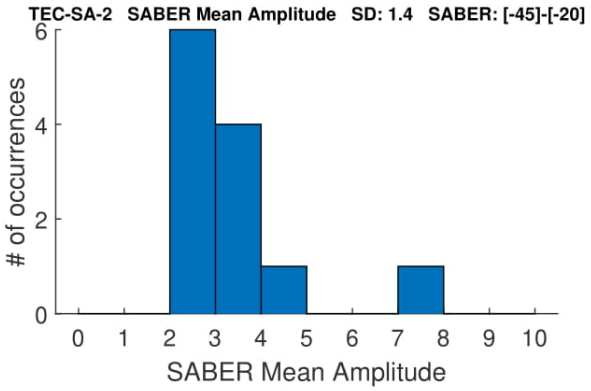

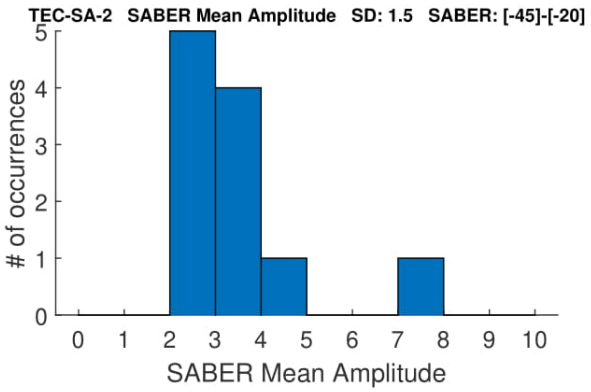

With Solar

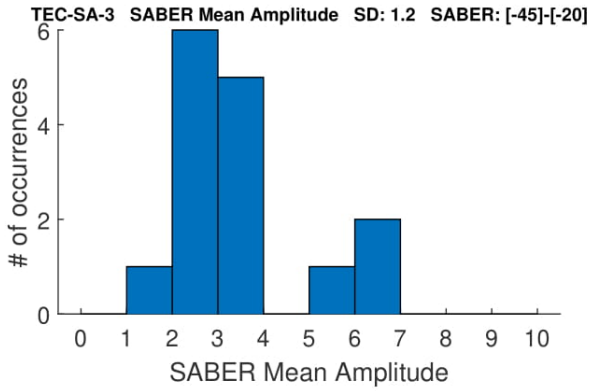

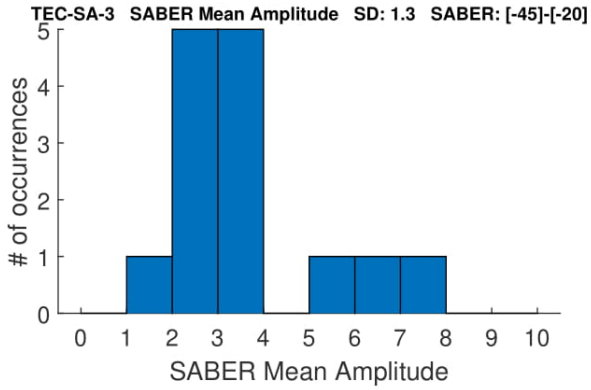

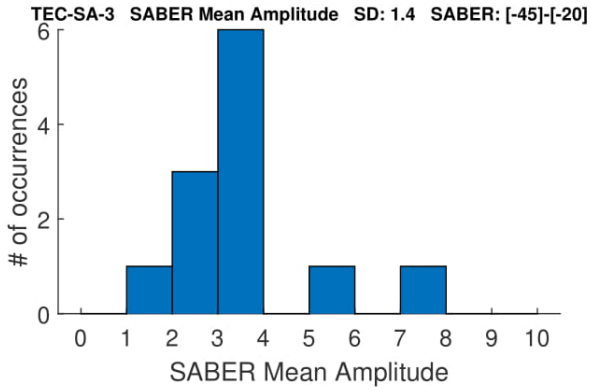

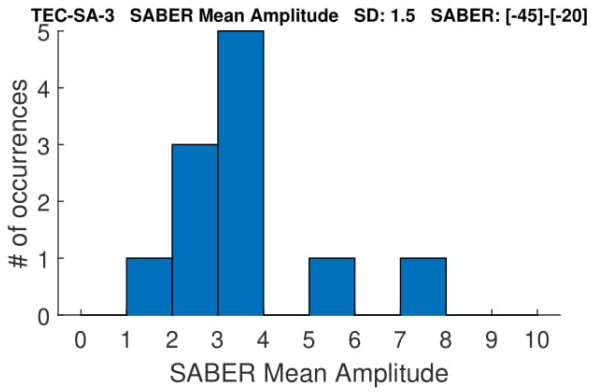

Eliminating Solar

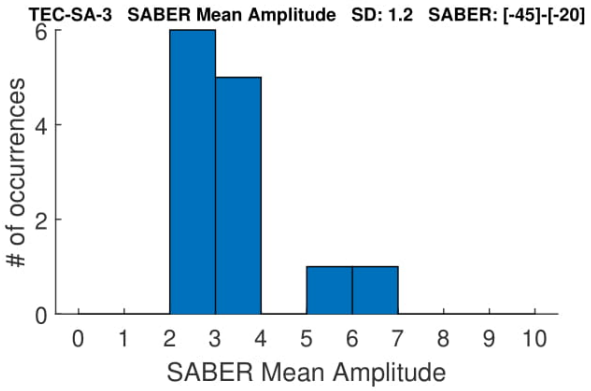

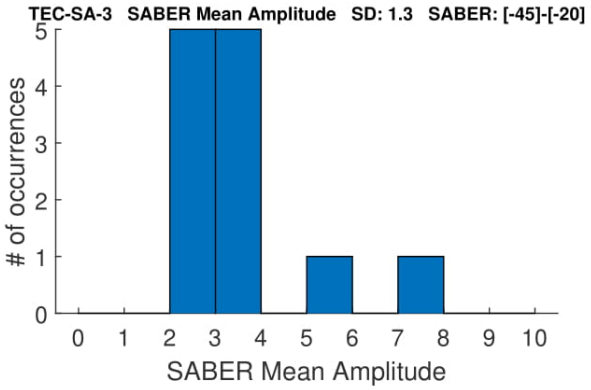

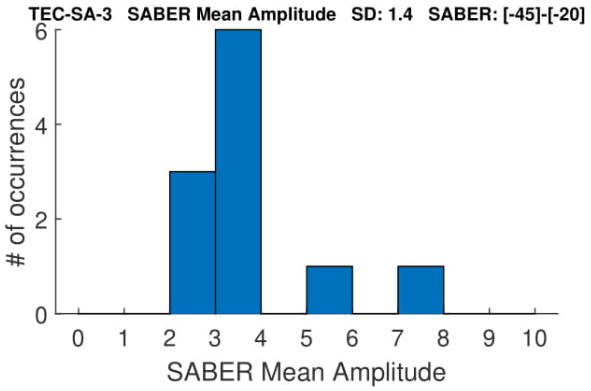

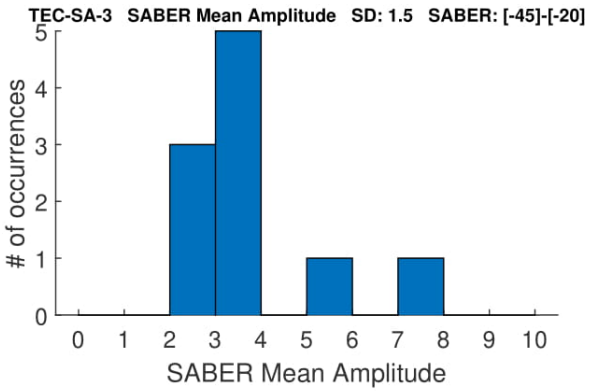

With Solar

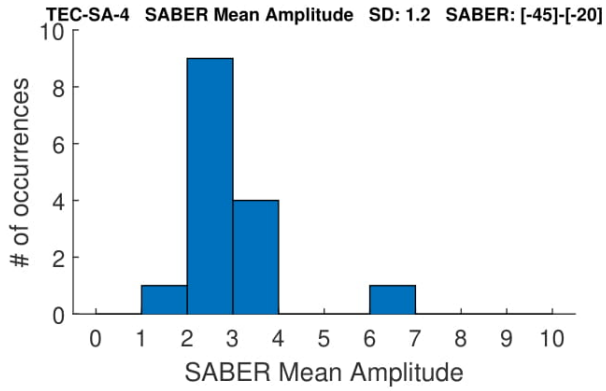

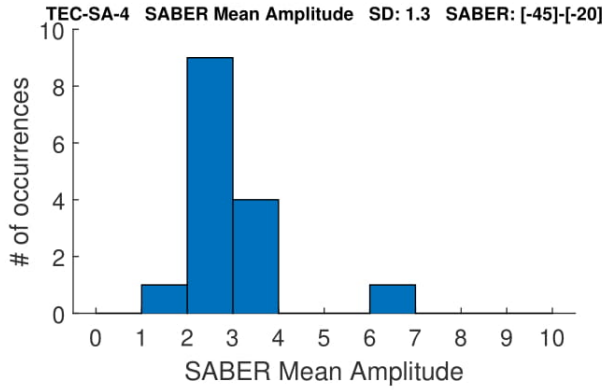

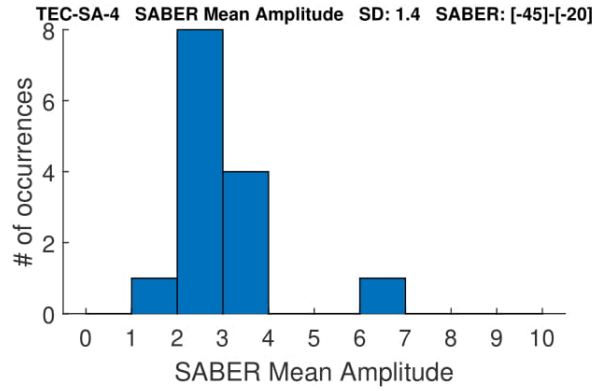

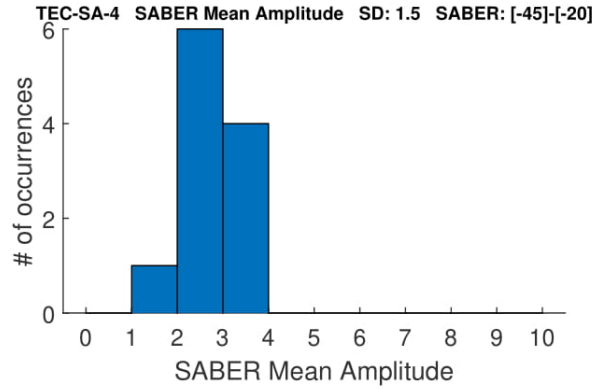

Eliminating Solar

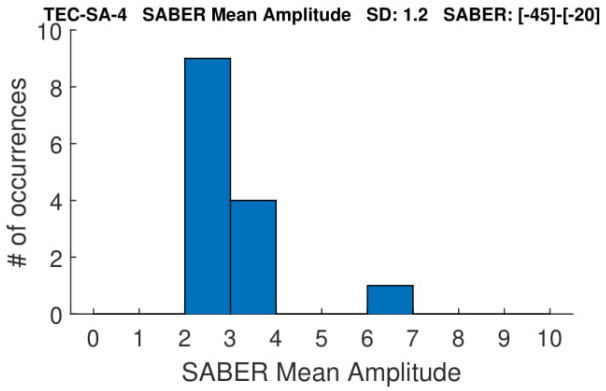

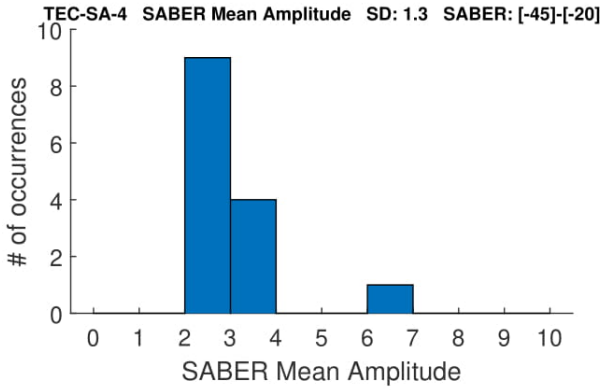

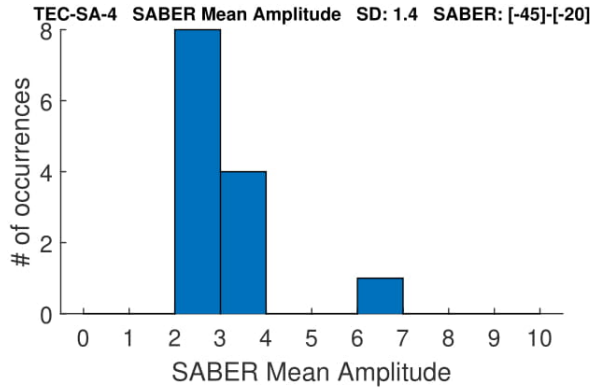

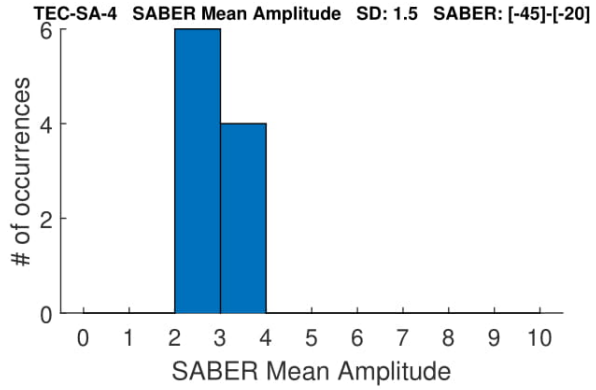

B.3 Number of Latitude Bands

This section contains the one of the types of location histograms described in Sections 3.3.2 and 4.3. These histograms display how many latitude bands the SABER events spans. These figures are similar to the left plot in 3.14.

With Solar

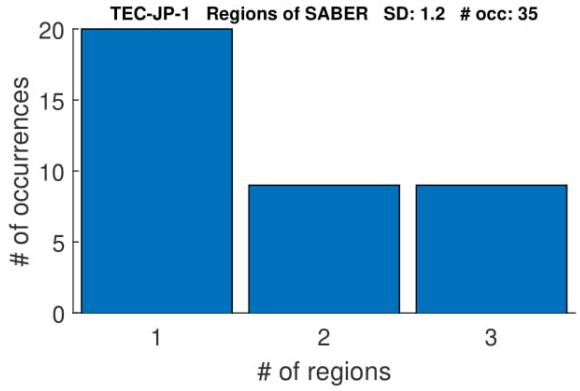

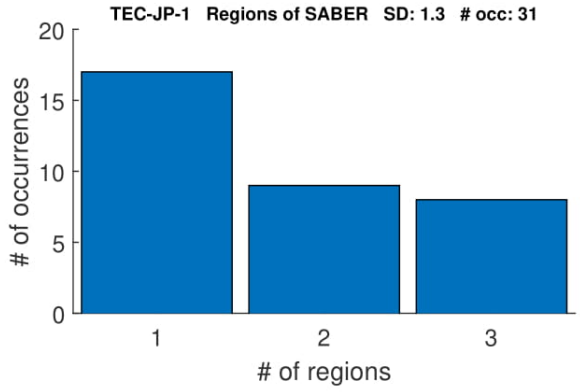

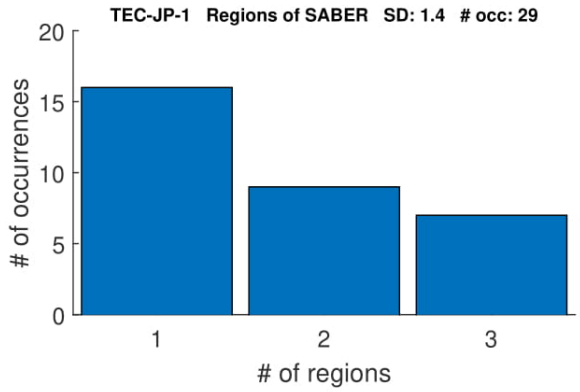

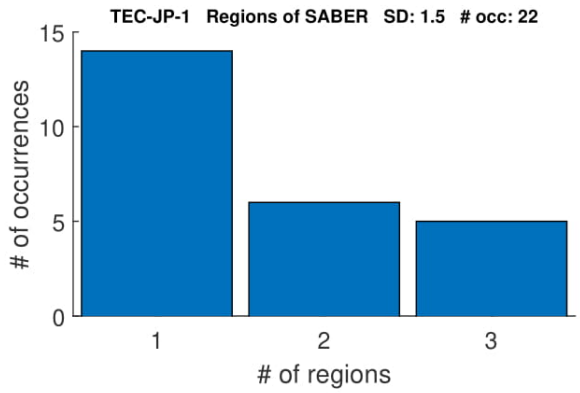

Eliminating Solar

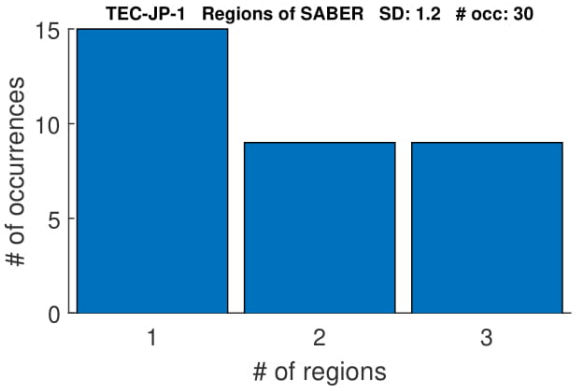

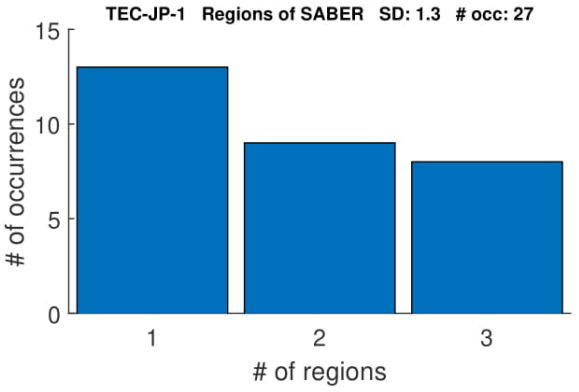

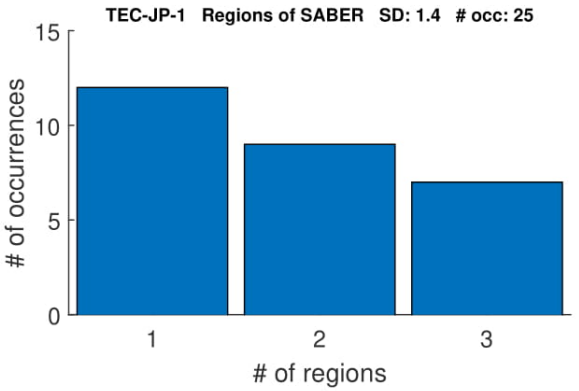

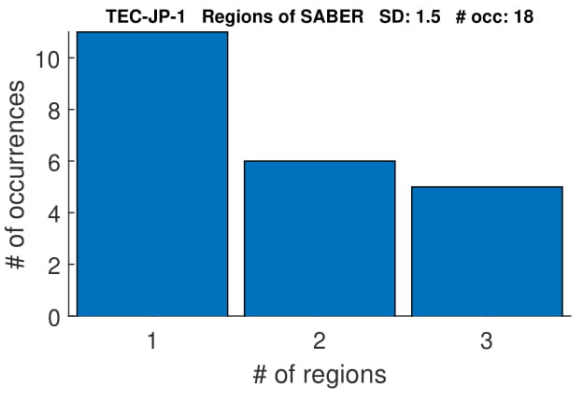

With Solar

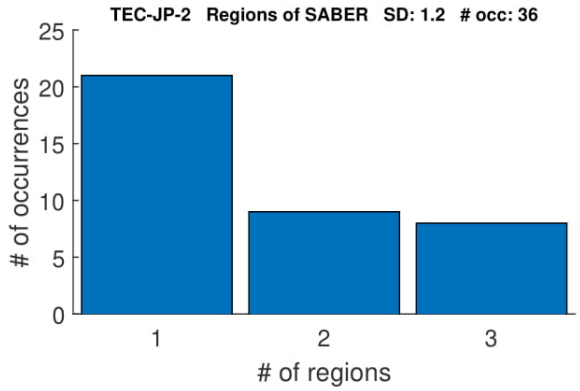

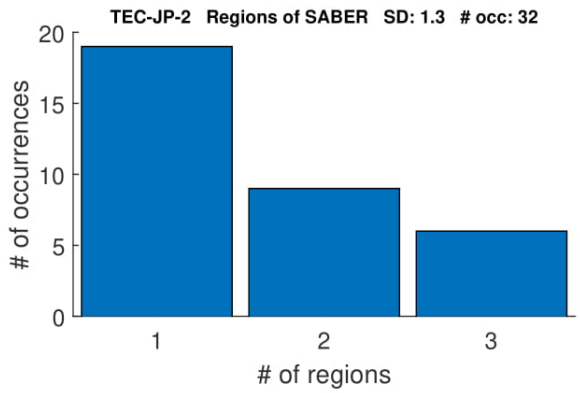

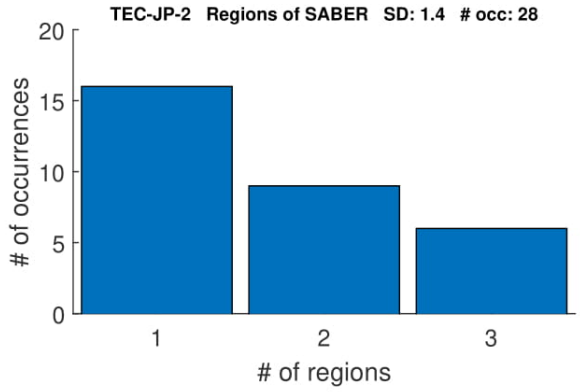

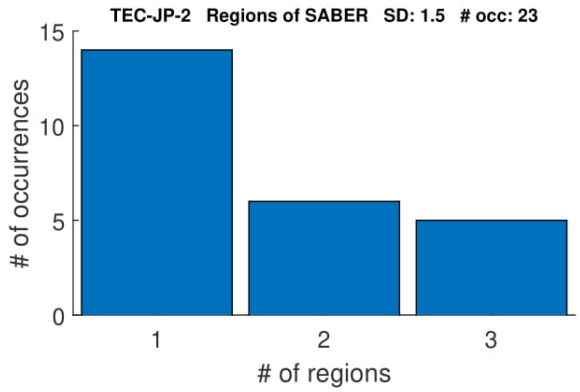

Eliminating Solar

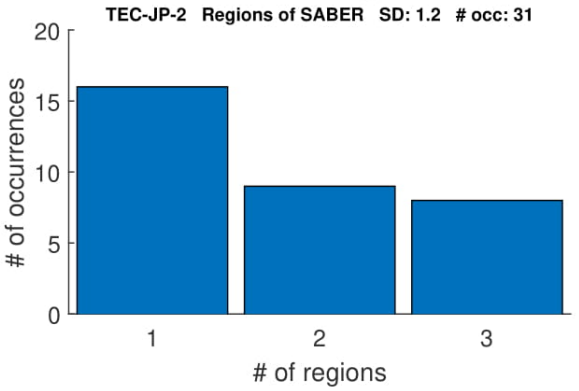

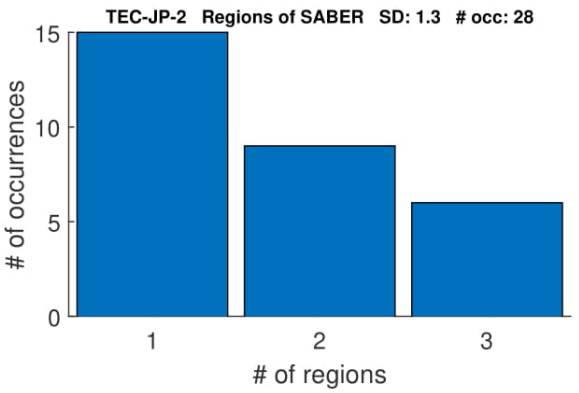

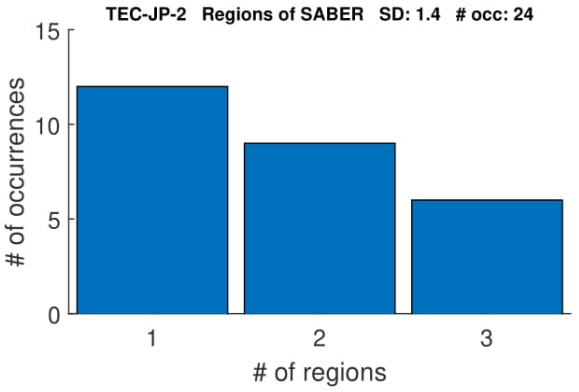

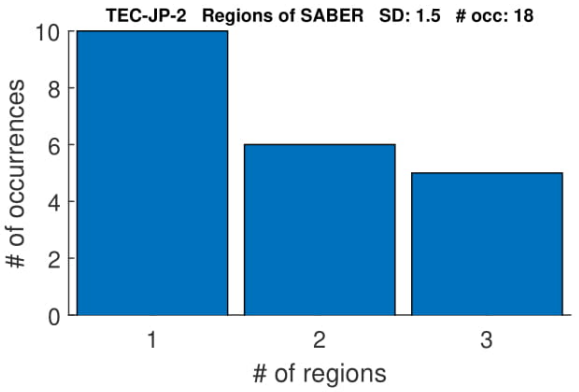

With Solar

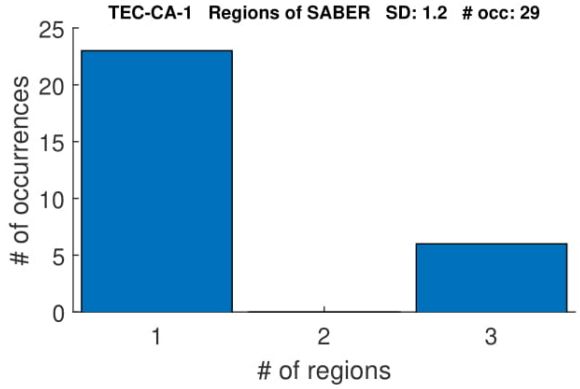

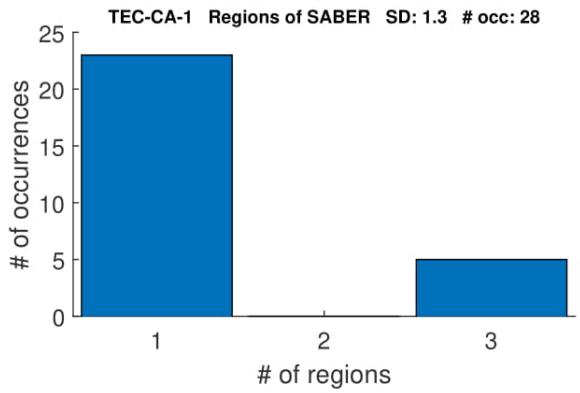

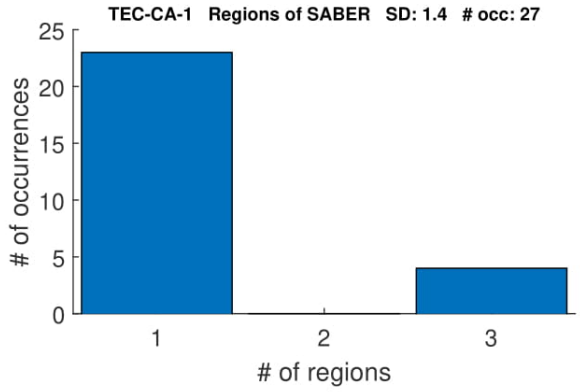

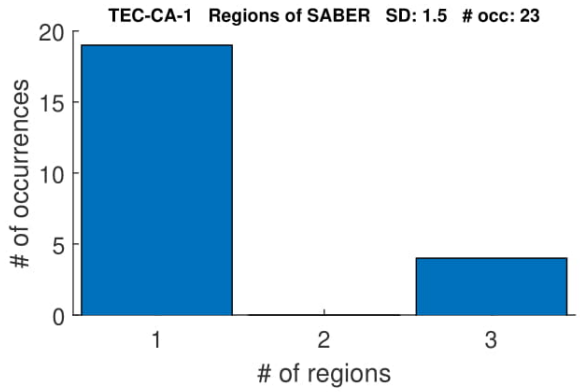

Eliminating Solar

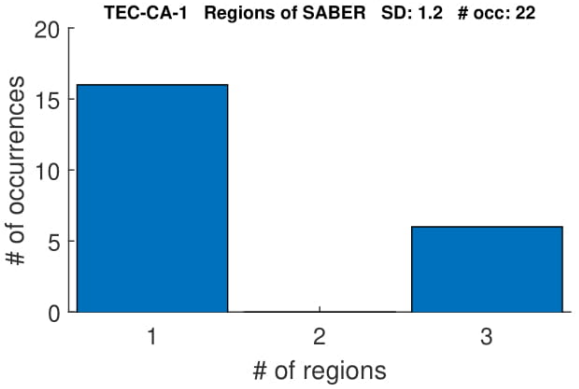

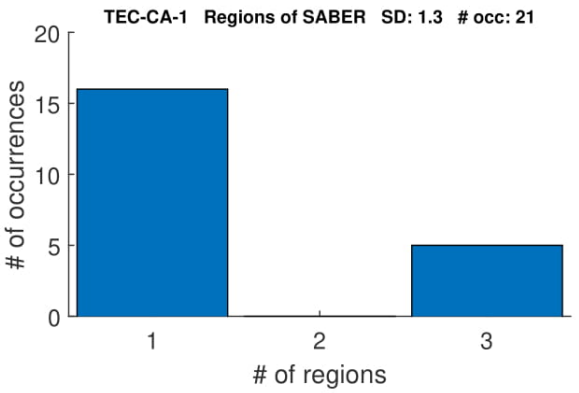

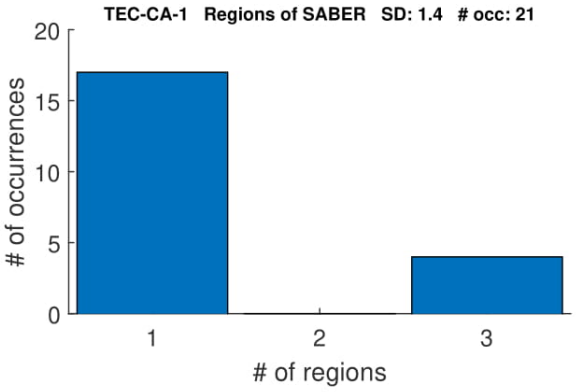

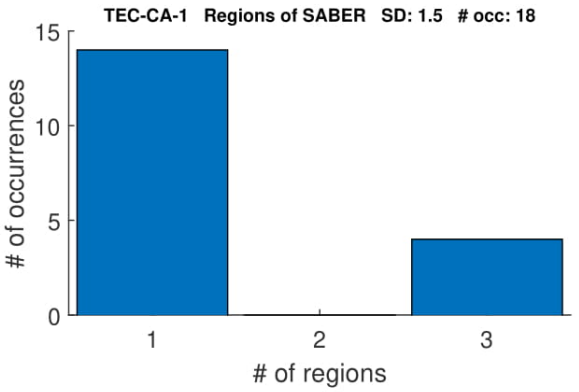

With Solar

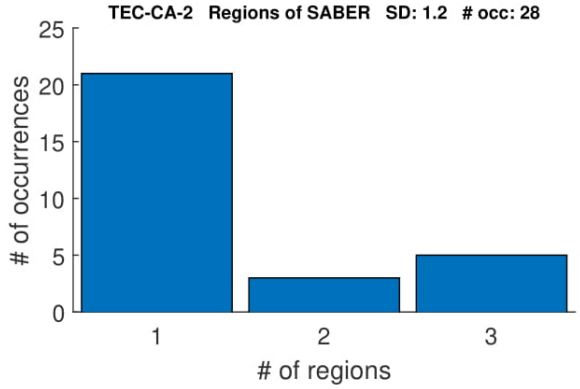

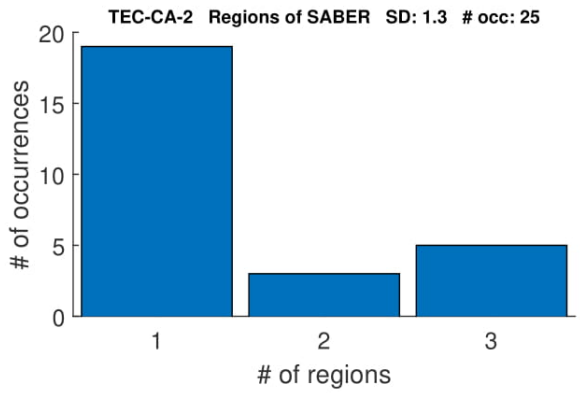

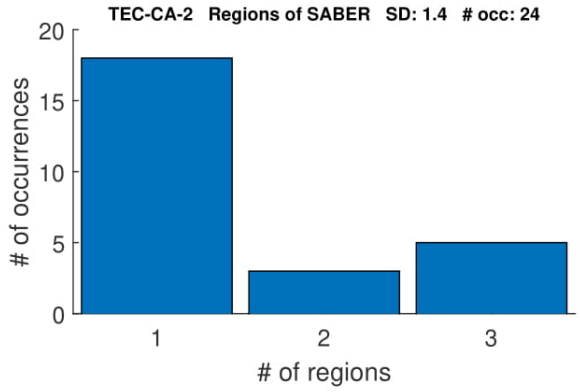

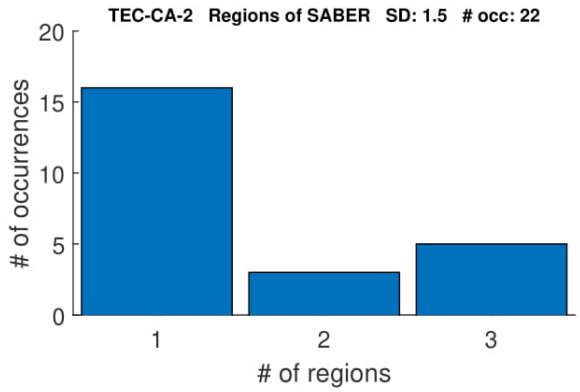

Eliminating Solar

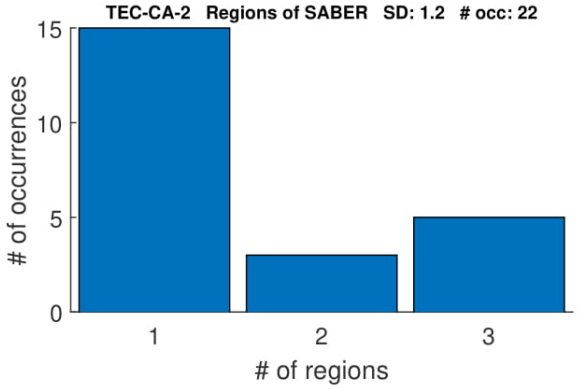

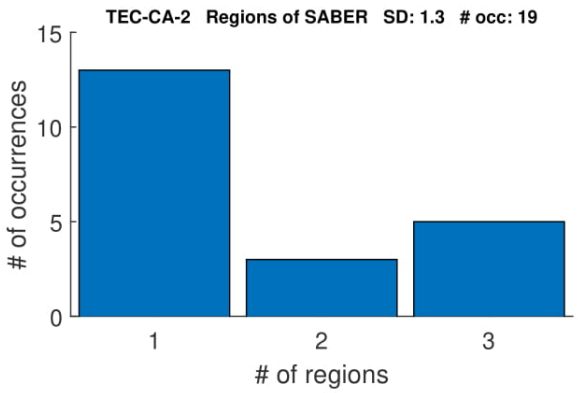

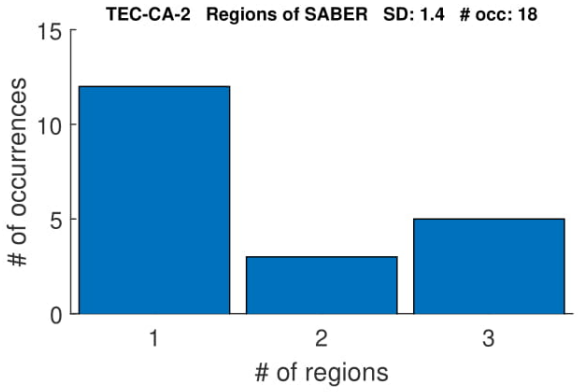

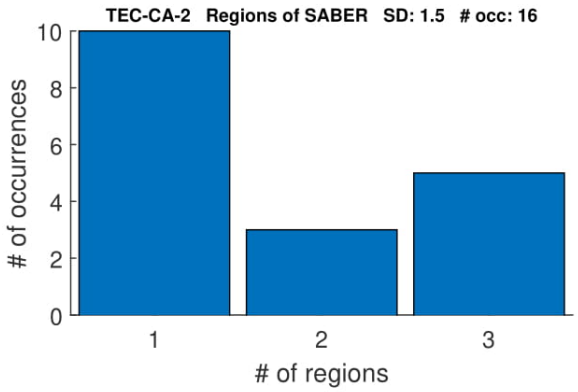

With Solar

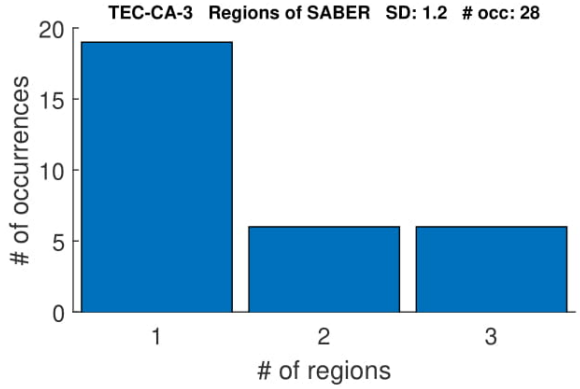

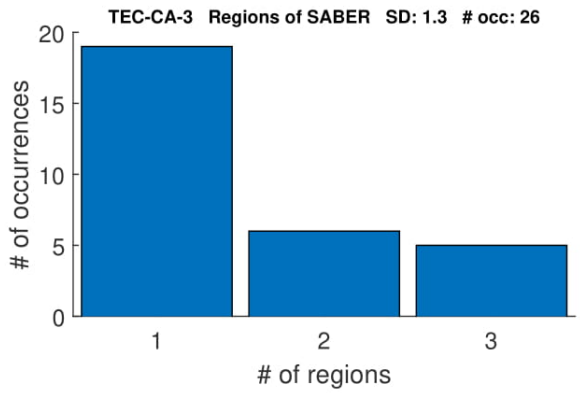

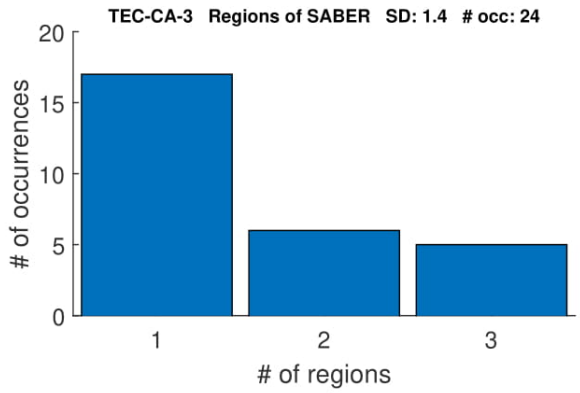

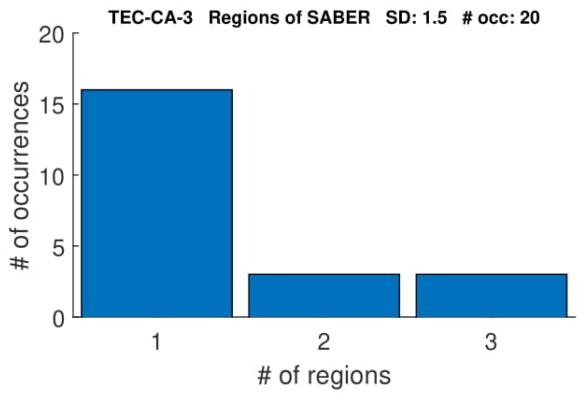

Eliminating Solar

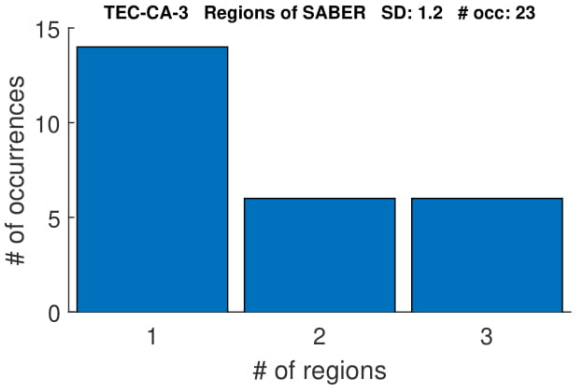

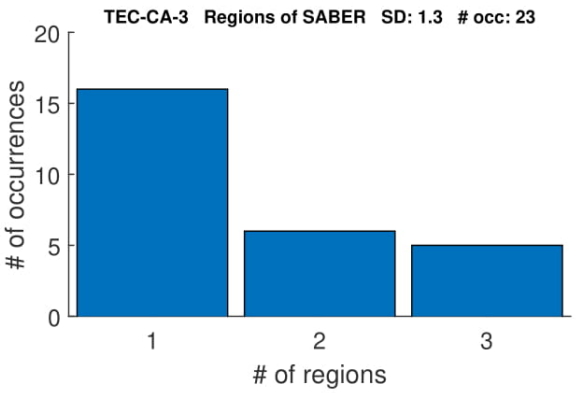

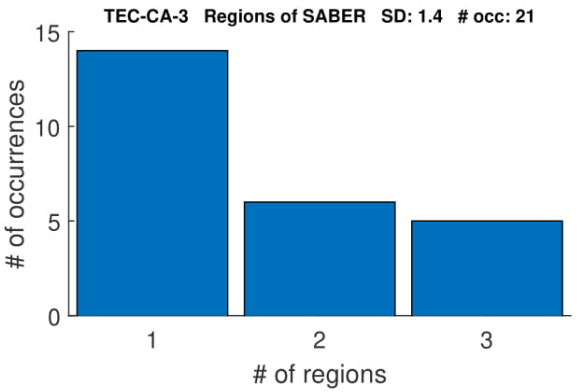

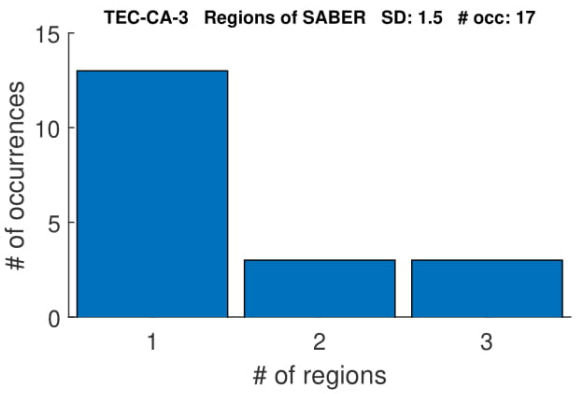

With Solar

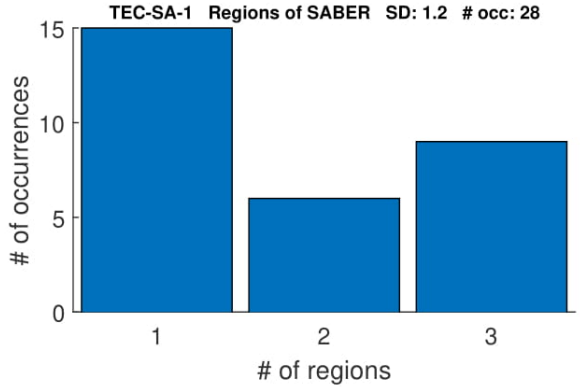

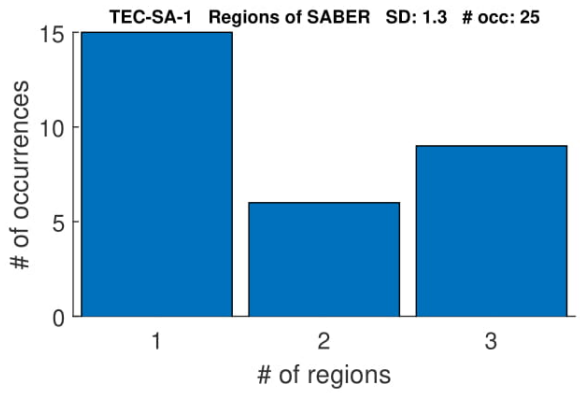

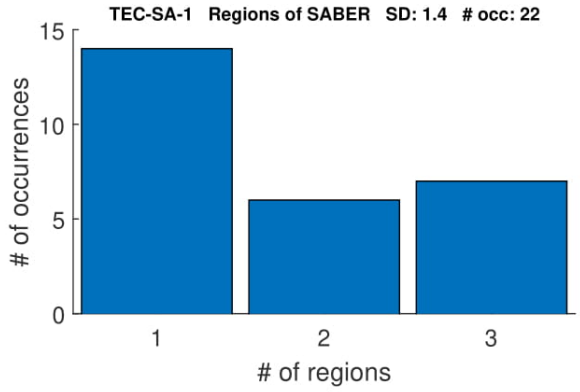

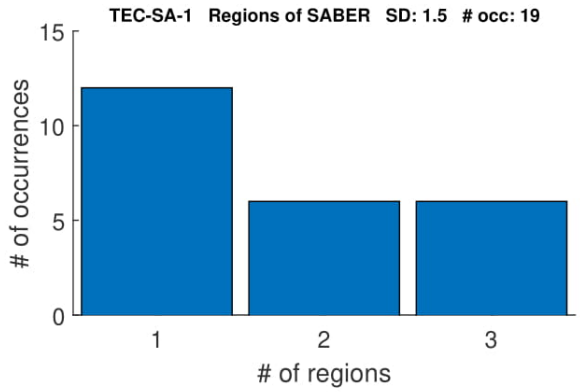

Eliminating Solar

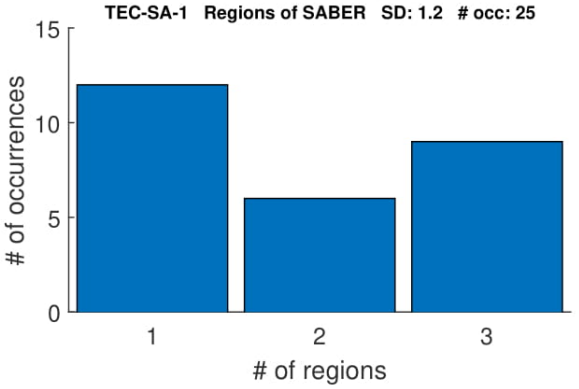

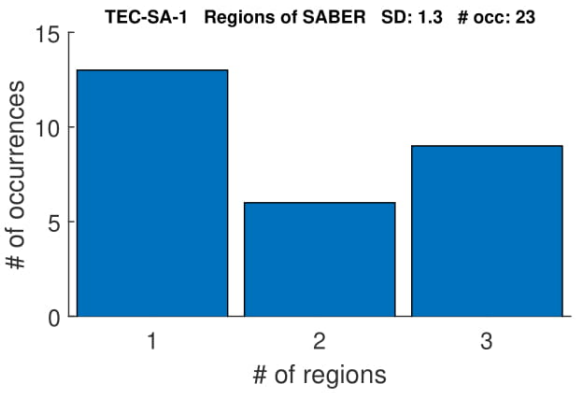

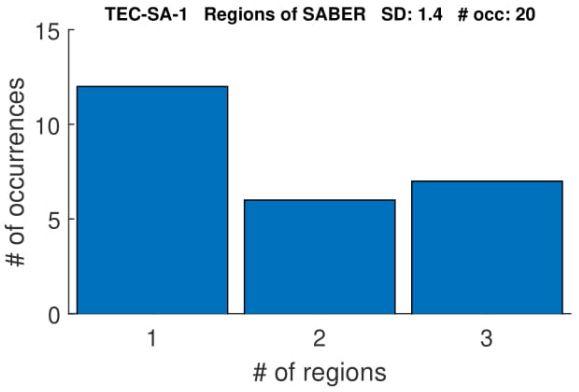

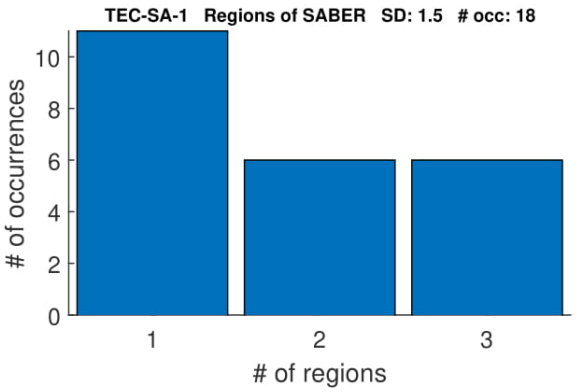

With Solar

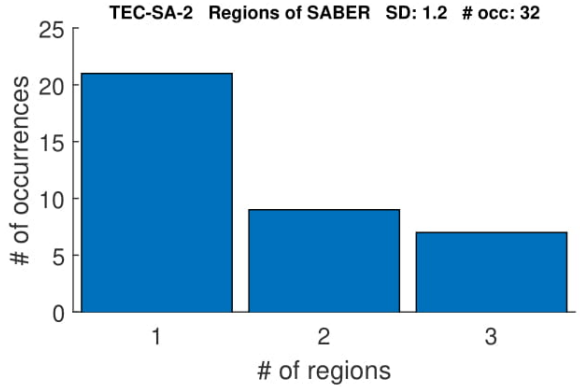

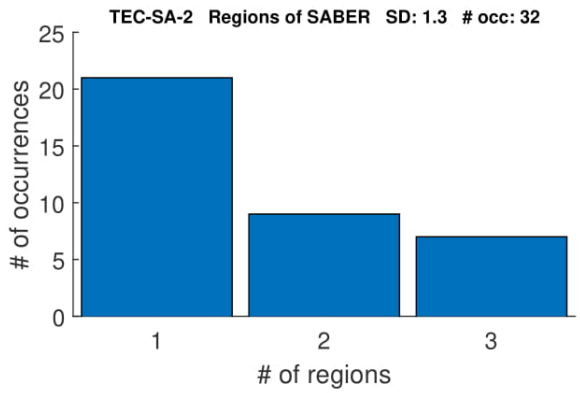

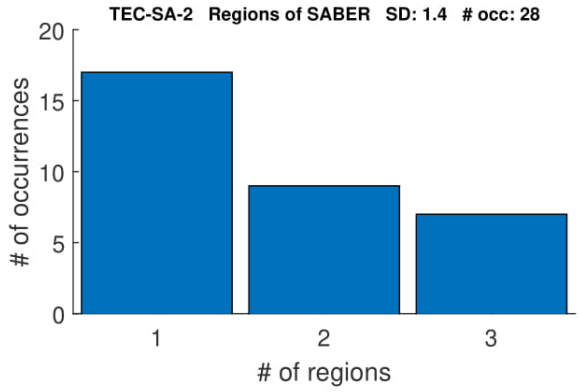

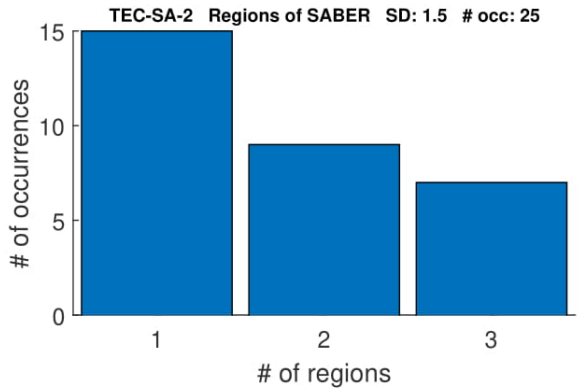

Eliminating Solar

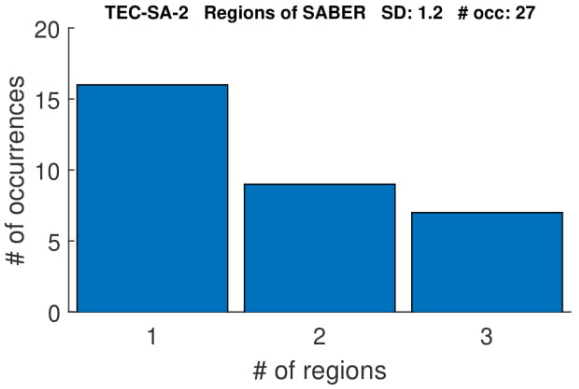

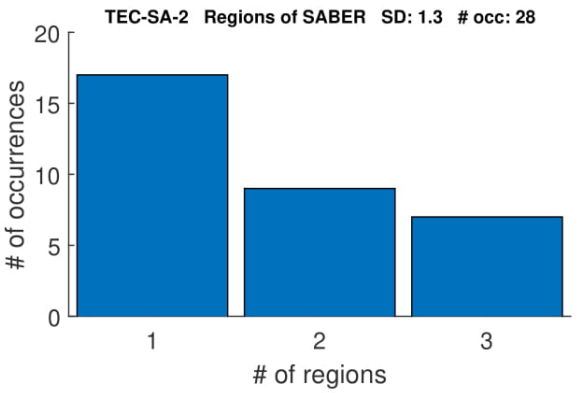

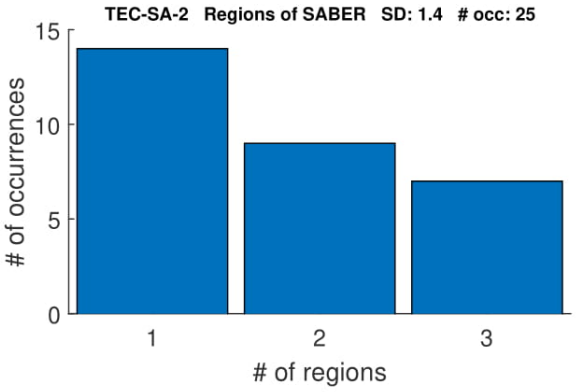

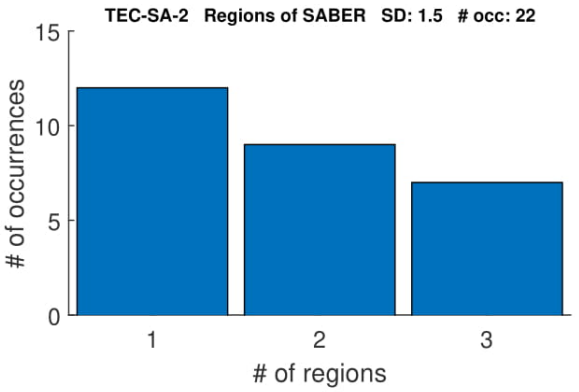

With Solar

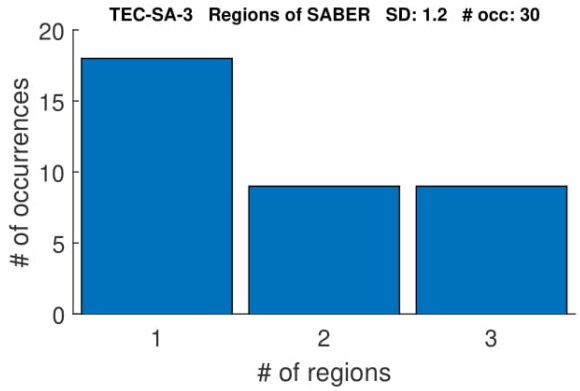

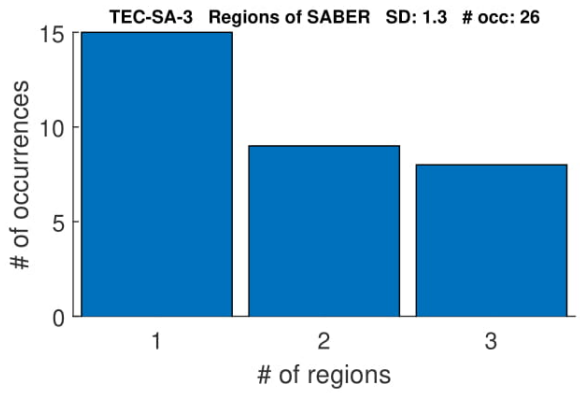

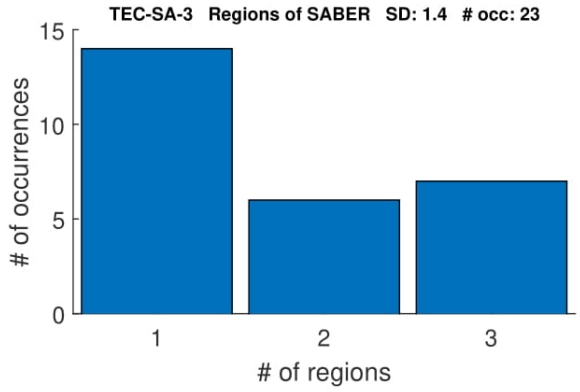

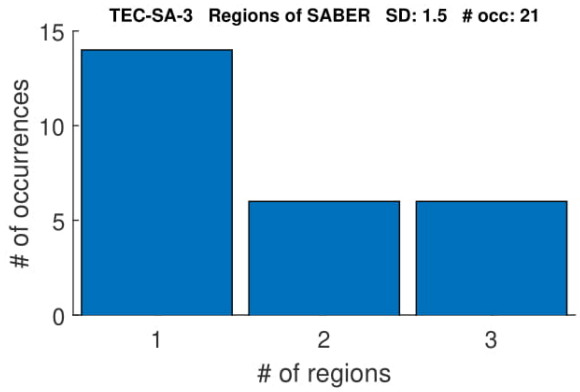

Eliminating Solar

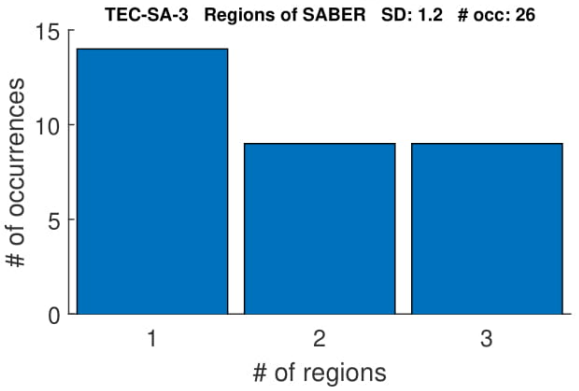

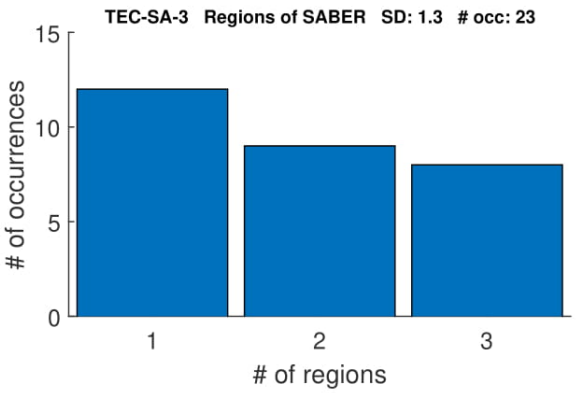

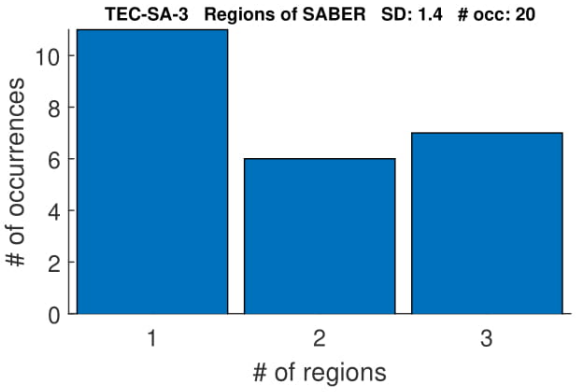

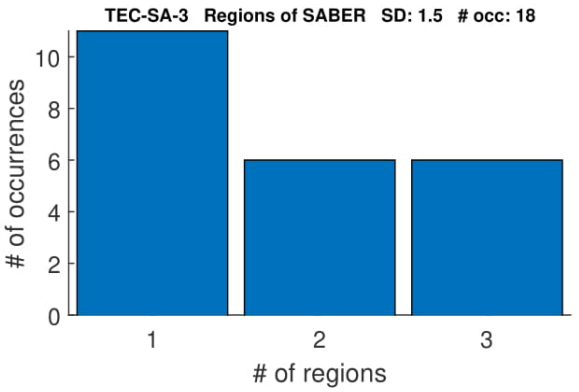

With Solar

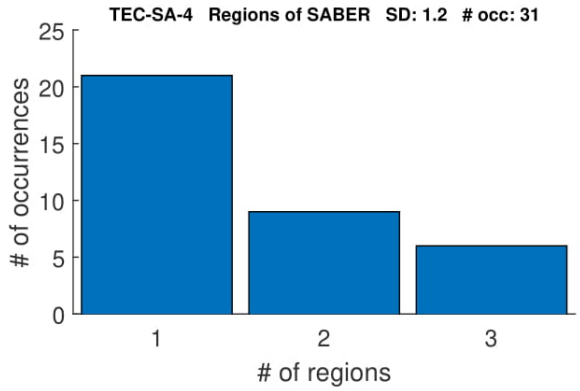

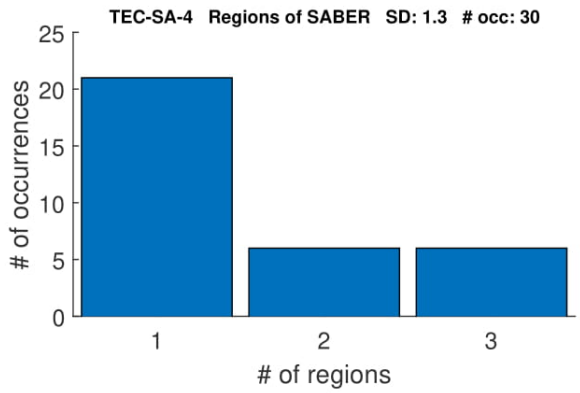

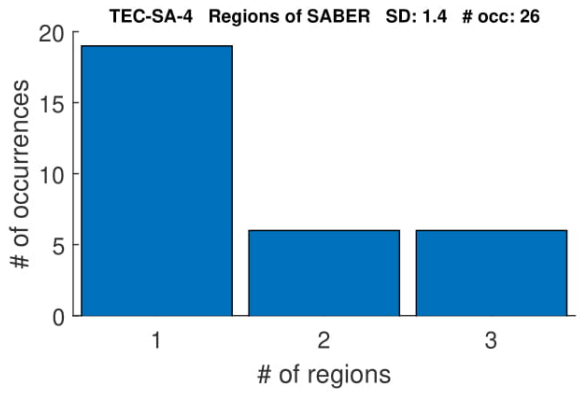

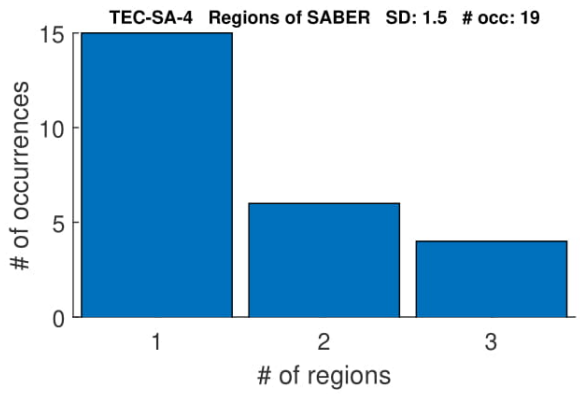

Eliminating Solar

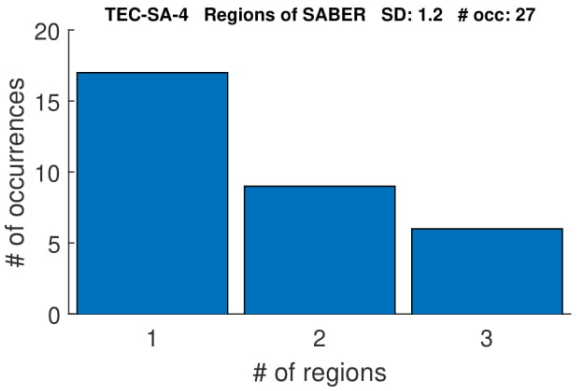

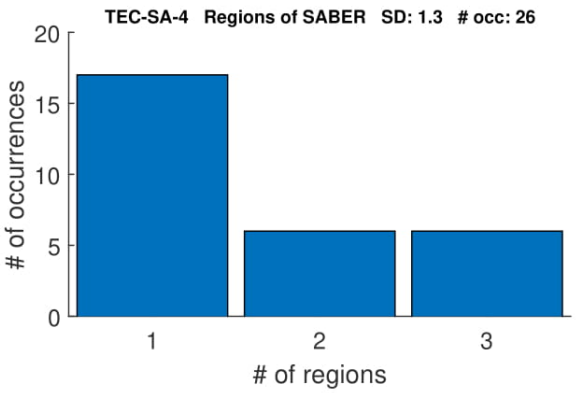

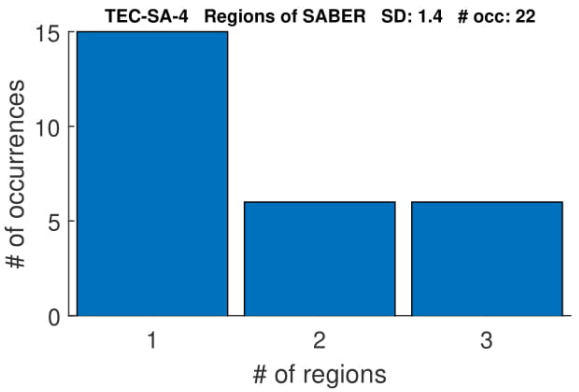

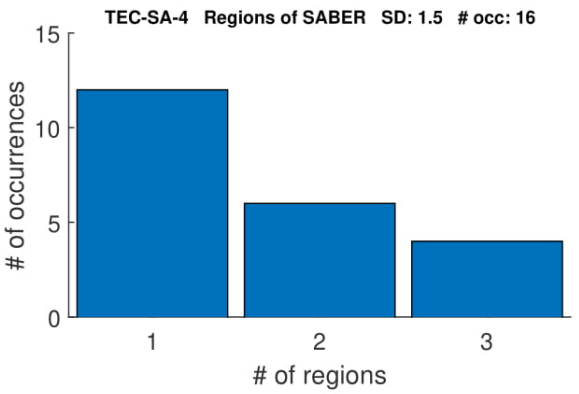

B.4 Specific Latitude Band

This section contains the one of the types of location histograms described in Sections 3.3.2 and 4.3. These histograms display the specific latitude band the SABER event occurs in. These figures are similar to the right plot in 3.14 and 4.4.

With Solar

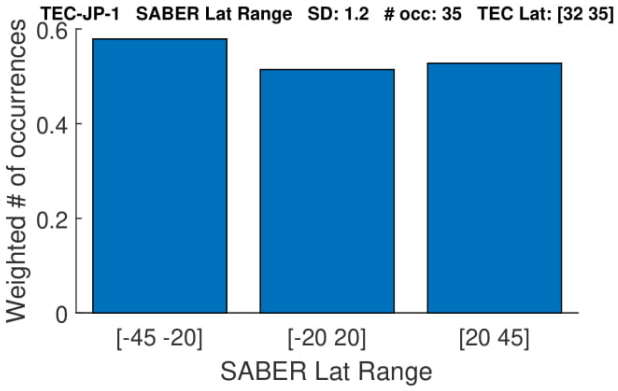

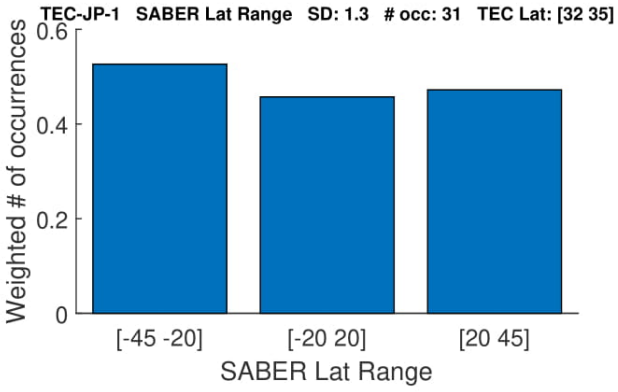

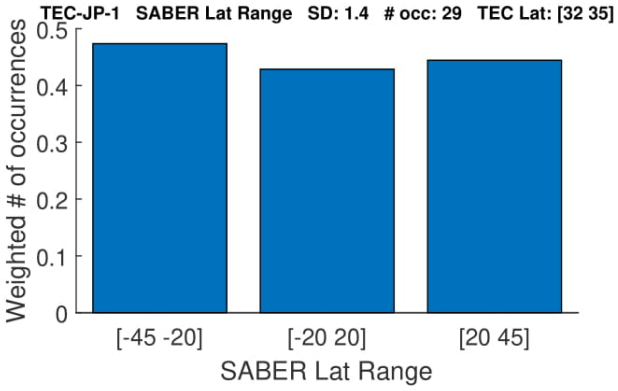

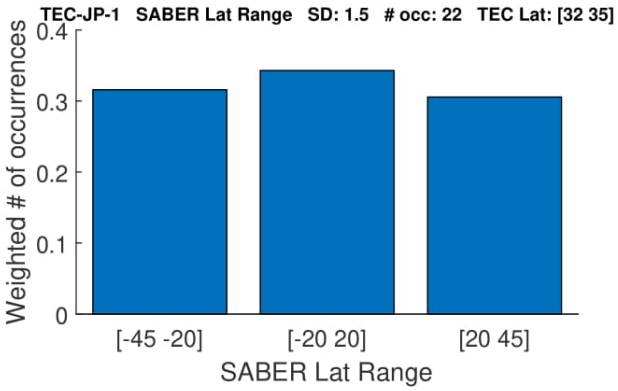

Eliminating Solar

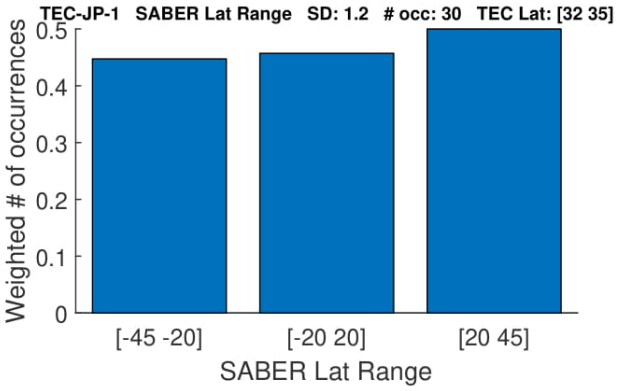

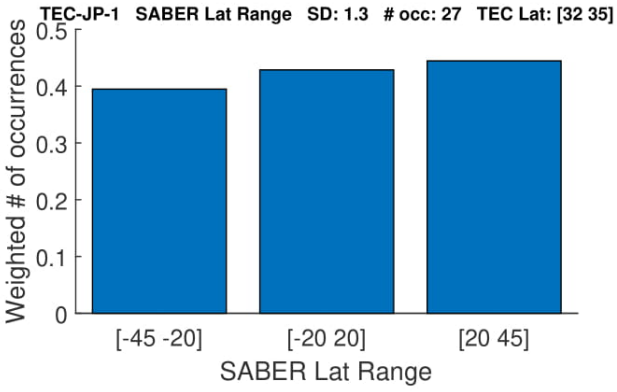

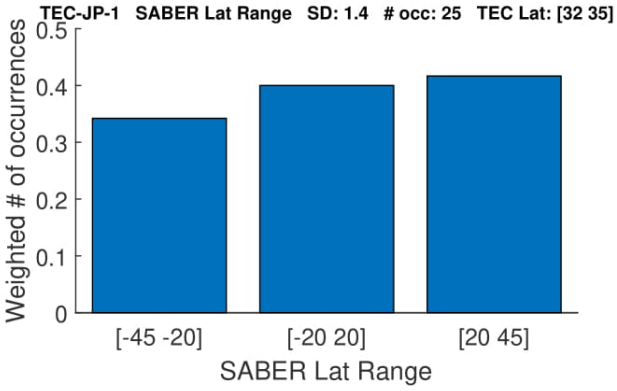

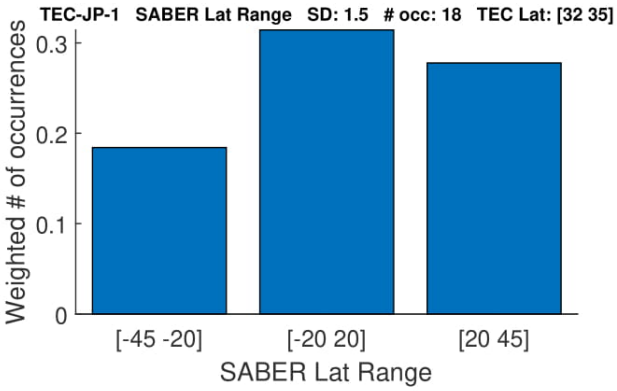

With Solar

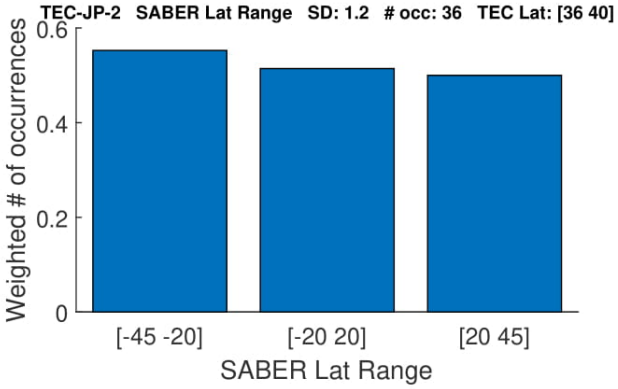

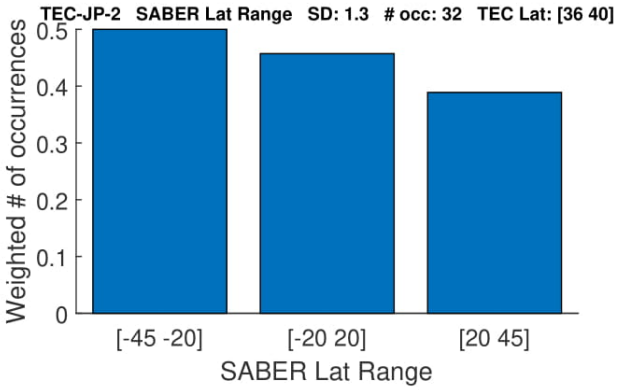

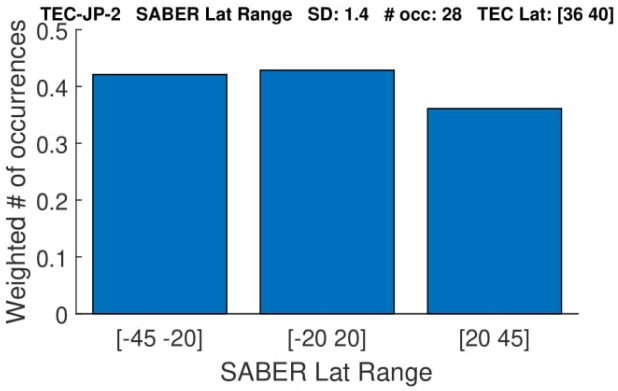

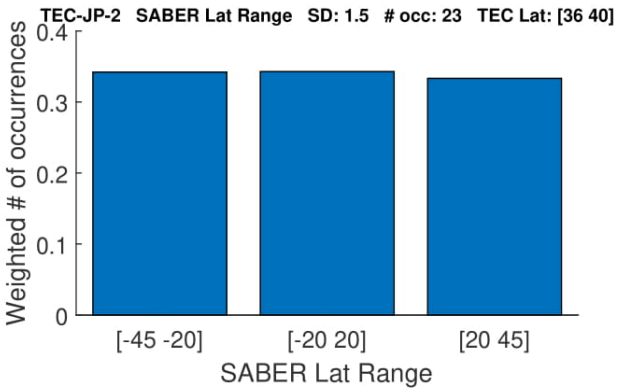

Eliminating Solar

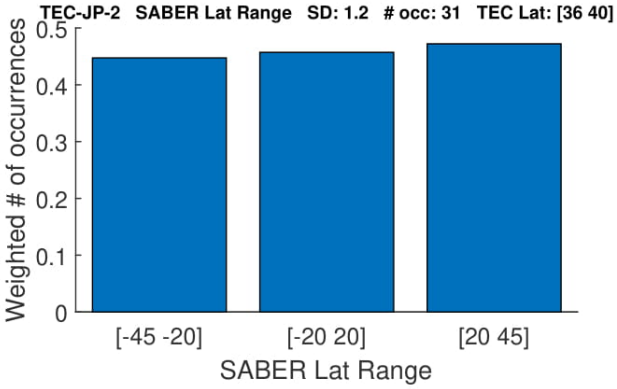

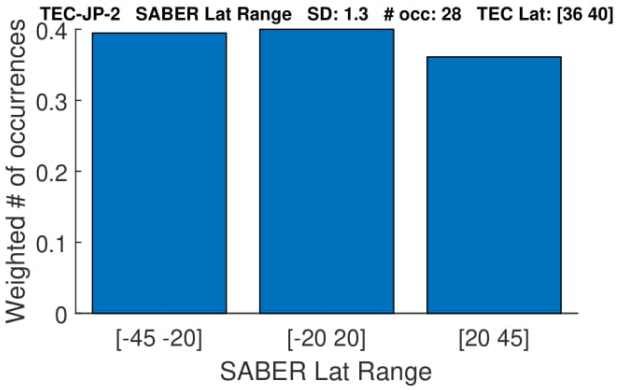

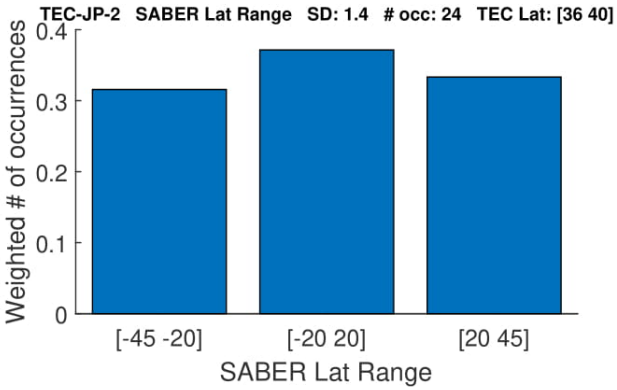

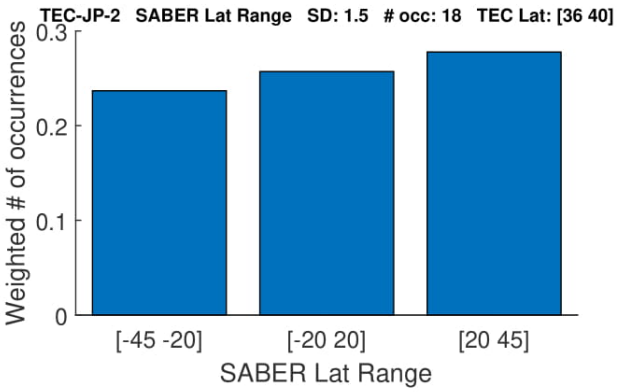

With Solar

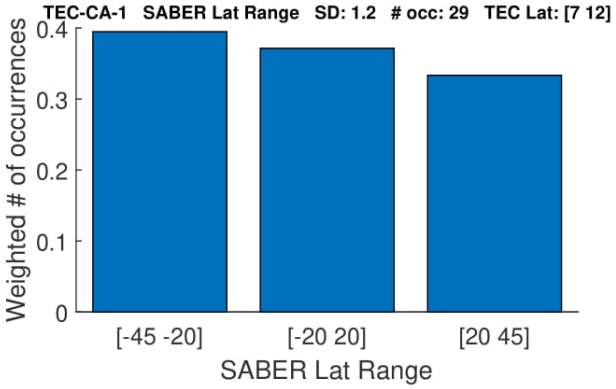

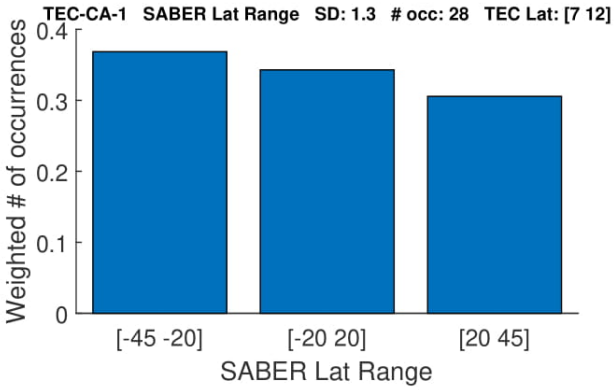

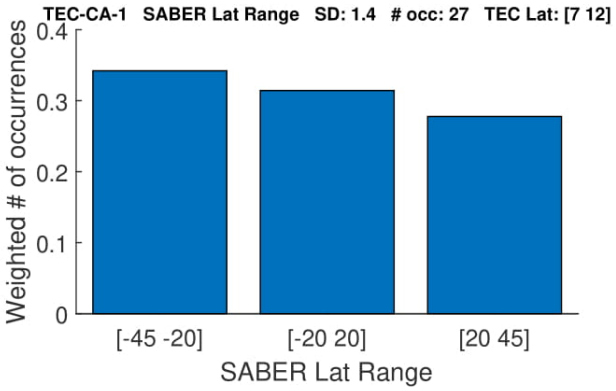

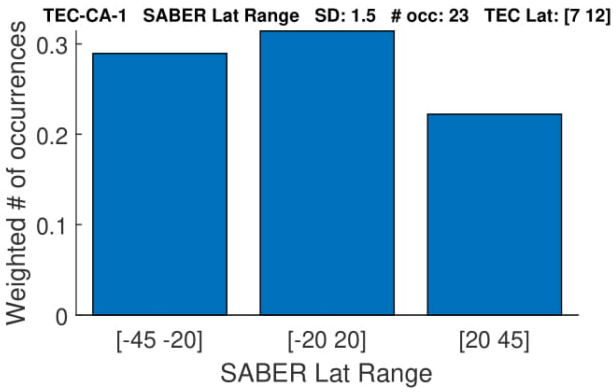

Eliminating Solar

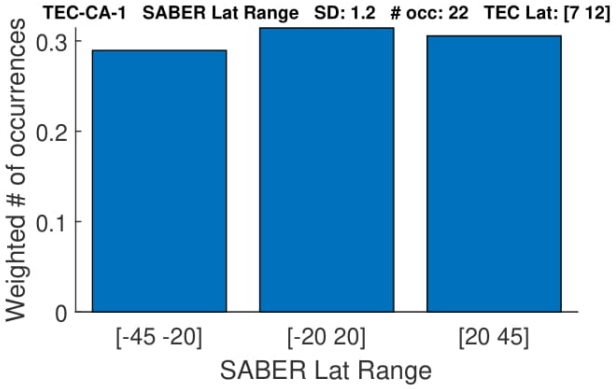

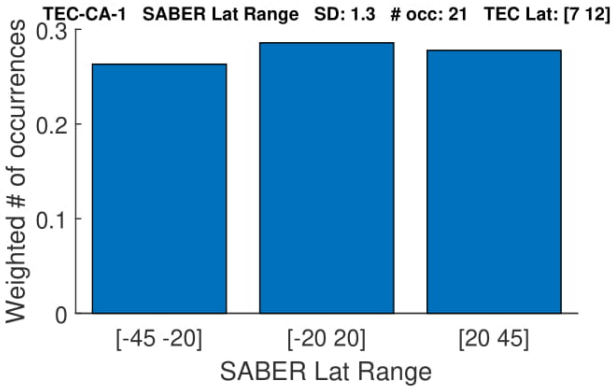

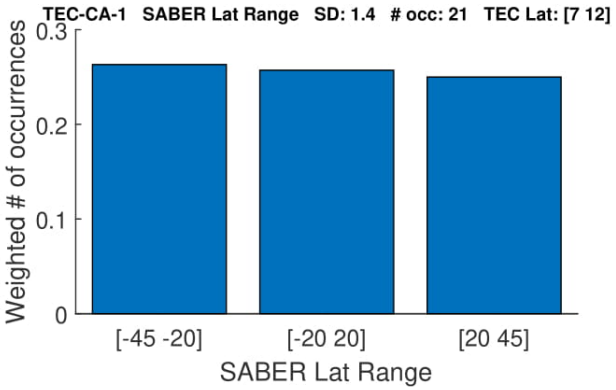

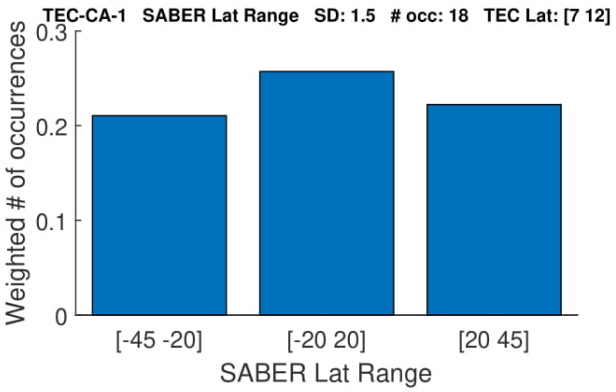

With Solar

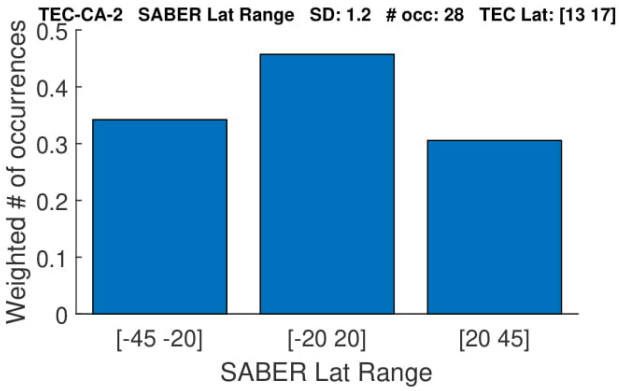

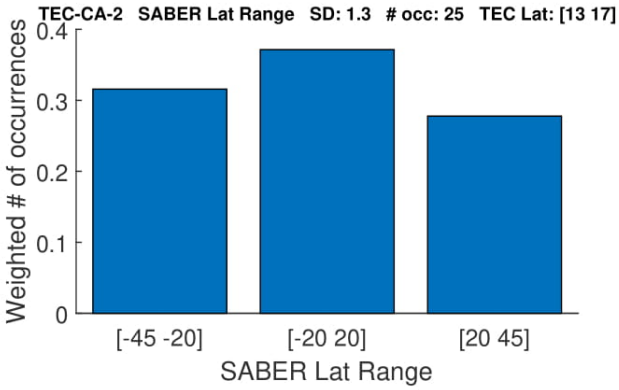

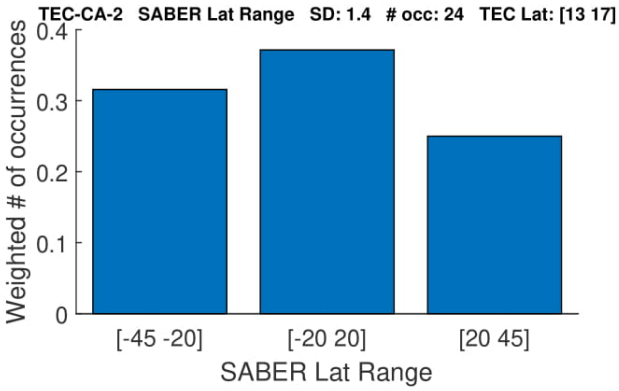

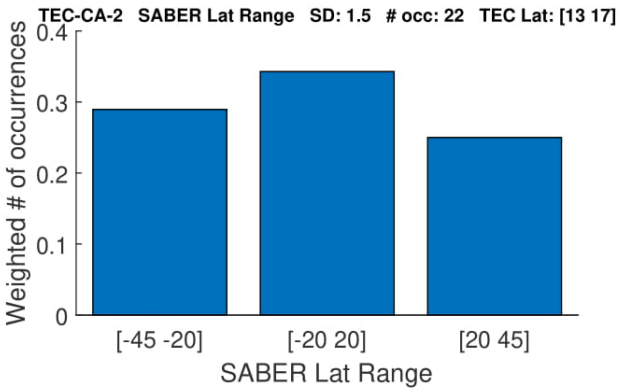

Eliminating Solar

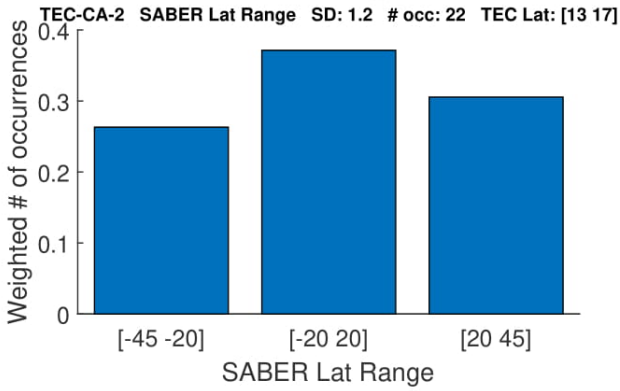

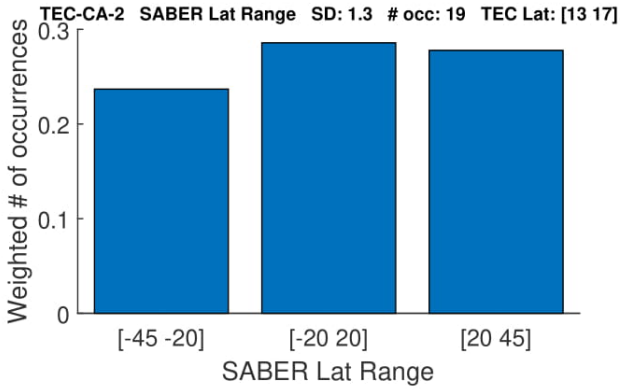

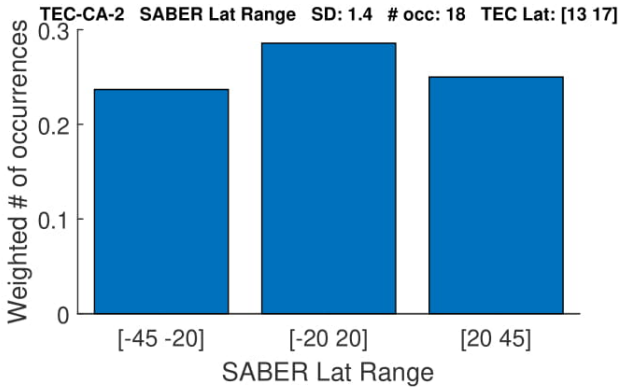

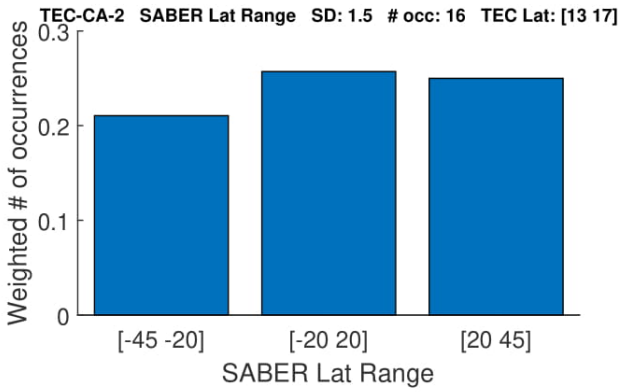

With Solar

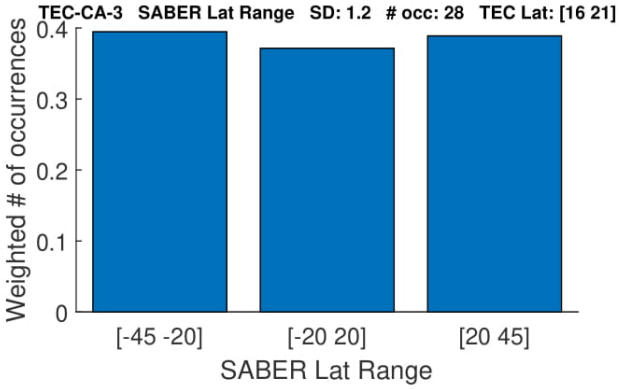

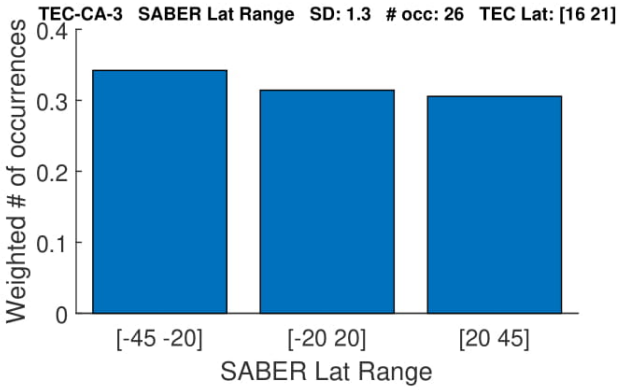

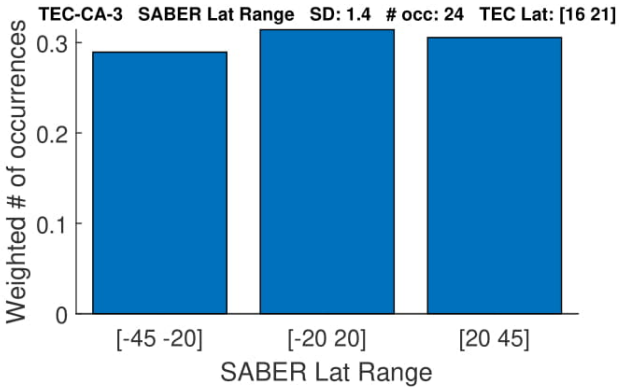

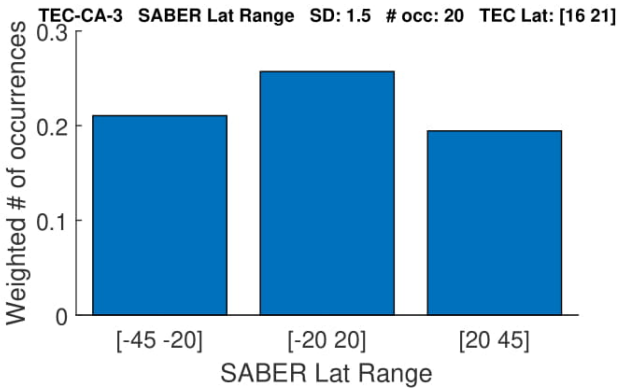

Eliminating Solar

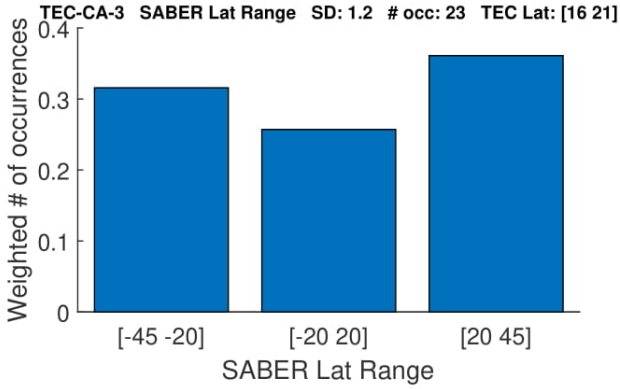

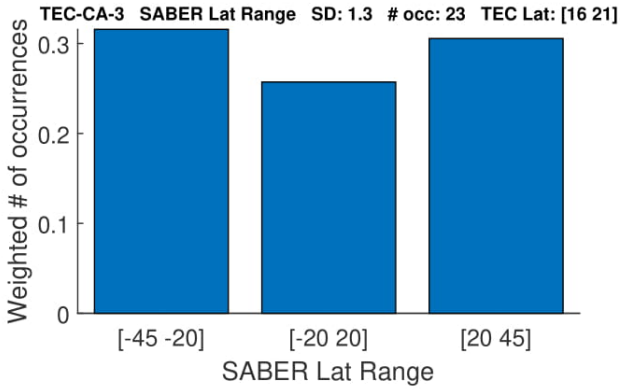

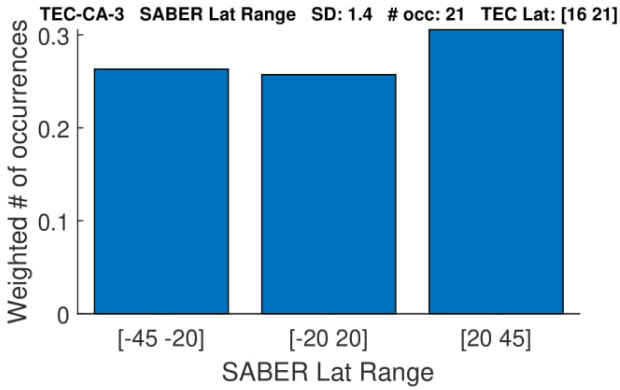

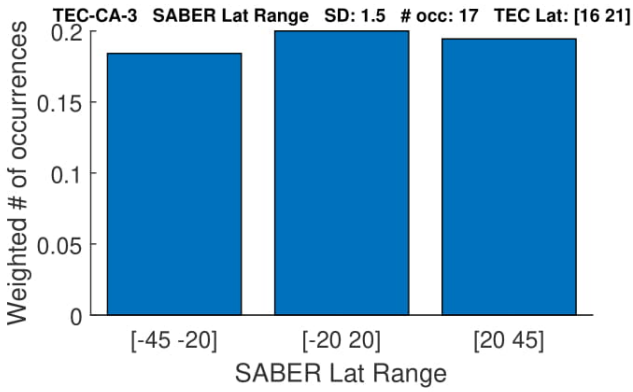

With Solar

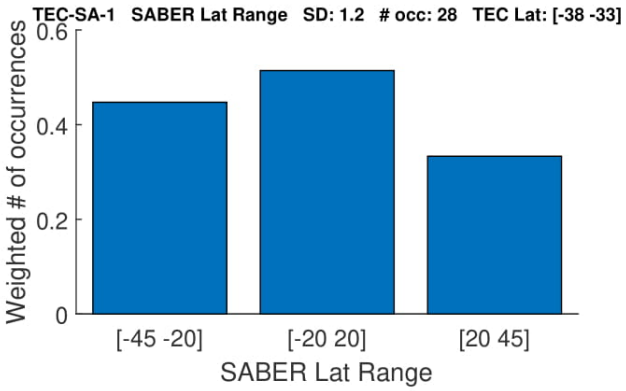

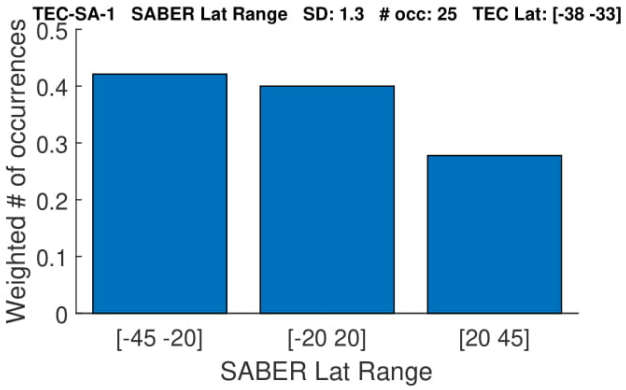

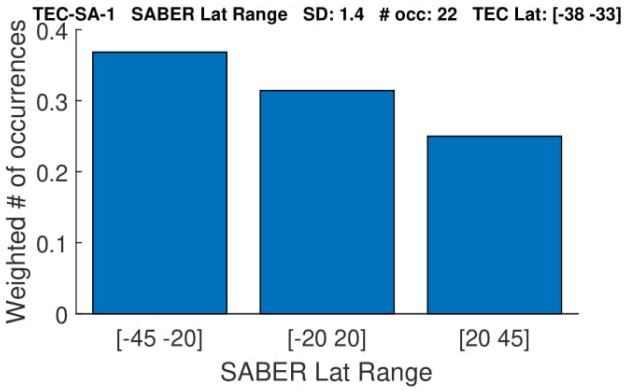

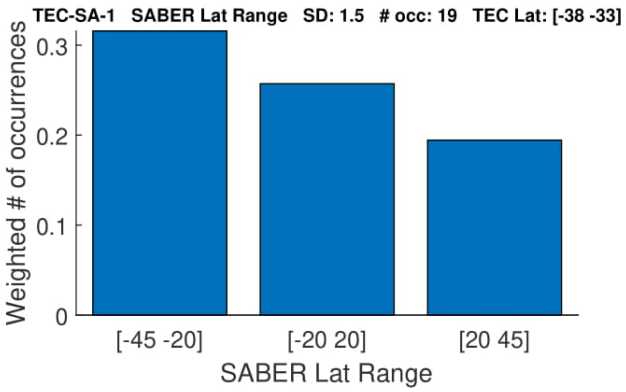

Eliminating Solar

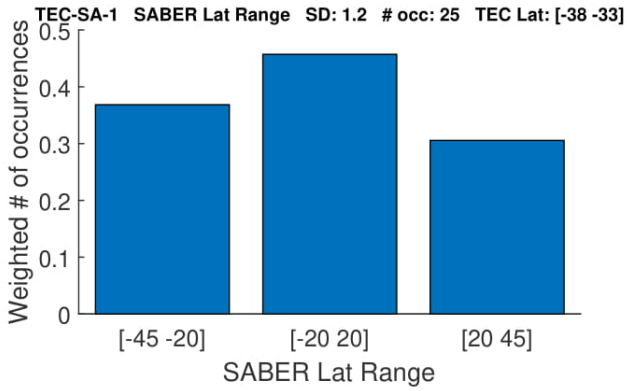

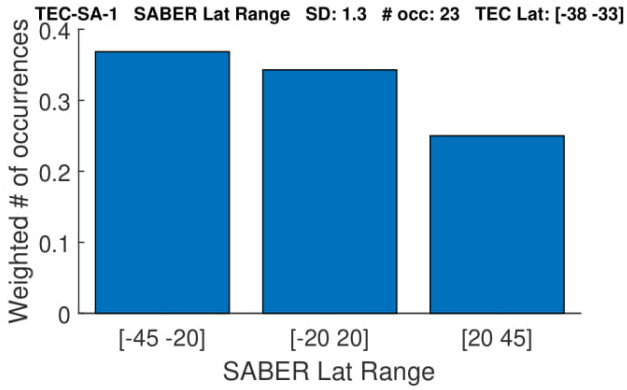

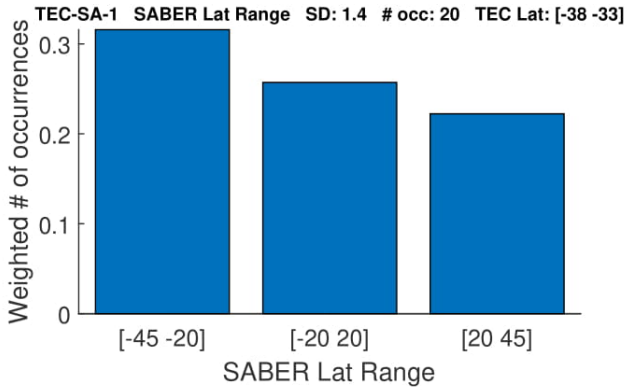

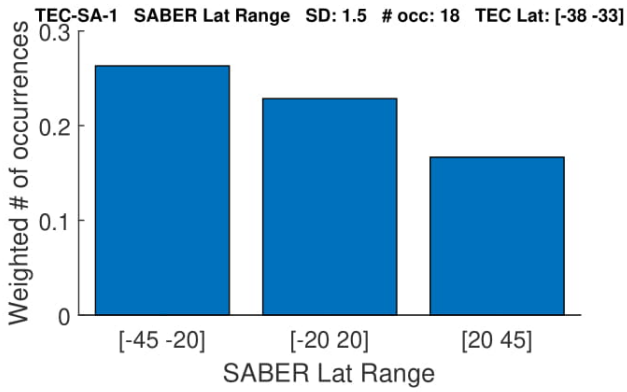

With Solar

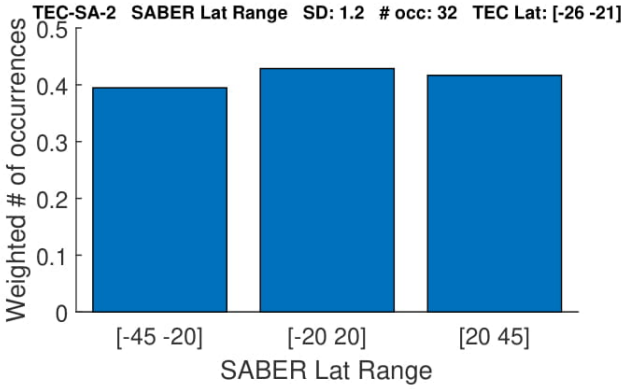

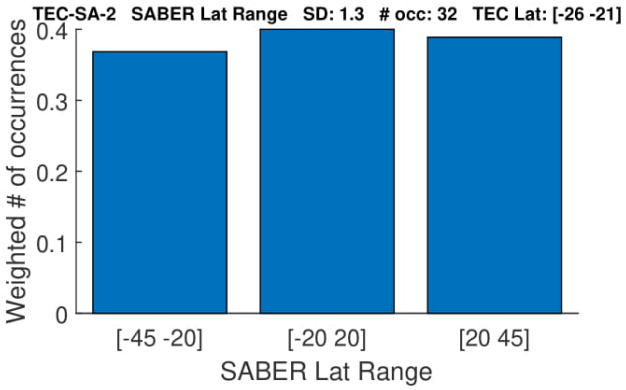

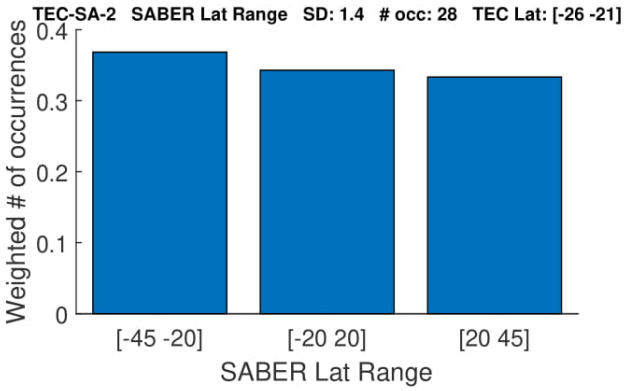

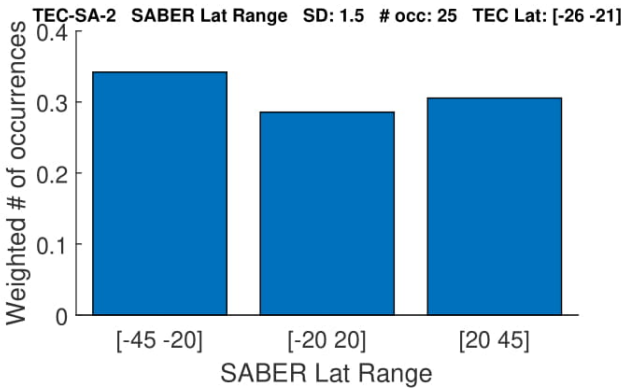

Eliminating Solar

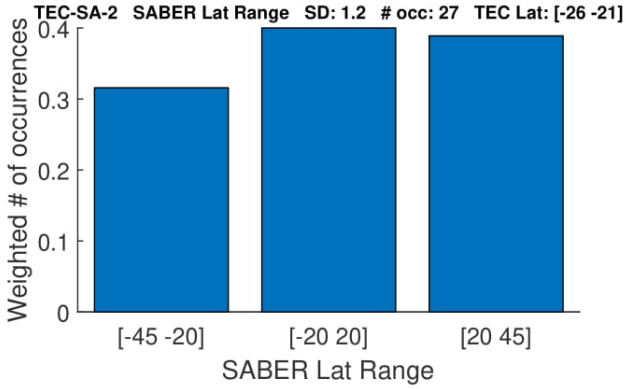

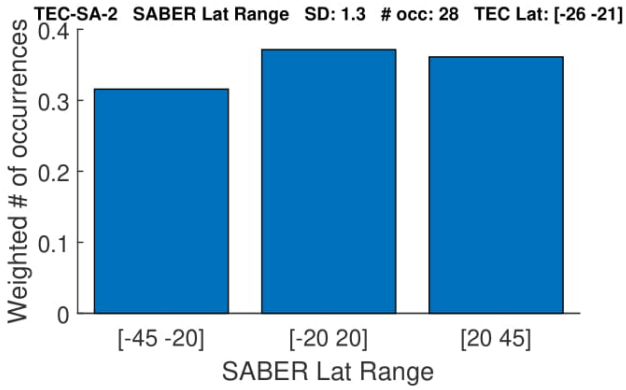

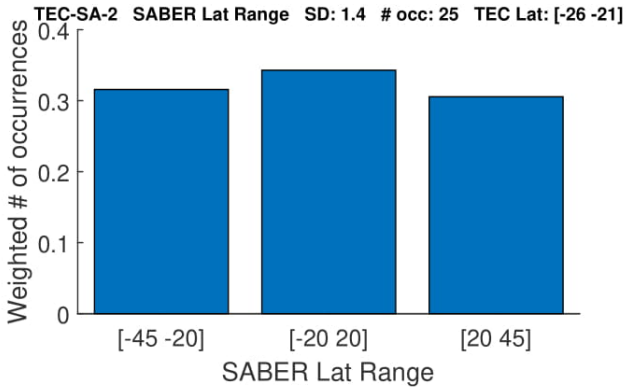

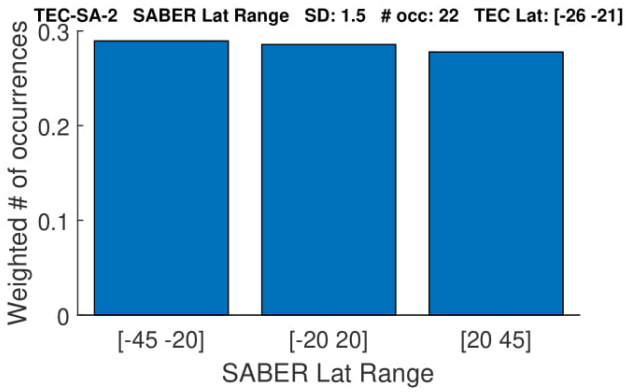

With Solar

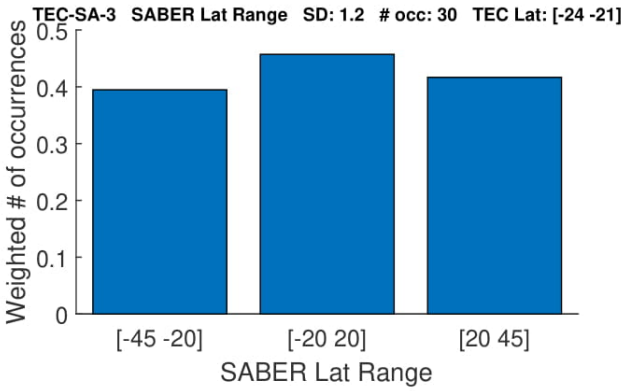

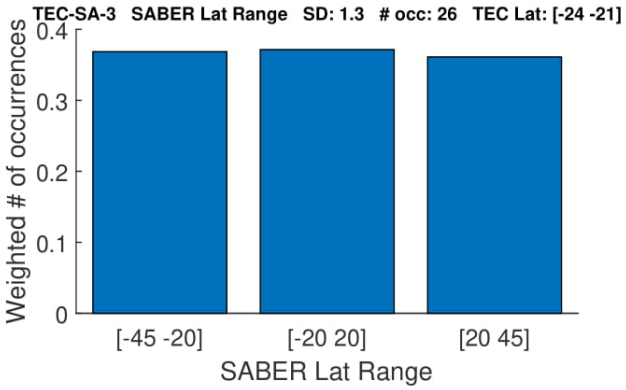

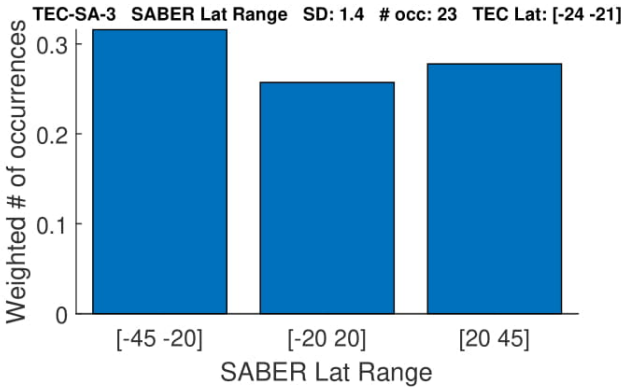

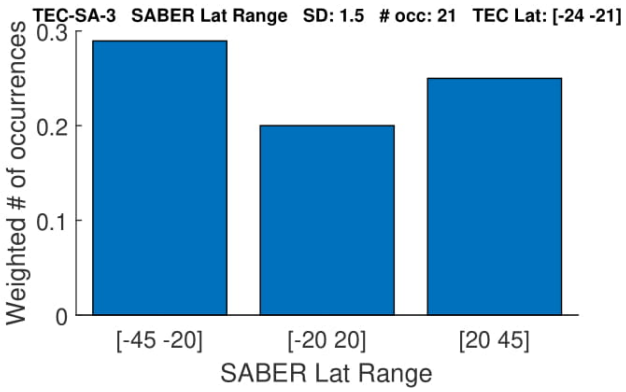

Eliminating Solar

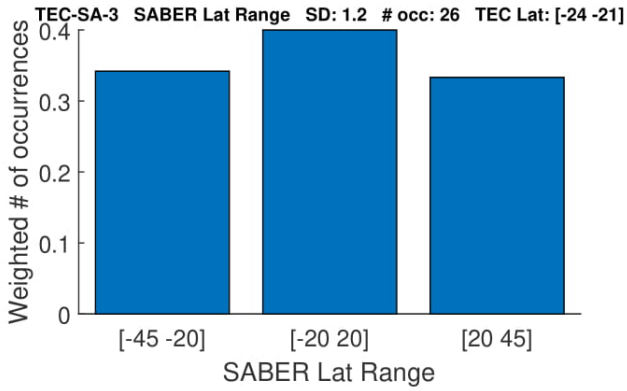

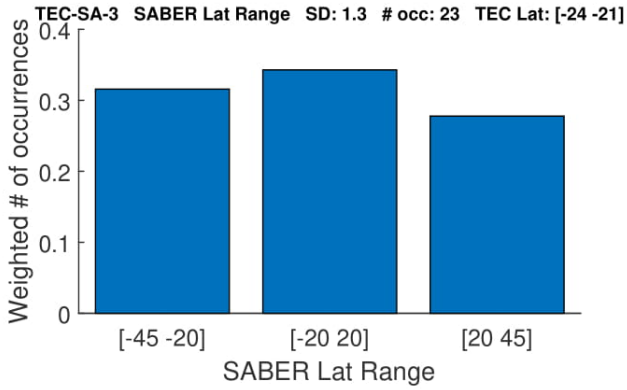

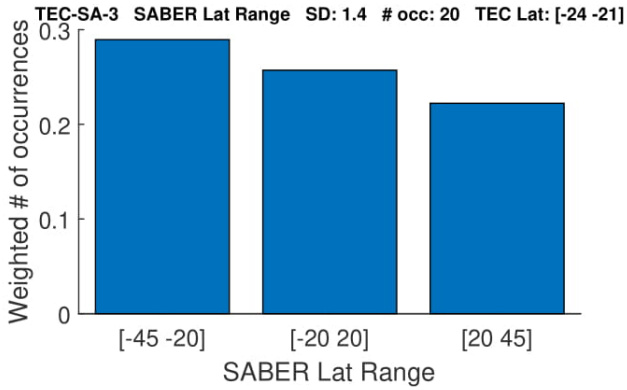

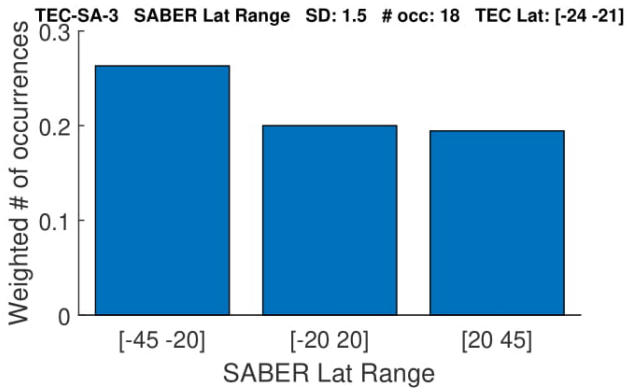

With Solar

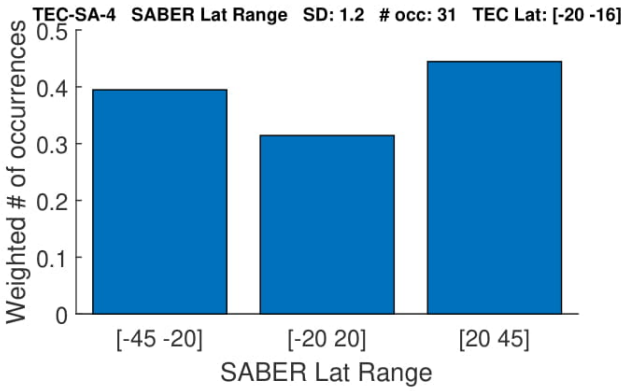

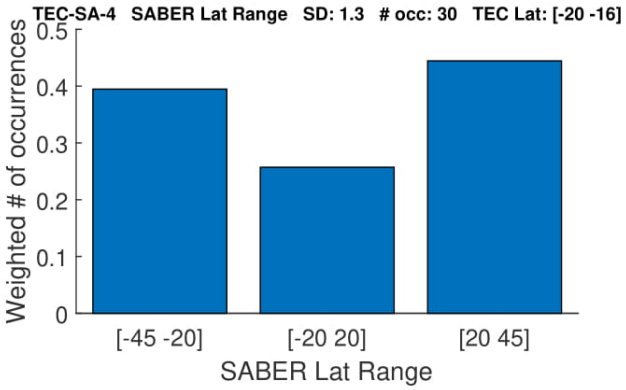

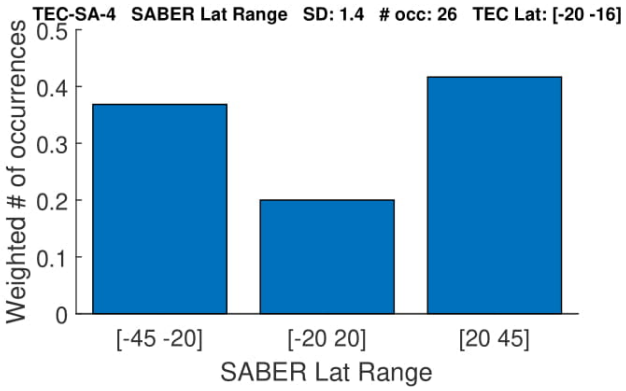

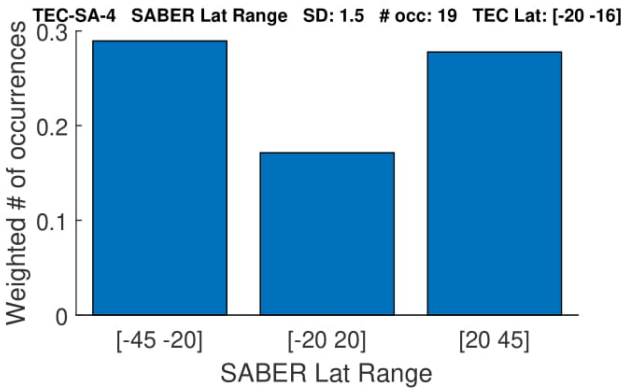

Eliminating Solar

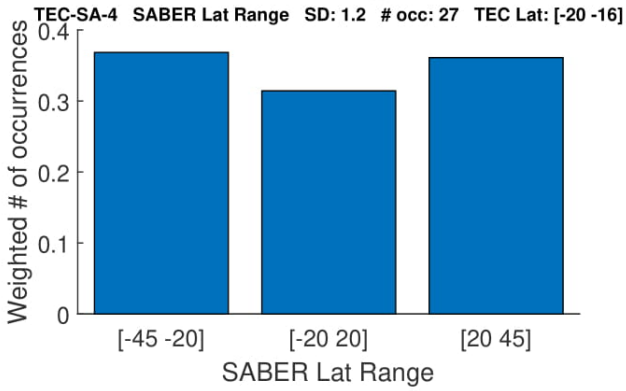

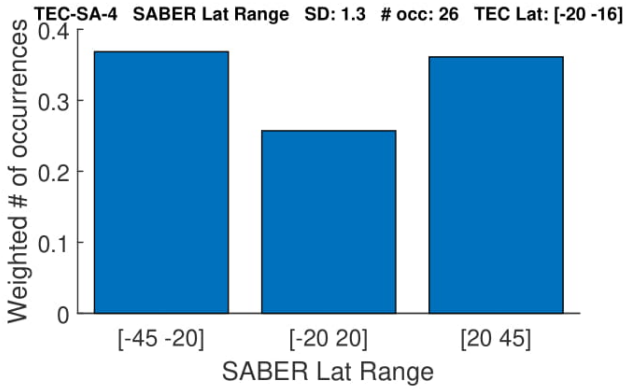

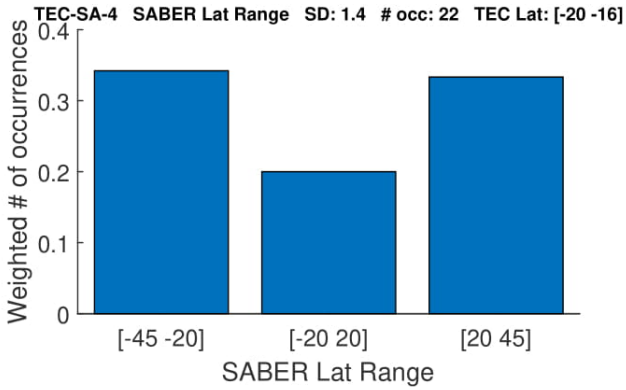

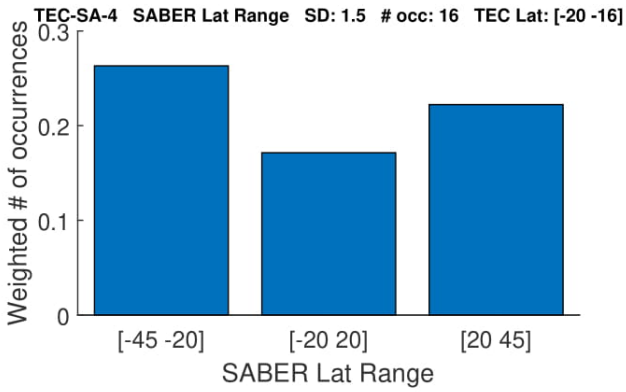

B.5 Solar Level

This section contains the one of the types of solar level histograms described in Sections 3.3.2 and 4.4. These histograms display the specific latitude band the SABER event occurs in. These figures are similar to 3.15.

With Solar

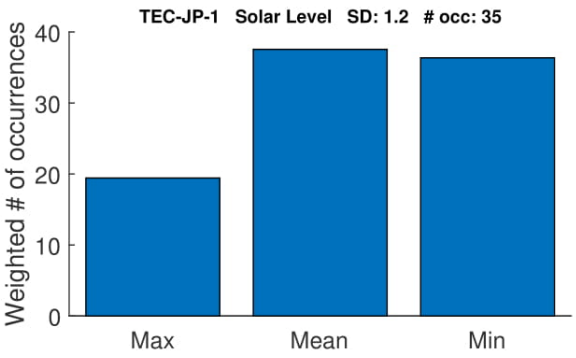

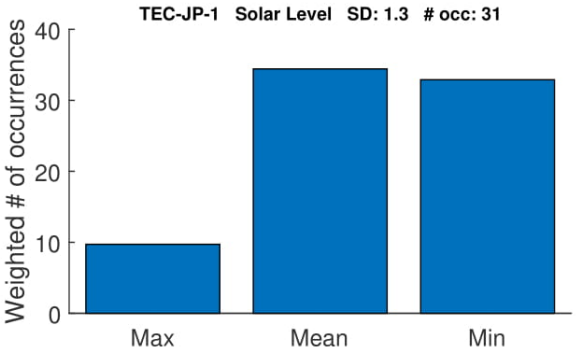

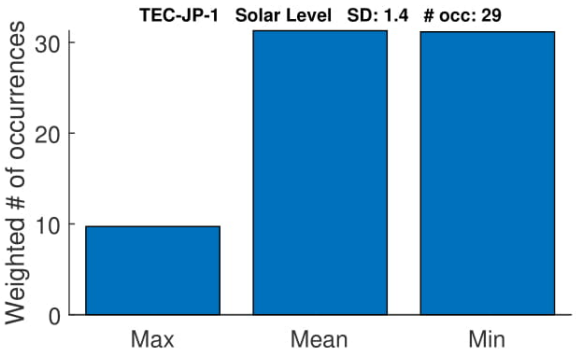

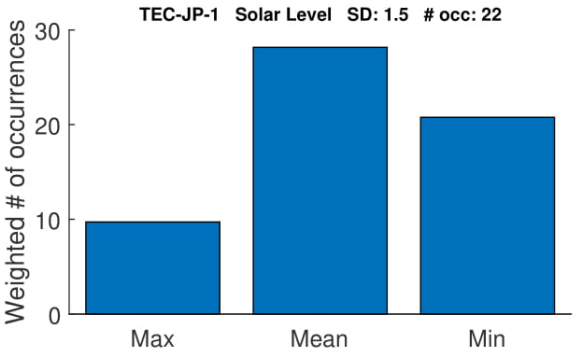

Eliminating Solar

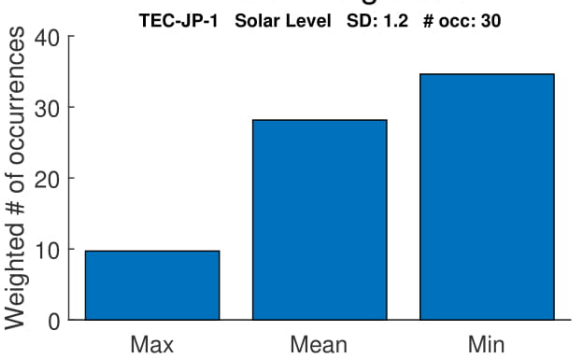

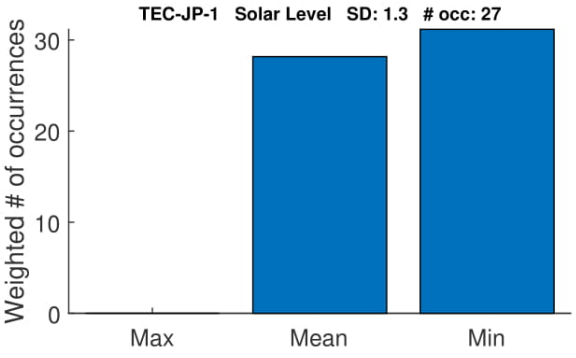

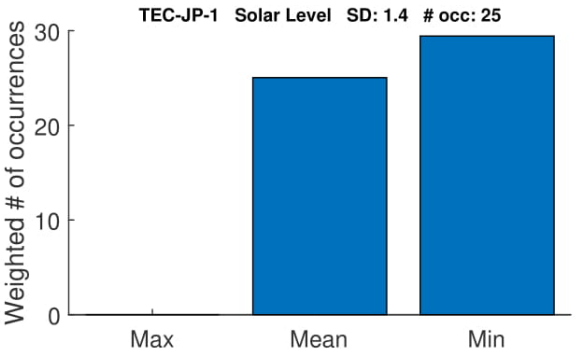

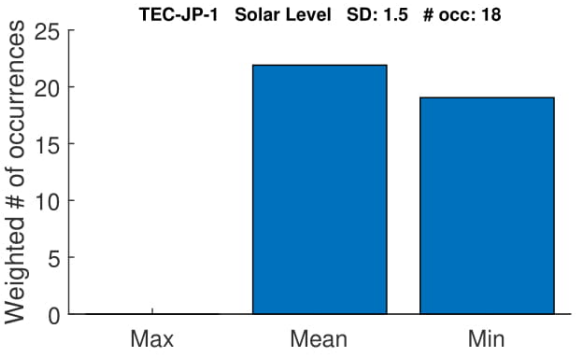

With Solar

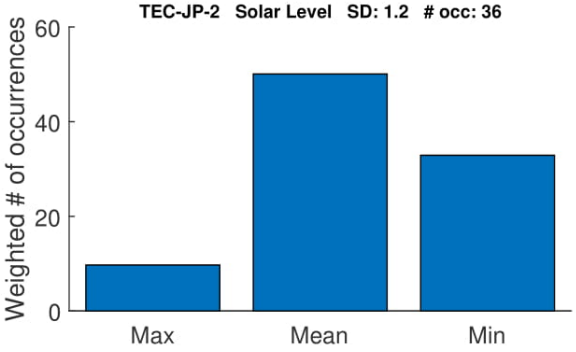

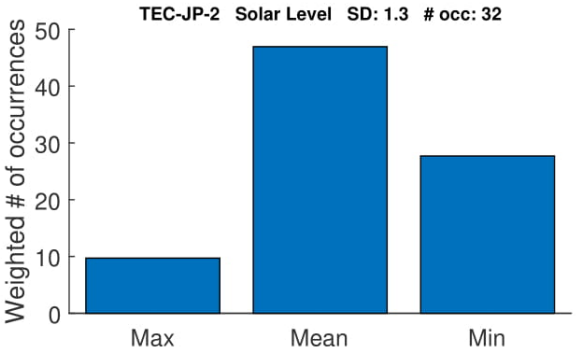

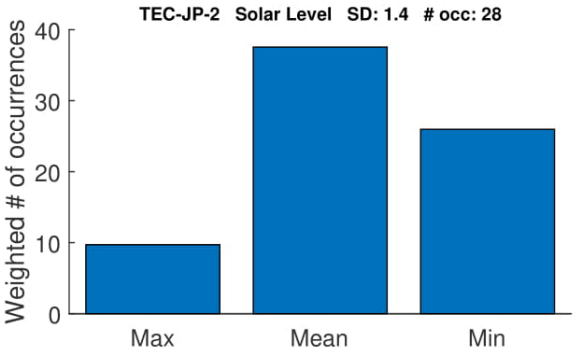

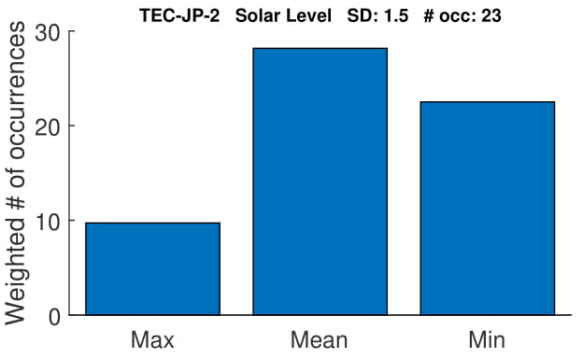

Eliminating Solar

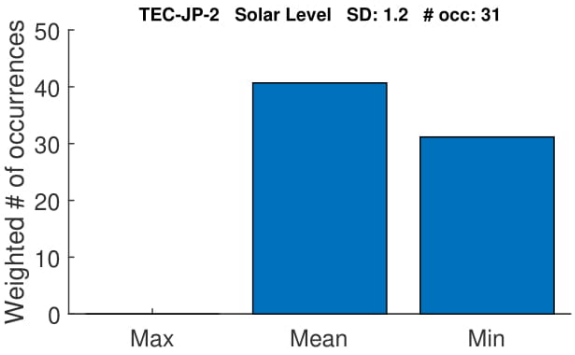

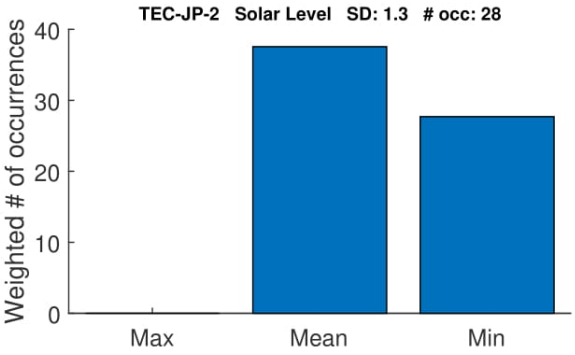

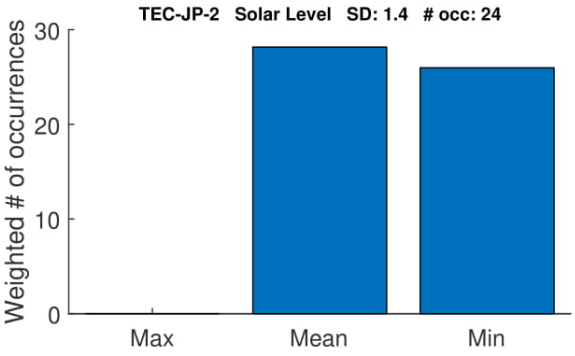

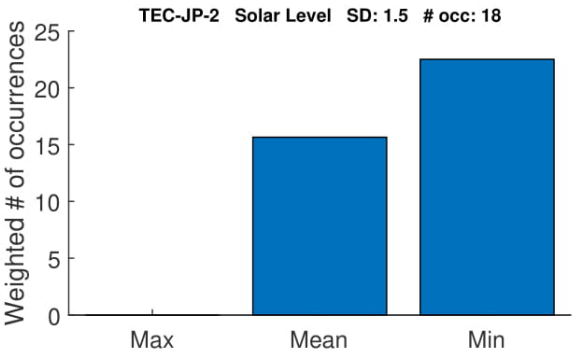

With Solar

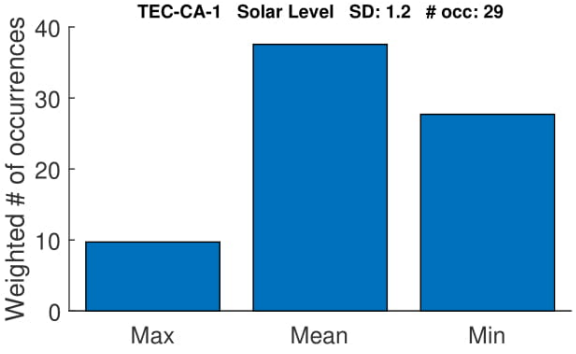

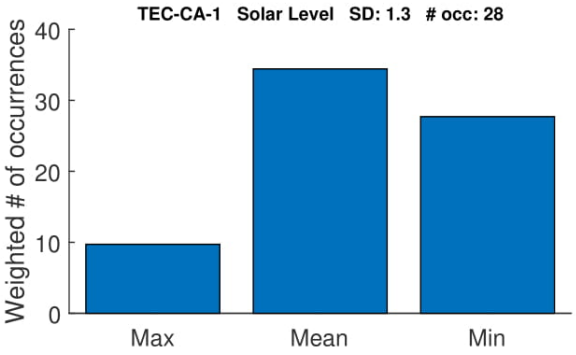

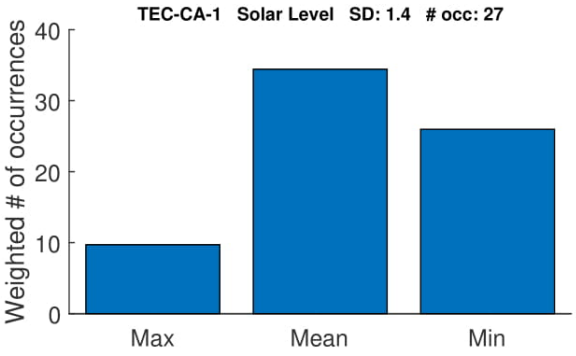

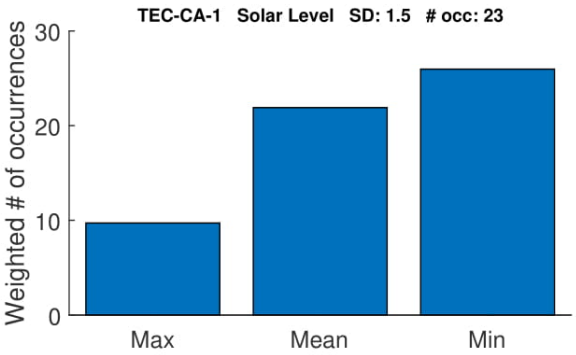

Eliminating Solar

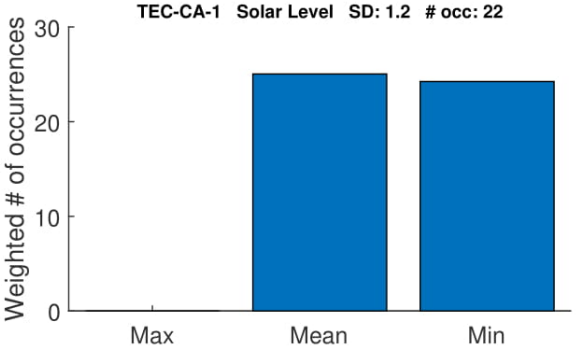

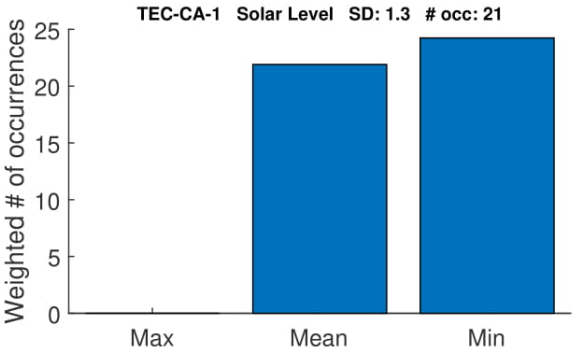

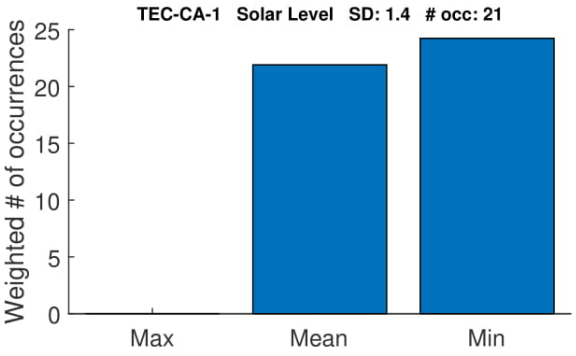

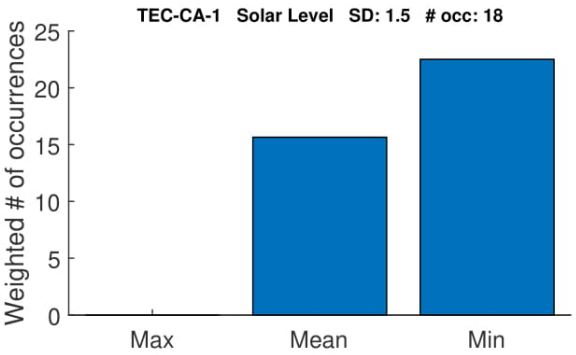

With Solar

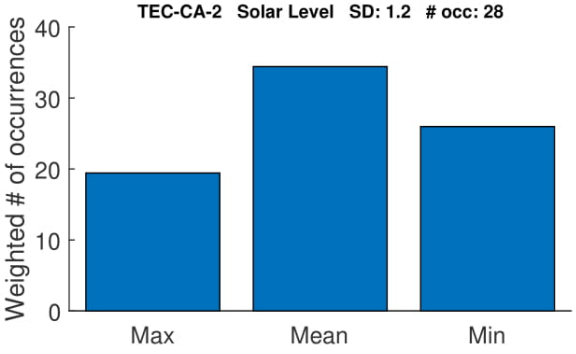

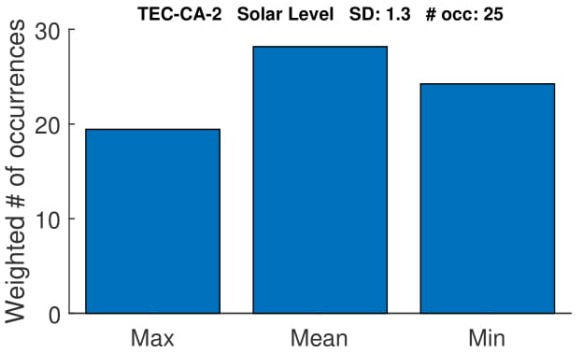

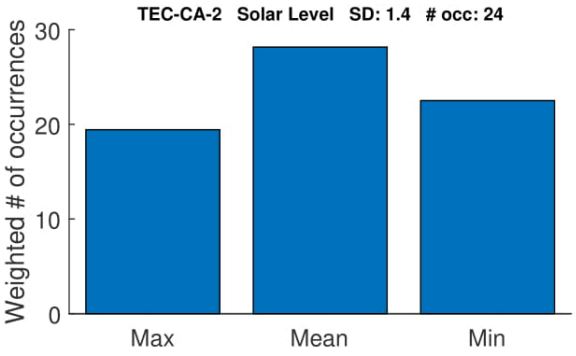

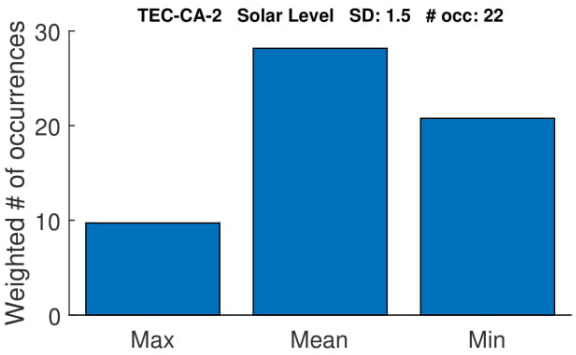

Eliminating Solar

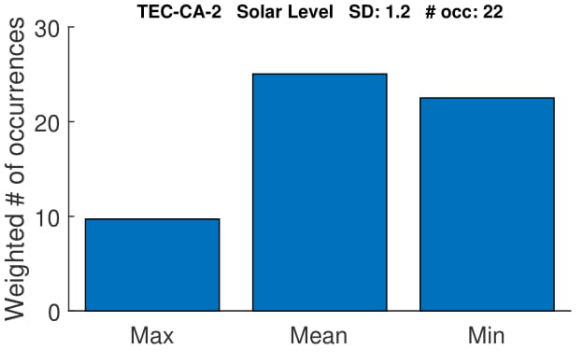

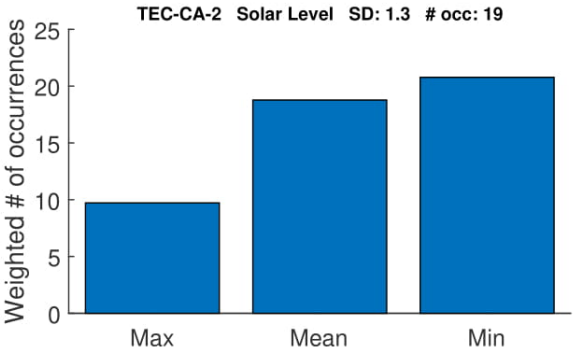

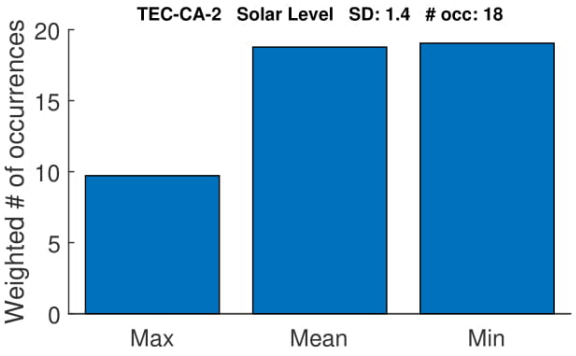

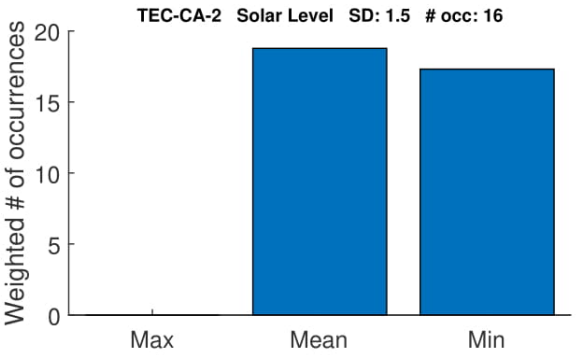

With Solar

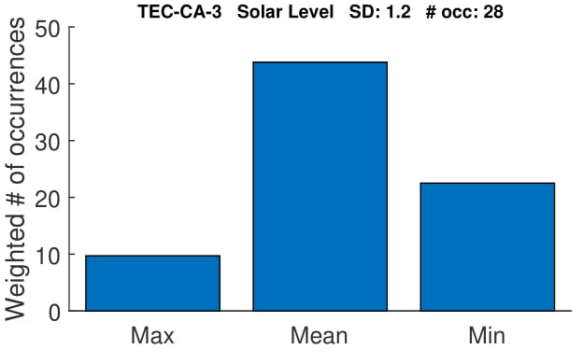

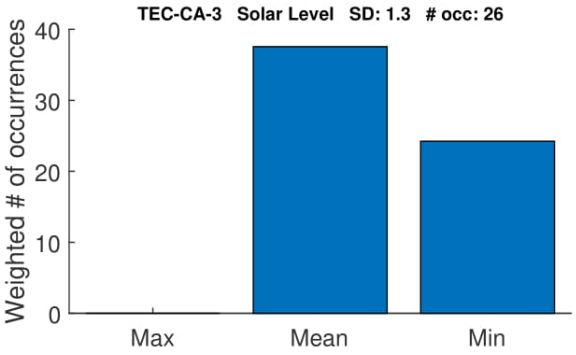

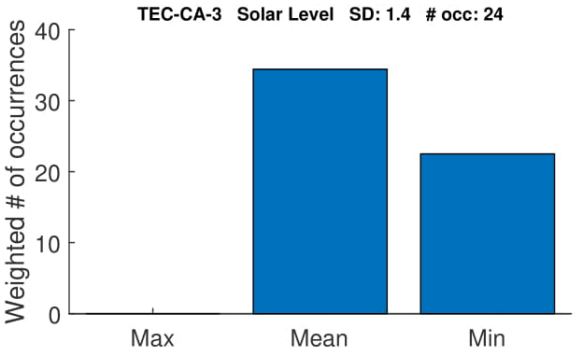

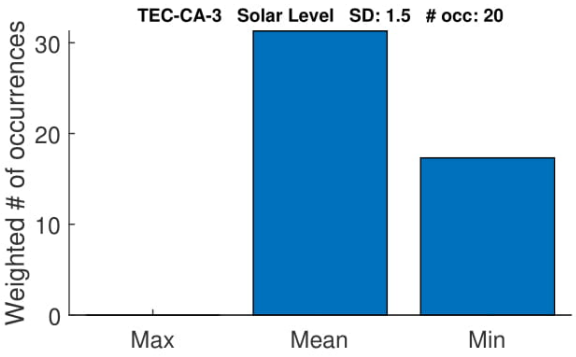

Eliminating Solar

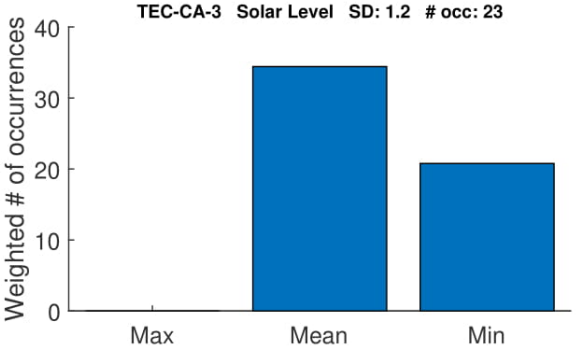

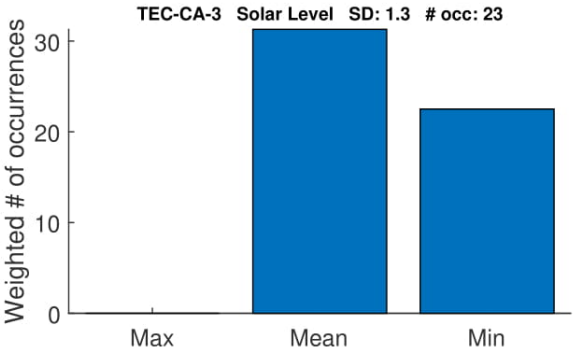

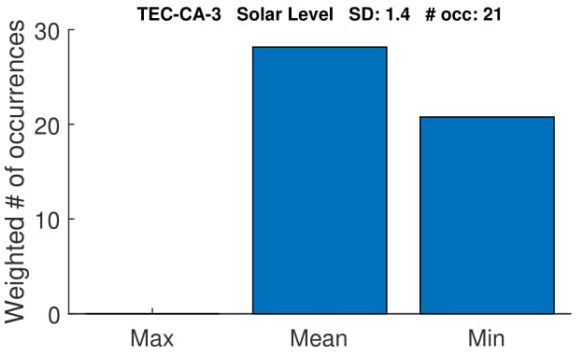

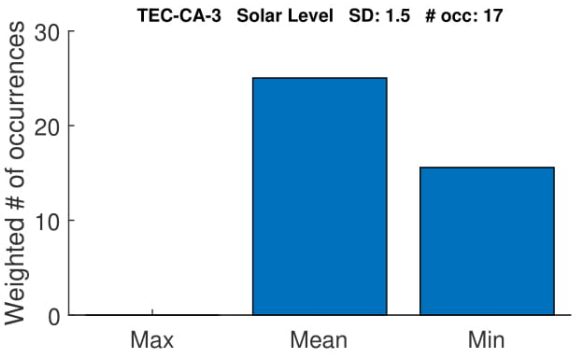

With Solar

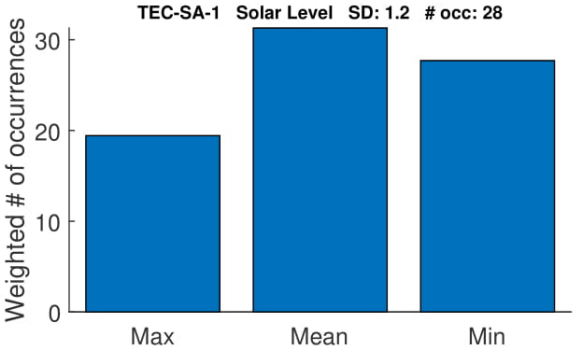

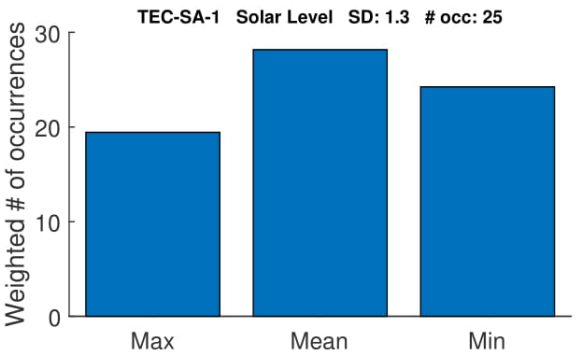

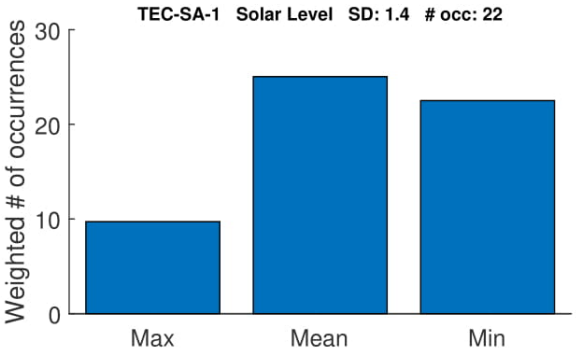

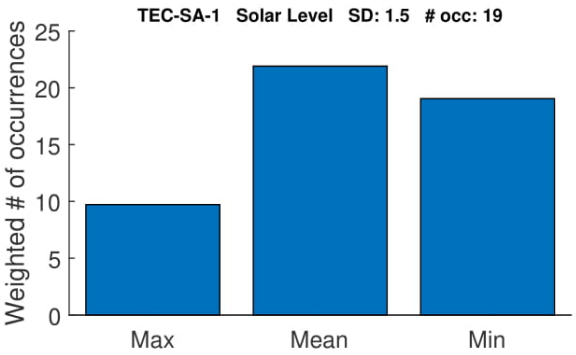

Eliminating Solar

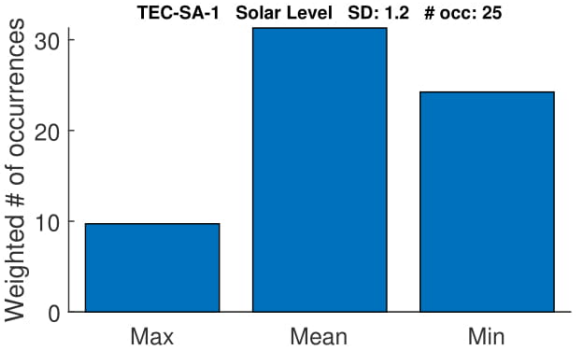

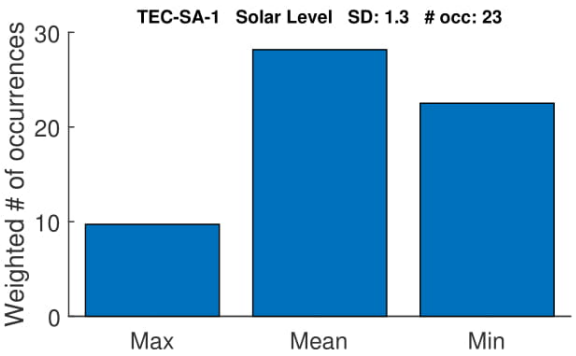

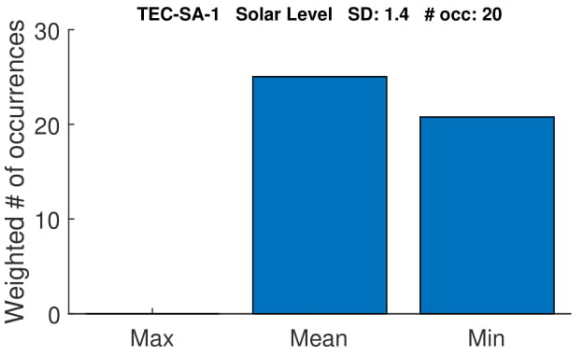

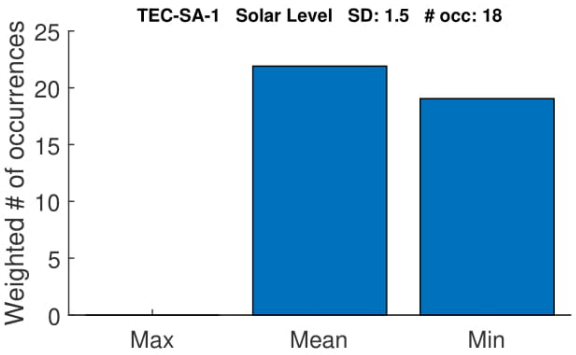

With Solar

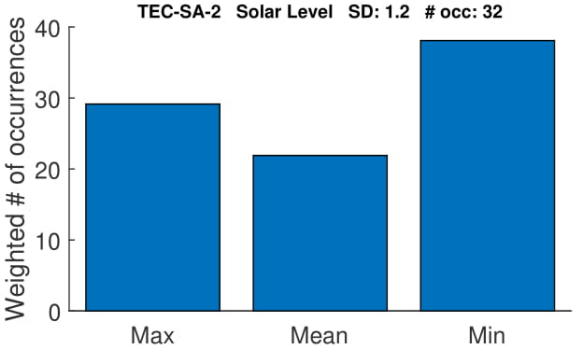

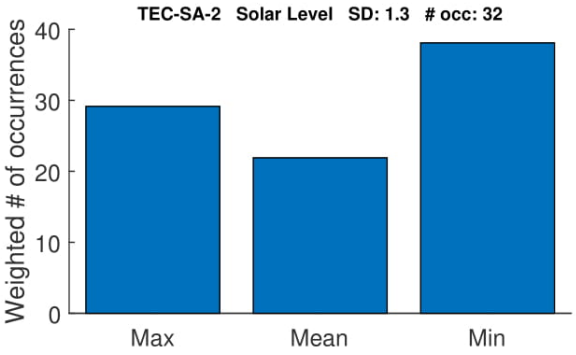

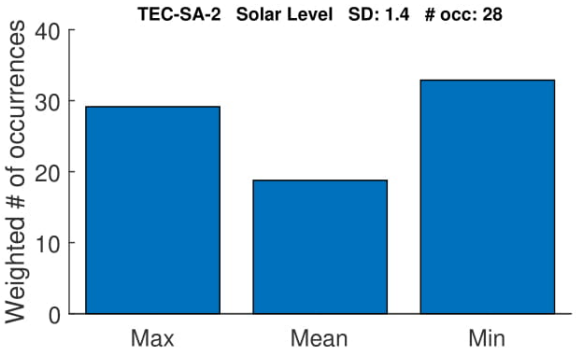

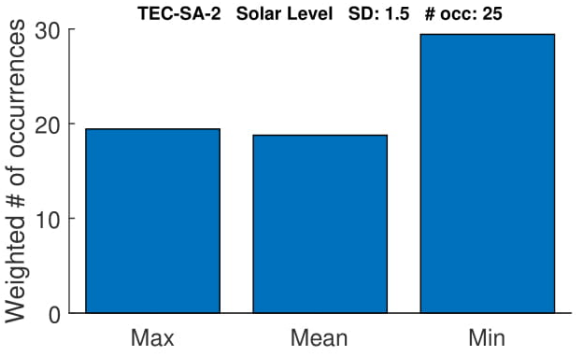

Eliminating Solar

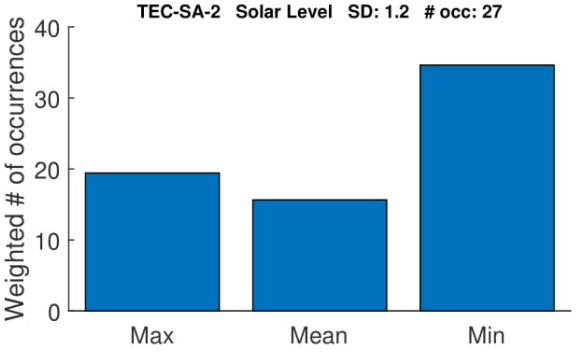

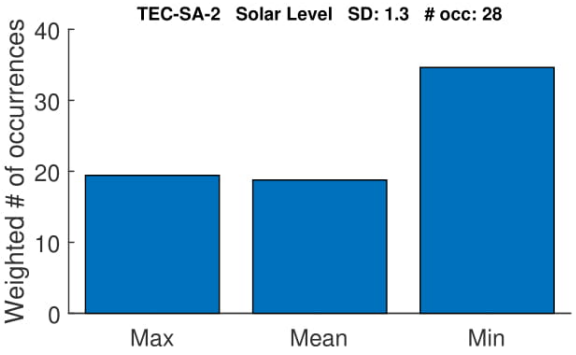

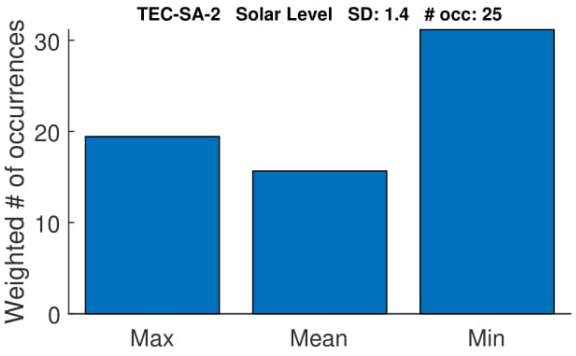

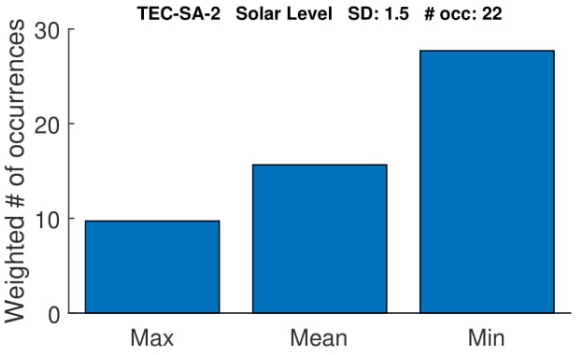

With Solar

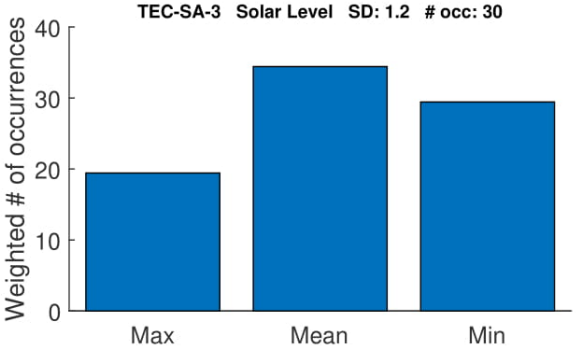

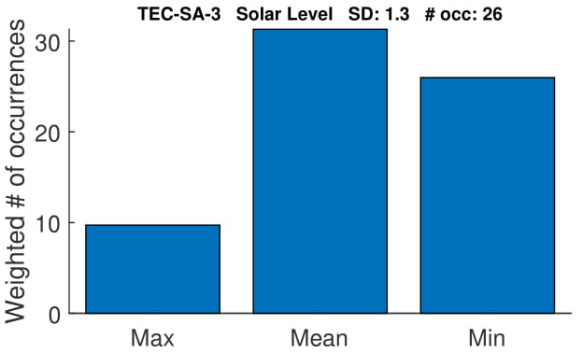

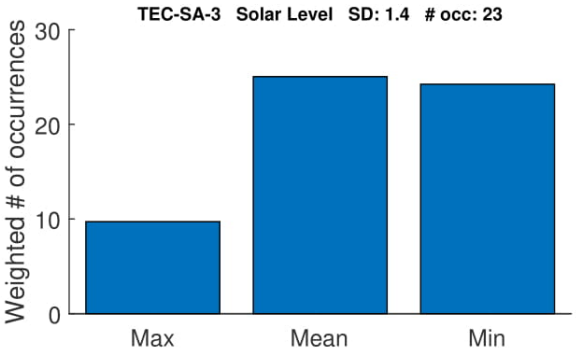

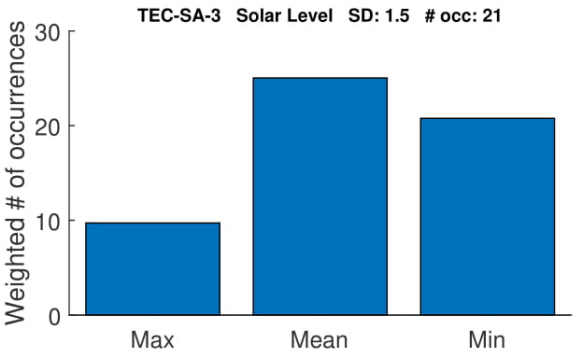

Eliminating Solar

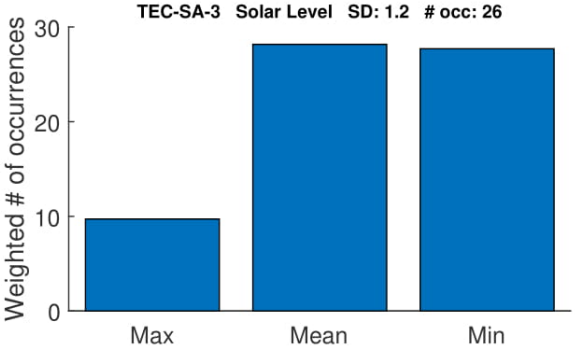

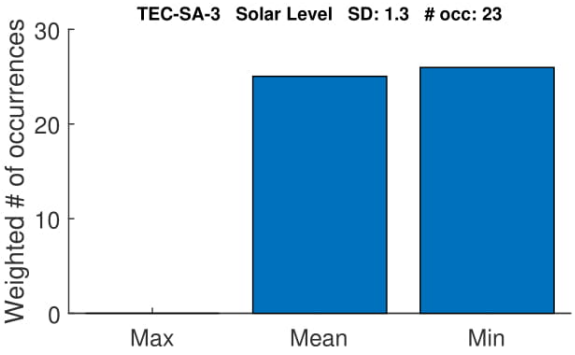

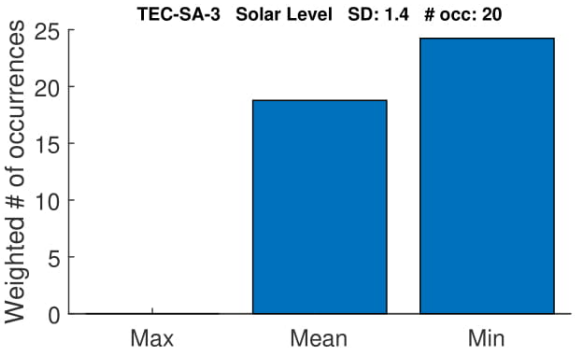

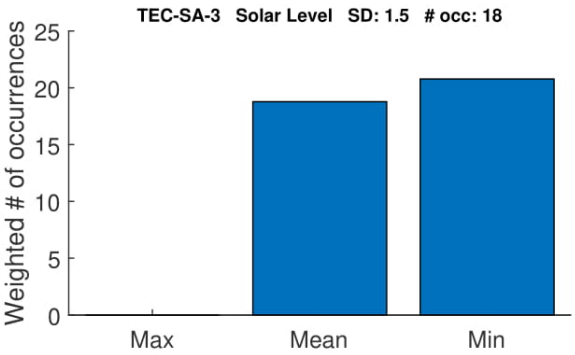

With Solar

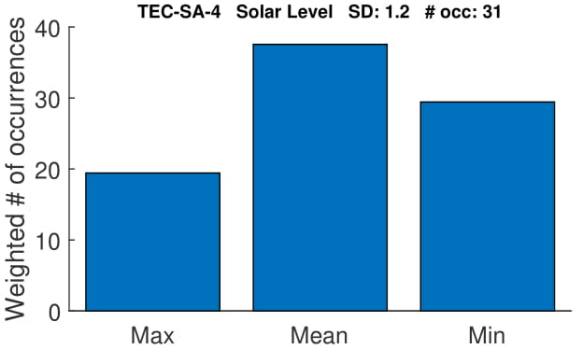

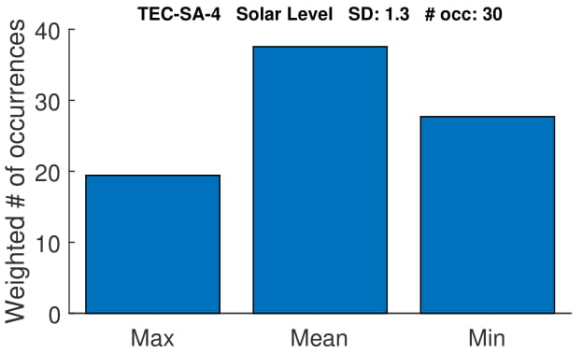

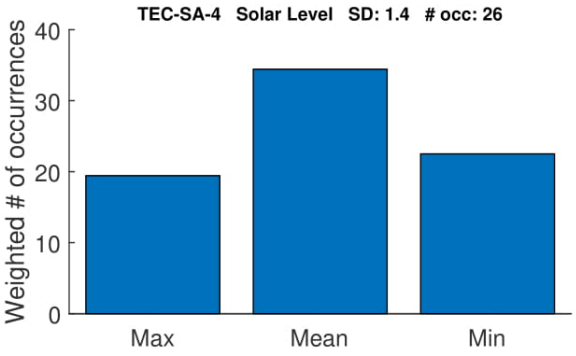

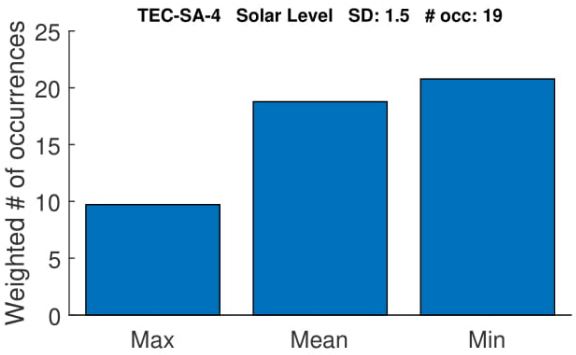

Eliminating Solar